

Université de Montréal

Sur la nature de la variabilité spectrale et photométrique périodique
d'étoiles Wolf-Rayet apparemment isolées

par

Thierry Morel

Département de physique

Faculté des arts et des sciences

Thèse présentée à la Faculté des études supérieures
en vue de l'obtention du grade de
Philosophiæ Doctor (Ph.D.)
en physique

Juillet, 1998

© Thierry Morel, 1998



QC
3
U54
1999
J.014

Revised edition 1971

Supplement reprinting reprinted editions of the series of nine
revised editions of the first four volumes

xxv

Series

Supplements

Supplements to the first four volumes

Supplements to the first four volumes
including the additional volumes
published since 1971, including
supplements to the first four volumes



Serials Section

May 1971

Université de Montréal
Faculté des études supérieures

Cette thèse intitulée:

Sur la nature de la variabilité spectrale et photométrique périodique
d'étoiles Wolf-Rayet apparemment isolées

présentée par:

Thierry Morel

a été évaluée par un jury composé des personnes suivantes:

Daniel Nadeau,	président-rapporteur
Nicole St-Louis,	directeur de recherche
Robert Lamontagne,	membre du jury
Alex W. Fullerton,	examinateur externe

Thèse acceptée le:99-03-26.....

SOMMAIRE

Il est depuis longtemps suspecté que les étoiles Wolf-Rayet *apparemment isolées* présentant des variations périodiques dans le profil de leurs raies spectrales, en photométrie ou en polarimétrie sont associées à un compagnon dégénéré (étoile à neutron ou trou noir), et constituent ainsi une phase évolutive dont l'existence, bien que prédicta par les modèles évolutifs des systèmes binaires massifs rapprochés, n'a pas encore été catégoriquement confirmée observationnellement.

Cependant, de récentes études ayant trait à la variabilité spectrale des étoiles OB laissent émettre quelques doutes quant à la pertinence de ce modèle, en démontrant que des vents largement asphériques peuvent se développer dans les étoiles de type précoce. Le scénario alternatif serait donc de considérer que la variabilité périodique observée n'est pas due à la présence d'un compagnon dégénéré affectant la structure à grande échelle du vent de l'étoile Wolf-Rayet, mais est au contraire induite par la modulation par rotation d'un vent nettement anisotropique.

Cet ouvrage présente les résultats d'un vaste programme d'observations spectroscopiques et photométriques (généralement simultanées) se proposant de lever l'ambiguïté sur la nature précise des étoiles Wolf-Rayet apparemment isolées dont la périodicité des variations est, soit depuis longtemps établie (WR 6), soit suspectée (WR 1, WR 134, WR 136).

Notre étude a permis de confirmer l'existence d'une périodicité de 2.3 jours pour l'étoile WR 134. En outre, nous présentons des arguments mettant en doute l'éventuelle association de WR 6 et WR 134 avec un compagnon dégénéré.

Alternativement, nous proposons que la variabilité périodique observée serait plutôt induite, à l'instar de nombreuses étoiles OB, par la rotation de structures azimutalement étendues dans le vent. Ce modèle est plus à même d'appréhender certains aspects de la variabilité, notamment la nature globalement différente du patron de variabilité selon l'époque d'observation, le caractère périodique des variations présentées par les raies spectrales formées à proximité du cœur stellaire, ou encore la causalité des variations affectant les parties internes et externes du vent. Cette assertion est également supportée par la déficience de rayons-X observée dans le contexte d'une accrétion du vent stellaire par un objet dégénéré.

La similitude des variations spectrales de l'étoile WR 1 avec celles des étoiles précitées laisse présumer qu'une variabilité de nature cyclique pourrait éventuellement être révélée dans un proche avenir. Dans ce cas de figure, nos données semblent imposer une limite inférieure de 5 jours pour une quelconque périodicité.

Le cas échéant, ces structures à grande échelle dans le vent des étoiles WR 6 et WR 134 doivent probablement leur formation à une activité photosphérique dont la nature précise reste à déterminer. L'existence de pulsations radiales ou non radiales du noyau, ou de structures magnétiques ("photosphériques" ou plus vraisemblablement d'origine fossile) pourrait néanmoins être à l'origine de ce phénomène.

TABLE DES MATIÈRES

SOMMAIRE	iii
TABLE DES MATIÈRES	v
LISTE DES TABLEAUX	vi
LISTE DES FIGURES	vii
LISTE DES ABRÉVIATIONS	viii
CHAPITRE 1: INTRODUCTION	1
1.1 Les étoiles Wolf-Rayet	1
1.1.1 Généralités	1
1.1.2 Classification	3
1.1.3 Statut évolutif et processus de formation	4
1.1.3.1 Formation par perte de masse	4
1.1.3.2 Formation par transfert de masse dans un système binaire massif rapproché	5
1.2 Variabilité à petite et grande échelle des étoiles WR	5
1.2.1 La nature fragmentée du vent des étoiles WR	5
1.2.2 Sur l'origine de la variabilité périodique	7

1.2.2.1	Présence d'un compagnon dégénéré?	7
1.2.2.2	Modulation par rotation d'un vent anisotropique?	11
1.3	Les motivations scientifiques de ce projet	13
1.4	Choix de l'échantillon	14
RÉFÉRENCES	16
CHAPITRE 2: OPTICAL SPECTROSCOPY OF EZ CANIS MAJORIS: INDICATION FOR LARGE-SCALE STRUCTURES IN A WOLF-RAYET WIND		31
2.1	Introduction	35
2.2	Observations and Reduction Procedure	40
2.2.1	Photometry	40
2.2.2	Spectroscopy	41
2.3	Results	42
2.3.1	Photometry	42
2.3.2	Spectroscopy	44
2.3.2.1	The Emission-line Variability	44
2.3.2.2	The P Cygni Profile Variability	50
2.3.2.3	“Temporal Variance Spectrum” Analysis	52
2.4	Discussion	54
2.4.1	A Compact Companion?	55

2.4.2 Toward an Interpretation	60	
2.4.3 A Hint of a Magnetic Field Structure?	63	
2.5 Conclusion	65	
RÉFÉRENCES	67	
CHAPITRE 3: COUPLED LINE-PROFILE AND CONTINUUM VARIATIONS IN EZ CANIS MAJORIS: IMPLICATIONS FOR THE DRIVING MECHANISM OF GLOBAL WIND STRUCTURES IN WOLF-RAYET WINDS		93
3.1 Introduction	96	
3.2 Observations	99	
3.2.1 Spectroscopy	99	
3.2.2 Photometry	101	
3.3 Results	101	
3.3.1 An Overview of the LPVs: He II λ 4686	101	
3.3.2 Similarities in the Pattern of Variability for Different Lines	102	
3.3.3 Correlated Continuum and Line-profile Variations	103	
3.3.4 Temporal Variance Spectrum	105	
3.3.5 Line Fluxes, FWHM and Skewness Variations	107	
3.4 Discussion	108	
3.4.1 Implications for the Binary Scenario	108	
3.4.2 Evidence for a Deep-seated Wind Variability	108	

3.4.3	The Cause of a Nonisotropic Base Outflow	110
3.4.3.1	Pulsations	110
3.4.3.2	Magnetic Fields	111
RÉFÉRENCES	114
CHAPITRE 4: A 2.3-DAY PERIODIC VARIABILITY IN THE APPARENTLY SINGLE WOLF-RAYET STAR WR 134: COLLAPSED COMPANION OR ROTATIONAL MODULATION?		133
4.1	Introduction	137
4.2	Observational Background	139
4.3	Observations and Reduction Procedure	141
4.3.1	Spectroscopy	141
4.3.2	Photometry	142
4.4	Results	144
4.4.1	Search for Short-term Periodicity	144
4.4.1.1	Spectroscopy	144
4.4.1.2	Photometry	147
4.4.2	Similarities of the Variations Across a Given Line Profile	149
4.4.3	Similarities Between the Variations of Different Lines . .	150
4.5	Discussion	151
4.5.1	The Duplicity of WR 134 Questioned	151

4.5.1.1	The Expected Emergent X-ray Luminosity	151
4.5.1.2	Modeling the Line-profile Variations Caused by an Ionizing X-ray Source	156
4.5.1.3	On the Origin of the Long-term Modulations	159
4.5.2	Wind-related Variability?	160
RÉFÉRENCES		164
CHAPITRE 5: AN INVESTIGATION OF THE LARGE-SCALE VARIABILITY OF THE APPARENTLY SINGLE WOLF-RAYET STAR WR 1		190
5.1	Introduction	193
5.2	Observations and Reduction Procedure	194
5.2.1	Photometry	194
5.2.2	Spectroscopy	195
5.2.2.1	Long-slit and Reticon Spectra	195
5.2.2.2	Echelle Spectra	196
5.3	Results	197
5.3.1	Continuum Flux Variations	197
5.3.2	An Overview of the Line-profile Variations	197
5.3.3	Temporal Variance Spectrum Analysis	198
5.3.4	The P Cygni Profile Variability	199
5.3.5	Correlated Line-profile Variations in Different Lines? . .	200

5.3.6 Centroid, FWHM, EW, and Skewness Variations	201
5.4 Comparison with Previous Studies	201
5.5 On the Presence of a Companion	203
5.5.1 A Non-degenerate Companion?	203
5.5.2 A Collapsed Companion?	204
5.6 Concluding Remarks	205
RÉFÉRENCES	207
CHAPITRE 6: CONCLUSION	222
RÉFÉRENCES	228
APPENDICE A: MONTAGE DES SPECTRES DE L'ETOILE WR 136	ix
REMERCIEMENTS	xxiv

LISTE DES TABLEAUX

1.1 Critères de classification spectroscopique des étoiles WR (d'après van der Hucht 1996a)	22
1.2 Caractéristiques générales des étoiles WR 1, WR 6, WR 134 et WR 136	23
2.1 Narrowband photometry of EZ CMa in 1995	73
2.1 Continued	74
2.1 Continued	75
2.2 Doppler velocities corresponding to the maxima of the TVS of different lines	76
2.3 Velocities of the prominent σ subpeaks observed in the P Cygni absorption components	77
3.1 Journal of spectroscopic observations	119
3.2 Differential UBV magnitudes of EZ CMa in 1994	120
4.1 Journal of spectroscopic observations	171
4.2 Journal of photometric observations	172
4.3 <i>IUE</i> SWP high resolution spectra of WR 134	173

5.1	Journal of photometric observations	210
5.2	Journal of spectroscopic observations	211
5.3	Projected velocities of the TVS subpeaks observed in some He II features	212
6.1	Caractéristiques générales de la variabilité d'étoiles WR apparemment isolées.	230

LISTE DES FIGURES

1.1 Spectre d'une étoile de type WN 5: WR 6.	24
1.2 Position des étoiles WR dans le diagramme HR selon le modèle atmosphérique de Koesterke & Hamann (1995).	25
1.3 Structure d'un vent stellaire sujet à des instabilités radiatives. D'après Feldmeier (1995).	26
1.4 Illustration de la propagation stochastique de petits sous-pics d'émission superposés sur les profils de raie d'étoiles WR. D'après Lépine & Moffat (1999).	27
1.5 Evolution d'un système binaire massif rapproché. Adapté de De Loore, de Grève, & de Cuyper (1975).	28
1.6 Structure du vent d'une étoile de type précoce en présence d'un compagnon dégénéré accrétant le flux stellaire. D'après Blondin (1994).	29
1.7 Simulations hydrodynamiques de structures à grande échelle dans le vent de ζ Puppis. D'après Cranmer & Owocki (1996).	30
2.1 Light curve of EZ CMa.	78
2.2 Time series of N IV λ 4058, He II λ 6560, and N V λ 4945.	79
2.3 Gray-scale plot of the time series of the residuals of N IV λ 4058, He II λ 4686, and He II λ 6560.	80

2.4	Estimation of the Doppler shifts associated with the different subpeaks traveling across the He II λ 6560 line-profile.	81
2.5	Red-wing intensity of He II λ 4686 measured at 4719 Å.	82
2.6	Gray-scale plot of the time series of N V λ 4945.	83
2.7	Equivalent widths of six selected transitions.	84
2.8	Comparison of the He II λ 4200, He II λ 4542, N V $\lambda\lambda$ 4604, 4620, and N V λ 4945 line-profiles associated with the minimum and the maximum EW values.	85
2.9	Skewness measurements for four selected transitions.	86
2.10	Comparison between the heliocentric radial velocities and the skewness measurements for He II λ 4686 and He II λ 6560.	87
2.11	Deviations of the full width at half-maximum around the mean value for six selected transitions.	88
2.12	Gray-scale plots of the time series of the P Cygni absorption components of He I λ 3889, He I λ 5876, and N V $\lambda\lambda$ 4604, 4620.	89
2.13	Intensity of the N V λ 4604 line-profile measured at 4588 Å. . . .	90
2.14	Superposition of the σ spectrum and the mean spectrum.	91
2.15	Comparison between the representative line-profiles of N IV λ 1718 for the low and high-velocity states as observed by <i>IUE</i> in 1995 January, with the one of 1983 September.	92
3.1	The y -magnitudes of EZ CMa for the periods HJD 2,448,281-2,448,294 and HJD 2,448,918-2,448,931; Narrowband light curve of EZ CMa for the period HJD 2,449,038-2,449,089.	121

3.2	<i>UBV</i> light curves of EZ CMa for the period HJD 2,449,383-2,449,450.	122
3.3	Time series of He II λ 4686 for the six different epochs.	123
3.3	Continued.	124
3.3	Continued.	125
3.4	Gray-scale plots of the time series of the residuals of He II λ 4686, He II λ 4859, and N V λ 4945 for epoch I.	126
3.5	Time series of N IV λ 4058 for epoch VI.	127
3.6	Correlation functions of He II λ 4686 for the different epochs. . .	128
3.7	Correlation function during epoch III for the spectral domain 4570- 4980 Å.	129
3.8	Gray-scale plot of the time series of the P Cygni components of N V $\lambda\lambda$ 4604, 4620 for epoch I.	130
3.9	Superposition of the TVS of epochs I, III, VI, and of 1995 January for the spectral domain 4575-4780 Å.	131
3.10	Deviations of the FWHM, skewness and line flux of He II λ 4686 as a function of phase, for the six epochs.	132
4.1	Power spectra of the skewness, centroid, and FWHM time series of He II λ 4686 for epoch I.	174
4.2	Skewness and centroid variations, deviations of the FWHM around the mean value, and EW variations of He II λ 4686 for each epoch, as a function of phase.	175
4.3	The PS of the rectified spectra of epoch I.	176

4.4	Gray-scale plots of the time series of the residuals of He II λ 4686 for each epoch, as a function of phase.	177
4.5	Photometry of WR 134 in 1992.	178
4.6	Photometry of WR 134 in 1992, folded with the $\mathcal{P} = 2.27$ day period.	179
4.7	Photometry of WR 134 in 1995.	180
4.8	Auto-correlation matrices of He II λ 4686 for each epoch.	181
4.9	Correlation matrices of He II λ 5412 with He II λ 4542, He II λ 4686, He II λ 4859, and C IV λ 5806 for epoch III.	182
4.10	Contours of constant ionization parameter $\log \xi$	183
4.11	Predicted X-ray luminosities in the 0.2-2.4 and 0.2-4.0 keV bands in the presence of an accreting compact companion.	184
4.12	The observed and modeled TVS.	185
4.13	Sketch of the geometry adopted for the photoionization cavity. .	186
4.14	The observed and modeled phase-dependent variations of He II λ 4686.	187
4.15	Variations of the P Cygni absorption troughs of He I λ 4471 and N V λ 4604 with phase.	188
4.16	The Stokes parameters Q and U of WR 134 in 1985-1986, folded with the $\mathcal{P} = 2.27$ day period.	189
5.1	Differential v magnitudes of WR 1 in 1996 September	213

5.2	Superposition of the 21 Echelle spectra acquired around HJD 2,450,344.873 for the spectral range encompassing He II λ 4686	214
5.3	Montage of the continuum-normalized, nightly mean spectra obtained in 1995 October and 1996 September for the spectral range encompassing He II λ 4686	215
5.4	Square root of the Temporal Variance Spectrum	216
5.5	Superposition for the spectral range encompassing N V $\lambda\lambda$ 4604, 4620 of the nightly means of 1995 October 12 and 1996 September 16	217
5.6	Superposition for the spectral range encompassing C IV λ 5806 and He I λ 5876 of nightly means observed in 1995 October, 1996 September and 1996 November	218
5.7	Correlation matrices of He II λ 5412 with He II λ 4686, He II λ 4859, and N V λ 4945	219
5.8	Continuum flux level variations, centroid variations, deviations of the FWHM around the mean value, EW variations, and skewness variations of He II λ 4686, as a function of the Heliocentric Julian Date of observation	220
5.9	Allowed values of (P, M_*) when adopting $K_{WR} \approx 70 \text{ km s}^{-1}$ and $K_{WR} \approx 22 \text{ km s}^{-1}$	221
A.1	Montage des spectres de l'étoile WR 136 pour le domaine spectral 4440-5005 Å.	x
A.1	Suite.	xi
A.1	Suite.	xii

A.1 Suite	xiii
A.1 Suite	xiv
A.2 Montage des spectres de l'étoile WR 136 pour le domaine spectral 5345-5930 Å	xv
A.2 Suite	xvi
A.2 Suite	xvii
A.2 Suite	xviii
A.2 Suite	xix
A.3 Valeurs de la TVS pour l'étoile WR 136 en 1995	xx
A.4 Variations selon le jour Julien d'observation de l'inclinaison, premier moment, largeur à mi-hauteur et largeur équivalente de la raie He II λ 4686 de l'étoile WR 136	xxi

LISTE DES ABRÉVIATIONS

c	Compact object
DAC	Discrete absorption component
HMXRB	High-mass X-ray binary
LBV	Etoile lumineuse bleue variable
LPV	Line-profile variations
MPS	Mean power spectrum
PS	Power spectrum
SB	Supergéante bleue
SR	Supergéante rouge
TVS	Temporal variance spectrum
UV	Ultraviolet
WC	Etoile Wolf-Rayet de la séquence du carbone
WN	Etoile Wolf-Rayet de la séquence de l'azote
WO	Etoile Wolf-Rayet de la séquence de l'oxygène
WR	Etoile Wolf-Rayet

CHAPITRE 1

INTRODUCTION

1.1 Les étoiles Wolf-Rayet

1.1.1 Généralités

Il y a maintenant plus d'un siècle, plus précisément en 1867, que deux astronomes français — Wolf & Rayet — observèrent des étoiles dont le spectre ne présentait que des raies spectrales en émission.¹ La nature de ces spectres surprit d'autant plus à l'époque, que ces raies en émission étaient extrêmement intenses et larges (largeur à mi-hauteur $\approx 2000 \text{ km s}^{-1}$). Ce n'est que bien plus tard qu'il a été justement proposé que ces raies spectrales étaient *exclusivement* formées dans un milieu (en l'occurrence un vent stellaire) en expansion rapide (Beals 1929).² Un spectre de l'étoile de type WN 5, WR 6, est présenté sur la Figure 1.1 (pour une description du système de classification des étoiles WR, voir §1.1.2).

Cent trente ans après leur découverte, on recense actuellement environ 200 étoiles Wolf-Rayet (WR) dans la Galaxie (van der Hucht 1996a), ainsi que de nombreuses autres dans le Groupe Local (Maeder & Conti 1994; Massey & Johnson 1998, et références citées). Il est maintenant bien établi que ce stade

¹Les étoiles WR 134 (voir chapitre 4) et WR 136 (voir Appendice A), toutes deux situées dans la constellation du Cygne, étaient parmi les étoiles initialement découvertes par ces deux astronomes.

²Sauf dans de rares cas, aucune raie d'origine photosphérique n'est observée dans le spectre des étoiles WR.

évolutif est vraisemblablement partagé par toutes les étoiles galactiques isolées de masse initiale supérieure à $25\text{--}35 M_{\odot}$, c'est-à-dire de type O. En outre, des processus de transfert de masse dans un système binaire rapproché sont également susceptibles de mener à la formation d'une étoile WR (§1.1.3.2). Le faible nombre d'étoiles WR observées n'est ainsi dû qu'à la relativement courte durée de cette phase évolutive (entre 10^5 et 10^6 années; Maeder & Meynet 1994). De plus, étant principalement concentrées dans le plan galactique, nombre d'entre elles subissent une extinction interstellaire considérable qui nous en empêche l'observation.

Les particularités spectrales des étoiles WR révèlent que la formation des raies d'émission s'opère dans un milieu gazeux en expansion rapide. La modélisation de l'atmosphère étendue de ces étoiles nécessite donc un traitement adéquat (e.g., Schaerer 1996): analyse hors équilibre hydrostatique, abandon de l'approximation plane-parallèle, etc. Les modèles théoriques les plus récents leur attribuent des températures effectives, ainsi que des luminosités extrêmement élevées (Hamann & Koesterke 1996; voir Fig.1.2). La masse d'une étoile WR s'échelonne entre cinq et plusieurs dizaines de masses solaires; une masse minimale de $72 M_{\odot}$ a été récemment reportée par Rauw et al. (1996a) pour l'étoile de type WN 7, WR 7.

Le taux de perte de masse des étoiles WR, qui est l'un des plus élevés des objets stellaires connus, constitue leur principale particularité. Le taux de perte de masse est généralement déduit de l'observation radio, et se situe entre 10^{-4} et $10^{-5} M_{\odot}/\text{an}$ (e.g., Abbott et al. 1986; Leitherer, Chapman, & Koribalski 1995). La vitesse terminale du vent est, quant à elle, déterminée grâce aux profils P Cygni présents dans le domaine ultraviolet (UV), et peut atteindre jusqu'à $5\,500 \text{ km s}^{-1}$ pour les étoiles WR les plus évoluées (Rochowicz & Niedzielski 1995). Du fait de ces particularités, les étoiles WR injectent une quantité importante d'énergie mécanique dans le milieu interstellaire; ceci ayant pour effet d'affecter grandement leur voisinage direct (Leitherer, Robert, & Drissen 1992). Elles contribuent éga-

lement substantiellement à l'enrichissement en métaux des galaxies (Meynet et al. 1997). Pour une revue des propriétés générales de ces étoiles, nous référons le lecteur à Abbott & Conti (1987) et van der Hucht (1992, 1996b).

1.1.2 Classification

Les étoiles WR sont subdivisées en trois principaux groupes: WN, WC et WO. Les étoiles WR ayant été, tout au moins en partie, “dénudées” de leurs couches externes durant leurs phases évolutives antérieures, leur vent stellaire révèle les produits de nucléosynthèse produits dans leurs couches initialement internes. Ainsi, les étoiles WN montrent la signature spectrale des produits de la nucléosynthèse CNO, soit l'azote et l'hélium, tandis que les étoiles WC montrent les produits de combustion de l'hélium: le carbone et l'oxygène. Proportionnellement à ces dernières, les rares étoiles WO sont enrichies en oxygène (et ceci au détriment de l'hélium et du carbone). A l'intérieur de chaque classe, on a défini une sous-classification: WN 2, ..., WN 11, WC 4, ..., WC 9, WO 1, ..., WO 5. Cette sous-classification est uniquement basée sur des critères spectroscopiques empiriques, et est grossièrement fonction du niveau d'ionisation/excitation des raies (voir Tableau 1.1).³ Il est important de réaliser que ce système de classification ne reflète que les propriétés générales du *vent* stellaire, et n'est donc pas révélateur des propriétés fondamentales de l'étoile que sont, par exemple, la température effective ou la luminosité bolométrique. Seule l'utilisation de modèles atmosphériques permet d'évaluer ces quantités (Fig.1.2). Par extension, on parle de WNE pour les étoiles WN 2-5, et de WNL pour les étoiles WN 5-11 (il en va de même pour les étoiles de type WC; la subdivision s'effectuant à partir du type WC 7).

³Un système de classification plus élaboré a été récemment proposé par Smith, Shara, & Moffat (1996). Voir également Crowther, De Marco, & Barlow (1998) pour un nouveau système de classification des étoiles WC et WO.

1.1.3 Statut évolutif et processus de formation

1.1.3.1 Formation par perte de masse

Comme suggéré précédemment, une étoile WR peut constituer le résultat final de l'évolution d'une étoile O *isolée* avant qu'elle n'explose en supernova. L'évolution d'une étoile massive dans le voisinage solaire peut être grossièrement schématisée comme suit (Maeder 1996):

- O → Of → WNL + abs. → WN 7 → (WNE) → WCL → WCE → (WO)
→ Supernova
Pour $M_{SP} \gtrsim 60 M_{\odot}$
- O → Of → LBV → WN 8 → WNE → WCE → Supernova
Pour $40 \lesssim M_{SP} \lesssim 60 M_{\odot}$
- O → (SB) → SR → (SB) → WNE → (WCE) → Supernova
Pour $25 \lesssim M_{SP} \lesssim 40 M_{\odot}$

où SB, SR et LBV réfèrent respectivement à une étoile supergéante bleue, rouge et dite lumineuse bleue variable (Humphreys & Davidson 1994). M_{SP} dénote la masse initiale de l'étoile sur la séquence principale. Les phases évolutives entre parenthèses sont incertaines ou de très courte durée. Le processus décrit ci-dessus est en accord avec diverses déterminations d'abondance (e.g., Eenens & Williams 1992; Nugis & Niedzielski 1995), ainsi qu'avec l'existence des objets de transition de type Ofpe/WN 9 (Nota et al. 1996) et WN/WC (Crowther, Smith, & Willis 1995). Il est à souligner que ce scénario évolutif est loin d'avoir été unanimement accepté (voir, e.g., Langer et al. 1994; Crowther et al. 1995). Ceci s'explique en partie par la sensibilité de ces modèles au traitement de la convection et du mélange par rotation, ainsi qu'aux valeurs du taux de perte de masse adoptées pour chaque stade évolutif. Concernant ce dernier point, le taux de perte de masse

étant relié à la métallicité du milieu interstellaire à partir duquel l'étoile s'est formée (selon $\dot{M} \propto Z^{0.5-1.0}$), le parcours évolutif diffère également d'une galaxie à l'autre, voire à l'intérieur d'une même galaxie. L'évolution d'étoiles massives dans différents environnements est décrite en détail par Maeder & Conti (1994) et Meynet (1995).

1.1.3.2 Formation par transfert de masse dans un système binaire massif rapproché

Un autre processus non négligeable pouvant mener à la formation d'une étoile WR — notamment dans les galaxies de faible métallicité — est de considérer l'évolution d'un système binaire massif rapproché O + O (Paczyński 1967; Dalton & Sarazin 1995). Au cours de son évolution, l'étoile primaire⁴ s'expandra et remplira son lobe de Roche. Une partie substantielle de l'enveloppe riche en hydrogène de cette étoile sera alors transférée à l'étoile secondaire par accrétion. Le résultat final est l'exposition du cœur de l'étoile primaire, qui sera alors observée comme étoile WR (pour de plus amples précisions, voir §1.2.2.1).

1.2 Variabilité à petite et grande échelle des étoiles WR

1.2.1 La nature fragmentée du vent des étoiles WR

Comme il a été souligné, les étoiles WR se distinguent par un taux de perte de masse remarquablement élevé, ainsi que par un vent stellaire accéléré à des vitesses considérables ($\approx 0.01 c$). Bien qu'il ait été admis pendant de nombreuses années que le mécanisme à l'origine de ce vent stellaire devait être fondamentalement différent de celui opérant dans les étoiles de type tardifs, il a fallu attendre le travail fondamental de Lucy & Solomon (1970) pour envisager

⁴Par étoile primaire, nous entendons l'étoile initialement la plus massive.

que le vent des étoiles de type précoce pouvait en fait être supporté par la pression exercée sur le gaz par l'absorption de la radiation par les raies de résonance présentes dans le domaine ultraviolet.⁵

Il est rapidement devenu évident que, du fait de la nature intrinsèquement instable de ce mécanisme à de petites perturbations de vitesse radiale, le vent devait être sujet à d'importantes instabilités radiatives (e.g., Carlberg 1980). De nos jours, il est maintenant bien établi que des chocs s'y développent inévitablement (Fig.1.3) et que l'écoulement est donc fragmenté. Un point saillant de ceci est que le vent peut être grossièrement défini comme étant constitué d'une "hiérarchie" de surdensités locales de matière (Robert 1992).

De telles inhomogénéités engendrées par des instabilités radiatives (ainsi que possiblement par des phénomènes de turbulence ou des instabilités thermiques dues à l'existence d'ondes d'Alfvén; voir Gonçalves, Jatenco-Pereira, & Opher 1998 pour ce dernier cas de figure) se manifestent observationnellement dans les étoiles WR par des variations à la limite des possibilités instrumentales. Cependant, leur existence a été indépendamment révélée par des observations infrarouges/millimétriques (Nugis 1996), en rayons-X (Willis & Stevens 1996), photométriques (Moffat & Shara 1986) ou encore polarimétriques (Robert et al. 1989). Le mouvement systématique de petits sous-pics d'émission superposés aux raies spectrales leur est également attribué (Moffat & Robert 1992; Lépine & Moffat 1999). La propension des ces micro-structures à apparaître de façon *stochastique* sur le profil de la raie, puis de s'éloigner systématiquement du centre de celui-ci sur une durée caractéristique de quelques heures accrédite l'idée qu'ils "stigmatisent" le mouvement des surdensités locales de matière se déplaçant vers les parties

⁵Contrairement aux étoiles OB, le moment transporté par le champ de radiation semble néanmoins insuffisant pour soutenir le vent des étoiles WR (i.e., $\eta = \dot{M}v_\infty/(L/c) \gg 1$; voir Tableau 1.2). Bien que plusieurs hypothèses semblent pouvoir être avancées afin de pallier à cette déficience (Willis & Crowther 1996), aucune explication réellement satisfaisante n'a été jusqu'à lors avancée.

externes du vent (Fig.1.4).

Il importe de souligner que *ces variations spectroscopiques de faible amplitude, quoique indubitablement présentes dans les étoiles WR incluses dans notre étude, sont largement dominées par des variations de plus grande amplitude, et qui plus est périodiques.*

1.2.2 Sur l'origine de la variabilité périodique

Depuis quelques années, il apparaît que certaines étoiles WR *apparemment isolées* présentent des variations dans tous les modes d'observation qui sont difficilement attribuables à la nature instable de leur vent discutée ci-dessus. Cette conclusion repose principalement sur la grande amplitude des variations spectroscopiques, photométriques et/ou polarimétriques observées (e.g., Lépine, Moffat, & Henriksen 1996; Anthokin et al. 1995; Drissen et al. 1989) ou, a fortiori, sur le caractère périodique de la variabilité pour quelques rares étoiles.⁶ Dans ce dernier cas, deux hypothèses peuvent être avancées afin de rendre compte de ce caractère périodique: une variabilité induite par la révolution orbitale d'un compagnon ne manifestant aucun signe évident de sa présence, ou une modulation par rotation d'un vent largement anisotropique. Ces deux scénarios sont discutés plus amplement ci-dessous.

1.2.2.1 Présence d'un compagnon dégénéré?

La nature strictement périodique des variations affectant certaines étoiles WR, conjuguée avec le manque total de signature spectrale d'un éventuel compagnon (i.e., manque de raies spectrales pouvant lui être attribuées dans le spectre intégré, absence de variations notables de vitesse radiale des raies de l'étoile WR

⁶Pour une illustration du type de variabilité photométrique et spectroscopique présenté par ces étoiles, nous référerons le lecteur aux figures 2.1 et 3.3 présentées ci-après.

induites par une hypothétique révolution orbitale, ou aucune dilution apparente du niveau de continuum de l'étoile WR) amène à penser que celui-ci serait, le cas échéant, un astre de relativement faibles masse et luminosité dans le domaine optique, vraisemblablement de nature dégénérée (étoile à neutron ou trou noir).

Cette conclusion est, d'ailleurs, supportée par les modèles évolutifs des systèmes binaires massifs rapprochés qui prédisent l'existence d'une phase évolutive où une étoile WR est associée à un objet dégénéré. Le parcours évolutif que décrit un tel système double massif peut être schématisé comme suit (voir la Figure 1.5):

- Stade I: On considère un système initialement constitué de deux étoiles de la séquence principale de type O, étant supposées évoluer comme deux étoiles isolées; la période orbitale est généralement de quelques jours.
- Stade II: L'étoile primaire, après avoir quitté la séquence principale, entre dans sa phase supergéante. Dès lors, elle remplit son lobe de Roche avec un subséquent transfert de masse vers l'étoile secondaire par le point de Lagrange intérieur. Des exemples de tels systèmes binaires, dits semi-détachés, sont rares (voir, e.g., Lorenz, Mayer, & Drechsel 1994). Il est à noter que ce processus peut s'avérer instable et conduire à une phase dite d'enveloppe commune (Rasio & Livio 1996).
- Stade III: Après cette courte première phase de transfert de masse (environ 30 000 ans), le système est dorénavant constitué d'une étoile WR — fruit de la perte par l'étoile primaire de ses couches externes riches en hydrogène — et d'une étoile O orbitant autour du centre de masse avec une période maintenant légèrement plus importante. Cette phase évolutive est couramment observée; environ 37 % des étoiles WR connues dans le voisinage solaire sont associées à un compagnon, de type O dans la plupart des cas (van der Hucht et al. 1988).
- Stade IV: L'étoile WR arrive à la fin de son évolution et explose en supernova.

Une récente détermination de la vitesse spatiale d'un échantillon de jeunes pulsars (Lyne & Lorimer 1994) suggère que, du fait de l'asymétrie de l'explosion, ces derniers acquièrent une vitesse considérable lors de leur formation ($\approx 300\text{-}500 \text{ km s}^{-1}$; Lorimer, Bailes, & Harrison 1997; Hansen & Phinney 1997).⁷ De ce fait, il est vraisemblable que la plupart de ces systèmes ne devraient plus être liés gravitationnellement après l'explosion (e.g., De Donder, Vanbeveren, & van Bever 1997). Dans certains cas favorables, une étoile O peut cependant demeurer associée avec une jeune étoile à neutron (ou un trou noir); le système est alors caractérisé par une vitesse spatiale élevée.

- Stade V: L'étoile O arrive maintenant à la fin de sa phase de brûlage de l'hydrogène et évolue en supergéante. Celle-ci engendre dès lors un intense vent stellaire (taux de perte de masse d'environ $10^{-5}\text{-}10^{-6} M_{\odot}/\text{an}$) dont l'accrétion sur le compagnon dégénéré produit une intense émission dans le domaine des hautes énergies (les luminosités en rayons-X approchent en général $10^{36} \text{ ergs s}^{-1}$). Voir Bildsten et al. (1997) pour les propriétés générales de ces systèmes.
- Stade VI: L'étoile O s'expand jusqu'à remplir à son tour son lobe de Roche; c'est la seconde phase de transfert de masse. Une importante partie de l'enveloppe est éjectée du système ($\approx 70\%$ d'après Dalton & Sarazin 1995). En vertu de cette perte de masse et de la conservation du moment angulaire orbital, l'étoile à neutron "spirale" à l'intérieur de l'atmosphère étendue de l'étoile O. De nombreuses incertitudes persistent quant à la nature exacte de ce processus. L'accrétion du vent stellaire par l'étoile à neutron peut s'avérer être supercritique et amener couramment à la formation de trous noirs (Brown 1995). Dans certains cas, les deux objets peuvent d'autre part "fusionner" (Thorne & Zytkow 1977).

⁷De nombreuses autres distributions de vitesse ont été récemment proposées dans la littérature, e.g., Fryer, Burrows, & Benz (1998).

- Stade VII: Fin de la seconde phase de transfert de masse. Une nébuleuse est formée suite à la masse perdue par le système lors de ce processus. Nous sommes dès lors en présence d'un système constitué d'un objet compact et d'une étoile dans la phase de brûlage de l'hélium.
- Stade VIII: La période de révolution du système, maintenant composé d'une étoile dégénérée et d'une étoile WR résultant de l'évolution ultérieure de l'étoile à hélium, s'est considérablement réduite et n'est plus que de quelques heures (van den Heuvel & De Loore 1973). Là encore, du fait du taux de perte de masse considérable des étoiles WR et de l'accrétion par le compagnon dégénéré du vent stellaire, une intense production de rayons-X est attendue. Cygnus X-3 est le seul objet dont l'appartenance à cette classe est fortement suspectée (van Kerkwijk 1993; van Kerkwijk et al. 1992, 1996). Cette source extrêmement intense en rayons-X ($L_X \approx 10^{38}$ ergs s^{-1}), est vraisemblablement constituée d'une étoile WNL et d'un trou noir orbitant avec une période d'environ 4.8 heures (Schmutz, Geballe, & Schild 1996). Cygnus X-3 montre des variations spectaculaires dans tous les modes d'observations (e.g., Fender et al. 1997).
- Stade IX: L'étoile WR explose à son tour en supernova. Deux objets dégénérés non liés gravitationnellement et de vitesse spatiale élevée sont créés ou, dans de très rares cas, un système double constitué de deux objets dégénérés (indifféremment étoile à neutron ou trou noir) est constitué. PSR 1913+16 a été le premier système de ce type découvert (Hulse & Taylor 1975).

Du fait des grandes capacités de calculs actuelles, il est maintenant possible de simuler l'évolution d'une population statistiquement représentative de systèmes doubles avec une variété de conditions initiales adéquatement choisies (i.e., rapport de masses stellaires, séparation orbitale, etc.). Les premières avancées dans ce domaine ont été réalisées dans les années 1970. Ces premières synthèses de population, où il a été supposé que le caractère anisotropique de l'explosion de l'étoile

primaire en supernova (durant le stade IV) communiquait une vitesse d'environ 100 km s^{-1} à l'étoile à neutron ainsi formée, aboutissaient à un taux de survie⁸ du système d'approximativement 80 % (de Grève, de Loore, & van Dessel 1977). Conséquemment, ceci suggérait qu'un nombre important de systèmes constitués d'une étoile WR et d'un objet dégénéré devaient être observables (jusqu'à 40 % de l'ensemble des WR observables selon Vanbeveren & Conti 1980). De récentes réévaluations de la vitesse acquise par l'étoile à neutron lors de sa formation ($v \approx 300\text{-}500 \text{ km s}^{-1}$) ont cependant amené à revoir considérablement à la baisse ces estimations. En effet, les modèles évolutifs les plus récents arrivent à un taux de survie de seulement 30 % en moyenne (Brandt & Podsiadlowski 1995), et que moins de 3 % (moins de 5 systèmes observables) de l'ensemble des étoiles WR seraient associées à un objet dégénéré (De Donder et al. 1997; Cerviño 1998).

La présence d'une étoile à neutron ou trou noir, orbitant dans le vent d'une étoile de type précoce a un effet drastique sur la structure et dynamique de celui-ci (Fig.1.6). Comme observé pour les systèmes constitués d'une étoile à neutron orbitant autour d'une étoile OB, d'importantes variations photométriques (e.g., Tjemkes, Zuiderwijk, & van Paradijs 1986) et spectroscopiques (e.g., Kaper, Hammerschlag-Hensberge, & Zuiderwijk 1994) (quasi) périodiques sont attendues.

1.2.2.2 Modulation par rotation d'un vent anisotropique?

Une alternative afin de rendre compte de la variabilité périodique observée est de considérer que le vent de l'étoile WR est fortement anisotropique. Dans ce modèle, le vent est constitué de structures à grande échelle de propriétés physiques significativement différentes, et ayant une durée de vie relativement longue (typiquement plusieurs périodes de rotation stellaire). Les variations spectroscopiques ou photométriques rencontrées seraient alors induites par la

⁸Nous entendons par là, la probabilité que le système reste lié gravitationnellement après l'explosion.

rotation apparente de ces structures sur le plan du ciel, et seraient donc modulées par la période de rotation stellaire.

Ces dernières années, un nombre considérable d'études ont démontré que la variabilité spectrale des étoiles O (progénitrices des étoiles WR) pouvait fort bien être accommodée par ce modèle. Cette conclusion repose principalement sur la similitude entre le temps de récurrence moyen des variations affectant les parties en absorption des profils P Cygni présents dans le domaine UV et la vitesse de rotation projetée de l'étoile (Kaper & Henrichs 1994; Kaper et al. 1996, 1997, 1998). De plus, de fortes présomptions laissent penser que ces structures pourraient prendre naissance à la base du vent, en réponse à des perturbations photosphériques (e.g., Prinja, Massa, & Fullerton 1995; Kaper et al. 1996).

Des simulations hydrodynamiques ont démontré que de telles perturbations photosphériques peuvent effectivement fortement influer sur les propriétés d'un vent stellaire supporté par la force radiative (Cranmer & Owocki 1996). Dans ces simulations appliquées à l'étoile de type O4 If, ζ Puppis, des régions photosphériques caractérisées par un flux radiatif plus élevé ont été artificiellement réparties de façon équidistante en longitude stellaire. De façon générale, ceci a pour effet d'occasionner la formation de structures azimutalement étendues, courbées par la rotation stellaire. On remarque que le flot de particules émergeant de ces régions caractérisées par une force radiative plus importante est plus dense, et est accéléré à des vitesses moindres que le vent "ambiant". Des chocs (ainsi que des zones de raréfaction) apparaissent à l'interface entre le flot ambiant et ces structures étendues, et induisent des variations spatiales particulièrement remarquables de la profondeur optique de Sobolev (Fig.1.7). Le phénomène de pulsations non radiales du cœur de l'étoile est un candidat sérieux pour ce qui est du mécanisme à l'origine de la formation de telles structures dans le vent des étoiles OB (Fullerton, Gies, & Bolton 1996). Néanmoins, et bien que leur existence puisse être légitimement questionnée en ce qui concerne les étoiles OB et WR,

des structures magnétiques émanant de la photosphère peuvent également être considérées.⁹

1.3 Les motivations scientifiques de ce projet

L'objet principal de ce projet a été d'entreprendre un vaste programme observationnel visant à révéler quel processus (compagnon dégénéré ou vent anisotropique) opérait dans les étoiles WR apparemment isolées potentiellement candidates pour une variabilité périodique. Les principales motivations scientifiques nous ayant amené à entreprendre ce travail sont les suivantes:

- Cygnus X-3 est le seul système jusqu'alors connu que l'on soupçonne d'être constitué d'un compagnon dégénéré orbitant autour d'une étoile WR (van Kerkwijk et al. 1996). Il reste à établir si cette déficience de systèmes observés comparée aux prédictions des modèles évolutifs des systèmes binaires massifs — notamment ceux adoptant un taux élevé de survie du système lors de l'explosion de l'étoile primaire en supernova — est avérée, ou résulte simplement d'un biais observationnel. Une détermination du statut des candidats WR les plus prometteurs permettrait d'explorer plus précisément ce point, et de reconsidérer, le cas échéant, les différents processus physiques opérant lors de l'évolution des systèmes binaires massifs à transfert de masse (§1.2.2.1).
- Hormis l'intérêt que représenterait en elle-même la détection de vents globalement anisotropiques parmi la population d'étoiles WR, ceci pourrait

⁹Les simulations hydrodynamiques de Cranmer & Owocki (1996) ne prennent pas en considération la possible existence de forces magnétiques; lesdites forces pouvant notamment affecter la dynamique d'un vent supposé être dans ce travail intégralement supporté par la force radiative. En outre, ce modèle exclut implicitement toute croissance d'instabilités radiatives (§1.2.1).

également indirectement suggérer — si l'on s'en tient aux résultats des modèles hydrodynamiques de Cranmer & Owocki (1996) — que ceci est engendré par l'existence de perturbations photosphériques. Dans ce cas de figure, et bien que ceci reste fort spéculatif, des instabilités du cœur stellaire induisant des pulsations (e.g., le mécanisme ϵ),¹⁰ ou des structures magnétiques émergeant de la photosphère pourraient être invoquées.

Concernant ce dernier point, des efforts, d'une part, théoriques (e.g., Maheswaran & Cassinelli 1994) et, d'autre part, observationnels (e.g., Henrichs et al. 1998) notables ont été entrepris ces dernières années afin d'étudier l'évolution du champ magnétique fossile durant la vie de l'étoile sur la séquence principale, et plus encore durant les phases ultérieures; malheureusement, ceci avec peu de résultats réellement probants.

1.4 Choix de l'échantillon

Lorsque ce projet a été initié en août 1994, celui-ci visait principalement à lever l'ambiguïté sur la nature de l'étoile WR 6 (WN 5; EZ CMa; HD 50896), dont la nature strictement périodique des variations (selon $\mathcal{P} \approx 3.77$ jours) en spectroscopie, photométrie et polarimétrie était déjà bien établie à l'époque (e.g., Firmani et al. 1980). Cet objet constitue le prototype d'étoile WR apparemment isolée présentant des variations cycliques, et a fait l'objet des chapitres 2 et 3 présentés ci-après. Ce projet a été par la suite étendu à l'étoile WR 134 (WN 6; HD 191765) pour laquelle une variabilité périodique dans le profil des raies spectrales selon $\mathcal{P} = 2.27 \pm 0.05$ jours était soupçonnée (McCandliss et al. 1994). Notre étude a notamment permis de confirmer le bien-fondé de cette proposition. Le chapitre 4 présente les résultats concernant cet objet. Le chapitre 5 est dédié à l'étoile WR 1 (WN 5; HD 4004); la similitude des variations spectroscopiques

¹⁰Seule l'étoile WR 66 (de type WN 8) semble présenter jusqu'alors une telle particularité (Antokhin et al. 1995; Rauw et al. 1996b).

avec celles des deux objets précités nous ayant amené à l'inclure dans la discussion (Niedzielski 1996).

Enfin, des spectres de l'étoile apparemment isolée WR 136 (WN 6; HD 192163) ont été collectés lors de diverses campagnes d'observations à l'Observatoire du Mont Mégantic en 1995. WR 136 est un candidat potentiel pour une périodicité spectrale dans le domaine optique selon $\mathcal{P} \approx 4.5$ jours (Koenigsberger, Firmani, & Bisiacchi 1980; Aslanov & Cherepashchuk 1981; Anthokin & Cherepashchuk 1985). (Les variations dans le domaine UV sont discutées par St-Louis et al. 1989). Malgré ce caractère variable — et possiblement périodique — visiblement bien établi, les variations que nous observons sont de bien moindre amplitude que pour WR 1, WR 6 ou WR 134. De plus, et ceci découle éventuellement de la faible amplitude des variations spectrales observées et/ou de notre relativement pauvre échantillonnage en temps, aucune périodicité de quelque ordre que ce soit n'apparaît dans nos données. Ceci nous amène à la conclusion que l'origine de la variabilité est de nature fondamentalement différente de celle des étoiles précitées (voir Lépine, Moffat, & Henriksen 1996) ou que nous l'avons malencontreusement observé durant une phase de relativement faible “activité” (comme occasionnellement observé pour WR 6; voir chapitre 3). De futures observations avec une meilleure couverture temporelle permettraient sans doute de clarifier ce point. Un montage des spectres est présenté dans l'Appendice A.

Les caractéristiques générales de ces quatre étoiles (WR 1, WR 6, WR 134 et WR 136) sont résumées dans le Tableau 1.2.

RÉFÉRENCES

- Abbott, D. C., Bieging, J. H., Churchwell, E., & Torres, A. V. 1986, ApJ, 303, 239
- Abbott, D. C., & Conti, P. S. 1987, ARA&A, 25, 113
- Antokhin, I. I., & Cherepashchuk, A. M. 1985, Sov. Astron. Lett., 11, 355
- Antokhin, I. I., Bertrand, J.-F., Lamontagne, R., Moffat, A. F. J., & Matthews, J. M. 1995, AJ, 109, 817
- Aslanov, A. A., & Cherepashchuk, A. M. 1981, Sov. Astron. Lett., 7, 265
- Beals, C. S. 1929, MNRAS, 90, 202
- Bildsten, L., et al. 1997, ApJS, 113, 367
- Blondin, J. M. 1994, ApJ, 435, 756
- Brandt, N., & Podsiadlowski, P. 1995, MNRAS, 274, 461
- Breysacher, J. 1981, A&AS, 43, 203
- Brown, G. E. 1995, ApJ, 440, 270
- Carlberg, R. G. 1980, ApJ, 241, 1131
- Cerviño, M. 1998, Thèse de Doctorat, LAEFF-INTA
- Chu, Y.-H., Gull, T. R., Treffers, R. R., Kwitter, K. B., & Troland, T. H. 1982, ApJ, 254, 562
- Crampton, D. 1971, MNRAS, 153, 303
- Cranmer, S. R., & Owocki, S. P. 1996, ApJ, 462, 469
- Crowther, P. A., Smith, L. J., Hillier, D. J., & Schmutz, W. 1995, A&A, 293, 427
- Crowther, P. A., Smith, L. J., Willis, A. J. 1995, A&A, 304, 269

- Crowther, P. A., De Marco, O., & Barlow, M. J. 1998, MNRAS, 296, 367
- Dalton, W. W., & Sarazin, C. L. 1995, ApJ, 440, 280
- De Donder, E., Vanbeveren, D., & van Bever, J. 1997, A&A, 318, 812
- De Loore, C., de Grève, J. P., & de Cuypere, J. P. 1975, Ap&SS, 36, 219
- Drissen, L., Robert, C., Lamontagne, R., Moffat, A. F. J., St-Louis, N., van Weeren, N., & van Genderen, A. M. 1989, ApJ, 343, 426
- Eenens, P. R. J., & Williams, P. M. 1992, MNRAS, 255, 227
- Feldmeier, A. 1995, A&A, 299, 523
- Fender, R. P., Burnell, S. J. B., Waltman, E. B., Pooley, G. G., Ghigo, F. D., & Foster, R. S. 1997, MNRAS, 288, 849
- Firmani, C., Koenigsberger, G., Bisiacchi, G. F., Moffat, A. F. J., & Isserstedt, J. 1980, ApJ, 239, 607
- Fryer, C. L., Burrows, A., & Benz, W. 1998, ApJ, 496, 333
- Fullerton, A. W., Gies, D. R., & Bolton, C. T. 1996, ApJS, 103, 475
- Gonçalves, D. R., Jatenco-Pereira, V., & Opher, R. 1998, ApJ, 501, 797
- de Grève, J. P., De Loore, C., & van Dessel, E. L. 1977, Ap&SS, 53, 105
- Hamann, W.-R., Koesterke, L., & Wessolowski, U. 1995, A&A, 295, 151
- Hamann, W.-R., & Koesterke, L. 1996, in Proceedings of the 33rd Liège International Astrophysical Colloquium, ed. J.-M. Vreux et al., 491
- Hansen, B. M. S., & Phinney, E. S. 1997, MNRAS, 291, 569
- Henrichs, H. et al. 1998, in ESO Proceedings: “Cyclical Variability in Stellar Winds”, 374
- Hulse, R. A., & Taylor, J. H. 1975, ApJ, 195, L51
- Humphreys, R. M., & Davidson, K. 1994, PASP, 106, 1025
- Johnson, H. M., & Hogg, D. E. 1965, ApJ, 142, 1033

- Kaper, L., Hammerschlag-Hensberge, G., & Zuiderwijk, E. J. 1994, A&A, 289, 846
- Kaper, L., & Henrichs, H. F. 1994, ApS&S, 221, 115
- Kaper, L., Henrichs, H. F., Nichols, J. S., Snoek, L. C., Volten, H., & Zwarthoed, G. A. A. 1996, A&AS, 116, 257
- Kaper, L., et al. 1997, A&A, 327, 281
- Kaper, L., Henrichs, H. F., Nichols, J. S., & Telting, J. H. 1998, A&A, sous presse
- Koenigsberger, G., Firmani, C., & Bisiacchi, G. F. 1980, Rev. Mex. Astron. Astrof., 5, 45
- Koesterke, L., & Hamann, W.-R. 1995, A&A, 299, 503
- Langer, N., Hamann, W.-R., Lennon, M., Najarro, F., Paulydrach, A. W. A., & Puls, J. 1994, A&A, 290, 819
- Leitherer, C., Robert, C., & Drissen, L. 1992, ApJ, 401, 596
- Leitherer, C., Chapman, J. M., & Koribalski, B. 1995, ApJ, 450, 289
- Lépine, S., Moffat, A. F. J., & Henriksen, R. N. 1996, ApJ, 466, 392
- Lépine, S., & Moffat, A. F. J. 1999, ApJ, sous presse
- Lorenz, R., Mayer, P., & Drechsel, H. 1994, A&A, 291, 185
- Lorimer, D. R., Bailes, M. & Harrison, P. A. 1997, MNRAS, 289, 592
- Lucy, L. B., & Solomon, P. M. 1970, ApJ, 159, 879
- Lyne, A. G., & Lorimer, D. R. 1994, Nature, 369, 127
- McCandliss, S. R., Bohannan, B., Robert, C., & Moffat, A. F. J. 1994, Ap&SS, 221, 155
- Maeder, A., & Meynet, G. 1994, A&A, 287, 803
- Maeder, A., & Conti, P. S. 1994, ARA&A, 32, 227
- Maeder, A. 1996, in Proceedings of the 33rd Liège International Astrophysical Colloquium, ed. J.-M. Vreux et al., 39

- Maheswaran, M., & Cassinelli, J. 1994, ApJ, 421, 718
- Massey, P., & Johnson, O. 1998, ApJ, 505, 793
- Meynet, G. 1995, A&A, 298, 767
- Meynet, G., Arnould, M., Prantzos, N., & Paulus, G. 1997, A&A, 320, 460
- Moffat, A. F. J., & Robert, C. 1992, in ASP Conf. Proc. 22, Nonisotropic and Variable Outflows From Stars, ed. L. Drissen, C. Leitherer, & A. Nota (San Francisco: ASP), 203
- Moffat, A. F. J., & Shara, M. M. 1986, AJ, 92, 952
- Moffat, A. F. J., et al. 1998, A&A, 331, 949
- Niedzielski, A. 1996, in Proceedings of the 33rd Liège International Astrophysical Colloquium, ed. J. M. Vreux et al., 277
- Nota, A., Pasquali, A., Drissen, L., Leitherer, C., Robert, C., Moffat, A. F. J., & Schmutz, W. 1996, ApJS, 102, 383
- Nugis, T., & Niedzielski, A. 1995, A&A, 300, 237
- Nugis, T. 1996, in Proceedings of the 33rd Liège International Astrophysical Colloquium, ed. J.-M. Vreux et al., 575
- Nugis, T., Crowther, P. A., & Willis, A. J. 1998, A&A, 333, 956
- Paczyński, B. 1967, Acta Astron., 17, 355
- Pollock, A. M. T. 1987, ApJ, 320, 283
- Pollock, A. M. T., Haberl, F., & Corcoran, M. F. 1995, in IAU Symp. 163, Wolf-Rayet Stars: Binaries, Colliding Winds, Evolution, ed. K. A. van der Hucht & P. M. Williams (Dordrecht: Kluwer), 512
- Prinja, R. K., Massa, D., & Fullerton, A. W. 1995, ApJ, 452, L61
- Rasio, F. A., & Livio, M. 1996, ApJ, 471, 366
- Rauw, G., Vreux, J.-M., Gosset, E., Hutsemékers, D., Magain, P., & Rochowicz, K. 1996a, A&A, 306, 771

- Rauw, G., Gosset, E., Manfroid, J., Vreux, J.-M., & Claeskens, J.-F. 1996b, A&A, 306, 783
- Robert, C. 1992, Thèse de Doctorat, Univ. Montréal
- Robert, C., Moffat, A. F. J., Bastien, P., Drissen, L., & St-Louis, N. 1989, ApJ, 347, 1034
- Rochowicz, K., & Niedzielski, A. 1995, Acta Astron., 45, 307
- Schaerer, D. 1996, A&A, 309, 129
- Schmutz, W., Geballe, T. R., & Schild, H. 1996, A&A, 311, L25
- Skinner, S. L., Itoh, M., & Nagase, F. 1998, New Astronomy, 3, 37
- Smith, L. F., Shara, M. M., & Moffat, A. F. J. 1996, MNRAS, 281, 163
- St-Louis, N., Smith, L. J., Stevens, I. R., Willis, A. J., Garmany, C. D., & Conti, P. S. 1989, A&A, 226, 249
- Thorne, K. S., & Zytkow, A. 1977, ApJ, 212, 832
- Tjemkes, S. A., Zuiderwijk, E. J., & van Paradijs, J. 1986, A&A, 154, 77
- Vanbeveren, D., & Conti, P. S. 1980, A&A, 88, 230
- van den Heuvel, E. P. J., & De Loore, C. 1973, A&A, 25, 387
- van der Hucht, K. A., Hidayat, B., Admiranto, A. G., Supelli, K. R., & Doom, C. 1988, A&A, 199, 217
- van der Hucht, K. A. 1992, A&A Rev., 4, 123
- van der Hucht, K. A. 1996a, in Proceedings of the 33rd Liège International Astrophysical Colloquium, ed. J.-M. Vreux et al., 1
- van der Hucht, K. A. 1996b, ApS&S, 238, 1
- van Kerkwijk, M. H. 1993, A&A, 276, L9
- van Kerkwijk, M. H., et al. 1992, Nature, 355, 703
- van Kerkwijk, M. H., Geballe, T. R., King, D. L., van der Klis, M., & van Paradijs, J. 1996, A&A, 314, 521

Willis, A. J., & Stevens, I. R. 1996, A&A, 310, 577

Willis, A. J., & Crowther, P. A. 1996, in Proceedings of the 33rd Liège International Astrophysical Colloquium, ed. J.-M. Vreux et al., 109

TABLEAU 1.1. Critères de classification spectroscopique des étoiles WR (d'après van der Hucht 1996a)^a

Etoiles WN	Premier critère	Autres critères
WN 2	N V faible ou absente	He II intense
WN 2.5	N V présente, N IV absente	
WN 3	N IV ≪ N V, N III faible ou absente	
WN 4	N IV ≈ N V, N III faible ou absente	
WN 4.5	N IV ≥ N V, N III faible ou absente	
WN 5	N III ≈ N IV ≈ N V	
WN 6	N III ≈ N IV, N V présente quoique faible	
WN 7	N III ≥ N IV, N III ≤ He II λ4686	He I faible P Cyg
WN 8	N III > N IV, N III ≈ He II λ4686	He I intense P Cyg
WN 9	N III ≥ N II, N IV absente	He I P Cyg
WN 10	N III ≈ N II	Raies de Balmer, He I P Cyg
WN 11	N II ≈ He II, N III faible ou absente	Raies de Balmer, He I P Cyg
<hr/>		
Etoiles WC		
WC 4	C IV intense, C II faible ou absente	O V modérée
WC 5	C III ≪ C IV	C III ≤ O V
WC 6	C III ≪ C IV	C III ≥ O V
WC 7	C III ≤ C IV	C III > O V
WC 8	C III ≥ C IV	C II absente, O V faible ou absente
WC 9	C III ≥ C IV	C II présente, O V faible ou absente
<hr/>		
Etoiles WO		
WO 1	O VI intense, O IV absente	C IV ≤ O V, C III absente
WO 2	O VI intense, O IV absente	C IV ≥ O V, C III absente
WO 3	O VI ≥ O IV	C IV > O V, C III absente
WO 4	O VI ≈ O IV	C IV > O V, C III absente
WO 5	O IV ≥ O VI	C IV > O V, C III absente

^a Les raies d'émission suivantes sont utilisées à des fins de classification:

- Type WN: N II λ3995, N III λλ4634, 4641, N III λ5314, N IV λλ3479, 3484, N IV λ4058, N V λ4603, N V λ4619 et N V λλ4933, 4944.
- Type WC: C III λ5696, C III/C IV λ4650, C IV λλ5801, 5812 et O V λλ5572, 5598.
- Type WO: C IV λλ5801, 5812, O IV λ3400, O V λλ5572, 5598 et O VI λλ3811, 3834.

TABLEAU 1.2. Caractéristiques générales des étoiles WR 1, WR 6, WR 134 et WR 136

	Type	Nébuleuse	α (2000)	δ (2000)	v	D (kpc)	z (pc) ^a	$(v_t)_{pec}$ (km s^{-1}) ^b
		(1)				(2)	(2)	(2)
WR 1	HD 4004	WN 5	—	0 ^h 43 ^m 28 ^s .4	64° 45' 44"	10.5	2.6	+ 87 33.1 ± 29.3
WR 6	HD 50896	WN 5	S 308	6 ^h 54 ^m 13 ^s .0	- 23° 55' 42"	6.9	1.6	- 273 42.1 ± 15.9
WR 134	HD 191765	WN 6	ANON MR100	20 ^h 10 ^m 14 ^s .1	36° 10' 36"	8.2	2.1	+ 56 40.0 ± 16.8
WR 136	HD 192163	WN 6	NGC 6888	20 ^h 12 ^m 06 ^s .5	38° 21' 18"	7.7	1.8	+ 77 40.0 ± 14.8

	$T_{2/3}$ (kK) ^c	$R_{2/3}$ (R_\odot) ^c	$\log L_*$ (L_\odot)	M_* (M_\odot)	v_∞ (km s^{-1})	\dot{M} ($10^{-5} M_\odot \text{ an}^{-1}$)	$\eta = \dot{M} v_\infty / (L/c)$	H/He ^d
	(3)	(3)	(3)	(3)	(4)	(5)		(6)
WR 1	40.0	3.0	5.0	9.1	2135	2.40	25.1	0.07:
WR 6	41.0	3.0	5.2	11.8	1915	1.90	11.2	0.2:
WR 134	39.4	2.8	5.2	11.1	1955	4.55	27.5	0.2:
WR 136	38.5	1.9	5.4	14.0	1705	6.25	20.8	0.54

	L_X ($10^{32} \text{ ergs.s}^{-1}$)		
	[0.2-2.4] keV	[0.2-4.0] keV	[0.5-10.0] keV
	(7)	(8)	(9)
WR 1	7.07 ± 2.85	—	—
WR 6	2.07 ± 0.10	6.2 ± 0.5	≈ 7
WR 134	0.46 ± 0.22	4.6 ± 1.6	—
WR 136	0.19 ± 0.08	0.6 ± 0.6	—

Références. — (1) WR 6: Chu et al. (1982) — WR 134: Crampton (1971) — WR 136: Johnson & Hogg (1965); (2) Moffat et al. (1998); (3) Hamann, Koesterke, & Wesselowski (1995); (4) Rochowicz & Niedzielski (1995); (5) Nugis, Crowther, & Willis (1998); (6) Nugis & Niedzielski (1995); (7) Pollock, Haberl, & Corcoran (1995); (8) Pollock (1987); (9) Skinner, Itoh, & Nagase (1998).

^a Distance perpendiculairement au plan galactique.

^b Vitesse tangentielle particulière après soustraction du mouvement autour du Soleil et de la rotation galactique.

^c $T_{2/3}$ réfère à la température effective régnant à un rayon $R_{2/3}$, où la profondeur optique de Rosseland, τ_R , est de 2/3.

^d Rapport d'abondance H/He par nombre.

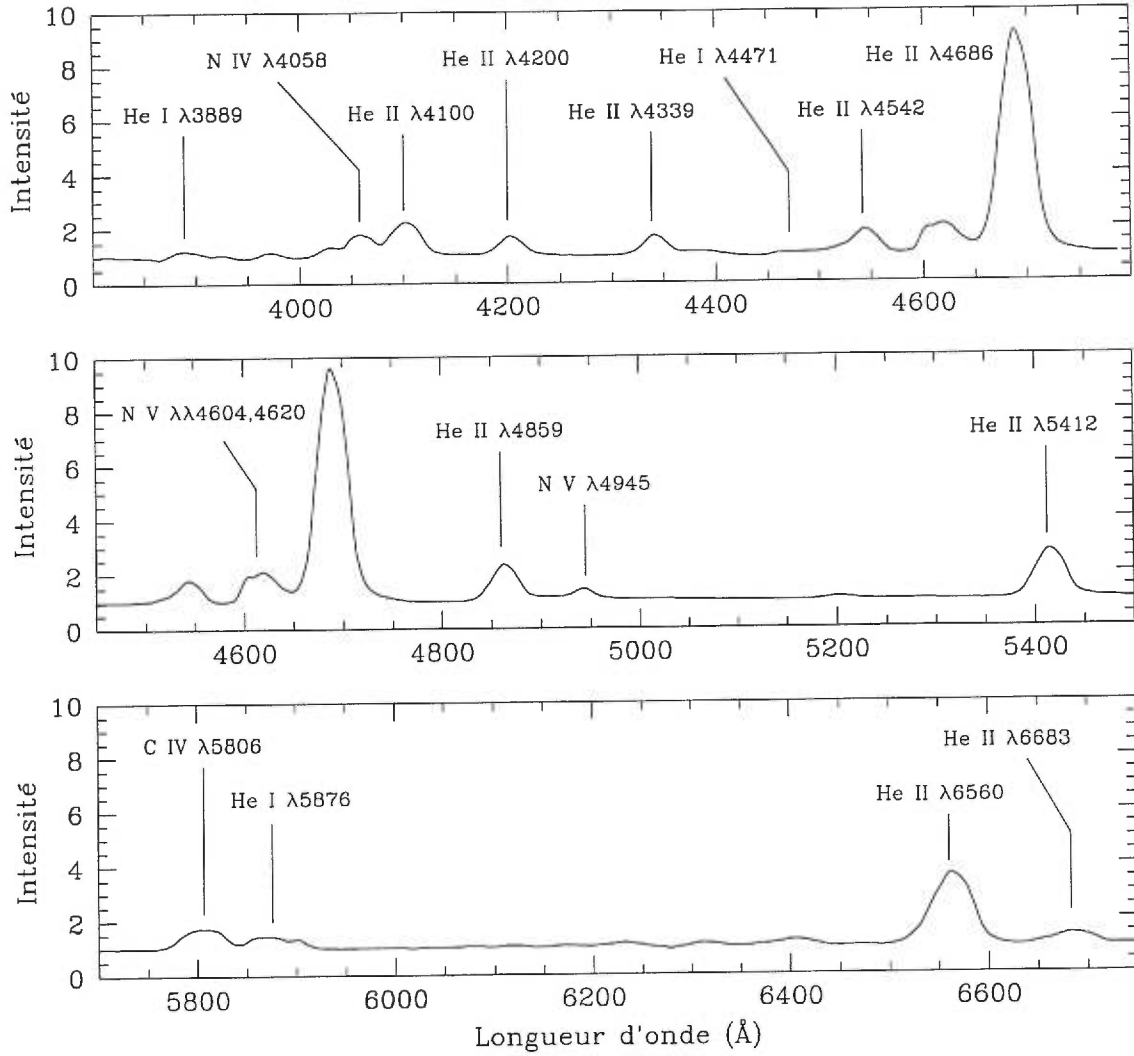


FIGURE 1.1. Spectre de l'étoile de type WN 5, WR 6, pour le domaine spectral 3800-6750 Å. Le continuum stellaire a été fixé à l'unité. Les principales raies spectrales sont identifiées par leur longueur d'onde dans le référentiel du laboratoire.

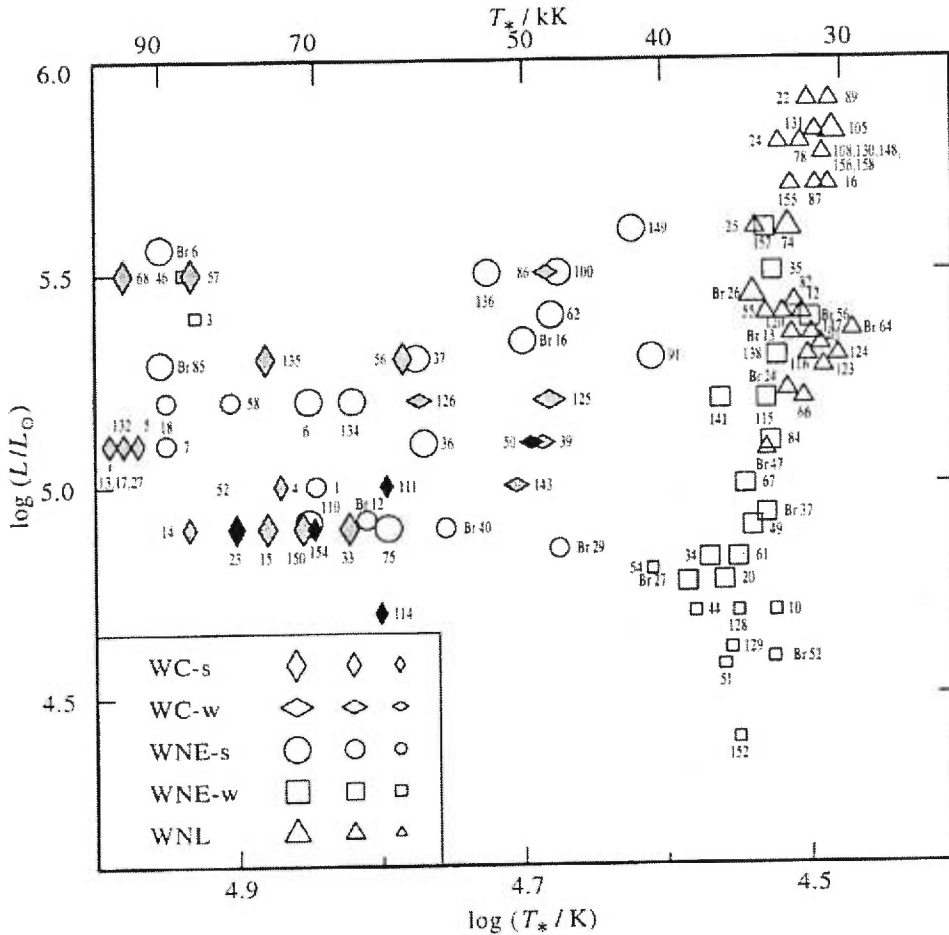


FIGURE 1.2. Position des étoiles WR dans le diagramme HR selon le modèle atmosphérique de Koesterke & Hamann (1995). T_* réfère à la température effective à un rayon où $\tau_R \approx 20$, et est donc notablement supérieure aux valeurs de $T_{2/3}$ tabulées dans le Tableau 1.2. Les étoiles WR sont identifiées par leur numéro usuel (van der Hucht et al. 1988; Breysacher 1981). Les étoiles WC dont le taux de confiance dans la position sur cette figure est élevé ou faible, sont respectivement présentées en symboles pleins ou hachurés. La taille des symboles est proportionnelle au taux de perte de masse exprimé en $\log [\dot{M} (\mathrm{M}_\odot/\mathrm{an})]$: $\gtrsim -4.2$ (grands symboles); $\lesssim -4.8$ (petits symboles) ou intermédiaire (tailles moyennes). Les symboles -w et -s indiquent si l'étoile présente des raies faibles ou intenses.

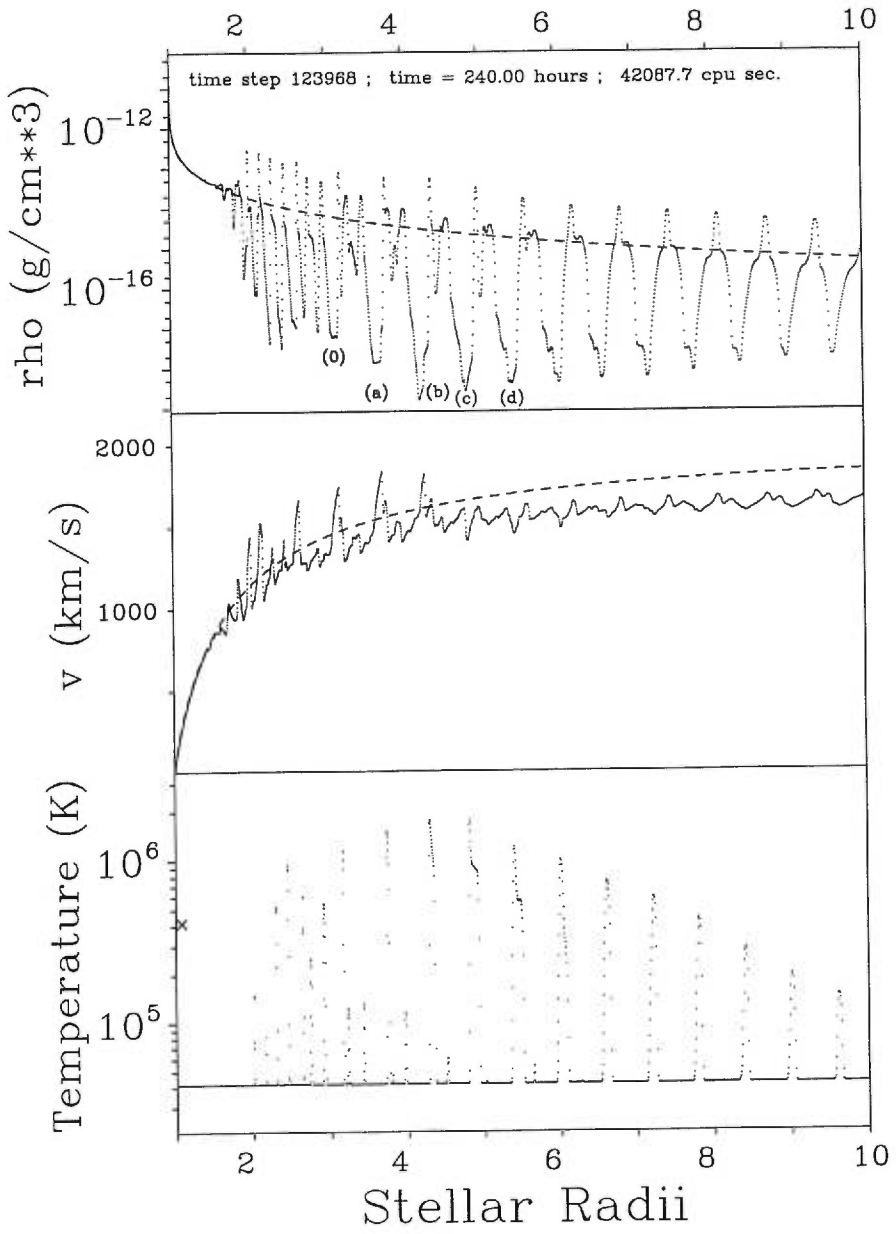


FIGURE 1.3. Illustration de la structure d'un vent stellaire (en l'occurrence, le modèle a adopté les paramètres de l'étoile O4 If, ζ Puppis) sous l'action d'ondes acoustiques photosphériques de période 5000 s et d'amplitude 1 %. La densité, vitesse et température du vent stellaire sont décrites en fonction de la distance à l'étoile. La ligne pointillée présente le résultat du modèle sans perturbations. D'après Feldmeier (1995).

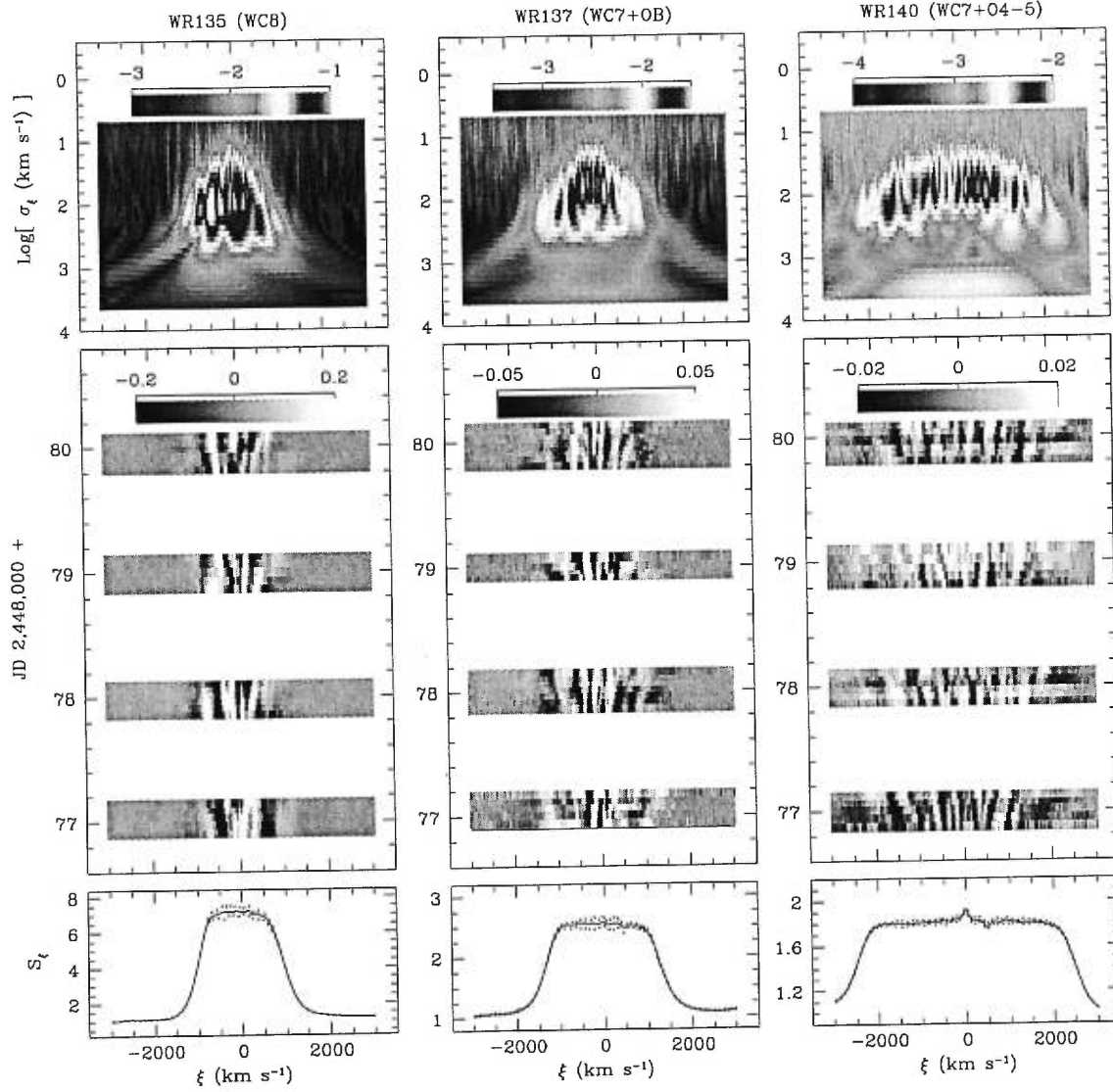


FIGURE 1.4. Illustration de la propagation stochastique de petits sous-pics d'émission superposés sur la raie C III $\lambda 5696$ des étoiles WR 135 (WC 8), WR 137 (WC 7 + OB) et WR 140 (WC 7 + O4-5). Chaque profil individuel, auquel a été soustrait le profil moyen, est arrangé en fonction du jour Julien d'observation. La partie supérieure de cette figure présente les résultats d'une analyse en ondelettes; pour de plus amples détails, voir Lépine & Moffat (1999).

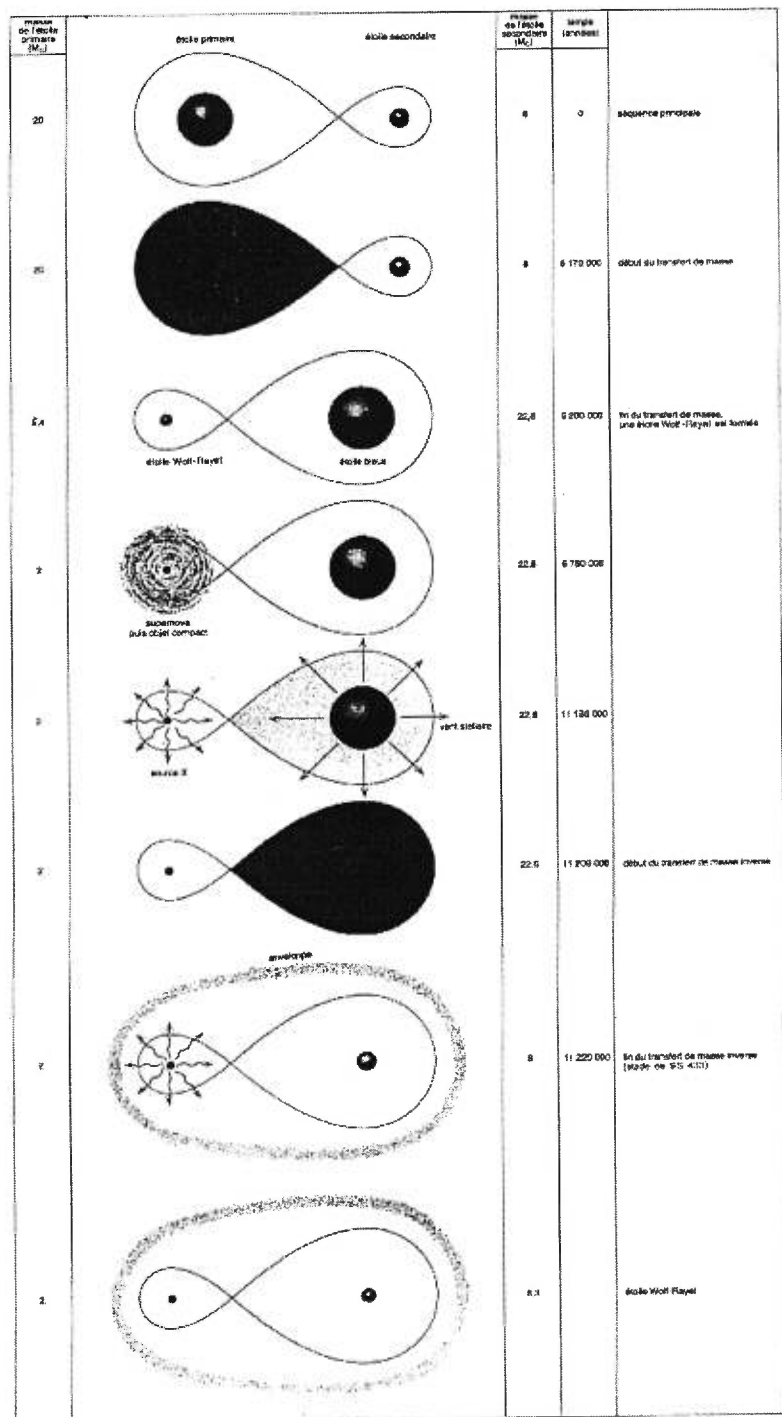


FIGURE 1.5. Evolution d'un système binaire massif rapproché. Ce schéma évolutif, où la première phase de transfert de masse intervient lors du brûlage en couche de l'hydrogène de l'étoile primaire, est souvent référencé dans la littérature au "cas B". Les masses initiales des étoiles sont de 20 et $8 M_{\odot}$. Adapté de De Loore, de Grève, & de Cuyper (1975).

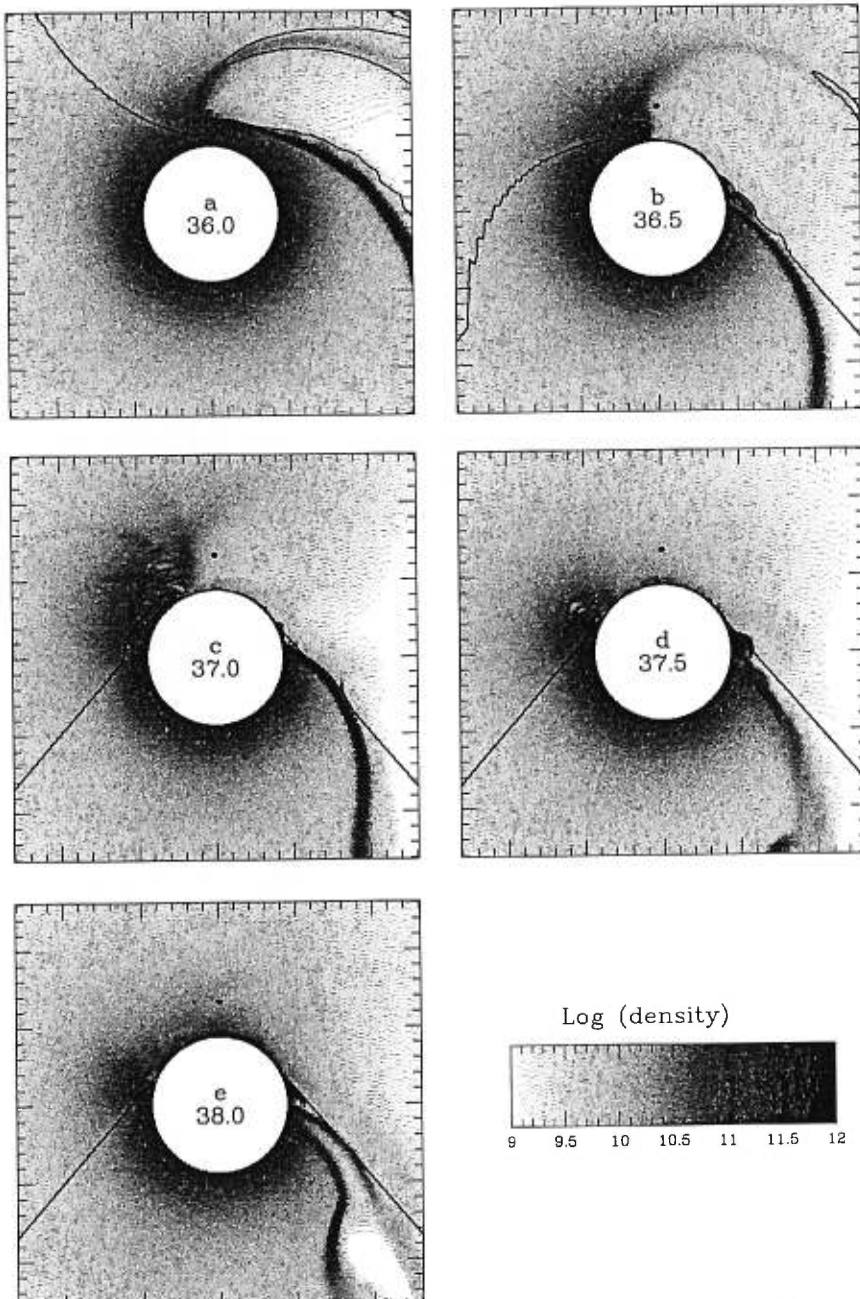


FIGURE 1.6. Structure du vent d'une étoile de type précoce en présence d'un compagnon dégénéré (en l'occurrence une étoile à neutron) accrétant le flux stellaire. Les paramètres utilisés dans ces simulations hydrodynamiques sont ceux du système Cen X-3. Les différentes teintes de gris sont proportionnelles à la densité du vent stellaire. Chaque encadré présente les résultats des simulations pour différentes valeurs de $\log L_X$ (exprimées en ergs s^{-1}). La source de rayons-X est identifiée par un point noir. La ligne continue marque la région où la dynamique du vent est fortement altérée. La révolution orbitale s'opère dans le sens inverse des aiguilles d'une montre. D'après Blondin (1994).

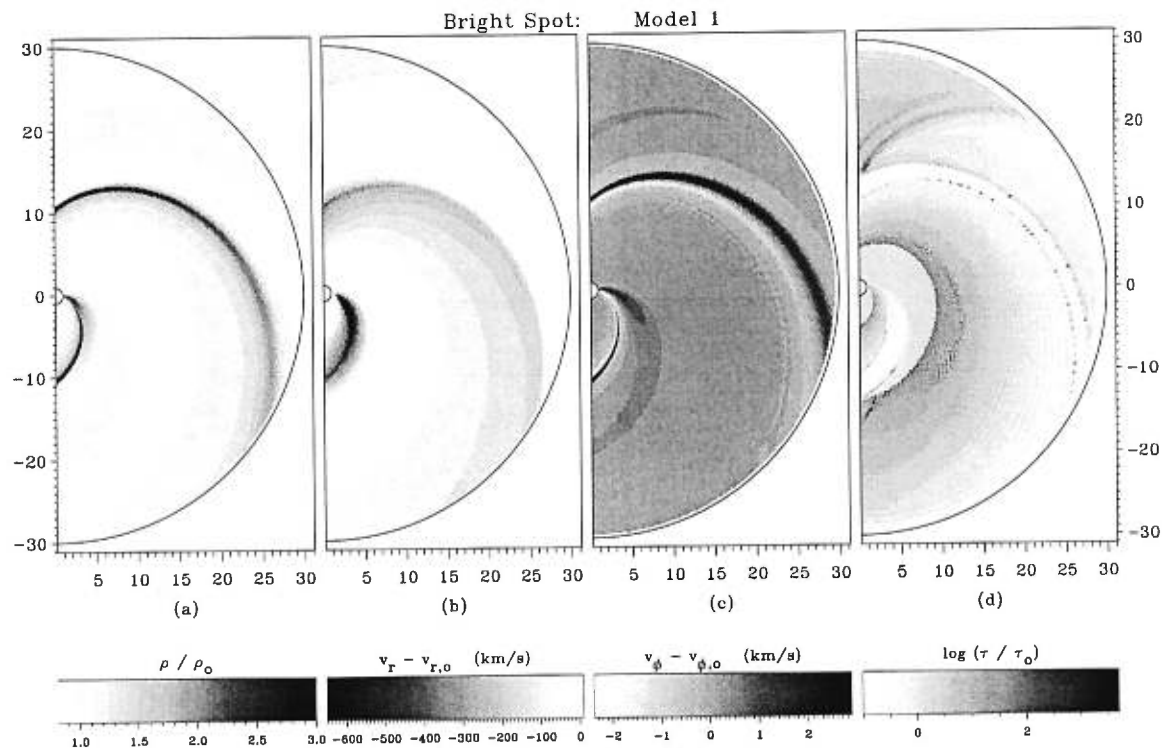


FIGURE 1.7. Structure en densité (ρ), vitesse radiale (v_r), vitesse azimutale (v_ϕ) et profondeur optique de Sobolev (τ) d'un vent stellaire supporté par la force radiative, après adjonction artificielle de 2 régions photosphériques diamétralement opposées caractérisées par un flux radiatif plus important. ρ_0 , $v_{r,0}$, $v_{\phi,0}$ et τ_0 : valeurs que prennent ces quantités en l'absence de perturbations. Les paramètres utilisés dans ces simulations hydrodynamiques sont ceux de l'étoile ζ Puppis. D'après Cranmer & Owocki (1996).

CHAPITRE 2

OPTICAL SPECTROSCOPY OF EZ CANIS MAJORIS: INDICATION FOR LARGE-SCALE STRUCTURES IN A WOLF-RAYET WIND

The Astrophysical Journal, **482**, 470 (1997)

OPTICAL SPECTROSCOPY OF EZ CANIS MAJORIS: INDICATION FOR LARGE-SCALE STRUCTURES IN A WOLF-RAYET WIND

Thierry Morel,^{1,2} Nicole St-Louis,¹ and Sergey V. Marchenko^{1,2,3}

Received 1996 August 19; accepted 1997 January 9

Article submitted to the Astrophysical Journal main section.

¹ Département de Physique, Université de Montréal, C.P. 6128, Succ. Centre-Ville, Montréal, Québec, Canada, H3C 3J7; and Observatoire du Mont Mégantic.

² Visiting Astronomer, University of Toronto Southern Observatory, Las Campanas, Chile.

³ Visiting Astronomer, Cerro Tololo Inter-American Observatory, National Optical Astronomy Observatories, operated by the Association of Universities for Research in Astronomy, Inc., under cooperative agreement with the National Science Foundation.

ABSTRACT

We have carried out optical spectroscopy of the Wolf-Rayet star EZ CMa during 20 consecutive nights in 1995 January in support of the *IUE* Mega-project. In parallel with this optical spectroscopy, we also monitored EZ CMa using narrowband photometry. The light curve was found to be remarkably stable when folded with the $P = 3.77$ day period, and it had a peak-to-valley amplitude of 0.1 mag.

The P Cygni absorption components of He I $\lambda 3889$ and He I $\lambda 5876$ display a similar global pattern of variability as was found for the simultaneously acquired UV profiles. The strengthening of the P Cygni absorption component of these transitions is associated with the maximum of the continuum flux. Conversely, the absorption trough of N V $\lambda 4604$ gradually disappears as the star brightens. Although the emission parts of the lines are variable at different levels, they all show the same pattern of variability, which consists of phase-dependent shifts of extra emission components superposed on the profiles.

A strong correlation is found between the continuum-light level and the equivalent width of most transitions. The line skewness and the full-width at half-maximum show a daily recurrence timescale, reflecting the light curve changes. We have addressed in a rigorous statistical way the significance of the variations by calculating the “temporal variance spectrum”. For any given line, we found enhanced variability at some velocities, although the whole profile displays a statistically significant level of variability.

Arguments against a compact companion as the cause of the observed periodic variability are presented. Instead, our observations strongly support the suggestion in the *IUE* Mega analysis that the atypical level of variability results from the rotation of a structured wind. We propose that the wind variability of EZ CMa is triggered by photospheric activity, or that the wind is controlled by

a large-scale magnetic field.

Subject headings: stars: individual (*EZ Canis Majoris*) — stars: mass loss — stars: Wolf-Rayet — ultraviolet: stars

2.1 Introduction

With the advent of modern detectors and the launch of various space observatories, the observations of early-type stars have increased dramatically, both in quantity and quality. Spectroscopic observations of such stars on a sufficiently long temporal baseline often reveal a high level of spectral variability. In fact, this phenomenon is so common among OB stars, that spectral variability is now widely recognized as one of their fundamental properties.

Intensive spectroscopic monitoring is therefore a powerful tool to collect fundamental information about the physical processes operating in their envelope and to derive the basic properties of the star itself (e.g., Henrichs 1995; Fullerton, Gies, & Bolton 1996). Wolf-Rayet (WR) stars are no exception, displaying time-dependent spectroscopic variations, frequently accompanied by changes in photometry and polarimetry. The line-profile variations (LPVs) can be schematically subdivided into two types: (a) small, stochastic emission peaks of various sizes moving across the optical emission lines away from the line center, which are often attributed to local inhomogeneities in the wind carried out by the global stellar outflow (Moffat et al. 1988; Robert 1992); (b) large-scale spectral variations simultaneously affecting a significant part of the profile (e.g., McCandliss et al. 1994).

A periodic pattern in the line-profile and photometric variability has generally been found for the stars showing the latter type of behavior. Thereby, binary modulation was naturally suggested as the cause of the observed variability, with the secondary being a compact object (neutron star or black hole; hereafter *c*). Indeed, these objects are single-lined, which precludes the presence of a bright OB companion. Furthermore, the existence of WR + *c* systems is predicted by the general theory of massive close binary evolution (van den Heuvel & de Loore 1973; Tutukov & Yungelson 1973; Vanbeveren 1991), although the theoretically

expected number is very low (De Donder, Vanbeveren, & van Bever 1997). On the other hand, since the timescale of the variability is comparable with the expected rotation period (a few days), rotational modulation of an inhomogeneous wind has also been suggested to account for the periodic LPVs.

The interest in these single-line WR stars showing periodic variations is twofold: (a) an observational constraint for the evolutionary model of massive close binaries comes from the paucity of WR + c systems discovered so far, the only unmistakably confirmed one being the strong X-ray emitter Cygnus X-3 (van Kerkwijk et al. 1996). Therefore, the identification of additional systems would be of considerable interest; (b) rotational modulation persisting during several cycles would be a strong indication of the existence of a “wind-photosphere connection” in the form of (non)radial pulsations or magnetic fields controlling the wind morphology and dynamics. Because time-resolved, high-quality observations are required, the search for WR + c systems is severely biased toward the apparently brightest objects and is therefore far from complete (see Cherepashchuk & Aslanov 1984 for the latest review).

Among the single-lined WR stars with periodic variations, the WN 5 star EZ CMa (WR 6; HD 50896) exhibits the most striking variations. Along with its firmly established periodic nature ($\mathcal{P} = 3.77$ days), it is usually considered as the most promising WR + c candidate. As a suspected high-mass X-ray binary (HMXRB), EZ CMa was monitored in the soft X-ray spectral domain ($\lesssim 5$ keV) by the *Einstein* and *ROSAT* observatories. Despite the paucity of the data, the X-ray flux was found to be variable on different timescales: from an hour (White & Long 1986), to a day (Willis et al. 1994). However, the nature of this X-ray variability is far from being completely clarified. In particular, Pollock (1989) criticized the statistical significance of the proposed hourly changes. Furthermore, whereas the *Einstein* observations showed a significant phase-modulation (Moffat et al. 1982), this is not apparent in the recent *ROSAT* data (Willis et al. 1994).

Presumably, the observations are subject to strong epoch-dependency, just as was found for the optical light curve and UV spectroscopic changes (see below).

The first visual photometric variability of this object was reported by Ross (1961). Subsequent observations established the periodic nature of the light variations, as well as its incoherence over several cycles (Firmani et al. 1980), a result that has been confirmed by all recent investigations (Duijsens et al. 1996, and references therein). Despite the various shapes of the light curves, the variations (if any) are always phased with the 3.77 day period. Likewise, the polarimetric curves share this epoch-dependency (Robert et al. 1992).

EZ CMa was chosen as an *IUE* target on several occasions. The first UV-line-profile variability was reported by Willis et al. (1986). During the first long-term monitoring of this star (seven consecutive days in 1983), Willis et al. (1989) noticed a reduced level of variability compared with some archival spectra, as well as smaller continuum-flux variations. The changes occurred mainly in the extreme blue edge of the P Cygni absorption troughs, i.e., at or above the terminal velocity of the unperturbed wind. In an attempt to reveal the presence of a compact companion, the authors searched for evidence of the so-called “Hatchett-McCray effect” (Hatchett & McCray 1977). Basically, the presence of a compact companion orbiting within the dense stellar wind will result in a drastic increase of the ionization state of the material in its vicinity. This will lead to the formation of an X-ray photoionization zone, where the radiative force will be quenched (Blondin 1994). Since the wind of WR stars is assumed to be radiatively driven, the dynamics in this region will be seriously altered. This can lead to a number of directly observed effects: (a) reduction of the wind terminal velocity during the passage of the compact companion in front of the WR component; (b) phase-dependent variations of the emission part of the profiles caused by the orbital revolution of the wind cavity around the WR star. The Hatchett-McCray effect has been observed in some HMXRBs (e.g., Kaper, Hammerschlag-Hensberge,

& van Loon 1993). Since this search was inconclusive for EZ CMa (albeit a tentative phase-dependent variability with a 1 day timescale was reported), the observed UV changes were ascribed to be intrinsic to the WR wind. A follow-up study based on a 6 day run in 1988 (St-Louis et al. 1993) showed a somewhat higher degree of activity, but nevertheless confirmed the conclusions of Willis et al. (1989), notably the existence of the 1 day recurrence timescale. Because the variations in the absorption and emission components of the major UV P Cygni profiles were not correlated, the linear extension of the material causing the changes was estimated to be of the order of the WR core radius. A different pattern of variability was observed in 1992 (St-Louis 1994; St-Louis et al. 1997). The phase-dependent appearance of an excess in P Cygni absorption at high-negative velocities ($v \gtrsim 2000 \text{ km s}^{-1}$) was accompanied by a reduced absorption at intermediate negative velocities ($1800 \gtrsim v \gtrsim 1000 \text{ km s}^{-1}$). This can also be seen in the 1995 UV observations (St-Louis et al. 1995, hereafter WRMEGA). The variability was interpreted as a rotationally induced crossing in the line of sight of faster and hotter regions of the wind.

The most comprehensive optical spectroscopic study secured so far (Firmani et al. 1980) provided the first evidence for the periodic nature of the LPVs. The observed phase-dependent variations were attributed to the disturbance of the stellar wind by an orbiting companion. The very small mass-function derived from the radial velocity perturbations [$f(M) \approx 0.015 M_{\odot}$], combined with a polarization estimation of the orbital inclination (McLean et al. 1979), led to a mass of the secondary typical of a neutron star: $1.32 \pm 0.15 M_{\odot}$. Ebbets (1979) also favored the binary hypothesis with the same conclusion regarding the nature of the secondary. This view was later supported by the detection of high-velocity interstellar lines in the high-resolution spectra of EZ CMa, which were interpreted as revealing the existence of an old supernova remnant in the line of sight of this WR star (Howarth & Phillips 1986; Nichols-Bohlin & Fesen 1986). However, the possibility of a direct association is not proven yet, mainly owing to the

controversial distance to EZ CMa (Howarth & Phillips 1986; Nichols & Fesen 1994). Thereafter, a growing number of studies have questioned the existence of a compact companion, since the radial velocity variations that are supposed to describe a hypothetical binary motion can easily be introduced by large-scale LPVs (e.g., Robert et al. 1992; St-Louis et al. 1993). An alternative approach was proposed by Underhill & Yang (1991), who interpreted the observed LPVs as a rotational modulation of a ringlike disk connected to the central star by ever-changing filaments.

Despite the wealth of optical spectroscopic data already collected, an investigation based on an intensive time-resolved data set taking advantage of the capacities of modern detectors was still lacking. The *IUE* MEGA campaign (Massa et al. 1995) provided a unique opportunity to carry out such a study, with 16 contiguous days of observation of three early-type stars: ζ Pup (O4 If[n]), HD 64760 (B0.5 Ib) and EZ CMa. For the latter, preliminary results were presented in WRMEGA. Simultaneously with this campaign, we have obtained an extensive set of optical spectroscopy and photometry, which will be discussed in this article.

The data acquisition and the reduction procedure will be presented in §2.2; §2.3 will summarize our photometric (§2.3.1) and spectroscopic results (§2.3.2). The possible duplicity of EZ CMa will be discussed in §2.4.1, while §2.4.2 will be devoted to an interpretation of the observed variability as rotationally induced. We will discuss the possible existence of localized or large-scale magnetic structures in §2.4.3. Finally, our main conclusions will be given in §2.5.

2.2 Observations and Reduction Procedure

2.2.1 Photometry

Our photometric data were obtained with the one-channel photometer of the 60 cm Lowell telescope at CTIO (S-20 phototube and cold box 57). In an attempt to follow any possible color variations in the continuum of EZ CMa, two narrowband filters were chosen: one with central wavelength $\lambda_0 = 3650 \text{ \AA}$ and full width at half-maximum FWHM = 100 Å (u filter), and the other with $\lambda_0 = 5140 \text{ \AA}$ and FWHM = 90 Å (v filter), the latter being the same as used during the three-month monitoring campaign in 1993 (Antokhin et al. 1994). Note that these filters are very close to the continuum (u, v) WR filters used by Smith (1968). We used “traditional” comparison stars, c1 = HD 50853 and c2 = HD 50711, in the following sequence of 15 s integrations through an 18'' or 25'' diaphragm: sky(u, v), c2(u, v), c1(u, v), WR(u, v), c1(u, v), WR(u, v), c1(u, v), c2(u, v), sky(u, v). The data were reduced using the extinction coefficients derived from observations of all available comparison stars: we have followed three additional objects, HD 5980, HD 64760, and HD 66811. We applied two sets of extinction coefficients: $k_u = 0.466$, $k_v = 0.137$ before 26/27 1995 January, and $k_u = 0.565$, $k_v = 0.203$ afterward. The journal of observations (Table 2.1) gives the heliocentric Julian dates (HJD), the phases, and the u and v magnitudes. The phases, as everywhere in this paper, were calculated according to the ephemeris of Lamontagne, Moffat & Lamarre (1986). The overall (c2 – c1) accuracy was: $\sigma(u) = 0.0049$ mag and $\sigma(v) = 0.0039$ mag.

In an attempt to confirm the short period, $\mathcal{P} \approx 0.11$ s, announced as a result of five nights of rapid photometry of EZ CMa in 1993 (Marchenko et al. 1994), we have obtained a significantly larger data set, comprising observations 1-2 times per night in the broadband V filter, with 0.02 s time resolution. Every ≈ 10 minute record of EZ CMa was immediately followed by the same length

record of the comparison star c1 to complete one cycle of fast photometry. In the “fast photometry” column of Table 2.1 the number of complete cycles is listed for each night. For a given night, two cycles were separated by a 2-4 hr interval.

2.2.2 Spectroscopy

Spectroscopic observations were secured in the interval 1995 January 10-29 at the 60 cm Helen Sawyer-Hogg telescope at the Las Campanas Observatory in Chile. The spectrograph was equipped with a Photometrics PM 512 chip.

In order to obtain a good compromise between resolution and spectral coverage, we selected the 600 lines mm⁻¹ diffraction grating blazed at 4700 Å in the first order, which gives 2.2 Å pixel⁻¹ reciprocal dispersion. We observed EZ CMa over a wide spectral domain in order to characterize the LPVs for lines with a broad range of excitation potential, i.e., to probe different line-formation regions. Accordingly, our spectra cover the following regions: 3700-4800 Å, 4450-5550 Å, and 5650-6750 Å. Three consecutive exposures (with unit exposure time ranging from about 50 s in the blue to 120 s in the yellow region) were combined to improve the signal-to-noise ratio, which is typically around 100 in the continuum of the net spectrum. We eliminated any spectrum showing a deviation obviously attributable to an inadequate rectification procedure or saturated exposures. This resulted in 85, 99 and 62 spectra for each spectral domain, respectively. We did not find any significant short-term (below 5 minutes) variability while grouping the exposures.

The standard reduction procedure (i.e., bias subtraction, flat-fielding, removal of cosmic rays, extraction of the spectra and wavelength calibration) was carried out using **IRAF**¹ reduction packages. The calibration lamp spectra

¹**IRAF** is distributed by the National Optical Astronomy Observatories, operated by the Association of Universities for Research in Astronomy, Inc., under cooperative agreement with the National Science Foundation.

were taken systematically before the star exposure in order to avoid any flexure problems. We used an argon lamp for the first two spectral regions and a neon lamp for the last one. Since we intended to characterize changes in the line profiles, which are often of the order of a few percent of the continuum level, the rectification of the spectra was one of the most crucial steps in the reduction procedure. We have carefully selected five to seven fixed wavelength continuum regions for each spectral domain, with an extent varying from 4 to 112 Å, and we have fitted the continuum with a Legendre polynomial of the fifth or sixth order.

We used the light curve to eliminate the variability induced by the continuum-light modulation in the following way: first, we binned the light curve to 0.01 phase resolution. Then, we multiplied all the rectified spectra in accordance to their phase ϕ by $10^{-0.4[m_v(\phi) - m_v(\min)]}$, where $m_v(\phi)$ and $m_v(\min)$ are the magnitudes for a given phase ϕ and at minimum light, respectively. The constant continuum level was subtracted before, and added back in after this procedure. Therefore, the remaining variations should be entirely attributable to the emission lines.

2.3 Results

2.3.1 Photometry

In Figure 2.1, we plot the light curve of EZ CMa folded with the $P = 3.77$ day period. Because of the extremely small amplitude of the $u - v$ color variations, we plot only the v -filter data (*filled dots*). The light curve covers five complete cycles. Its small (for a fixed phase) scatter indicates that, during our observations, the 3.77 day periodicity completely dominated the shape of the light curve. Open symbols (*middle panel*) denote the value $2.5 \times \log [F(\lambda_1) + F(\lambda_2)]$, where the wavelengths $\lambda_1 = (1689 \pm 9)$ Å and $\lambda_2 = (1860 \pm 40)$ Å are continuum-dominated regions in the *IUE* spectrum of EZ CMa. This far-ultraviolet light curve was shifted by a constant value to match the minimum (phases 0.5–0.8) in v light. It

is clear that the amplitude increases toward the far ultraviolet. This, along with the fact that the P Cygni absorption component of N V $\lambda 4604$ disappears at $\phi = 0.1\text{--}0.5$ (§2.3.2.2), strongly suggests that the temperature at the base of the wind of EZ CMa increases during maximum light.

Inspired by the positive detection of a short, $\mathcal{P} \approx 0.11$ s ($f = 9.048$ Hz), period during V -band photometric observations in 1993 (Marchenko et al. 1994), which could be related to the rapid rotation of a neutron star, we performed a more systematic search in 1995. All the ≈ 10 minute records (around 3×10^4 data bins, 0.02 s each) of EZ CMa and the comparison star were Fourier-transformed to create a mean power spectrum (MPS) of the whole run: a total of 23 records for EZ CMa and 21 records of the comparison star. The MPS of EZ CMa appeared to be featureless when applying the 1 % or 0.5 % detectability thresholds (Bendat & Piersol 1986; Marchenko et al. 1994).

Because the orbital parameters of the hypothetical neutron star are not known, any comprehensive search for periodic signals must allow for the Doppler shifts induced by orbital revolution. As a first approximation, we assumed a circular orbit. Hence, the search for periodicities was performed by varying K (the radial velocity amplitude) and the “zero” orbital phase of the compact companion (the moment when the companion passes in front of the WR star). We have chosen the grid: $K = 100\text{--}600$ km s $^{-1}$ with 12.5 km s $^{-1}$ steps, and orbital phases $\phi = 0^\circ\text{--}360^\circ$ with $20^\circ\text{--}15^\circ\text{--}10^\circ$ steps, the larger step applies to the smaller K .

The same procedure was applied to the 1993 data (nine records of EZ CMa). Note that this processing, which is different from the one used in Marchenko et al. (1994), might slightly change the previously found frequencies (i.e., $f = 9.048$ Hz). There are some encouraging similarities between the 1993 and 1995 data sets. We found significant signals at:

- $f = 1.094$ Hz (1993) and $f = 1.096$ Hz (1995) for $K = 300$ km s $^{-1}$;

- $f = 1.490 \text{ Hz}$ (1993) and $f = 1.487 \text{ Hz}$ (1995) for $K = 412 \text{ km s}^{-1}$;
- $f = 1.714 \text{ Hz}$ (1993) and $f = 1.699 \text{ Hz}$ (1995) for $K = 588 \text{ km s}^{-1}$;
- $f = 1.782 \text{ Hz}$ (1993) and $f = 1.796 \text{ Hz}$ (1995) for $K = 450 \text{ km s}^{-1}$;
- $f = 2.649 \text{ Hz}$ (1993) and $f = 2.650 \text{ Hz}$ (1995) for $K = 450 \text{ km s}^{-1}$;
- $f = 9.036 \text{ Hz}$ (1993) and $f = 9.038 \text{ Hz}$ (1995) for $K = 450 \text{ km s}^{-1}$.

However, practically all features in the combined spectrum are generated by the individual power spectrum of the record obtained at HJD 2,449,747.794 under unfavorable weather conditions. When it is removed from the 1995 data set, the combination of the remaining 22 power spectra produces a practically featureless MPS. This casts serious doubt on the significance of any 1993-1995 similarities.

2.3.2 Spectroscopy

2.3.2.1 The Emission-line Variability

The Morphological Behavior of the Spectral Lines The high degree of activity observed in optical photometry and in the UV spectra (WRMEGA) is also reflected by our optical data set. The emission lines demonstrate a remarkable level of variability on an hourly timescale. The temporal behavior of these variations is strictly coherent over the five cycles covered by the observations. Excluding N V $\lambda 4945$ (its subtle variations cannot be easily related to the LPVs of other transitions), we found that the same variability pattern affects all the emission-line profiles with the possibility of small phase lags. Also, the variability of the He I $\lambda 5876$ emission component is difficult to associate with that of other transitions since this line is severely blended with unresolved telluric and interstellar lines. The *degree* of variability, however, varies from one line to another. In particular, the characteristics of the helium line or C IV $\lambda 5806$ LPVs also apply to N IV

$\lambda 4058$, although the changes are more dramatic for the latter. The behavior of three lines, N IV $\lambda 4058$, He II $\lambda 6560$ and N V $\lambda 4945$, is displayed in Figure 2.2. The representative profiles resulting from 0.05-phase binning are compared with the mean template profile (*dashed line*). This template spectrum was constructed by giving an equal weight to every 0.05 bin, irrespective of the number of spectra in a given bin. The LPVs of the helium lines often show recurrent structures with a timescale of about 1 day (see, for example, the similarity between the profiles at $\phi \approx 0.125, 0.425$ and 0.725), indicating that nearly the same wind state is encountered three times per cycle. Similarities are also found for profiles taken about $\phi \approx 0.2$ apart ($\phi \approx 0.275, 0.625$ and 0.925). Finally, we note the appearance of a well-defined double-peaked profile at $\phi \approx 0.8$. The similarity of the LPVs affecting all the transitions can readily be seen in Figure 2.3, where we present a gray-scale plot of the residuals from the mean profile for three selected lines: N IV $\lambda 4058$, He II $\lambda 4686$ and He II $\lambda 6560$. The pattern of variability can be attributed to various extra emission components waving around the line center. This complex behavior is somewhat similar to the one found (with a period of 2.27 days) in the He II transitions of the WN 6 star WR 134 (McCandliss et al. 1994). It is extremely difficult to follow consistently the motion of these individual extra emission features over the entire cycle. Although their motion is readily seen within the velocity range of about $\pm 1500 \text{ km s}^{-1}$, an extension of the variability to higher Doppler shifts is discernible up to at least $\pm 2000 \text{ km s}^{-1}$ (Figs. 2.3b and 2.3c), which roughly corresponds to the value of the wind terminal velocity ($\approx 1900 \text{ km s}^{-1}$; Prinja, Barlow, & Howarth 1990; Rochowicz & Niedzielski 1995). The significance of these high-velocity changes will be rigorously demonstrated in §2.3.2.3.

In order to investigate the dynamics of the extra emission features appearing in Figure 2.3, we have measured their radial velocity by determining the wavelength at which the total flux of the feature is divided into two equal parts. The results are presented in Figure 2.4 for He II $\lambda 6560$. Since the emission lines probe

the conditions of the wind averaged over the entire stellar envelope, it is likely that overlap in velocity space of different extra emission components, as well as opacity effects considerably complicate the observed pattern of variability. It is, however, remarkable that the *bluest* excursions of these substructures coincide with the occurrence of the brightness maxima at $\phi \approx 0.15$ and 0.40 (compare Figs.2.1 and 2.4). In particular, no extra emission is observed at high-negative velocities during minimum light ($\phi \approx 0.5\text{--}0.8$).

In order to quantify the nature of the variability displayed by all transitions at $v \gtrsim + 2000 \text{ km s}^{-1}$, we have measured the wing intensity of He II $\lambda 4686$ for a fixed wavelength (here 4719 \AA , which corresponds to $v \approx + 2140 \text{ km s}^{-1}$; the red-wing variability reaches a maximum at this velocity, see §2.3.2.3). The results (Fig.2.5) bear a striking similarity with the light curve and suggest a causal relationship. This variability could be partially related to the variations at negative-to-zero velocities brought to the positive domain by electron scattering (Hillier 1984, 1991). However, the relative amplitude of the variations at $v \sim + v_\infty$ exceeds the variations in the $-v_\infty\text{-}0$ domain (§2.3.2.3). In addition, there is a clear anticorrelation between the intensities measured at $+ v_\infty$ and $- v_\infty$ (see §2.4.1). Thus, these positive-velocity changes might reflect the genuine changes of the wind structure at $|v| \sim v_\infty$.

As mentioned previously, N V $\lambda 4945$ does not display a high degree of variability. However, the LPVs inherent in this line are significant (§2.3.2.3) and show some phase dependency (Fig.2.6). The variability is mainly restricted to the uppermost part of the profile and seems to differ from the variations of the “typical” lines discussed above (compare Figs.2.2b and 2.2c between $\phi \approx 0.525$ and 0.675). However, these differences do not clearly indicate that this line is not sensitive to the same time-dependent physical conditions as the other transitions. In particular, we note that the line-peak intensity is also enhanced at $\phi \approx 0.3$.

Equivalent Width Variations For each line, we have measured the equivalent width (EW) within a fixed wavelength range. As much as possible, this range was chosen in order to minimize the contribution of blends. The results (which were normalized for comparison) are shown for six selected lines in Figure 2.7. Note that the plotted variations reflect the net changes of emissivity after allowance for the continuum level changes. The EW variations reach a maximum value (20 %) for He II $\lambda 4542$ and N V $\lambda\lambda 4604, 4620$. Lower level changes are detected in He II $\lambda 4686$ and N IV $\lambda 4058$, while the variations observed in other lines (such as He II $\lambda 4200$ or N V $\lambda 4945$) are comparable with the measurement errors.

In Figure 2.8, the line profiles corresponding to the maximum and minimum EW values are plotted for four transitions. The different responses to a change in the physical conditions are noticeable for the two Pickering lines He II $\lambda 4200$ and He II $\lambda 4542$. Since He II $\lambda 4542$ is blended with multiple lines of N III around 4513 Å, we were compelled to restrict our measurements to the region 4526-4578 Å. Even accounting for a possible distinct behavior of the N III transitions, it seems unlikely that the amplitude of the EW variations can decrease sufficiently to remove the observed difference. As a possible explanation of this peculiarity one can invoke the argument of Conti, Leep, & Perry (1983): this line might be at the verge of the optically thick/thin case, exposing particular sensitivity to the variations of the continuum flux.

In the case of the doublet N V $\lambda\lambda 4604, 4620$, the high amplitude of the observed EW variations can mostly be explained by the appearance and disappearance of the P Cygni absorption components (§2.3.2.2). According to Hillier (1988), collisional excitation is an important process in the formation of these lines. Therefore, they must be highly sensitive to the temperature fluctuations occurring at the base of the wind (Fig.2.1), i.e., in the vicinity of the line formation zone (this doublet is formed at $\approx 3 R_c$, where R_c is the stellar core radius; P. Crowther 1995, private communication). As far as the lines exhibiting the largest

changes are concerned, the equivalent width variations are strongly correlated with the continuum flux level: the equivalent width decreases as the star fades.

Skewness Variations In order to quantify the phase-related changes in the line asymmetry (Fig.2.2), we have calculated the skewness of the line profiles:

$$\beta^{1/2} = \mu_3/\mu_2^{3/2}, \quad (2.1)$$

where

$$\mu_n = \sum_j (\lambda_j - \bar{\lambda})^n I_j / \sum_j I_j, \quad (2.2)$$

and

$$\bar{\lambda} = \sum_j \lambda_j I_j / \sum_j I_j. \quad (2.3)$$

Here, I_j is the intensity of the line at the wavelength λ_j . We have measured the skewness above a given intensity in order to avoid the blended part of the profile. The results are plotted in Figure 2.9 for four selected transitions. The 1 day recurrence timescale inferred visually (see above) appears clearly for most of the lines (e.g., He II $\lambda 4686$), excluding N V $\lambda 4945$. This result is reminiscent of the 1 day recurrence timescale found in the EW of the UV absorption components by Willis et al. (1989) and St-Louis et al. (1993). No comparative information can be gained from these data since, for a given transition, both the amplitude and the shape of the curves depend on the chosen intensity level above which the skewness value was determined (compare the values of Figs.2.9 and 2.10 for He II $\lambda 4686$ and He II $\lambda 6560$).

Radial Velocity Variations Because most of the optical lines of EZ CMa are blended and asymmetric, the difficulties in the determination of radial velocity variations are well known. The reliability of the results strongly depends on the method used as well as on its applicability range. Consequently, we excluded from our measurements the uppermost highly variable part of the profiles, which

does not reflect in a straightforward manner (i.e., via orbital motion) a possible binary manifestation. We also excluded the lowest part in order to avoid the line wings and the blend contributions. The measurements were restricted to the ranges 3–6.5 and 1.35–2.5 of the continuum level for He II λ 4686 and He II λ 6560, respectively. Finally, instead of Gaussian fitting, we prefer the half-flux method, which measures the wavelength where the selected part of the profile is equally divided with respect to the line flux. Typical results for He II λ 4686 and He II λ 6560 are shown in the upper part of Figure 2.10. The semi-amplitude of the variations amounts to $\approx 100 \text{ km s}^{-1}$. In both cases, this is significantly higher than the measurement errors (about 15 km s^{-1}).² In the lower part of the figure, we plot the skewness values calculated for the portion of the profile where the velocity measurements were performed (i.e., base and top excluded). We conclude that changes in the line profiles are likely to contribute significantly to the radial velocities changes. Support for this comes from the 1 day recurrence timescale found in the radial velocity curves (upper part of Fig.2.10), suggesting that these data do not reflect a $P = 3.77$ day binary motion. Accordingly, we doubt the reliability of these measurements as a source to derive any eventual orbital parameters.

Full-width at Half-maximum Variations In order to measure the full-width at half-maximum (FWHM), we fitted the different lines by a Gaussian profile. For various representative line-profile shapes, it was found that the measurements derived by this method correlate very well with the values directly measured on the profile. Typical deviations around the mean value are shown in Figure 2.11 for selected transitions. Three main conclusions can be drawn from this graph: (a) the semi-amplitude of the variations over one cycle is always quite large (of the order of 100 km s^{-1}); (b) for all lines, a clear phase-dependency of the FWHM is found

²Unfortunately, the low resolution of the spectra does not allow us to refer to a reliable fiducial mark. Therefore, this quantity was derived from the characteristic dispersion of the measurements for different consecutive exposures.

with a 1 day recurrence timescale. N V $\lambda 4945$ is the only line that does not clearly show this pattern; the latter could be due to the measurement uncertainties, which are considerably higher for this weak line; (c) slight time delays appear between different lines. We have chosen the phase location of the first maximum as a reference point. In the first group, consisting of He II $\lambda 3968$ and He II $\lambda 4200$, this maximum occurs at $\phi \approx 0.1$, whereas for the other transitions (He II $\lambda 4686$, He II $\lambda 5412$ and He II $\lambda 6560$) it appears at $\phi \approx 0.2$. The existence of this time delay can be reinforced when one compares the location of the other local extrema for He II $\lambda 3968$ and He II $\lambda 4686$. This could be a consequence of the different radial extensions of the line-formation regions in a WR wind (e.g., Niedzielski 1994). In particular, He II $\lambda 3968$ and He II $\lambda 4200$ are formed deeper in the wind (maximum emissivity at $3\text{-}6 R_c$: Hillier 1987; P. Crowther 1995, private communication) than He II $\lambda 4686$ ($\approx 10 R_c$: Hillier 1987).

2.3.2.2 The P Cygni Profile Variability

Since the simultaneous UV observations have revealed dramatic changes in the P Cygni absorption components (WRMEGA), we searched for similar LPVs in the optical P Cygni profiles. Two lines in our sample clearly present a P Cygni absorption component: He I $\lambda 3889$ and N V $\lambda 4604$. Also of interest is He I $\lambda 5876$, but its absorption trough is severely blended with C IV $\lambda 5806$.

Figure 2.12a presents the temporal behavior of the He I $\lambda 3889$ absorption component. The variability pattern for this line shares many similarities with N IV $\lambda 1718$ (WRMEGA). During maximum light, the line develops an enhanced absorption trough at velocities above the estimated wind terminal velocity. Of importance is the fact that the maximum absorption strength at high-negative velocities ($\gtrsim 2000 \text{ km s}^{-1}$) does not exactly coincide with the variability at intermediate negative velocities ($\approx 1400 \text{ km s}^{-1}$), as was seen for the UV lines (WRMEGA). Rather, a lack of absorption at this velocity is observed with some

delay, at $\phi \approx 0.3$ and 0.55.

Although the bluest part of the He I $\lambda 5876$ line does not reach the continuum level in EZ CMa, a violet displaced absorption component is clearly seen for WR stars of various subtypes (e.g., Robert 1992). The gross variations affecting the region where C IV $\lambda 5806$ and He I $\lambda 5876$ merge are thus most likely related to the variations of this helium absorption trough. The absorption is deepest at light curve maxima (Fig. 2.12b), i.e., at $\phi \approx 0.15, 0.45$ and 0.90, gradually changing its location toward higher velocities, in close resemblance to He I $\lambda 3889$.

One of the most puzzling characteristics of the present series of spectra is the temporal variations of N V $\lambda 4604$, which gradually changes from a typical P Cygni profile to a pure emission-line profile on an hourly timescale. As illustrated in Figure 2.12c, a weak absorption trough on the blue side of N V $\lambda 4604$ appears at $\phi \approx 0.0$ and $\phi \approx 0.5$ –0.8. Comparison of Figures 2.12c and 2.1 shows that the development of this absorption component is completely controlled by the continuum flux variations. This is highlighted in Figure 2.13, where we show the line intensity at 4588 Å ($v \approx -1025$ km s $^{-1}$) as a function of phase. Contrary to He I $\lambda 3889$ and He I $\lambda 5876$, for which the P Cygni absorption strengthens at maximum light, the weak absorption component in N V appears only as the star fades. The quasi-simultaneous photometric and spectroscopic observations performed by Firmani et al. (1980) led also to the same conclusion. In view of the strong epoch-dependency of the variability in this star, it is remarkable that the same behavior can be noticed in data secured about 20 years ago. A comparison of the spectroscopic data of Smith & Willis (1994) with the photometry performed by Duijsens et al. (1996), both obtained in 1991 January, also supports this tight correlation. A subsequent paper (Morel et al., in preparation) based on a large data set of optical spectra secured over a much longer timescale will further confirm the long-term consistency of this result.

2.3.2.3 “Temporal Variance Spectrum” Analysis

As shown in Figure 2.2, even a simple inspection by eye is sufficient to roughly deduce the temporal behavior of the LPVs. However, the precise characterization of these variations could be greatly influenced by the photon statistics in the region of interest. In order to rigorously estimate the significance of the LPVs, we applied the “temporal variance spectrum” analysis (TVS; Fullerton 1990).

In order to describe the LPVs for a collection of N spectra, we produced a reference spectrum \bar{S}_j as a mean weighted by the signal-to-noise in the continuum associated with each individual exposure. We placed the N rectified spectra in a matrix $S(i, j)$, where i and j denote the spectrum and the pixel (or wavelength bin) numbers, respectively. Then, we have calculated the weighted differences:

$$D_{ij} = \left(\frac{\sigma_{0j}}{\sigma_{ij}} \right) (S_{ij} - \bar{S}_j), \quad (2.4)$$

where σ_{0j} is the reciprocal of the rms S/N of the spectral time series (see Fullerton et al. 1996), and σ_{ij} are the elements of the matrix giving the noise associated with the element S_{ij} . In our case, we can reasonably assume that σ_{ij} is given by the Poisson statistics, i.e., by the square root of the count number (in electrons) accumulated at a given pixel. The overall variation for a collection of N spectra will be:

$$(TVS)_j = \frac{1}{N-1} \sum_{i=1}^N D_{ij}^2 - (\sigma_j^{cal})^2, \quad (2.5)$$

where σ_j^{cal} is introduced in order to eliminate any spurious variability induced by an imperfect wavelength calibration. Following Malanushenko (1988), this quantity can be expressed by the relation:

$$\sigma_j^{cal} = \nabla \bar{S}_j \delta_j, \quad (2.6)$$

where $\nabla \bar{S}_j$ is the derivative of the mean spectrum, and δ_j the precision of the wavelength calibration in Å (we have estimated δ_j to be 15 km s^{-1}).

In order to assess the significance of the LPVs, we compare in the lower panels of Figures 2.3, 2.6, and 2.12 the values of $(\text{TVS})_j^{1/2}$ (expressed in terms of the amplitude of the deviations as a percentage of the normalized continuum) with $[\sigma_{0j}^2 \chi_{N-1}^2(99\%)]^{1/2}$. Accounting for the noise level in the line profile, any value of $(\text{TVS})_j^{1/2}$ above this threshold ensures that the line-profile variability is significant at the 99 % level. An inspection of Figures 2.3, 2.6, and 2.12 shows that this condition is satisfied over the entire profile of all lines (excluding N V $\lambda 4945$), confirming that the high-velocity variability discussed in §2.3.2.1 has a physical meaning.

In the following, we will discuss the ratio of $(\text{TVS})_j^{1/2}$ to the mean spectrum (hereafter σ), which allows us to estimate the relative importance of the line-to-line variability. This quantity (*dashed line*, and expressed as the amplitude of the deviations as a percentage of the line intensity at a given wavelength) is overplotted on the mean spectrum in Figure 2.14. Several characteristics of the LPVs can be readily deduced from this plot. In particular, the LPVs create some local maxima of σ along the line profiles. This effect was also noticed for WR 134 by Vreux et al. (1992), and by Robert (1992). Concerning EZ CMa, the same result was found by Robert et al. (1992) for He II $\lambda 5412$ (see their Fig.13).

Of interest is the remarkable degree of variability, not only at intermediate to high-negative velocities, but also at high-positive velocities (Tables 2.2 and 2.3). This is particularly noticeable for He II $\lambda 4686$. Its red wing (around + 2140 km s⁻¹; see Table 2.2) displays an intense peak in the σ spectrum; the size of the deviations amount to $\approx 6\%$ of the line intensity at this velocity.

Since the great majority of optical transitions present a significant level of variability at high-positive velocity, it is likely that the red-wing variability of C IV $\lambda 5806$ affects in some way the variability pattern of the absorption component of He I $\lambda 5876$ discussed in §2.3.2.2. However, mainly because of the similarities between the behavior of He I $\lambda 5876$ and He I $\lambda 3889$, we believe that the variations

intrinsic to the He I absorption trough dominate in Figure 2.12c.

In general, the relative amplitude of the LPVs is higher for lines formed in the outer parts of the wind. This is clearly demonstrated by the decrease of σ along the He II Pickering sequence (Fig.2.14). Interestingly, the integral of σ over the extent of a given transition is not correlated with the level of its EW variations (§2.3.2.1).

2.4 Discussion

All our observations point to a strictly coherent phase-dependent behavior of the variability over five consecutive 3.77 day cycles and can be summarized as follows:

- (a) Extra emission subpeaks are found to travel across all the line profiles (Fig.2.3); the bluest excursions of these features coincide with the light curve maxima (Fig.2.4).
- (b) The brightening of the star causes an increase of the EWs, although the amplitude of the EW variations is different from line to line (Fig.2.7).
- (c) A 1 day recurrence timescale within the 3.77 day cycle appears in the FWHM, radial velocities, and skewness measurements (Figs.2.9, 2.10 and 2.11).
- (d) For the He I transitions exposing a blue absorption edge, we observe an enhanced absorption at high velocities at maximum light (Figs.2.12a and 2.12b).
- (e) The P Cygni absorption component of N V λ 4604 disappears as the star brightens (Fig.2.12c).
- (f) There are some zones of enhanced variability along the line profiles (Fig.2.14).

For further discussion, we shall refer to the model of the “unperturbed wind”, i.e., the wind in (relative) absence of variability. The spectra obtained during the 1983 *IUE* campaign are particularly well suited for the creation of

a reference spectrum for the “quiet” wind, since they were obtained during a relatively quiescent stellar state (Willis et al. 1989). Two N IV $\lambda 1718$ profiles representative of the WRMEGA low- and high-velocity states (referring to the blueward extension of the P Cygni absorption components) are compared with the 1983 mean profile in Figure 2.15. Although some differences are evident, the 1983 profile morphology resembles more the 1995 low-velocity state profile. Therefore, we conclude that the part of the envelope that is seen projected on the stellar disk between $\phi \approx 0.5$ and $\phi \approx 0.8$ is *relatively* unperturbed.

2.4.1 A Compact Companion?

The assumption that the unperturbed wind is related to the minimum of the continuum flux has serious implications for the interpretation of the variability. Indeed, if the perturbations are caused by the presence of a compact companion, the latter would have to be placed in front of the WR star at $\phi \approx 0.1\text{--}0.2$ (i.e., at maximum light), as occurs in low-mass X-ray binaries (LMXRB; van Paradijs 1983). Without further advocating the similarity between our case and LMXRBs, we discuss below the binary scenario with the hypothetical companion in front at $\phi \approx 0.1\text{--}0.2$.

If we assume the presence of a compact companion, we have to explain the simultaneous strengthening of the P Cygni absorption components of the He I transitions and the “evaporation” of the N V $\lambda 4604$ (and probably N V $\lambda 4620$) absorption components at $\phi \approx 0.1\text{--}0.5$ and $\phi \approx 0.9$. As the ionization cavity around a neutron star crosses the line of sight, one should observe a reduced absorptivity (or emissivity) at intermediate-to-high velocities accompanied by a reduced wind velocity (see §2.1). The latter is in complete contradiction to what we observe in EZ CMa: maximum light (hypothetical companion in front) corresponds to maximum wind velocity (WRMEGA and our Fig.2.12).

The influence of the hypothetical companion on the EWs of the emission lines strictly depends on the location of the companion's orbit relative to the line formation zones (Marchenko et al. 1996). In general, one expects a minimum in the EWs of the He II (and probably He I) emission lines during the passage of the companion in front of the WR star. This is also not observed in EZ CMa.

Considering the fact that the deepest minimum in the light curve of wind-fed HMXRBs with negligible X-ray heating of the primary (which is expected for EZ CMa because of its low X-ray flux; see below) occurs when the compact companion is in front (e.g., van Paradijs, Hammerschlag-Hensberge, & Zuiderwijk 1978; van Genderen 1981; Pakull et al. 1983), one can argue that the companion is in fact in front at $\phi \approx 0.6\text{--}0.7$. This would be consistent with the decrease of the wind velocity at this phase, as well as the decrease of high-speed absorption in He I lines, but cannot account for the appearance of the absorption trough in N V $\lambda 4604$. Note also that this maximum of N V absorption at $v \approx -900 \text{ km s}^{-1}$ coincides with the maximum emissivity at the same velocity in the N IV and He II lines (Fig.2.3). This virtually eliminates the possibility of the companion being in front of the WR star at minimum continuum flux.

The clear indication of the intensity variations at high-positive velocities ($v \sim +v_\infty$; Fig.2.5) deserves special attention. To quantify them, we have measured the intensity of He II $\lambda 4686$ and He II $\lambda 6560$ at the highest positive velocities (v_p) corresponding to the maxima of the TVS, together with the intensities at $v \sim -v_p$ in the same spectrum, i.e., at $v = -1910$ and $+2140 \text{ km s}^{-1}$ for He II $\lambda 4686$, $v = -1700$ and $+1920 \text{ km s}^{-1}$ for He II $\lambda 6560$ (see Table 2.2). Both measurements indicate anticorrelated changes with correlation coefficients ranging from -0.44 (He II $\lambda 4686$) to -0.47 (He II $\lambda 6560$), i.e., being significant at a greater than 95 % statistical level. At first sight, the interpretation is straightforward: the “void” in the WR wind at $v = -v_p$ created by the X-ray source reappears at $v = +v_p$, half an orbital phase later, causing the negative correlation at $v = \pm v_p$. However,

there is one fundamental difficulty. Because of the low level of the observed X-ray flux, we expect the zone of the high ionization to be fairly restricted, with an especially well-defined edge at the side facing the densest parts of the wind (i.e., between the ionizing X-ray source and the WR star). This means that the position (in velocity space) of the “void” in the WR wind cannot depend on the line transition. However, we observe significant differences of the maxima of the TVS at high-positive/negative velocities in different lines (Table 2.2: He II $\lambda 6560$ vs He II $\lambda 4686$). Moreover, the maximum of the TVS for He II $\lambda 6560$ at -1700 km s^{-1} is placed right at the minimum of the variability of N IV $\lambda 1718$ (compare with Fig.3 of WRMEGA). This indicates that the spatial location of the “void” in the WR wind is transition-dependent. This cannot be reconciled with the strictly spatially limited zone shaped by the ionizing X-ray flux from the hypothetical companion.

Since the wind is strongly disrupted between $\phi \approx 0.8$ and $\phi \approx 1.5$ (Fig.2.12c), the azimuthal extension of the perturbed zone should be very substantial. This may occur if the compact companion is surrounded by a very large photoionized cavity. However, the low X-ray flux of EZ CMa argues against this conclusion. The other possibility is that the compact companion is trailed by some kind of disturbance such as a photoionization wake (Fransson & Fabian 1980), which would suggest some delayed reaction of the profiles. However, this cannot fit the fact that the N V absorption trough vanishes starting from $\phi \approx 0.8$ (Fig.2.12c), i.e., *long before* the suggested passage of the companion in front of the WR star ($\phi \approx 0.1\text{--}0.2$), and once again gains some strength for a short time at $\phi \approx 0.0$ (Fig.2.13). Furthermore, the formation of a photoionization wake is only possible for systems with low \dot{M}/L_X ratio (Blondin et al. 1990). Since EZ CMa has a strong wind but is not a strong X-ray emitter, the formation of such a vastly extended structure is very unlikely, additionally owing to the high X-ray opacity of the WR wind.

Other facts are also difficult to account for in the context of the binary hypothesis:

- The complex and epoch-dependent shape of the light curve is particularly difficult to reconcile with the binary interpretation. Wind-fed HMXRBs are generally characterized by a *stable* double-wave light curve shape, slightly distorted by reflection effects (e.g., Hutchings 1974; van Paradijs et al. 1978; Tjemkes, Zuiderwijk, & van Paradijs 1986). In particular, the occasional complete lack of variations of EZ CMa (Firmani et al. 1980; Duijzens et al. 1996) is not common for HMXRBs.
- The same conclusion also applies to the polarization curves. The behavior of EZ CMa (Robert et al. 1992) is not typical for HMXRBs (e.g., Dolan & Tapia 1988).
- A major drawback of the binary scenario arises also from the X-ray observations. The star was below the detection limit of the *UHURU* (2–6 keV) and *HEAO-1* (10–25 keV) satellites, which implies a X-ray luminosity below 1.5×10^{34} and 4.8×10^{33} ergs s⁻¹, respectively (Stevens & Willis 1988). Furthermore, the *ROSAT* and *Einstein* satellites placed an upper limit of 10^{33} ergs s⁻¹ on the emissivity in the soft X-ray band (Moffat et al. 1982; Willis et al. 1994). The data can be well described by a thermal spectrum with $kT_X \approx 0.5$ keV. Both L_X and T_X are extremely low compared to any HMXRB (e.g., Haberl, White, & Kallman 1989). This discrepancy might arise from the difference in orbital parameters and stellar wind properties since the amount of material accreted onto a neutron star (and the X-ray luminosity) scales as $F_* a^{-2} v^{-4}$, where F_* is the mass flux at the primary's surface, a is the binary separation, and v is the radial outflow velocity at the neutron star location (e.g., Waters et al. 1988). However, detailed calculations have shown that this is not a viable explanation for the observed 2 orders of magnitude deficit (Stevens & Willis 1988). This dichotomy

between the X-ray properties of HMXRBs and EZ CMa could then be viewed as significant. We note also that the same calculations applied to other wind-fed HMXRBs were in reasonable agreement with the X-ray observations (White 1985; Kaper et al. 1993).

This deficiency in the X-ray flux of EZ CMa could be overcome in different ways: (a) the X-ray emission suffers a strong extinction in the dense WR stellar wind (Moffat & Seggewiss 1979). This suggestion was challenged by others (Vanbeveren, van Rensbergen, & de Loore 1982); (b) the accretion is made impossible by centrifugal (or magnetic) inhibition (Stella, White, & Rosner 1986); (c) the conversion of gravitational energy into X-ray emission is much less efficient than usually assumed.

It seems, however, fairly contrived to invoke these mechanisms for which the efficiency is unknown. As for single early-type stars, the X-ray emission could merely be intrinsic to the stellar wind and result from shocks associated with dynamical instabilities (Baum et al. 1992). In short, no firm indication suggests at present that the X-ray emission of EZ CMa is particularly different from that of bona fide single WR stars.

Finally, we question some arguments proposed in support of the duplicity of EZ CMa:

- Since massive X-ray binaries are believed to be high-velocity objects (van Oijen 1989), it is of interest to determine if EZ CMa is indeed a runaway star. This assertion was first proposed by Moffat (1982), who suggested that its unusual height above the galactic plane for a population I star (≈ 315 pc for a distance of 1.8 kpc) arose from a possible recoil after a supernova explosion. However, EZ CMa is certainly dynamically associated with its surrounding ring nebula S 308, as well as with a cavity in the interstellar H I gas (Arnal & Cappa 1996). Since the systemic radial velocity inferred

for both objects shows little, if any, departure from the galactic rotation curve at this distance, the status of EZ CMa as a runaway star has since weakened (Chu et al. 1982; Pismis & Quintero 1982; Arnal & Cappa 1996).

- It has been suggested (e.g., Cherepashchuk & Aslanov 1984) that the optical nebulae surrounding some WR stars could be a fossil product of secondary mass exchange in a massive binary system. However, recent hydrodynamical simulations (García-Segura, Langer, & McLow 1996) show that this process is not required to reproduce global nebular morphologies, as in the case of S 308.

Could the companion be a main-sequence star? Since its mass should be about solar (Firmani et al. 1980), this implies a very large initial mass ratio, which is unlikely (Garmany, Conti, & Massey 1980). Other arguments such as: the softness of the X-ray emission (see White & Long 1986), the ragged and multipeaked shape of the skewness and radial velocity phase dependencies (see Lewis et al. 1993), and the complicated LPV pattern compared to the usual fairly smooth S-wave shape for binary systems seem to reject this possibility.

2.4.2 Toward an Interpretation

All the arguments presented above favor a variability induced by the rotational modulation of an inhomogeneous outflow, as already suggested in WRMEGA. Is it possible in this context to account for points (a)–(f) listed at the beginning of this section?

The point that certainly deserves the highest attention is the disappearance of the P Cygni absorption component of N V $\lambda 4604$ at $\phi \approx 0.1\text{--}0.5$. It is worth remembering that this line is formed in close vicinity of the stellar core: the outer boundary of the line formation zone can be put at $r \approx 10 R_c$ for a WN 5 star (Marchenko et al. 1997).

At this point, it might be relevant to examine the variation of the Sobolev line optical depth as a function of radial distance from the star r and azimuthal angle ϕ . For a given transition ($i \rightarrow j$), this quantity can be expressed by the relation ($\mu = 1$):

$$\tau(r, \phi) \sim \left[\frac{n_i(r, \phi)}{g_i} - \frac{n_j(r, \phi)}{g_j} \right] \left| \frac{\partial v(r, \phi)}{\partial r} \right|^{-1}. \quad (2.7)$$

Depending on the value of the angle ϕ , the line optical depth will be the result of the competition between two quantities — the difference in the population of the atomic levels n_i, n_j , and the radial gradient of the outflow velocity.

Suppose that we observe a “bright” zone of the wind projected on the stellar disk. The only way to produce the disappearance of the nitrogen P Cygni absorption component is either to invoke a steeper velocity gradient in the region where the bulk of emission of N V $\lambda\lambda 4604, 4620$ originates and/or to change the population levels. In fact, it is difficult to disentangle the contribution of both effects since the ionization/population balance and the velocity field are intimately linked in the radiation-driven wind theory.

We propose that the increase in the wind temperature occurring at the $\tau \approx 2/3$ “surface” at $\phi \approx 0.1\text{--}0.5$ (deduced from the color variations of the UV-optical continuum; Fig.2.1) leads to a possible rearrangement of the ionization (for N^{3+} and lower stages) as well as the level population balance (overpopulating high levels) in the vicinity of the star. This in turn affects the magnitude of the radiative force since henceforth the new dominant ionic species have their transition wavelengths differently distributed with regard to the maximum of the emergent flux. The resulting changes in the velocity field, combined with a possible altering of the populations of the atomic levels of N^{4+} , cause the replacement of the absorption component of N V $\lambda 4604$ by emission at $v \approx -900 \text{ km s}^{-1}$. Concerning the cause of the LPVs occurring at velocities exceeding the wind terminal velocity, we note that the nitrogen transitions are important

contributors to the radiative force acting in hot-star winds (see Table 5 of Abbott 1982). Therefore, a change in the opacity produced by the nitrogen (and possibly iron) ions in the core's vicinity could lead to a redistribution of the momentum deposited by the radiative force throughout the large wind volume. In particular, at phases $\phi \approx 0.1\text{--}0.5$ (maximum flux), the far-UV transitions that contribute substantially to the flow acceleration might become relatively less opaque. This will lead in turn to an excess of momentum deposited in the remote parts of the wind, and acceleration of the wind beyond v_∞ (compared to the quiet state). Because of this momentum deposition at large radii, the σ spectrum reveals a high level of variability at high velocities (§2.3.2.3; Tables 2.2 and 2.3). This could also explain why the transitions formed farther out in the wind (the He II Pickering lines with decreasing principal quantum number) present progressively higher amplitude of variability (§2.3.2.3). Note that the necessity of an additional acceleration of the wind at $v \gtrsim v_\infty$ was suggested for EZ CMa by Hillier (1988) in order to improve the model fits to the observed profiles.

The morphological changes of the P Cygni absorption components (Figs.2.12a and 2.12b), can be related to the pattern of variability in the pure emission lines (Fig.2.3). A careful look at Figure 2.4 shows that an excess of emission appears at $v \approx -1600 \text{ km s}^{-1}$ and $v \approx -2300 \text{ km s}^{-1}$ at $\phi \approx 0.25, 0.55, 0.90$ and $0.15, 0.45$, respectively (these velocities are indicated by two dashed lines in this figure). These are roughly the phases when we observe an excess of emission and an enhanced absorption at these velocities in Figures 2.12a and 2.12b. Therefore, the observed P Cygni variability is likely to be due to the motion across the stellar disk of the same zones which produce the extra emission features on the pure emission-line profiles (Fig.2.3). The looplike trajectories of the extra emission components suggest that they are involved in limb-to-center movement induced by the stellar rotation. This is reminiscent of the behavior of the corotating interaction regions in OB stars (Cranmer & Owocki 1996). In this context, note also the gradual increase of the velocity of the extra absorption seen in He I $\lambda 5876$ (Fig.2.12b) at

$\phi \approx 0.15, 0.45$ and 0.9 .

Additionally, we suggest in accordance with St-Louis et al. (1997), that the 1 day recurrence timescale found in the skewness and FWHM measurements highlights the reaction of the wind on the changing conditions at the base of the wind, i.e., on the variable flux emerging from the stellar core.

2.4.3 A Hint of a Magnetic Field Structure?

Our observations of EZ CMa suggest that the wind variability may be induced by some kind of “photospheric” activity such as (non)radial pulsations or magnetic fields. The question of the existence of (non)radial pulsations in WR stars remains open (Vreux 1985; Matthews & Beech 1987). Until now, no compelling observational evidence has been put forward. Although Blecha, Schaller, & Maeder (1992) claimed the existence of a 627 s periodicity in the light curve of the WN 8 star WR 40, subsequent observations carried out by four independent groups were unable to confirm this result (e.g., Martinez et al. 1994).

Some attempts have been made to search for rapid light variations in EZ CMa that could possibly be linked to pulsational instabilities. Moffat & Haupt (1974), Lindgren, Lundström, & Stenholm (1975), and Cherepashchuk (1981) reported the absence of short *periodic* variability (down to 1 hr). Interestingly, such rapid oscillations (\approx 20 minutes) were reported by Matthews, Moffat, & Marchenko (1992a) and Bratschi & Blecha (1996), but the intermittent nature of this phenomenon (in both cases, once during the entire observation period) makes its interpretation difficult. On the other hand, the uniqueness of the $\mathcal{P} = 3.77$ day period clearly shows up in the intensive photometric monitoring secured by Antokhin et al. (1994). This period seems to be too long for any conceivable (non)radial mode (Glatzel, Kiriakidis, & Fricke 1993).

Matthews et al. (1992a) proposed that the abrupt brightness increase of \approx

0.008 mag that lasted about 10 minutes in their photometric data may result from a reconnection of magnetic field lines. In that case, the local magnetic field strength would be of the order of 1000 G. Drissen et al. (1989) and Robert et al. (1992) reported a lack of significant circular polarization in broadband continuum, thus excluding cyclotron emission in a large magnetic field, but providing no serious constraints on the possibility of a small magnetic field. McLean et al. (1979) used circular line polarimetry to place a limit of (300 ± 600) G for the regular component strength. However, it is worth noting that any quantitative estimation of the magnetic field of EZ CMa is loosely constrained since a *local* surface field could easily escape detection (Barker et al. 1981).

From a theoretical standpoint, it is not excluded (but by no means certain) that a local magnetic field with a strength of some hundred G is sufficient to control the wind morphology via creation of magnetically active zones. Although significant attempts have been made to include the effects of a global magnetic field on the wind structure and dynamics (e.g., Friend & McGregor 1984; Cassinelli, Ignace, & Bjorkman 1995), this question remains to be fully addressed theoretically. Such local “photospheric” magnetic activity is capable, at least qualitatively, of explaining the epoch-dependency and the nature of the variations. We note that the recognition that WR stars could present discrete absorption components (DACs) in their UV resonance lines (Prinja & Smith 1992), as do the majority of O stars, leads to the suggestion that the mechanism inducing the observed variability in both classes of objects is not fundamentally different. It has been suggested (Cranmer & Owocki 1996) that the DAC phenomenon is related to the formation of corotating interaction regions (Hundhausen 1972, chap.5). These regions emerge from active zones in the stellar photosphere. The development of such large-scale structures is therefore not excluded for EZ CMa. Their curvature induced by the stellar rotation (St-Louis et al. 1997) can introduce small time delays observed in the FWHM variations (§2.3.2.1). These structures must be relatively long-lived in order to account for the 5 cycle stability found in our data,

as well as for the light curve shape, which can keep the same global pattern on a monthly timescale (Duijzens et al. 1996). In this context, however, the possible existence of magnetic activity for WR stars in conjunction with a presumable lack of surface convective zones remains to be explained.

Another possibility is that the wind of EZ CMa is controlled by a large-scale magnetic structure perhaps of fossil origin (e.g., Brown, Shore, & Sonneborn 1985). We note that an interpretation of the variability of EZ CMa in terms of a bipolar density enhancement has been already given by Matthews et al. (1992b). On the other hand, it has been proven that early-type stars can possess complicated magnetic field configuration geometry as a result of the evolution of the fossil field (Thompson & Landstreet 1985). In order to produce the strong-epoch dependency displayed by EZ CMa, this structure should be at some point variable, if not in global morphology, at least in local manifestations.

2.5 Conclusion

Beyond the difficulty of accounting for all the observational aspects presented in this paper, we believe that a relatively coherent picture can be drawn in terms of the rotation of a single WR star with a structured wind. This view is supported by spectropolarimetric studies that emphasized the distorted nature of the wind of EZ CMa (Schulte-Ladbeck et al. 1991, 1992). A contrario, the binary hypothesis hardly finds any support from our observations.

In our interpretation, the variability is induced by the azimuthal dependency of the ionization balance and line opacities prevailing at the base of the outflow. Since the altered opacity modifies the action of the radiative force, the wind is structured in zones differing by their dynamical and physical properties. The streams coming from the active zones at $\phi \approx 0.1\text{--}0.5$ and $\phi \approx 0.9$ possess different properties compared to the ambient wind. As they are carried by stellar rotation,

this leads to the complicated pattern of LPVs seen in our data. This is not surprising, considering the sensitivity of the P Cygni profiles to changes in the wind conditions (e.g., Castor & Lamers 1979; Hamann 1980; Prinja & Howarth 1984).

These observations tend to support the “wind-photosphere connection” for which a growing amount of evidence is now presented for O stars (e.g., Reid & Howarth 1996). Support for this assertion comes from the tight correlation between the changes of the UV continuum flux and spectroscopic variations (WRMEGA; Willis et al. 1989), which signifies that the changes at/near the stellar core drive the wind variability. Although (non)radial pulsations cannot be completely ruled out, magnetic fields are serious candidates for controlling the morphology of EZ CMa’s wind. To achieve a complete understanding of the physical processes operating in the envelope of early-type stars, it would be desirable to consider the possible influence of large-scale or localized magnetic field structures on the wind properties. From this point of view, the search for magnetic fields in these objects deserves serious and systematic attention. This could be, for example, accomplished via the detection of circular polarization in very high-resolution and high S/N spectropolarimetric data.

Acknowledgments: It is a pleasure to thank B. Duffee and F. McAuliffe for their excellent support during this campaign, Paul Crowther for his calculations of the line-formation region of He II λ 3968 and N V $\lambda\lambda$ 4604, 4620, as well as Tony Moffat for discussions and suggestions helping to improve the presentation. We wish to thank the Natural Sciences and Engineering Research Council (NSERC) of Canada and the Fonds pour la Formation de Chercheurs et l’Aide à la Recherche (FCAR) of Québec for financial support.

RÉFÉRENCES

- Abbott, D. C. 1982, ApJ, 259, 282
- Antokhin, I. I., Bertrand, J.-F., Lamontagne, R., & Moffat, A. F. J. 1994, AJ, 107, 2179
- Arnal, E. M., & Cappa, C. E. 1996, MNRAS, 279, 788
- Barker, P. K., Landstreet, J. D., Marlborough, J. M., Thompson, I., & Maza, J. 1981, ApJ, 250, 300
- Baum, E., Hamann, W.-R., Koesterke, L., & Wesselowsky, U. 1992, A&A, 266, 402
- Bendat, J. S., & Piersol, A. G. 1986, Random Data Analysis and Measurement Procedures (New York: Wiley)
- Blecha, A., Schaller, G., & Maeder, A. 1992, Nature, 360, 320
- Blondin, J. M. 1994, ApJ, 435, 756
- Blondin, J. M., Kallman, T. R., Fryxell, B. A., & Taam, R. E. 1990, ApJ, 356, 591
- Bratschi, P., & Blecha, A. 1996, A&A, 313, 537
- Brown, D. N., Shore, S. N., & Sonneborn, G. 1985, AJ, 90, 1354
- Cassinelli, J. P., Ignace, R., & Bjorkman, J. E. 1995, in IAU Symp. 163, Wolf-Rayet Stars: Binaries, Colliding Winds, Evolution, ed. K. A. van der Hucht & P. M. Williams (Dordrecht: Kluwer), 191
- Castor, J. I., & Lamers, H. J. G. L. M. 1979, ApJS, 39, 481
- Chalabaev, A., & Maillard, J. P. 1983, A&A, 127, 279
- Cherepashchuk, A. M. 1981, MNRAS, 194, 755

- Cherepashchuk, A. M., & Aslanov, A. A. 1984, *Ap&SS*, 102, 97
- Chu, Y.-H., Gull, T. R., Treffers, R. R., Kwitter, K. B., & Troland, T. H. 1982, *ApJ*, 254, 562
- Conti, P. S., Leep, E. M., & Perry, D. N. 1983, *ApJ*, 268, 228
- Crammer, S. R., & Owocki, S. P. 1996, *ApJ*, 462, 469
- De Donder, E., Vanbeveren, D., & van Bever, J. 1997, *A&A*, 318, 812
- Dolan, J. F., & Tapia, S. 1988, *A&A*, 202, 124
- Drissen, L., Robert, C., Lamontagne, R., Moffat, A. F. J., St-Louis, N., van Weeren, N., & van Genderen, A. M. 1989, *ApJ*, 343, 426
- Duijzens, M. F. J., van der Hucht, K. A., van Genderen, A. M., Schwarz, H. E., Linders, H. P. J., & Kolkman, O. M. 1996, *A&AS*, 119, 37
- Ebbets, D. 1979, *PASP*, 91, 804
- Firmani, C., Koenigsberger, G., Bisiacchi, G. F., Moffat, A. F. J., & Isserstedt, J. 1980, *ApJ*, 239, 607
- Fransson, C., & Fabian, A. C. 1980, *A&A*, 87, 102
- Friend, D. B., McGregor, K. B. 1984, *ApJ*, 282, 591
- Fullerton, A. W. 1990, Ph.D. Thesis, Univ. Toronto
- Fullerton, A. W., Gies, D. R., & Bolton, C. T. 1996, *ApJS*, 103, 475
- García-Segura, G., Langer, N., & McLow, M.-M. 1996, *A&A*, 316, 133
- Garmany, C. D., Conti, P. S., & Massey, P. 1980, *ApJ*, 242, 1063
- Glatzel, W., Kiriakidis, M., & Fricke, K. J. 1993, *MNRAS*, 262, L7
- Haberl, F., White, N. E., & Kallman, T. R. 1989, *ApJ*, 343, 409
- Hamann, W.-R. 1980, *A&A*, 84, 342
- Hatchett, S., & McCray, R. 1977, *ApJ*, 211, 552
- Henrichs, H. F. 1995, in Multi-Site Continuous Spectroscopy, ed. L. Huang, D. S. Zhai, C. Catala, & B. H. Foing, 11

- Hillier, D. J. 1984, ApJ, 280, 744
- Hillier, D. J. 1987, ApJS, 63, 965
- Hillier, D. J. 1988, ApJ, 327, 822
- Hillier, D. J. 1991, A&A, 247, 455
- Howarth, I. D., & Phillips, A. P. 1986, MNRAS, 222, 809
- Hundhausen, A. J. 1972, Coronal Expansion and Solar Wind (Berlin: Springer)
- Hutchings, J. B. 1974, ApJ, 188, 341
- Kaper, L., Hammerschlag-Hensberge, G., & van Loon, J. Th. 1993, A&A, 279, 485
- Lamontagne, R., Moffat, A. F. J., & Lamarre, A. 1986, AJ, 91, 925
- Lewis, D., Moffat, A. F. J., Matthews, J. M., Robert, C., & Marchenko, S. V. 1993, ApJ, 405, 312
- Lindgren, H., Lundström, I., & Stenholm, B. 1975, A&A, 44, 219
- McCandliss, S. R., Bohannan, B., Robert, C., & Moffat, A. F. J. 1994, Ap&SS, 221, 155
- McLean, I. S., Coyne, G. V., Frecker, J. E., & Serkowski, K. 1979, ApJ, 231, L141
- Malanushenko, V. P. 1988, Trudu Tartusskoi Astofis. Observatorii, 92, 60
- Marchenko, S. V., Antokhin, I. I., Bertrand, J.-F., Lamontagne, R., Moffat, A. F. J., Piceno, A., & Matthews, J. M. 1994, AJ, 108, 678
- Marchenko, S. V., Moffat, A. F. J., Eenens, P. R. J., Cardona, O., Echevarria, J., & Hervieux, Y. 1997, ApJ, in press
- Marchenko, S. V., Moffat, A. F. J., Lamontagne, R., & Tovmassian, G. H. 1996, ApJ, 461, 386
- Martinez, P., Kurtz, D., Ashley, R., & Tripe, P. 1994, Nature, 367, 601
- Massa, D., et al. 1995, ApJ, 452, L53

- Matthews, J. M., & Beech, M. 1987, *ApJ*, 313, L25
- Matthews, J. M., Moffat, A. F. J., & Marchenko, S. V. 1992a, *A&A*, 266, 409
- Matthews, J. M., St-Louis, N., Moffat, A. F. J., Drissen, L., Koenigsberger, G., Cardona, O., & Niemela, V. S. 1992b, in *ASP Conf. Proc. 22, Nonisotropic and Variable Outflows From Stars*, ed. L. Drissen, C. Leitherer, & A. Nota (San Francisco: ASP), 130
- Moffat, A. F. J. 1982, in *IAU Symp. 99, Wolf-Rayet Stars: Observations, Physics, Evolution*, ed. C. W. H. de Loore & A. J. Willis (Dordrecht: Kluwer), 263
- Moffat, A. F. J., Drissen, L., Lamontagne, R., & Robert, C. 1988, *ApJ*, 334, 1038
- Moffat, A. F. J., Firmani, C., McLean, I. S., & Seggewiss, W. 1982, in *IAU Symp. 99, Wolf-Rayet Stars: Observations, Physics, Evolution*, ed. C. W. H. de Loore & A. J. Willis (Dordrecht: Kluwer), 577
- Moffat, A. F. J., & Haupt, W. 1974, *A&A*, 32, 435
- Moffat, A. F. J., & Seggewiss, W. 1979, *A&A*, 77, 128
- Nichols, J. S., & Fesen, R. A. 1994, *A&A*, 291, 283
- Nichols-Bohlin, J., & Fesen, R. A. 1986, *AJ*, 92, 642
- Niedzielski, A. 1994, *A&A*, 282, 529
- Pakull, M., van Amerongen, S., Bakker, R., & van Paradijs, J. A. 1983, *A&A*, 122, 79
- Pismis, P., & Quintero, A. 1982, in *IAU Symp. 99, Wolf-Rayet Stars: Observations, Physics, Evolution*, ed. C. W. H. de Loore & A. J. Willis (Dordrecht: Kluwer), 305
- Pollock, A. M. T. 1989, *ApJ*, 347, 409
- Prinja, R. K., Barlow, M. J., & Howarth, I. D. 1990, *ApJ*, 361, 607
- Prinja, R. K., & Howarth, I. D. 1984, *A&A*, 133, 110
- Prinja, R. K., & Smith, L. J. 1992, *A&A*, 266, 377

- Reid, A. H. N., & Howarth, I. D. 1996, A&A, 311, 616
- Robert, C. 1992, Ph.D. Thesis, Univ. Montréal
- Robert, C., et al. 1992, ApJ, 397, 277
- Rochowicz, K., & Niedzielski, A. 1995, Acta Astron., 45, 307
- Ross, L. W. 1961, PASP, 73, 354
- Schulte-Ladbeck, R. E., Nordsieck, K. H., Taylor, M., Nook, M. A., Bjorkman, K. S., Magalhães, A. M., & Anderson, C. M. 1991, ApJ, 382, 301
- Schulte-Ladbeck, R. E., et al. 1992, ApJ, 391, L37
- Smith, L. F. 1968, MNRAS, 140, 409
- Smith, L. J., & Willis, A. J. 1994, Ap&SS, 221, 189
- Stella, L., White, N. E., & Rosner, R. 1986, ApJ, 308, 669
- Stevens, I. R., & Willis, A. J. 1988, MNRAS, 234, 783
- St-Louis, N. 1994, Ap&SS, 221, 197
- St-Louis, N., Dalton, M. J., Howarth, I. D., Willis, A. J., & Conti, P. S. 1997, ApJ, submitted
- St-Louis, N., Dalton, M. J., Marchenko, S. V., Moffat, A. F. J., & Willis, A. J. 1995, ApJ, 452, L57 (WRMEGA)
- St-Louis, N., Howarth, I. D., Willis, A. J., Stickland, D. J., Smith, L. J., Conti, P. S., & Garmany, C. D. 1993, A&A, 267, 447
- Thompson, I. B., & Landstreet, J. D. 1985, ApJ, 289, L9
- Tjemkes, S. A., Zuiderwijk, E. J., & van Paradijs, J. 1986, A&A, 154, 77
- Tutukov, A. V., & Yungelson, L. R. 1973, Nauch. Inf. Astrosov. Acad. Nauk USSR, 27, 58
- Underhill, A. B., & Yang, S. 1991, ApJ, 368, 588
- van Genderen, A. M. 1981, A&A, 96, 82

- van den Heuvel, E. P. J., & De Loore, C. 1973, A&A, 25, 387
- van Kerkwijk, M. H., Geballe, T. R., King, D. L., van der Klis, M., & van Paradijs, J. 1996, A&A, 314, 521
- van Oijen, J. G. J. 1989, A&A, 217, 115
- van Paradijs, J. A. 1983, in Accretion-Driven Stellar X-Ray Sources, ed. W. H. G. Lewin & E. P. J. van der Heuvel (Cambridge: Cambridge Univ. Press), 189
- van Paradijs, J. A., Hammerschlag-Hensberge, G., & Zuiderwijk, F. J. 1978, A&AS, 31, 189
- Vanbeveren, D. 1991, Space Sci. Rev., 56, 249
- Vanbeveren, D., van Rensbergen, W., & de Loore, C. 1982, A&A, 115, 69
- Vreux, J.-M. 1985, PASP, 97, 274
- Vreux, J.-M., Gosset, E., Bohannan, B., & Conti, P. S. 1992, A&A, 256, 148
- Waters, L. B. F. M., Taylor, A. R., van den Heuvel, E. P. J., Habets, G. M. H. J., & Persi, P. 1988, A&A, 198, 200
- White, N. E. 1985, in Interacting Binaries, ed. P. P. Eggleton & J. E. Pringle (Dordrecht: Reidel), 249
- White, R. L., & Long, K. S. 1986, ApJ, 310, 832
- Willis, A. J., Howarth, I. D., Smith, L. J., Garmany, C. D., & Conti, P. S. 1989, A&AS, 77, 269
- Willis, A. J., Schild, H., Howarth, I. D., & Stevens, I. R. 1994, Ap&SS, 221, 321
- Willis, A. J., van der Hucht, K. A., Conti, P. S., & Garmany, D. 1986, A&AS, 63, 417

TABLEAU 2.1. Narrowband photometry of EZ CMa in 1995

HJD – 2,440,000	Phase	$u(\text{WR} - \text{c1})$	$u(\text{c2} - \text{c1})$	$v(\text{WR} - \text{c1})$	$v(\text{c2} - \text{c1})$	Rapid Photometry
9730.5864	0.808	– 0.594	0.362	0.790	0.310	—
9730.6965	0.837	– 0.605	0.349	0.785	0.304	
9730.7655	0.855	– 0.602	0.360	0.770	0.303	
9730.8171	0.869	—	—	0.778	0.301	
9732.5952	0.341	– 0.663	0.349	0.721	0.306	—
9732.6829	0.364	– 0.673	0.351	0.723	0.313	
9732.8557	0.410	– 0.648	0.354	0.740	0.305	
9733.6656	0.625	– 0.561	0.352	0.822	0.306	—
9733.7450	0.647	– 0.574	0.353	0.809	0.308	
9733.8308	0.669	– 0.578	0.352	0.806	0.298	
9734.5461	0.859	– 0.622	0.356	0.768	0.307	1
9734.6280	0.881	– 0.634	0.357	0.758	0.307	
9734.7792	0.921	– 0.620	0.348	0.756	0.302	
9734.8225	0.933	– 0.611	0.357	0.774	0.313	
9735.5551	0.127	– 0.699	0.346	0.721	0.302	1
9735.6195	0.144	– 0.688	0.351	0.705	0.307	
9735.6750	0.159	– 0.690	0.347	0.706	0.304	
9735.7328	0.174	– 0.692	0.348	0.702	0.304	
9735.8059	0.194	– 0.680	0.338	0.714	0.309	
9735.8474	0.205	– 0.674	0.361	0.714	0.305	
9736.5702	0.397	– 0.653	0.355	0.732	0.300	2
9736.6239	0.411	– 0.660	0.349	0.733	0.310	
9736.7108	0.434	– 0.648	0.353	0.738	0.300	
9736.7777	0.452	– 0.634	0.358	0.750	0.302	
9736.8095	0.460	– 0.640	0.348	0.747	0.304	
9736.8472	0.470	– 0.632	0.347	0.754	0.305	
9737.5537	0.658	– 0.602	0.352	0.794	0.299	2
9737.6080	0.672	– 0.591	0.357	0.797	0.315	
9737.6970	0.696	– 0.595	0.347	0.793	0.315	
9737.7631	0.713	– 0.591	0.353	0.798	0.310	
9737.7962	0.722	– 0.594	0.356	0.790	0.306	
9737.8223	0.729	– 0.588	0.352	0.785	0.308	
9738.5516	0.923	– 0.614	0.351	0.774	0.303	2
9738.6087	0.938	– 0.612	0.353	0.776	0.311	
9738.6972	0.961	– 0.595	0.350	0.786	0.312	

TABLEAU 2.1. Continued

HJD - 2,440,000	Phase	$u(\text{WR} - \text{c1})$	$u(\text{c2} - \text{c1})$	$v(\text{WR} - \text{c1})$	$v(\text{c2} - \text{c1})$	Rapid Photometry
9738.7564	0.977	- 0.597	0.349	0.792	0.309	
9738.7872	0.985	- 0.592	0.351	0.793	0.307	
9738.8195	0.994	- 0.593	0.350	0.791	0.316	
9738.8506	0.002	- 0.604	0.354	0.784	0.310	
9739.5510	0.188	- 0.675	0.350	0.718	0.304	2
9739.6063	0.203	- 0.671	0.353	0.720	0.311	
9739.6918	0.226	- 0.662	0.349	0.733	0.307	
9739.7538	0.242	- 0.653	0.351	0.734	0.304	
9739.7846	0.250	- 0.664	0.356	0.725	0.309	
9739.8133	0.258	- 0.659	0.352	0.728	0.311	
9739.8535	0.269	- 0.649	0.356	0.729	0.305	
9740.5700	0.459	- 0.644	0.363	0.735	0.309	—
9740.6046	0.468	- 0.637	0.341	0.741	0.311	
9740.6562	0.482	- 0.626	0.351	0.760	0.308	
9741.5515	0.720	- 0.592	0.354	0.785	0.308	1
9741.5877	0.729	- 0.600	0.350	0.787	0.303	
9741.6200	0.737	- 0.599	0.351	0.783	0.307	
9741.6513	0.746	- 0.604	0.344	0.782	0.310	
9741.7075	0.761	- 0.605	0.358	0.772	0.310	
9741.7679	0.777	- 0.604	0.350	0.784	0.310	
9741.7977	0.785	- 0.602	0.350	0.784	0.312	
9741.8260	0.792	- 0.597	0.357	0.784	0.308	
9742.5518	0.985	- 0.590	0.352	0.799	0.312	2
9742.6006	0.998	- 0.590	0.355	0.794	0.306	
9742.6791	0.019	- 0.601	0.349	0.785	0.312	
9742.7104	0.027	- 0.609	0.353	0.778	0.306	
9742.7681	0.042	- 0.610	0.348	0.780	0.309	
9742.7986	0.051	- 0.628	0.341	0.767	0.306	
9742.8274	0.058	- 0.626	0.350	0.764	0.305	
9743.5456	0.249	- 0.658	0.361	0.738	0.310	2
9743.5955	0.262	- 0.659	0.355	0.728	0.305	
9743.6495	0.276	- 0.660	0.352	0.732	0.312	
9743.7026	0.291	- 0.652	0.349	0.738	0.311	
9743.7255	0.297	- 0.660	0.348	0.738	0.306	
9743.7804	0.311	- 0.663	0.347	0.725	0.308	

TABLEAU 2.1. Continued

HJD - 2,440,000	Phase	$u(\text{WR} - \text{c1})$	$u(\text{c2} - \text{c1})$	$v(\text{WR} - \text{c1})$	$v(\text{c2} - \text{c1})$	Rapid Photometry
9743.8107	0.319	- 0.669	0.357	0.727	0.309	
9743.8414	0.327	- 0.658	0.345	0.727	0.308	
9744.5517	0.516	- 0.592	0.348	0.782	0.300	2
9744.6008	0.529	- 0.588	0.361	0.798	0.307	
9744.6535	0.543	- 0.584	0.349	0.798	0.305	
9744.7074	0.557	- 0.590	0.339	0.803	0.313	
9744.7600	0.571	- 0.585	0.346	-	0.309	
9744.7885	0.579	- 0.601	0.344	0.806	0.309	
9744.8148	0.586	- 0.587	0.351	0.788	0.315	
9744.8420	0.593	- 0.607	0.343	0.787	0.309	
9745.5512	0.781	- 0.591	0.353	0.794	0.307	2
9745.5987	0.794	- 0.599	0.354	0.790	0.309	
9745.6523	0.808	- 0.598	0.352	0.782	0.310	
9745.7049	0.822	- 0.595	0.357	0.797	0.305	
9745.7591	0.837	- 0.607	0.359	0.784	0.307	
9745.7865	0.844	- 0.605	0.354	0.784	0.308	
9745.8124	0.851	- 0.613	0.349	0.778	0.315	
9745.8387	0.858	- 0.610	0.351	0.777	0.310	
9746.5583	0.049	- 0.624	0.351	0.769	0.308	1
9746.6089	0.062	- 0.633	0.345	0.755	0.301	
9746.6536	0.074	- 0.648	0.348	0.750	0.311	
9746.7076	0.089	- 0.659	0.353	0.738	0.314	
9746.8162	0.117	- 0.678	0.347	0.719	0.310	
9747.5841	0.321	- 0.656	0.362	0.737	0.313	1
9747.6388	0.336	- 0.660	0.354	0.735	0.311	
9747.7242	0.358	- 0.662	0.351	0.738	0.309	
9747.8227	0.384	- 0.671	0.361	0.731	0.308	
9748.5760	0.585	- 0.585	0.353	0.793	0.307	—
9748.6332	0.600	- 0.597	0.354	0.789	0.302	
9748.7168	0.622	- 0.606	0.349	0.790	0.310	
9748.7629	0.634	- 0.591	0.349	0.797	0.311	
9748.8137	0.648	-	0.348	0.804	0.310	
9749.6736	0.876	- 0.637	0.355	0.770	0.311	2
9749.7257	0.890	- 0.618	0.351	0.773	0.307	
9749.7946	0.908	- 0.609	0.354	0.773	0.301	

TABLEAU 2.2. Doppler velocities corresponding to the maxima of the TVS of different lines^a

N IV λ 4058	He II λ 4200	He II λ 4339	He II λ 4542	He II λ 4686	He II λ 4859
				- 1910	
					- 1070
- 960	- 810	- 770	- 780		
- 140	- 130	- 170	- 200	- 260	- 120
	+ 1140	+ 1120	+ 1140		+ 1180
			+ 1740	+ 2140	

N V λ 4945	He II λ 5412	C IV λ 5806	He II λ 6560	He II λ 6683
			- 1700	
	- 1270	- 1290		- 1270
- 740				
+ 60	- 230		- 260	- 230
	+ 1160		+ 1190	
	+ 1800		+ 1920	

^a In km s⁻¹ and referred to the laboratory rest wavelength (note that the lines may have different "systemic" velocities in a WR wind, e.g., the difference between N V and the He II lines may amount to about 350 km s⁻¹ (Smith & Willis 1994).

TABLEAU 2.3. Velocities of the prominent σ subpeaks observed in the P Cygni absorption components^a

N IV λ 1718	He I λ 3889	He I λ 4471	N V λ 4604	N V λ 4620	He I λ 5876
- 2300		- 1940			- 2120
- 1100	- 1280	- 1330	- 890	- 930	- 1380

^a In km s⁻¹ and referred to the laboratory rest wavelength.

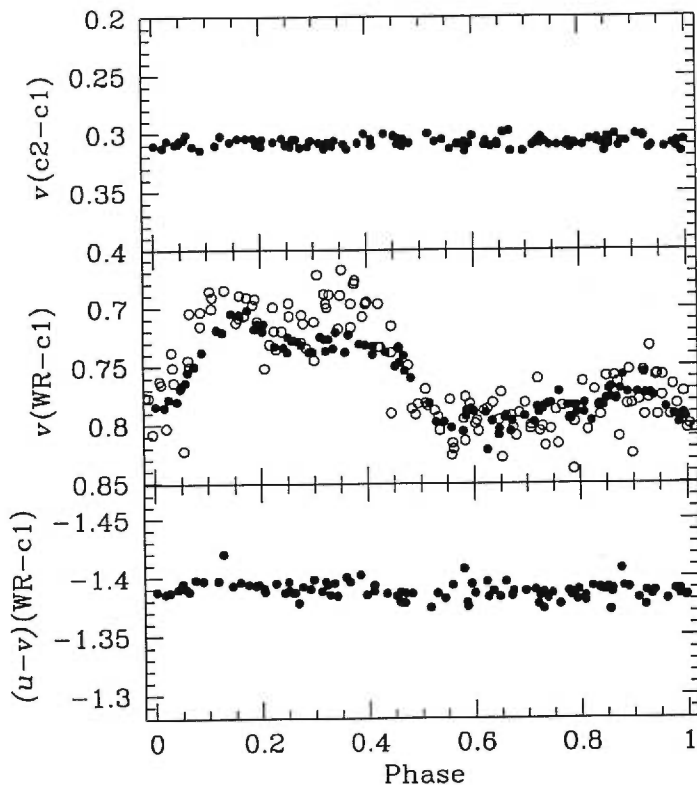


FIGURE 2.1. Light curve of EZ CMa. *Upper panel:* differential v magnitudes for the c1 and c2 comparison stars. *Central panel:* v -filter light curve (*filled dots*); combined *IUE* continuum (*open symbols*; see text). *Bottom panel:* $u - v$ color variations.

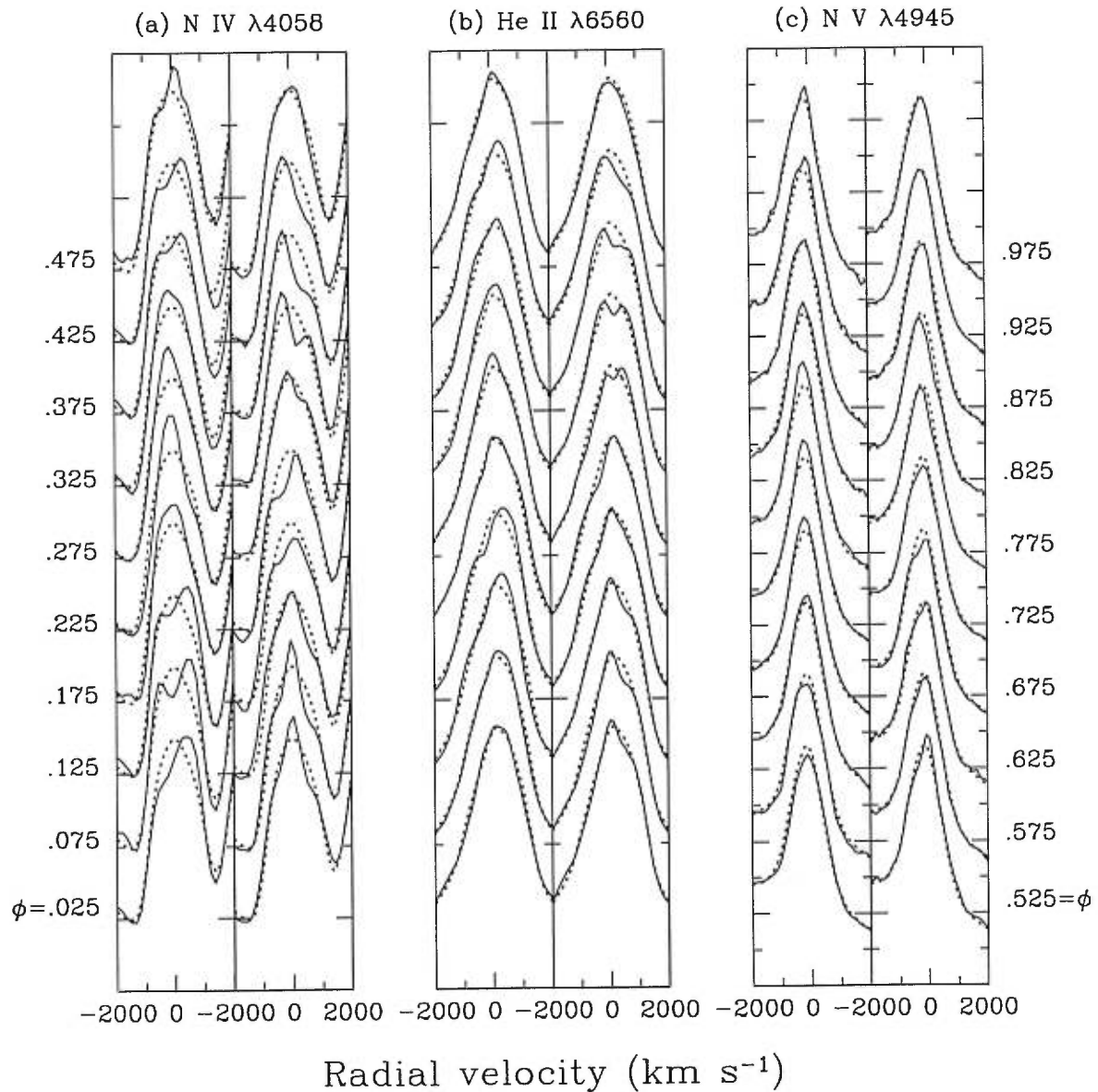


FIGURE 2.2. Time series of (a) N IV $\lambda 4058$, (b) He II $\lambda 6560$, and (c) N V $\lambda 4945$. The rectified spectra were binned to a 0.05 phase interval. The corresponding mean phases are indicated on both sides of this plot. The mean profile is overplotted as a dashed line. The intensities are in arbitrary units.

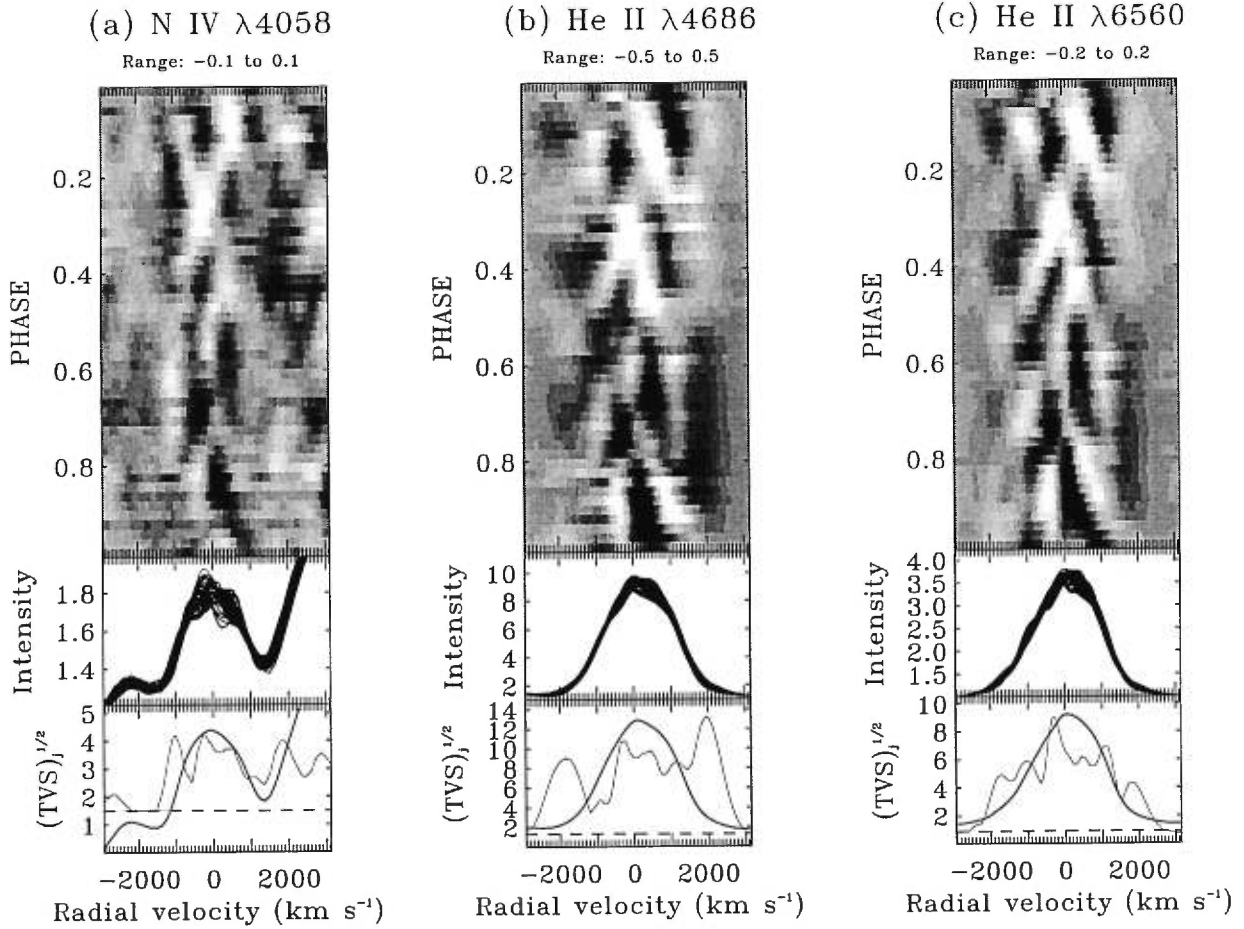


FIGURE 2.3. Gray-scale plot of the time series of the residuals of (a) N IV $\lambda 4058$, (b) He II $\lambda 4686$, and (c) He II $\lambda 6560$. These residuals (the mean profile subtracted from the individual profiles) were binned to a 0.02 phase interval. An extra emission component appears brighter in these plots. The middle panel presents the superposition of the different rectified profiles. The values of $(\text{TVS})_j^{1/2}$ (§2.3.2.3) and the mean profile (in arbitrary units) are presented in the lower panel. The horizontal dashed line indicates the 99 % variability detection threshold. All velocities are heliocentric.

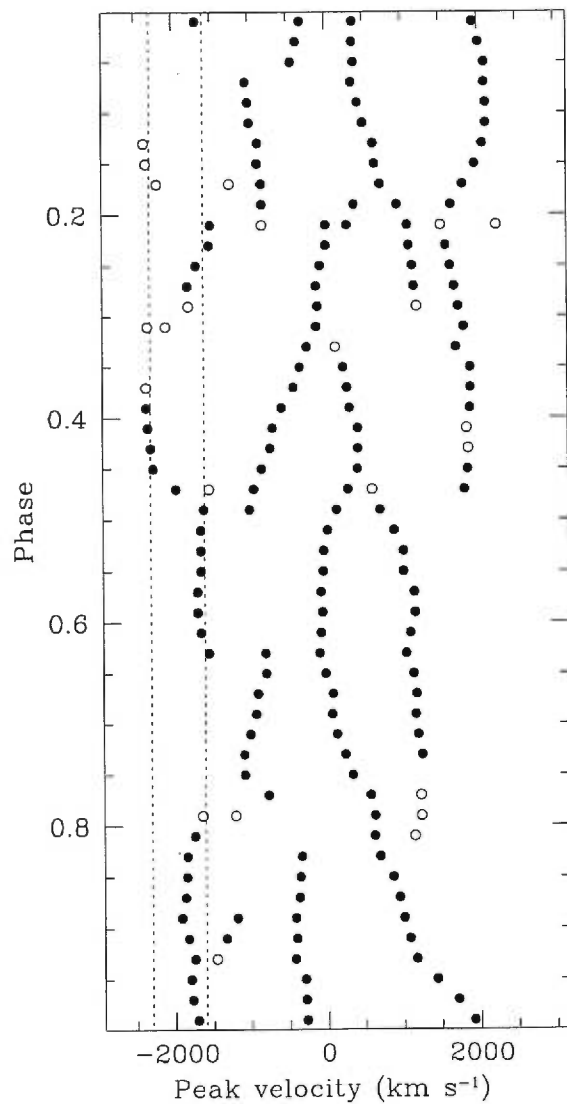


FIGURE 2.4. Estimation of the Doppler shifts (referred to the laboratory rest wavelength) associated with the different subpeaks traveling across the He II $\lambda 6560$ line-profile. Measurements indicated with a black dot possess a higher degree of confidence. The dashed lines indicate the isovelocities -1600 and -2300 km s^{-1} (see text).

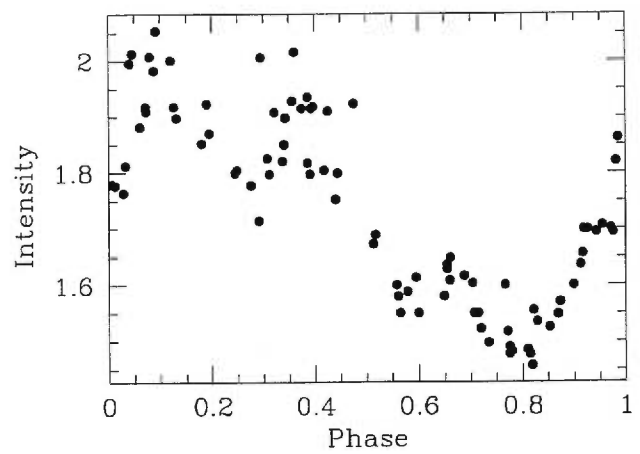


FIGURE 2.5. Red-wing intensity of He II $\lambda 4686$ measured at 4719 Å.

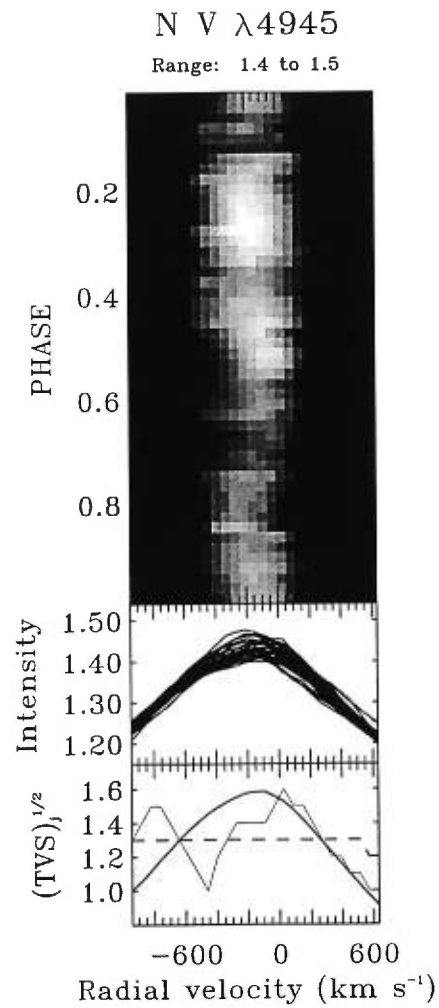


FIGURE 2.6. Gray-scale plot of the time series of N V λ 4945. The rectified spectra were binned to a 0.02 phase interval. The middle panel presents the superposition of the different rectified profiles. The value of $(\text{TVS})_j^{1/2}$ (§2.3.2.3) and the mean profile (in arbitrary units) are presented in the lower panel. The horizontal dashed line indicates the 99 % variability detection threshold. All velocities are heliocentric.

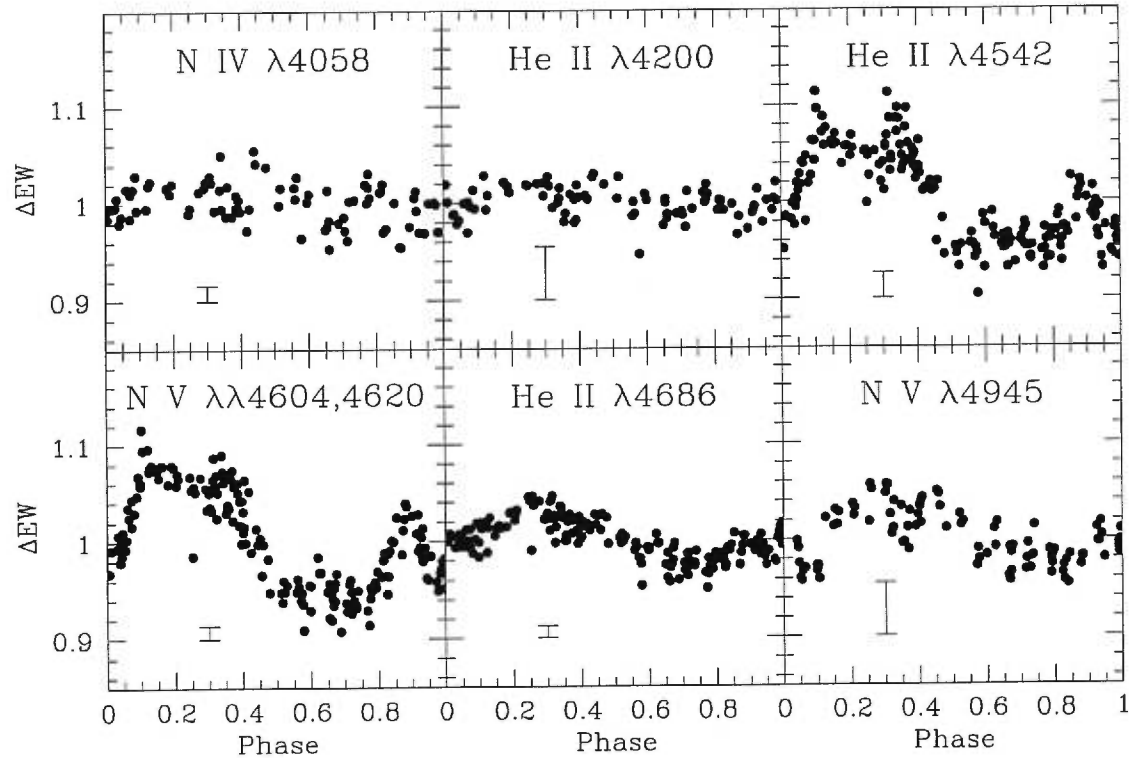


FIGURE 2.7. Equivalent widths (normalized to the mean value) of six selected transitions. The error bars (2σ) were calculated according to Chalabaev & Maillard (1983).

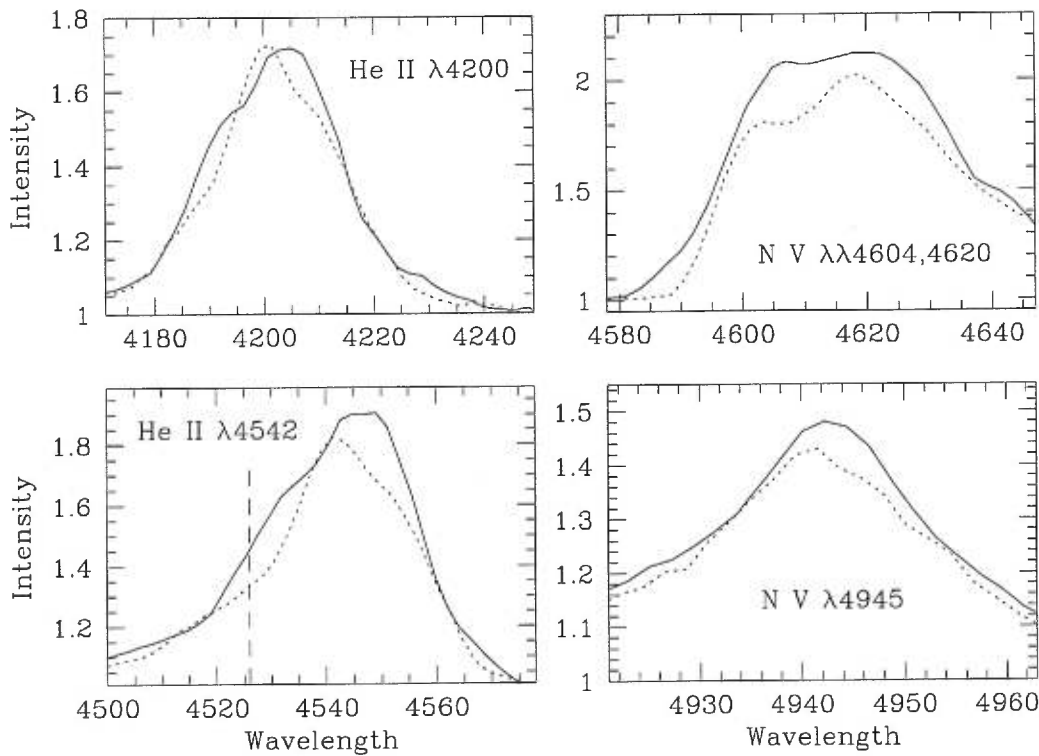


FIGURE 2.8. Comparison of the He II $\lambda 4200$, He II $\lambda 4542$, N V $\lambda\lambda 4604, 4620$, and N V $\lambda 4945$ line-profiles associated with the minimum (*dashed line*; $\phi \approx 0.579$ for the helium transitions, $\phi \approx 0.839$ for N V $\lambda 4945$) and the maximum EW values (*solid line*; $\phi \approx 0.120$ for the helium transitions, $\phi \approx 0.256$ for N V $\lambda 4945$). The wavelength range of these figures corresponds to the limits where the equivalent width measurements were performed (except for He II $\lambda 4542$: longward of 4526 Å).

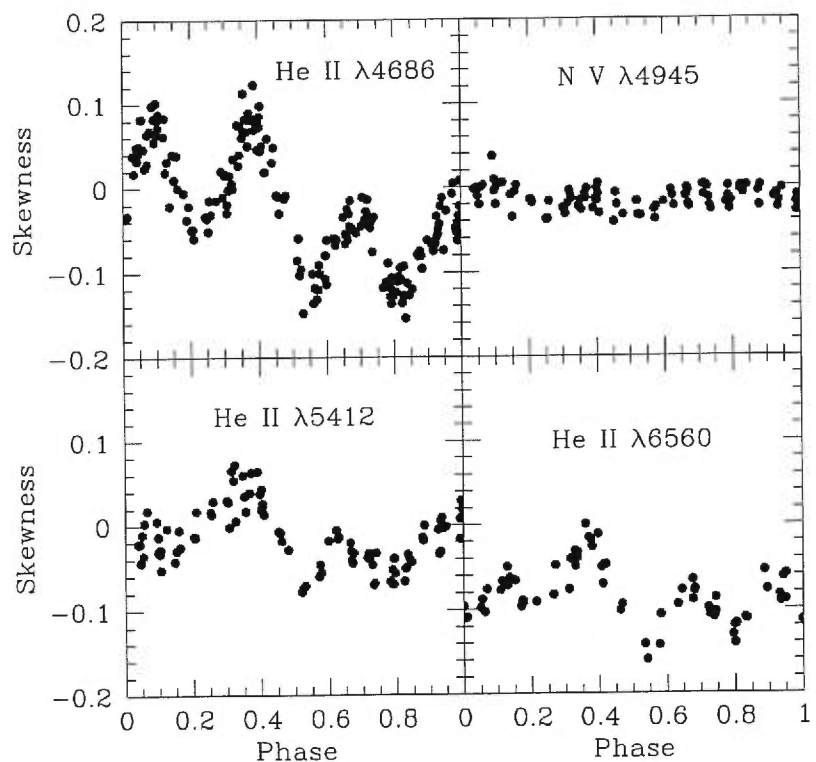


FIGURE 2.9. Skewness measurements for four selected transitions.

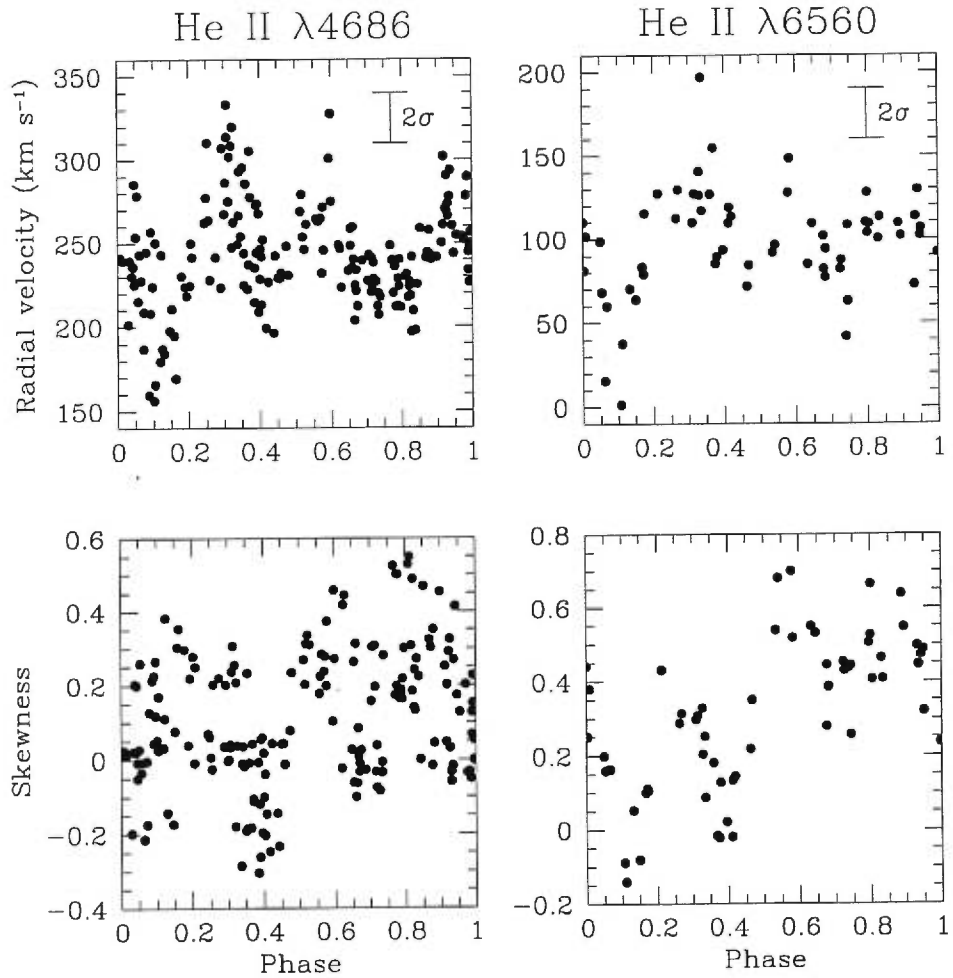


FIGURE 2.10. Comparison between the heliocentric radial velocities and the skewness measurements for He II $\lambda 4686$ (*left panels*) and He II $\lambda 6560$ (*right panels*). Both measurements were performed for the intensity ranges 3-6.5 and 1.35-2.5 for He II $\lambda 4686$ and He II $\lambda 6560$, respectively.

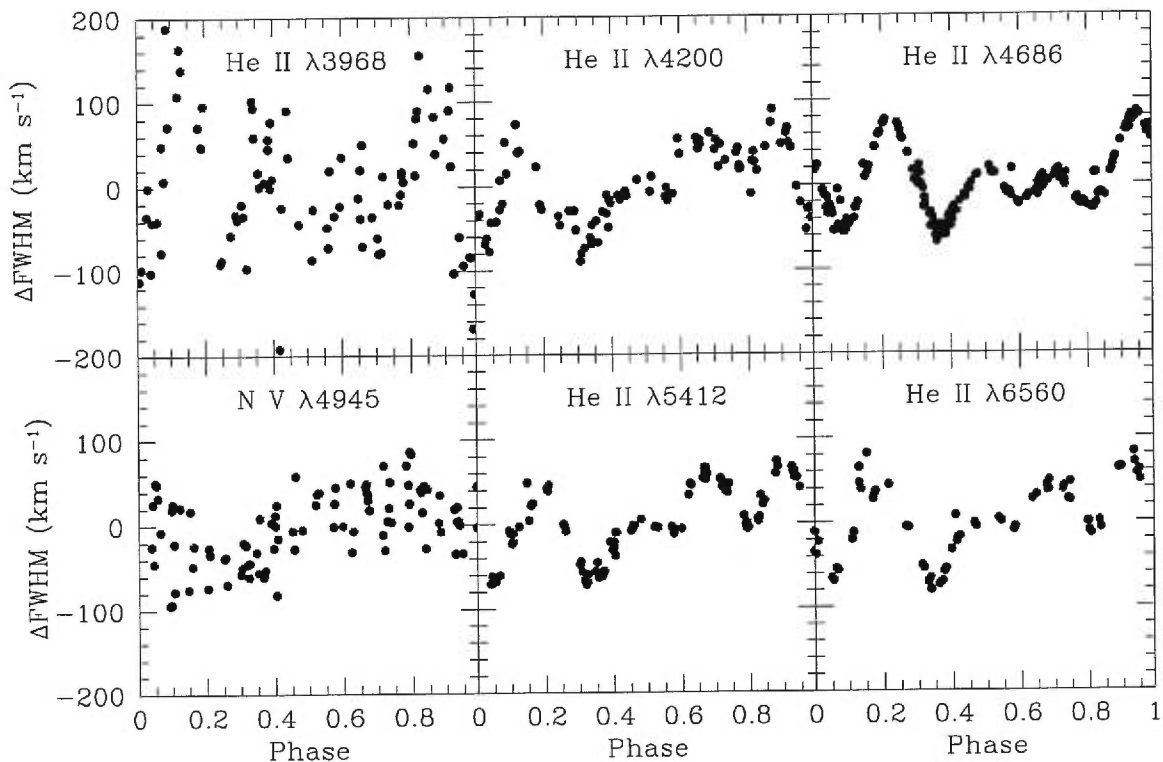


FIGURE 2.11. Deviations of the full width at half-maximum around the mean value for six selected transitions.

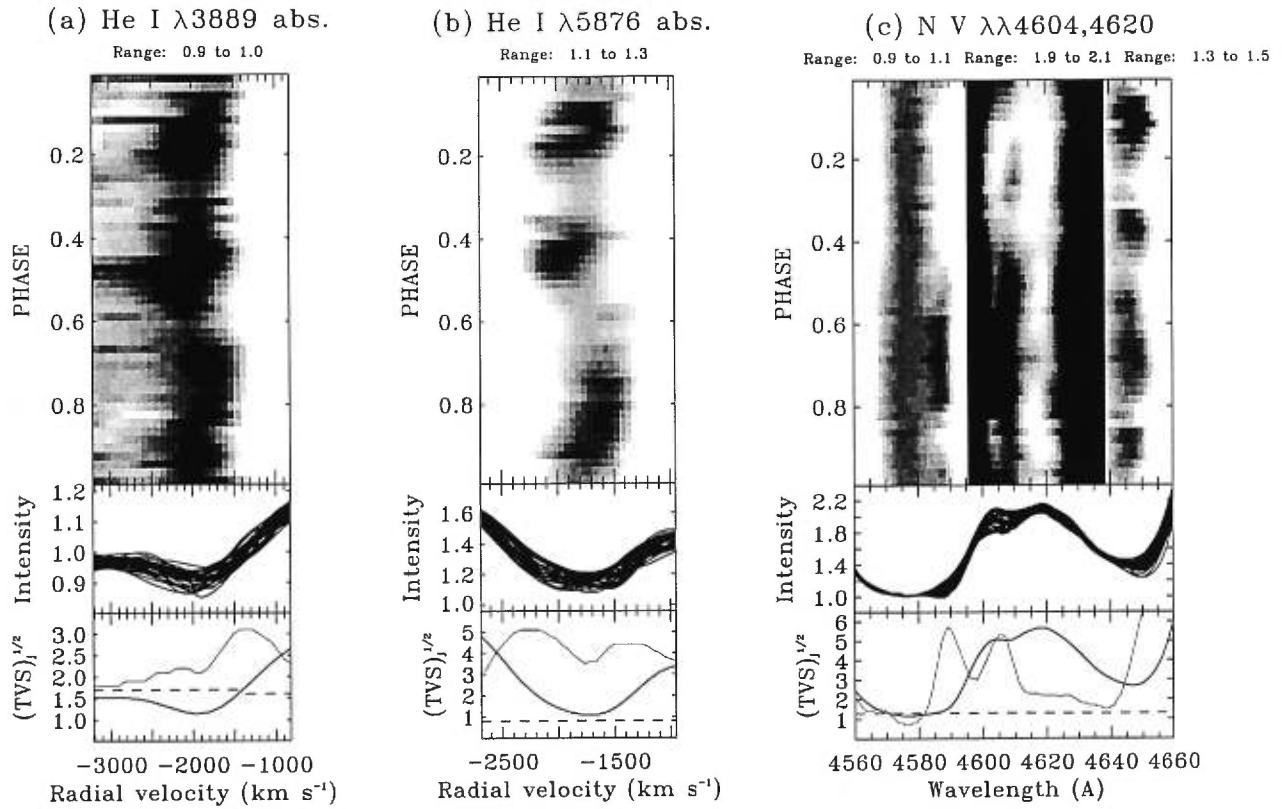


FIGURE 2.12. Gray-scale plots of the time series of the P Cygni absorption components of (a) He I $\lambda 3889$, (b) He I $\lambda 5876$, and (c) N V $\lambda\lambda 4604, 4620$. In (c), the selected wavelength domain is displayed for three different intensity intervals. The blue wing variability of He II $\lambda 4686$ is shown at the very right panel of this figure.

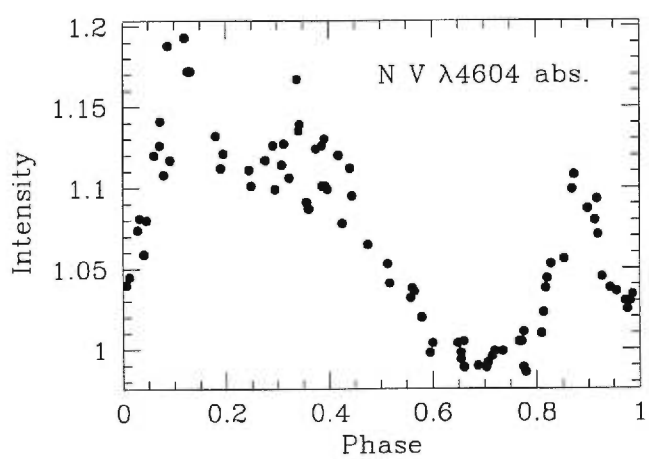


FIGURE 2.13. Intensity of the N V $\lambda 4604$ line-profile measured at 4588 Å.

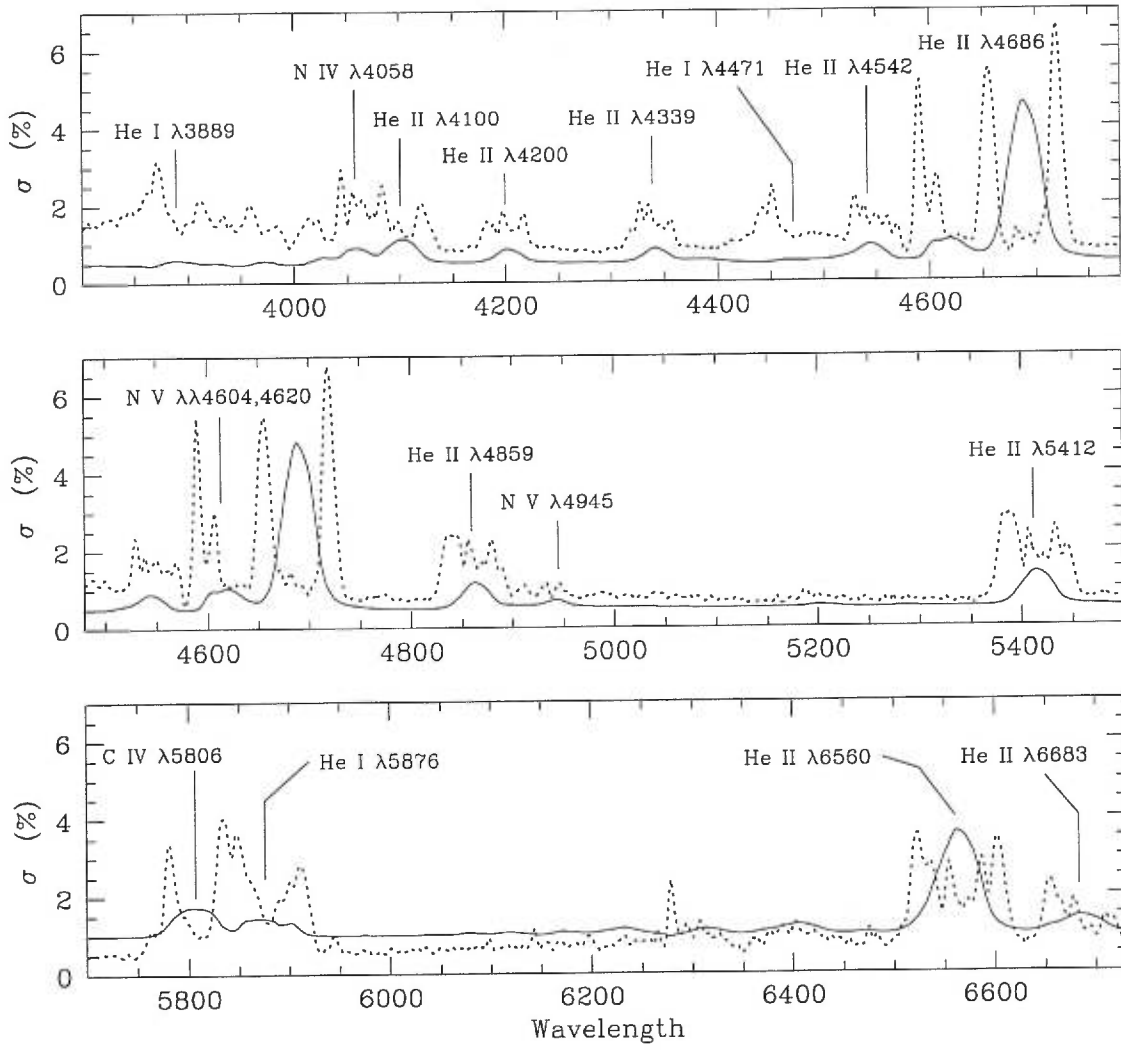


FIGURE 2.14. Superposition of the σ spectrum (*dashed line*) and the mean spectrum (*solid line*, arbitrary units). Small imperfections of the wavelength calibration lead to spurious peaks at the location of the interstellar and telluric lines (for example around 6279 Å).

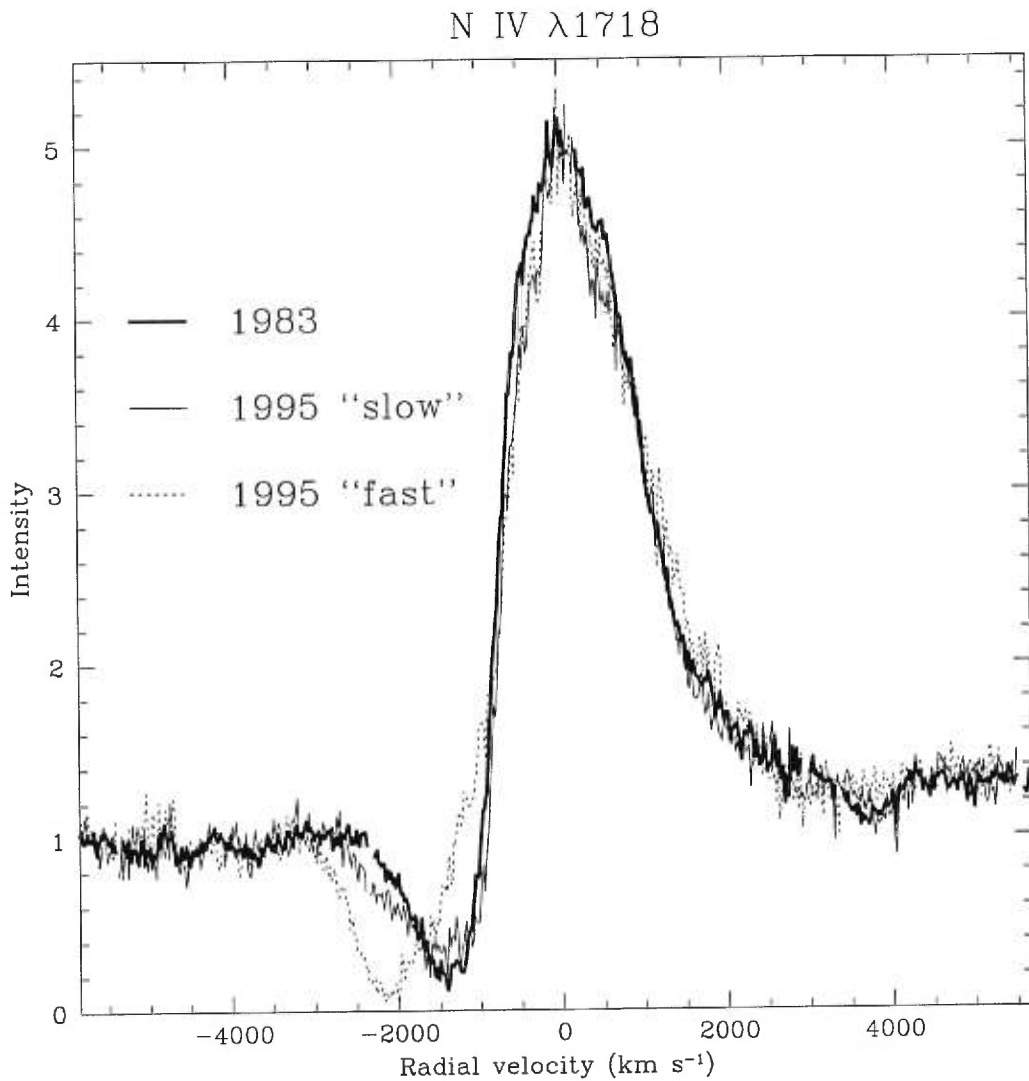


FIGURE 2.15. Comparison between the representative line-profiles of N IV $\lambda 1718$ for the low- (*thin line*) and high-velocity states (*dotted line*) as observed by *IUE* in 1995 January, with the one of 1983 September (*thick line*). The 1995 spectra were corrected for the changes of the continuum flux (§2.2.2).

CHAPITRE 3

COUPLED LINE-PROFILE AND CONTINUUM VARIATIONS IN EZ CANIS MAJORIS: IMPLICATIONS FOR THE DRIVING MECHANISM OF GLOBAL WIND STRUCTURES IN WOLF-RAYET WINDS

The Astrophysical Journal, 498, 413 (1998)

**COUPLED LINE-PROFILE AND CONTINUUM
VARIATIONS IN EZ CANIS MAJORIS:
IMPLICATIONS FOR THE DRIVING MECHANISM
OF GLOBAL WIND STRUCTURES IN
WOLF-RAYET WINDS**

Thierry Morel,¹ Nicole St-Louis,¹ Anthony F. J. Moffat,¹ Octavio Cardona,²
Gloria Koenigsberger,³ and Grant M. Hill⁴

Received 1997 August 20; accepted 1997 December 11

Article submitted to the Astrophysical Journal main section.

¹ Département de Physique, Université de Montréal, C.P. 6128, Succ. Centre-Ville, Montréal, Québec, Canada, H3C 3J7; and Observatoire du Mont Mégantic.

² Instituto Nacional de Astrofísica, Optica y Electrónica, Apdo. Postal 51, Puebla, Pue. 72000, México.

³ Instituto de Astronomía, UNAM, Apdo. Postal 70-264, México D.F. 04510, México.

⁴ National Research Council, Herzberg Institute of Astrophysics, Dominion Astrophysical Observatory, 5071 West Saanich Road, Victoria, British Columbia, Canada, V8X 4M6; present address: McDonald Observatory, HET, P. O. Box 1337, Fort Davis, TX.

ABSTRACT

EZ CMa is an apparently unusual Wolf-Rayet star of the nitrogen sequence that exhibits strong variations on a period of 3.77 days with coherency lasting typically about 10 cycles. We have used an extensive set of optical spectroscopic observations to investigate a possible link between its line-profile and photometric continuum variability. Despite the strong epoch dependency of the variations, a persistent correlation is found between changes in the wind line profiles ($\mathrm{N}\ \mathrm{V}$ $\lambda\lambda 4604, 4620$ in particular) and in continuum flux emanating near the stellar core.

We suggest that these observations give further support to the idea that the physical conditions prevailing in the vicinity of the star's photosphere have a significant impact on the wind structure and that a spatial dependence of these conditions at the base of the outflow induces the formation of azimuthal wind structures in EZ CMa. The epoch-dependent nature of the variability could be related to long-term behavior of corotating magnetic structures, although pulsational instabilities constitute a viable alternative.

Subject headings: stars: individual (EZ Canis Majoris) — stars: mass loss — stars: Wolf-Rayet

3.1 Introduction

Although a few early investigations of spectral variability of OB stars concluded that, in some cases, the outflow is probably far from being spherically symmetric or steady (e.g., Ebbets 1982; Grady, Snow, & Timothy 1983), it is only recently that a global view of the phenomenon and a comprehensive picture have begun to emerge (e.g., Howarth, Prinja, & Massa 1995; Massa, Prinja, & Fullerton 1995; Prinja, Massa, & Fullerton 1995; Kaper et al. 1996, 1997; Kaufer et al. 1996a, 1996b; Reid & Howarth 1996; Prinja, Fullerton, & Crowther 1996). In the light of these studies, some fundamental conclusions can be drawn: (i) the timescale of the wind line-profile variations (LPVs) is generally compatible with the stellar rotation period, which could imply that the variability is induced by the rotational modulation of a large-scale inhomogeneous outflow and (ii) there is some evidence for a direct link between photospheric and wind activity, pointing to mechanisms such as photospheric magnetic structures or (non)radial pulsations to trigger the formation of such aspherical winds.

Hydrodynamical simulations by Cranmer & Owocki (1996) have indeed demonstrated that an azimuthal dependence of the radiative flux emanating from the photosphere (due, e.g., to pulsations; Fullerton, Gies, & Bolton 1996) can lead to a structured wind with streams curved by the stellar rotation outflowing at different speeds from the “active” regions. In essence, an analogy can be made with the “corotating interaction regions” which are characteristic features of the solar corona (Hundhausen 1972; Gosling 1996). The ability of this conceptually simple model to reproduce the behavior of the “discrete absorption components” (DACs) moving shortward in the P Cygni absorption components of the UV resonance lines of most O stars raises the possibility that the development of such structures could be widespread among the OB-star population (Cranmer & Owocki 1996; Owocki, Cranmer, & Fullerton 1995). Their possible occurrence in hot-star winds was first discussed from a qualitative viewpoint by Mullan (1984,

1986) and Harmanec (1991).

The existence of globally aspherical outflows in Wolf-Rayet (WR) stars is currently a matter of debate, although the lack of depolarization (compared to continuum polarization) across the emission lines of the majority of these objects suggests that in first approximation the outflows are spherically symmetric (Schulte-Ladbeck 1995; Harries, Hillier, & Howarth 1998). However, although most of the spectral and photometric variability displayed by single WR stars can generally be ascribed to the strong stochastic inhomogeneities at relatively small scales, which may be ubiquitous in all radiatively driven outflows (Moffat & Robert 1992; Eversberg, Lépine, & Moffat 1998), a small number of remarkable WR stars present systematic, large-scale spectral variations, which are probably induced by an additional phenomenon, possibly the same that generates DACs in O-star winds (Lépine, Moffat, & Henriksen 1996). In addition, these WR stars are among the few that present strong, variable depolarization in their line profiles (see, e.g., Schulte-Ladbeck et al. 1992). Hence, a global departure from isotropic outflow could constitute a natural explanation for these observed large-scale changes. Furthermore, recent intensive photometric and spectroscopic monitoring of WN 8 stars has shown that physical processes operating in the deepest (“invisible”) layers of their winds could be, as in OB stars, responsible for their intrinsically high level of variability (Marchenko et al. 1998).

What might turn out to be the “prototype” of this class is the WN 5 (WN 4 in the new three-dimensional system of Smith, Shara, & Moffat 1996) star EZ CMa (WR 6, HD 50896), which exhibits an unusual and striking periodic variability (with $\mathcal{P} = 3.77$ days) in spectrophotometry (Firmani et al. 1980), continuum photometry (Antokhin et al. 1994), and polarimetry (Robert et al. 1992). Because of the periodicity of the changes and the lack of detection of a normal stellar companion, some authors have suggested that this WR star harbors a compact companion (Ebbets 1979; Firmani et al. 1980). This appealing

conclusion has, however, often been questioned on various grounds in the literature (e.g., Stevens & Willis 1988; Willis et al. 1989; St-Louis et al. 1993). The controversial nature of this object is illustrated by the fact that models including an orbiting neutron star companion or variability intrinsic to the wind itself have both been claimed to give an acceptable fit to the spectroscopic data (Matthews et al. 1992b; Koenigsberger 1995). Recently, further arguments were presented against the possible duplicity of this object (Morel, St-Louis, & Marchenko 1997; hereafter, MSM); rather, it has been suggested that the unique 3.77 day period, known for a long time in all modes of observation, is induced by the rotational modulation of the structured WR envelope. This conclusion was also reached by St-Louis et al. (1995, 1998) from an analysis of spectral variability in the ultraviolet. In view of the tight correlation found between the photometric and spectroscopic changes, the triggering of the wind variability by some process (probably of magnetic or pulsational origin) operating near the stellar core was also proposed.

In this paper, we present an extensive set of optical spectroscopic observations spread over 3 years (1991-1994). In view of the well-known epoch-dependent nature of the spectroscopic and photometric variability of EZ CMa (St-Louis et al. 1993, 1995; Duijsens et al. 1996), the main goal of this study is to investigate the relationship between the level of continuum flux emerging from the inner stellar wind, closest to the stellar core, and the spectroscopic changes, on a much longer timescale than done by MSM. To achieve this, we will discuss the pattern of spectral variability at different epochs in connection with (quasi-)simultaneously acquired archival, as well as new, optical light curves.

Following a description of the spectroscopic data and of their reduction (§3.2.1), we will present new *UBV* light curves in §3.2.2. The LPVs will be discussed in §3.3, while §3.4.1 will emphasize their direct link with the photometric variations. Finally, the cause of a nonisotropic base outflow will be explored in

§3.4.2.

3.2 Observations

3.2.1 Spectroscopy

We observed EZ CMa on several occasions between 1991 and 1994. The journal of observations is presented in Table 3.1, which lists successively the epoch number, the date of the spectroscopic observations, the interval of the observations in Heliocentric Julian Days, the observatory name, the number of spectra obtained, the selected spectral domain, the reciprocal dispersion of the spectra, and the typical signal-to-noise ratio (S/N) in the continuum. The last three columns of Table 3.1 indicate which data set was used for the correction of the continuum variability (see below). Part of this large data set (epochs I and III) has already been briefly discussed by St-Louis (1994). A detailed description of the epoch I data set is presented by Cardona et al. (1998).

Standard reduction procedures (i.e., bias subtraction, flat-fielding, removal of cosmic-ray events, background subtraction, extraction of the spectra, and wavelength calibration) were carried out using **IRAF**¹ software packages. For the rectification of the spectra with respect to the continuum, a third- to sixth-order Legendre polynomial was fitted to carefully selected line-free regions. For the last three epochs, consecutive exposures obtained over short periods of time (generally a few minutes) were combined, leading to a significantly higher S/N in the net spectrum (Table 3.1). No short-term variations were detected from one exposure to another. Note that the timescales involved are too short to detect any significant motion of “blobs”.

¹IRAF is distributed by the National Optical Astronomy Observatories, operated by the Association of Universities for Research in Astronomy, Inc., under cooperative agreement with the National Science Foundation.

In order to remove the contribution to the line variability induced by the rectification process combined with the changing continuum flux, we applied the method described in MSM, i.e., we multiplied each rectified spectrum corresponding to a given phase ϕ by $10^{-0.4[m(\phi)-m(\min)]}$, where $m(\phi)$ and $m(\min)$ are the magnitudes at phase ϕ (the light curves were binned to 0.05 phase resolution) and at minimum light, respectively. The constant continuum level in the rectified spectrum was subtracted before this procedure and added back in afterward. Because of the epoch-dependent nature of the photometric changes, the spectra were corrected (when possible) by quasi-simultaneously acquired photometric data. These data were taken from the literature (see Table 3.1) and were supplemented by new broadband light curves obtained in 1994 by the Automatic Photometric Telescope (see §3.2.2). Since we will continually refer to the light curves presented by Duijsens et al. (1996) and Antokhin et al. (1994) throughout this paper, these are reproduced for the sake of clarity in Figure 3.1. Note that the panels give calibrated (*top*) and differential magnitudes (*bottom*). Unfortunately, the spectroscopic and photometric data do not coincide (or even overlap) in some cases. This problem is most severe for the spectra from epochs II and III during which, to our knowledge, no optical light curves were recorded. However, as pointed out by St-Louis et al. (1998), the UV continuum variations observed during epoch III are very similar to the optical continuum variations observed during epoch I (Fig.3.1, *top*). Because the UV and optical continuum flux are strictly related (MSM), this light curve was adopted for epoch III, as well as for epoch II. For the other cases, the desynchronization never exceeds two weeks (epoch IV), an interval that is sufficiently short to expect no gross changes in the light curve shape or amplitude.

3.2.2 Photometry

New photometric data were obtained in order to help establish a reference for epoch VI. EZ CMa was monitored during the period 1994 January 31-April 8 using Johnson *UBV* filters with one of the 0.25 m automatic telescopes on Mount Hopkins (Young et al. 1991). HD 50853 and HD 50711 were used as comparison (c1) and check (c2) stars, respectively. The following sequence of 10 s integrations in each filter was used to derive the differential magnitudes listed in Table 3.2: c2, sky, c1, WR, c1, WR, c1, WR, c1, sky, c2. The internal standard deviations are also quoted in Table 3.2. The mean external standard deviations of the ($c_2 - c_1$) data are 0.006, 0.004, and 0.005 mag for the *U*, *B*, and *V* filters, respectively. These values are typical of the accuracy achieved by this robotic telescope (Strassmeier & Hall 1988). The flux in each of the three filters suffers from various line emission contributions (Duijsens et al. 1996): 22 % (*U*), 30 % (*B*), and 11 % (*V*). The data are plotted as a function of phase in Figure 3.2. The phases, as everywhere in this paper, are calculated according to the ephemeris of Lamontagne, Moffat, & Lamarre (1986).

3.3 Results

3.3.1 An Overview of the LPVs: He II $\lambda 4686$

In order to display the LPVs as conspicuously as possible, and because the variations were strictly repeatable from one cycle to another during our observing runs (which covered at most five cycles; Table 3.1), we have grouped the individual spectra for a given epoch into 0.05 phase resolution bins. Also, we have chosen to illustrate the LPVs by means of the strong He II $\lambda 4686$ emission line. As will be shown below (§3.3.2), this transition exhibits variations that are very much representative of those affecting the majority of the other spectral lines present

in the spectrum of EZ CMa. We compare the individual binned spectra with the corresponding mean spectrum of each epoch in Figures 3.3a-3.3f for the spectral range encompassing He II $\lambda 4686$. Remarkable phase-dependent changes in the line-peak morphology are observed. Also, this data set nicely exhibits the well-known epoch dependency (on a typical timescale of weeks to months) displayed by this star. At this point, we emphasize that some caution must be taken when making a direct comparison between different epochs. Because of the period uncertainty (accurate, at best, to the third decimal place), substantial phase shifts can occur if the observing runs are separated by some years, as is the case here. Even allowing for such potential slippage, however, there is little doubt that the pattern of variability has dramatically changed between epochs I and II (secured as little as only ≈ 70 cycles apart; Table 3.1). In addition to the line-peak variability, significant smaller changes (see §3.3.4) are also present in the line wings out to at least $v \approx \pm 2500 \text{ km s}^{-1}$.

3.3.2 Similarities in the Pattern of Variability for Different Lines

We present in Figures 3.4a-3.4b gray-scale plots of the residual deviations from the mean spectrum of He II $\lambda 4686$ and He II $\lambda 4859$ from epoch I, for which we have obtained the best phase coverage. These residual spectra were binned to 0.02 phase resolution and are arranged as a function of phase in the upper portion of each panel. As illustrated, these two He II transitions share the same pattern of variability, with only a small phase lag of the stronger He II $\lambda 4686$ line behind He II $\lambda 4859$. This similarity between the LPVs affecting all the He II transitions is also observed for the other epochs and seems to constitute a definite feature of the wind variability of EZ CMa (see MSM).

Figure 3.4c displays the gray-scale plot of N V $\lambda 4945$. This transition is of interest since it is formed relatively close to the stellar core, contrary to other transitions such as He II $\lambda 4686$. The bulk of emission in the nitrogen and helium

lines arises at about 2.5 and 12 stellar core radii, respectively (P. A. Crowther 1995, private communication). Although significant (see §3.3.4), the LPVs in this line are very subtle, even accounting for its weakness (MSM), and cannot easily be linked to those in the helium transitions discussed above. However, N V $\lambda 4945$ shares with the He II lines the peculiarity of also exhibiting cyclical changes according to the 3.77 day period (the variations are coherent over the three cycles covered by the observations). This suggests that the variability is rooted to processes operating in the deep layers of the wind. There is also a hint in Figure 3.4c that the structures in N V $\lambda 4945$ are seen earlier in phase than those in the He II lines (as N IV $\lambda 4058$ in 1995; MSM).

The relatively good phase coverage achieved during epoch VI allows one to characterize fairly well the N IV $\lambda 4058$ LPVs (Fig.3.5). As can be seen, this transition is extremely sensitive to time-dependent wind conditions. Owing to the modest changes in the line-profile morphology of He II $\lambda 4686$ (Fig.3.3f), it is not clear from this data set whether these N IV LPVs are — as found by MSM — similar to the variations in the He II line. Two states within the cycle can be defined: one with a strongly enhanced blue peak ($\phi \approx 0.175\text{--}0.325$ and $\phi \approx 0.575\text{--}0.725$) and red peak ($\phi \approx 0.875\text{--}0.075$), respectively. Note the abrupt ($\Delta\phi = 0.1$; ≈ 9 hr) shift between these two “states” at $\phi \approx 0.125$.

3.3.3 Correlated Continuum and Line-profile Variations

In order to search for a possible correlation between the line-profile and the photometric (continuum) variations, we have calculated the Spearman rank-order correlation coefficient (Press et al. 1992) between the line intensity at a given wavelength and the continuum flux level. The binned spectra of Figure 3.3 were used in this procedure, along with the continuum flux at the corresponding phase, which was determined by binning the light curves to 0.05 phase resolution. For epoch VI, we have averaged the U , B , V light curves displayed in Figure 3.2.

We stress that the rectified spectra used in this procedure have been corrected for the effect of the continuum flux variability (§3.2.1); that is to say, the line-profile variations reflect the genuine changes in the line emissivity at any given projected velocity. The results for each epoch (we have excluded epoch IV because of the poor phase coverage of the light curve [Fig.3.1, *top*] but included the data from 1995 January [MSM]) are displayed in Figure 3.6 for the spectral region encompassing He II $\lambda 4686$. The horizontal lines indicate the 99.0 % and 99.9 % confidence levels for a significant (anti)correlation. Although this investigation yields negative results at these levels for epochs II and V, the line intensity in some velocity regions is occasionally directly linked to the level of continuum flux for epochs I, III, and VI, as well as for the data acquired in 1995 January. For example, a positive correlation is observed for epochs I and III and in 1995 January between the line intensity and the level of continuum flux at $v \approx + 2000 \text{ km s}^{-1}$.

This correlation is particularly remarkable for epoch III, for which the line intensity at -1600 , $+300$, and $+2200 \text{ km s}^{-1}$ is strongly ($> 99.9 \%$) positively correlated with the continuum flux level, whereas it is anticorrelated at $+1200 \text{ km s}^{-1}$.² This result is reminiscent of the anticorrelated variations at the same blueward and redward projected outflow velocity observed in the H α line of the O supergiant HD 152408 by Prinja & Fullerton (1994). These (anti)correlations observed during epoch III in EZ CMa are probably a result of the oscillation between rather flat-topped and triangular profiles (Fig.3.3c) observed at minimum and maximum continuum flux, respectively ($\phi \approx 0.2$ and $\phi \approx 0.6$, respectively; see Fig.3.1, *top*). Similar phase-dependent changes in the line-profile “morphology” were also observed in 1994 (Georgiev & Ivanov 1995). The correlation function is displayed in Figure 3.7 for the entire spectral domain covered during epoch

²Note that this appearance of both correlated and anticorrelated variations between the line intensity in some given velocity regions and the continuum flux ensures that it is not an artifact of a systematically (under)overestimated correction of the continuum variability (§3.2.1).

III. Clearly, the phenomenon described above is by no means restricted to He II $\lambda 4686$; a very similar correlation pattern is also observed for the other transitions, including N V $\lambda 4945$. In particular, the correlation across the line profiles of He II $\lambda 4686$ and He II $\lambda 4859$ are indistinguishable. Note that because the spectra were continuum normalized (§3.2.1), the continuum sections show no significant correlation.

The indication found by MSM of a cyclical, simultaneous modulation of the wind properties and the continuum flux emanating near the stellar core was primarily provided by the inverse correlation existing between the strength of the absorption troughs of N V $\lambda\lambda 4604, 4620$ and the level of continuum flux. The same phenomenon is observed in the present data sets and is quantitatively confirmed by the correlation measurements (e.g., Fig.3.7). For *all* epochs, the alternation between filling in and strengthening of these violet absorption edges coincides exactly with maximum and minimum continuum flux, respectively.³ For illustration, the gray-scale plot of N V $\lambda\lambda 4604, 4620$ during epoch I is displayed in Figure 3.8. and can be compared with the continuum light curve of the same epoch in Figure 3.1 (*top*).

3.3.4 Temporal Variance Spectrum

As described by MSM, we have calculated the values of the temporal variance spectrum (TVS) (Fullerton et al. 1996), which give a statistical assessment of the variability level at a given wavelength. This quantity (expressed in terms of the typical “size” of the deviations from a template-weighted mean spectrum in percentage of the continuum flux) is shown, along with the 99.0 % confidence level for variability, in the lower panels of Figures 3.4a-3.4c and Figure 3.8. The TVS of

³The phase location of the maximum for epoch IV is dubious because of the severe undersampling of this light curve. Note, however, a maximum at $\phi \approx 0.6-0.7$ in the intensive photometric data gathered about 1 month later by Duijsens et al. (1996).

He II $\lambda 4686$ and He II $\lambda 4859$ are very similar (Figs.3.4a-3.4b), highlighting their similar behavior pointed out previously on other grounds (§3.3.2). *Significant* variations in He II $\lambda 4686$ occur at velocities exceeding the wind-terminal velocity deduced from the bluest saturated point of the UV resonance P Cygni absorption components ($v_\infty \approx 1900 \text{ km s}^{-1}$; Prinja, Barlow, & Howarth 1990).

In Figure 3.9, we compare the TVS for epochs I, III, VI, and for 1995 January for the region encompassing N V $\lambda\lambda 4604, 4620$ and He II $\lambda 4686$ (the number of spectra acquired during the other epochs is too small to yield significant information). It is fairly difficult to assess whether the variability takes place preferentially at the same characteristic velocities from one epoch to another, as recently proposed by Ivanov et al. (1998). Reasons for this are multiple. First, the TVS is particularly sensitive to imperfections in the wavelength calibration (although we tried to minimize this; for more details, see MSM), leading to artificially enhanced variability in the steepest parts of the lines. Second, the reciprocal dispersion of the spectra and phase coverage vary from one epoch to another and can also influence its overall shape. In an effort to assess the influence of the phase coverage on the resultant TVS, we have calculated the TVS for epoch I after rejection of the spectra with $0.0 < \phi < 0.2$, then $0.2 < \phi < 0.4$, and so on. This procedure provided us with five TVS whose subpeaks are detected in each case to within $\sigma \approx 20 \text{ km s}^{-1}$. In comparison, the subpeaks at ≈ -1600 and $\approx +2000 \text{ km s}^{-1}$ in He II $\lambda 4686$ (where the TVS is unaffected by shift of the profile) during epochs I, III, VI, and 1995 January (Fig.3.9) present a significantly higher velocity dispersion: $\sigma \approx 110 \text{ km s}^{-1}$. Therefore, although it would certainly be questionable to draw firm conclusions regarding the long-term behavior of the TVS on the basis of the present data set, preferential variability occurring at significantly different locations across the line profile from one epoch to another is suggested.

3.3.5 Line Fluxes, FWHM and Skewness Variations

Figure 3.10a presents the variations in the line flux of He II $\lambda 4686$ across the wavelength range 4647-4765 Å as a function of phase for each epoch. Note that the plotted variations reflect the net change of emissivity after allowance for the continuum level changes (§3.2.1). MSM found a significant positive correlation between the level of continuum flux and the line flux of this He II transition. However, such a correlation is marginal in this data set for epochs II and VI (compare with Figs.3.1 [top] and 3.2).

Two other quantities, the line skewness and FWHM of He II $\lambda 4686$, are also plotted for the different epochs in Figures 3.10b-3.10c, respectively. The skewness gives information on the degree of asymmetry of a given line: zero if it is symmetric, negative or positive if it is skewed longward or shortward in wavelength, respectively. The skewness measurements were restricted to flux levels above two in units of the continuum. A Gaussian fit to the entire profile was applied to determine the FWHMs. Both quantities show evidence for phase-related variations at most epochs. Furthermore, a phase dependence with three relative minima per cycle is suggested for the FWHM variations of epoch I, at $\phi \approx 0.0, 0.4$, and 0.75 . Relative maxima in skewness appear at these same phases. This is reminiscent of the 1 day recurrence timescale reported in the past, e.g., in the EWs of the UV P Cygni absorption components (Willis et al 1989; St Louis et al. 1993) or in the optical line-profile FWHM and skewness values (MSM). For the other epochs, however, it is important to note that the situation may be quite different.

3.4 Discussion

3.4.1 Implications for the Binary Scenario

In the following discussion, we restrict ourselves to an interpretation of the variability in terms of a single star. The main reason behind this choice is that the possibility of an orbiting low-mass companion as the cause of the 3.77 day variability was discussed in length in MSM and appeared to be unlikely. It is of interest, however, to briefly discuss here the implication of these new observations on the binary scenario. In this context, the phase-dependent LPVs presented by N V λ 4945 are noteworthy (Fig.3.4c). If we assume a 3.77 day circular orbit, a canonical mass of the companion of $1.44 M_{\odot}$, and reasonable parameters for EZ CMa ($M_* \approx 11.8 M_{\odot}$, $R_* = 2.7 R_{\odot}$; Hamann, Koesterke, & Wesselowsky 1995), we obtain an orbital separation of $a \approx 9 R_*$. Since the line-formation region of N V λ 4945 does not extend beyond $\approx 4 R_*$ (P. A. Crowther 1995, private communication), it would be difficult to explain how the secondary would significantly perturb these deep layers of the wind via X-ray photoionization, owing in particular to the very high X-ray opacity of the material in this region and the low level of X-ray flux observed (e.g., Stevens & Willis 1988).

3.4.2 Evidence for a Deep-seated Wind Variability

The analysis of the present data supports a direct link between the line-profile and photometric variations in EZ CMa. Compelling lines of evidence for this are the following: (i) filling in or strengthening of, for *all* epochs presented here, the violet absorption edge of N V λ 4604 (and N V λ 4620), at maximum or minimum continuum flux, respectively (see, e.g., Fig.3.8); (ii) a significant correlation is occasionally observed between the intensity changes affecting parts of the emission line profiles and the level of continuum flux (e.g., Fig.3.6). Although

it is not clear why this correlation stands out more clearly at some epochs, it is remarkable in view of the large wind volume sampled by the emission lines, compared to the P Cygni absorption components; (iii) the peaks of the correlation function during epoch III (Fig.3.6) coincide with the TVS subpeaks for this epoch (Fig.3.9), suggesting that the changes in the most variable parts of the profile are directly linked to the variations of the continuum flux.

This often-observed link between the LPVs and the optical continuum flux emanating close to the stellar core (Hillier 1987) suggests that the wind variability of EZ CMa is rooted to a (azimuthal) spatial dependence of the radiative flux emanating at the base of the outflow. In support of this conclusion, note that the quiescent state of UV spectral variability observed by Willis et al. (1989) was related to a UV continuum flux constant within 0.02 mag.

As demonstrated in the hydrodynamical simulations of Cranmer & Owocki (1996), azimuthal changes in the radiative flux (i.e., driving force) at the very base of an early-type stellar outflow are likely to lead to the formation of wind streams. We propose that this process is operating in EZ CMa. Detailed modeling (beyond the scope of this paper) is required to investigate whether this model is able to account for the observational aspects presented here, notably the correlation observed in Figure 3.6. Apparently in EZ CMa, as for the B supergiant HD 64760 (Fullerton et al. 1997), there is a strong epoch dependency of the physical conditions at the very base of the outflow, leading to observed wind structure that is different from one epoch to another. This introduces the epoch-dependent patterns of variability observed (Fig.3.3), although the rotation period of the star, which is probably modulating the changes, is always observed.

3.4.3 The Cause of a Nonisotropic Base Outflow

An interesting issue regarding our global understanding of WR stars is to uncover what underlying physical phenomena operating near (or at) the star's photosphere give rise to the observed wind variations. In this context, pulsations and magnetic structures naturally come to mind.

3.4.3.1 Pulsations

Theoretical investigations of the stability of WR stars to the ϵ -mechanism (Maeder 1985; Schaller 1991; Cox & Cahn 1988) have shown that the radial fundamental mode is likely to be excited for very deficient hydrogen stars such as EZ CMa (Nugis & Niedzielski 1995). The period of this fundamental mode is predicted to be about 40 minutes for a WNE star. In addition to this, strange-mode instabilities appear in the models of Kiriakidis, Glatzel, & Fricke (1996), with periods of the order 5-10 minutes (Glatzel, Kiriakidis, & Fricke 1993). In contrast, nonradial pulsations are unlikely to prevail in WR stars (Cox & Cahn 1988; Maeder & Schaller 1991), except perhaps in the objects that are in the H-shell-burning phase (Noels & Scuflaire 1986). From an observational point of view, two objects have been claimed to present periodic photometric variations that could be attributed to pulsational instabilities, namely the two WN 8 stars WR 40 (Blecha, Schaller, & Maeder 1992; but see Martinez et al. 1994) and WR 66 (Antokhin et al. 1995; Rauw et al. 1996). The *unique* 3.77 day period associated with EZ CMa (Antokhin et al. 1994) seems significantly too long to be associated with pulsations and is more likely to be related to the rotation period. It is, however, important to note that two independent studies found evidence for *transient* rapid (quasi-?)periodic photometric fluctuations (\approx 20 minutes) in EZ CMa (Matthews, Moffat, & Marchenko 1992; Bratschi & Blecha 1996). Owing to the unknown nature of the coupling between short-term variations

at the very base of the wind such as these *intermittent* variations and the wind conditions, pulsations still cannot be ruled out as driver of the variability. Further investigations are needed to challenge this possibility.

3.4.3.2 Magnetic Fields

Magnetic fields are another possible mechanism that might cause the variability. They can act on the wind either as (i) localized “surface” magnetic features or (ii) a large-scale (e.g., dipole or quadrupole) magnetic field probably of fossil origin. One class of objects that have been shown to possess such large-scale magnetic fields are the B-type helium-peculiar stars whose properties are often discussed in the context of the “oblique rotator model” (Shore & Brown 1990). In this model, the magnetic axis is tilted with respect to the rotational axis, leading to a dramatic surface abundance gradient with a subsequent rotational modulation of the spectral lines of these species as different parts of the stellar disk cross the observer’s line of sight. The stellar wind is magnetically controlled with the material flowing out freely along the open field lines near the magnetic poles but being trapped at the magnetic equator (Shore 1987). A similar model was recently proposed for the young O7 V star θ^1 Ori C by Stahl et al. (1996).

An overview of the photometric characteristics of EZ CMa (Robert et al. 1992; Duijsens et al. 1996; MSM) leads to the conclusion that the observed practically *continuous* changes in the light curve morphology (see Marchenko & Moffat 1998) could fit naturally into a picture where extended magnetic regions on the stellar core experience changes in their activity on a monthly timescale. Moreover, the long-term (≈ 6.6 yr) variability in the star’s luminosity hinted at by the data of Duijsens et al. (1996) could be related to cyclic magnetic activity (see, e.g., Baliunas & Vaughan 1985). Finally, possible flares in EZ CMa have been independently reported by Matthews et al. (1992a) and Duijsens et al. (1996).

However, there exists a fundamental difficulty related to the generation of such a magnetic activity. Although Schaefer (1996) found evidence in his evolutionary models for a small convective zone close to the surface of WNL stars, WR stars are believed to lack the outer and extended convective zone required for the creation of a dynamo-generated magnetic field. At present, there are no satisfactory alternatives to account for the putative formation of photospheric magnetic structures in WR stars. A more complete description of the internal structure of these objects is required to address this issue. This problem is somewhat reminiscent of the Herbig Ae/Be stars, for which alternative mechanisms for the creation of a corona have been invoked in order to account for their X-ray and LPVs properties (Tout & Pringle 1995).

Thus, some preference should perhaps be given to the existence of a large-scale, fossil corotating magnetic structure because it is less dependent on a mechanism to create and sustain magnetic activity in the envelope of EZ CMa. Although global fields have been proposed in order to explain the (very similar to EZ CMa) epoch-dependent photometric variations presented by some Be stars (Balona, Sterken, & Manfroid 1991), the major drawback of this model is that it cannot easily account for the long-term changes observed. If confirmed by more intensive time-resolved X-ray observations, the lack of phase-locked variability suggested by the *ROSAT* data (Willis & Stevens 1996) would challenge the relevance of the oblique rotator model to EZ CMa (see Gagné et al. 1997; Babel & Montmerle 1997).

Finally, it is not clear whether the inconclusive searches for magnetic fields in EZ CMa conducted so far (see the circular polarization observations of McLean et al. 1979 in low-resolution spectral mode; Drissen et al. 1989; Robert et al. 1992) are telling or are due, for instance, to orientation effects (Barker et al. 1981) or other constraints (e.g., lack of sufficient spectral resolution or sensitivity to weak fields). Polarimetric and radio observations of O stars (which are the precursors

of WR stars) put generous upper limits of some hundred gauss on the strength of any large-scale ordered fields (Bohlender 1994; Bieging, Abbott, & Churchwell 1989). If the same field limits apply also to EZ CMa, their detection would be extremely difficult even with present state-of-the-art polarimetric techniques. A more promising avenue might be via the detection of the Hanle effect in UV lines (Ignace, Nordsieck, & Cassinelli 1997).

Acknowledgments: We would like to thank D. Fortier and B. Sanscartier for their help in the reduction procedure. We acknowledge I. I. Antokhin and D. Duijzens for their permission to reproduce Figures 3.1 (*top*) and 3.1 (*bottom*), respectively. We thank S. V. Marchenko for a careful reading of this manuscript. T. M., N. S.-L., A. F. J. M., and G. M. H. wish to thank the Natural Sciences and Engineering Research Council (NSERC) of Canada and the Fonds pour la Formation de Chercheurs et l'Aide à la Recherche (FCAR) of Québec for financial support.

RÉFÉRENCES

- Antokhin, I. I., Bertrand, J.-F., Lamontagne, R., & Moffat, A. F. J. 1994, AJ, 107, 2179
- Antokhin, I. I., Bertrand, J.-F., Lamontagne, R., Moffat, A. F. J., & Matthews, J. M. 1995, AJ, 109, 817
- Babel, J., & Montmerle, T. 1997, ApJ, 485, L29
- Baliunas, S. L., & Vaughan, A. H. 1985, ARA&A, 23, 379
- Balona, L. A., Sterken, C., & Manfroid, J. 1991, MNRAS, 252, 93
- Barker, P. K., Landstreet, J. D., Marlborough, J. M., Thompson, I., & Maza, J. 1981, ApJ, 250, 300
- Bieging, J. H., Abbott, D. C., & Churchwell, E. B. 1989, ApJ, 340, 518
- Blecha, A., Schaller, G., & Maeder, A. 1992, Nature, 360, 320
- Bohlender, D. A. 1994, in IAU Symp. 162, Pulsation, Rotation and Mass Loss in Early-Type Stars, ed. L. A. Balona, H. F. Henrichs, & J. M. Le Contel (Kluwer: Dordrecht), 155
- Bratschi, P., & Blecha, A. 1996, A&A, 313, 537
- Cardona, O., St-Louis, N., Koenigsberger, G., Vazquez, G. A., Piceno, G., Moffat, A. F. J., Georgiev, L. N., & Ivanov, M. M. 1998, in preparation.
- Chalabaev, A., & Maillard, J. P. 1983, A&A, 127, 279
- Cox, A. N., & Cahn, J. H. 1988, ApJ, 326, 804
- Cranmer, S. R., & Owocki, S. P. 1996, ApJ, 462, 469
- Driessen, L., Robert, C., Lamontagne, R., Moffat, A. F. J., St-Louis, N., van Weeren, N., & van Genderen, A. M. 1989, ApJ, 343, 426

- Duijzens, M. F. J., van der Hucht, K. A., van Genderen, A. M., Schwarz, H. E., Linders, H. P. J., & Kolkman, O. M. 1996, A&AS, 119, 37
- Ebbets, D. 1979, PASP, 91, 804
- Ebbets, D. 1982, ApJS, 48, 399
- Eversberg, T., Lépine, S., & Moffat, A. F. J. 1998, ApJ, 494, 799
- Firmani, C., Koenigsberger, G., Bisacchi, G. F., Moffat, A. F. J., & Isserstedt, J. 1980, ApJ, 239, 607
- Fullerton, A. W., Gies, D. R., & Bolton, C. T. 1996, ApJS, 103, 475
- Fullerton, A. W., Massa, D. L., Prinja, R. K., Owocki, S. P., & Cranmer, S. R. 1997, A&A, 327, 699
- Gagné, M., Caillault, J.-P., Stauffer, J. R., & Linsky, J. L. 1997, ApJ, 478, L87
- Georgiev, L. N., & Ivanov, M. M. 1995, in IAU Symp. 163, Wolf-Rayet Stars: Binaries, Colliding Winds, Evolution, ed. K. A. van der Hucht & P. M. Williams (Dordrecht: Kluwer), 54
- Glatzel, W., Kiriakidis, M., & Fricke, K. J. 1993, MNRAS, 262, L7
- Gosling, J. T. 1996, ARA&A, 34, 35
- Grady, C. A., Snow, T. P., & Timothy, J. G. 1983, ApJ, 271, 691
- Hamann, W.-R., Koesterke, L., & Wessolowski, U. 1995, A&A, 295, 151
- Harmanec, P. 1991, in ESO workshop on Rapid Variability of OB-Stars: Nature and Diagnostic Value, ed. D. Baade (Garching: ESO), 265
- Harries, T. J., Hillier, D. J., & Howarth, I. D. 1998, MNRAS, in press
- Hillier, D. J. 1987, ApJS, 63, 947
- Howarth, I. D., Prinja, R. K., & Massa, D. 1995, ApJ, 452, L65
- Hundhausen, A. J. 1972, Coronal Expansion and Solar Wind (Berlin: Springer)
- Ignace, R., Nordsieck, K. H., & Cassinelli, J. P. 1997, ApJ, 486, 550

- Ivanov, M. M., Georgiev, L. N., Koenigsberger, G., & Valchev, T. S. 1998, A&A, submitted
- Kaper, L., Henrichs, H. F., Nichols, J. S., Snoek, L. C., Volten, H., & Zwarthoed, G. A. A. 1996, A&AS, 116, 257
- Kaper, L., et al. 1997, A&A, 327, 281
- Kaufer, A., Stahl, O., Wolf, B., Gäng, Th., Gummersbach, C. A., Kovács, J., Mandel, H., & Szeifert, Th. 1996a, A&A, 305, 887
- Kaufer, A., et al. 1996b, A&A, 314, 599
- Kiriakidis, M., Glatzel, W., & Fricke, K. J. 1996, MNRAS, 281, 406
- Koenigsberger, G. 1995, in IAU Symp. 163, Wolf-Rayet Stars: Binaries, Colliding Winds, Evolution, ed. K. A. van der Hucht & P. M. Williams (Dordrecht: Kluwer), 538
- Lamontagne, R., Moffat, A. F. J., & Lamarre, A. 1986, AJ, 91, 925
- Lépine, S., Moffat, A. F. J., & Henriksen, R. N. 1996, ApJ, 466, 392
- McLean, I. S., Coyne, G. V., Frecker, J. E., & Serkowski, K. 1979, ApJ, 231, L141
- Maeder, A. 1985, A&A, 147, 300
- Maeder, A., & Schaller, G. 1991, in IAU Symp. 143, Wolf-Rayet Stars and Interrelations with Other Massive Stars in Galaxies, ed. K. A. van der Hucht & B. Hidayat (Dordrecht: Kluwer), 167
- Marchenko, S. V., & Moffat, A. F. J. 1998, ApJ, submitted
- Marchenko, S. V., Moffat, A. F. J., Eversberg, T., Hill, G. M., Tovmassian, G. H., Morel, T., & Seggewiss, W. 1998, MNRAS, in press
- Martinez, P., Kurtz, D., Ashley, R., & Tripe, P. 1994, Nature, 367, 601
- Massa, D., Prinja, R. K., & Fullerton, A. W. 1995, ApJ, 452, 842
- Matthews, J. M., Moffat, A. F. J., & Marchenko, S. V. 1992a, A&A, 266, 409

- Matthews, J. M., St-Louis, N., Moffat, A. F. J., Drissen, L., Koenigsberger, G., Cardona, O., & Niemela, V. S. 1992b, in ASP Conf. Proc. 22, Nonisotropic and Variable Outflows From Stars, ed. L. Drissen, C. Leitherer, & A. Nota (San Francisco: ASP), 130
- Moffat, A. F. J., & Robert, C. 1992, in ASP Conf. Proc. 22, Nonisotropic and Variable Outflows From Stars, ed. L. Drissen, C. Leitherer, & A. Nota (San Francisco: ASP), 203
- Morel, T., St-Louis, N., & Marchenko, S. V. 1997, ApJ, 482, 470 (MSM)
- Mullan, D. J. 1984, ApJ, 283, 303
- Mullan, D. J. 1986, A&A, 165, 157
- Noels, A., & Scuflaire, R. 1986, A&A, 161, 125
- Nugis, T., & Niedzielski, A. 1995, A&A, 300, 237
- Owocki, S. P., Cranmer, S. R., & Fullerton, A. W. 1995, ApJ, 453, L37
- Press, W. H., Teukolsky, S. A., Vetterling, W. T., & Flannery, B. P. 1992, Numerical Recipes (Cambridge: Cambridge Univ. Press), 634
- Prinja, R. K., Barlow, M. J., & Howarth, I. D. 1990, ApJ, 361, 607
- Prinja, R. K., & Fullerton, A. W. 1994, ApJ, 426, 345
- Prinja, R. K., Massa, D., & Fullerton, A. W. 1995, ApJ, 452, L61
- Prinja, R. K., Fullerton, A. W., & Crowther, P. A. 1996, A&A, 311, 264
- Rauw, G., Gosset, E., Manfroid, J., Vreux, J.-M., & Claeskens, J.-F. 1996, A&A, 306, 783
- Reid, A. H. N., & Howarth, I. D. 1996, A&A, 311, 616
- Robert, C., et al. 1992, ApJ, 397, 277
- Schaerer, D. 1996, A&A, 309, 129
- Schaller, G. 1991, in ASP Conf. Proc. 11, Confrontation Between Stellar Pulsation and Evolution, ed. C. Cacciati & G. Clementini (San Francisco: ASP), 304

- Schulte-Ladbeck, R. E., Nordsieck, K. H., Taylor, M., Bjorkman, K. S., Magalhães, A. M., & Wolff, M. J. 1992, *ApJ*, 387, 347
- Schulte-Ladbeck, R. E. 1995, in IAU Symp. 163, Wolf-Rayet Stars: Binaries, Colliding Winds, Evolution, ed. K. A. van der Hucht & P. M. Williams (Dordrecht: Kluwer), 176
- Shore, S. N. 1987, *AJ*, 94, 731
- Shore, S. N., & Brown, D. N. 1990, *ApJ*, 365, 665
- Smith, L. F., Shara, M. M., & Moffat, A. F. J. 1996, *MNRAS*, 281, 163
- Stahl, O., et al. 1996, *A&A*, 312, 539
- Stevens, I. R., & Willis, A. J. 1988, *MNRAS*, 234, 783
- St-Louis, N., Howarth, I. D., Willis, A. J., Stickland, D. J., Smith, L. J., Conti, P. S., & Garmany, C. D. 1993, *A&A*, 267, 447
- St-Louis, N. 1994, *Ap&SS*, 221, 197
- St-Louis, N., Dalton, M. J., Marchenko, S. V., Moffat, A. F. J., & Willis, A. J. 1995, *ApJ*, 452, L57
- St-Louis, N., Dalton, M. J., Howarth, I. D., Willis, A. J., & Conti, P. S. 1998, in preparation
- Strassmeier, K. G., & Hall, D. S. 1988, *ApJS*, 67, 439
- Tout, C. A., & Pringle, J. E. 1995, *MNRAS*, 272, 528
- Willis, A. J., Howarth, I. D., Smith, L. J., Garmany, C. D., & Conti, P. S. 1989, *A&AS*, 77, 269
- Willis, A. J., & Stevens, I. R. 1996, *A&A*, 310, 577
- Young, A. T., et al. 1991, *PASP*, 103, 221

TABLEAU 3.1. Journal of spectroscopic observations

Epoch	Date	Spectroscopy					Photometry		
		HJD –		Number of spectra	Spectral coverage (Å)	Dispersion (Å pix ⁻¹)	S/N	HJD –	
		2,440,000	Observatory ^a					2,440,000	Filter
Epoch	Date	HJD –	Observatory ^a	Number of spectra	Spectral coverage (Å)	Dispersion (Å pix ⁻¹)	S/N	HJD –	Filter
I	91 Jan	8280-8291	SPM	283	4435-5020	1.04	≈ 150	8281-8294	y
II	91 Oct	8550-8563	UTSO	11	3750-4575	1.60	≈ 100	"	y
				11	4200-5025	1.60			
III ^b	92 Jan	8642-8655	UTSO	21	4550-5050	0.97	≈ 130	"	y
IV	92 Oct	8900-8917	UTSO	11	3620-4540	2.16	≈ 225	8918-8931 ^c	y
				11	4165-5210	2.16			
V	93 Mar	9046-9053	UTSO	8	3640-4505	2.16	≈ 230	9038-9089	5140 Å
				8	4110-4975	2.16			
				8	5115-5980	2.16			
VI	94 Mar	9428-9445	UTSO	18	4000-4820	1.60	≈ 220	9383-9450	U, B, V

^a SPM: San Pedro Mártir Observatory 2.1 m; UTSO: University of Toronto Southern Observatory 0.6 m.

^b Simultaneous *IUE* spectra were collected during the period HJD 2,448,643-2,448,649 (St-Louis et al. 1998).

^c For the correction of the continuum variability in the spectra, this light curve was interpolated.

References. — (1) Duijzens et al. (1996); (2) Antokhin et al. (1994); (3) this study.

TABLEAU 3.2. Differential UBV magnitudes of EZ CMa in 1994^a

HJD - 2,440,000	ϕ	U (mag)		B (mag)		V (mag)	
		WR - C1	C2 - C1	WR - C1	C2 - C1	WR - C1	C2 - C1
9383.7621	0.714	-0.412 (0.007)		0.325 (0.004)		0.642 (0.004)	
9384.7424	0.975	-0.395 (0.006)	0.437 (0.001)	0.337 (0.006)	0.370 (0.007)	0.646 (0.004)	0.296 (0.002)
9386.7674	0.512	-0.416 (0.017)		0.362 (0.017)		0.684 (0.016)	
9389.7288	0.299	-0.416 (0.008)	0.428 (0.007)	0.325 (0.005)	0.372 (0.008)	0.641 (0.002)	0.302 (0.001)
9393.7138	0.357	-0.426 (0.003)	0.433 (0.008)	0.334 (0.011)	0.366 (0.011)	0.641 (0.005)	0.291 (0.011)
9394.7733	0.638	-0.413 (0.012)					
9398.6893	0.678	-0.422 (0.004)	0.434 (0.001)	0.318 (0.007)	0.372 (0.007)	0.634 (0.002)	0.296 (0.005)
9399.6918	0.944	-0.386 (0.009)	0.412 (0.011)	0.355 (0.004)		0.663 (0.004)	0.258 (0.018)
9403.6895	0.006	-0.409 (0.008)	0.427 (0.005)	0.336 (0.005)	0.376 (0.003)	0.661 (0.005)	0.304 (0.003)
9406.7253	0.812	-0.382 (0.006)	0.434 (0.001)	0.337 (0.003)	0.366 (0.002)	0.679 (0.001)	0.301 (0.010)
9410.6881	0.864	-0.369 (0.011)		0.339 (0.007)	0.365 (0.012)	0.668 (0.012)	0.300 (0.005)
9411.6878	0.130	-0.397 (0.012)	0.440 (0.002)	0.335 (0.005)	0.364 (0.016)	0.656 (0.005)	0.286 (0.015)
9412.6970	0.398	-0.426 (0.009)	0.438 (0.014)	0.331 (0.004)	0.376 (0.005)	0.649 (0.003)	0.290 (0.002)
9416.6966	0.460	-0.417 (0.006)	0.421 (0.008)	0.322 (0.004)	0.369 (0.004)	0.637 (0.005)	0.283 (0.009)
9417.6934	0.724	-0.426 (0.006)	0.436 (0.017)	0.322 (0.008)	0.376 (0.005)	0.646 (0.006)	0.282 (0.006)
9418.6903	0.989	-0.396 (0.016)	0.435 (0.013)	0.333 (0.005)	0.373 (0.012)	0.680 (0.009)	0.310 (0.008)
9423.6696	0.311	-0.443 (0.004)	0.437 (0.005)	0.281 (0.012)	0.357 (0.013)	0.626 (0.008)	0.294 (0.009)
9424.6679	0.576			0.355 (0.015)		0.673 (0.012)	
9427.6584	0.370	-0.443 (0.014)	0.427 (0.016)	0.298 (0.005)	0.368 (0.004)	0.614 (0.000)	0.295 (0.003)
9429.6499	0.899	-0.396 (0.007)	0.453 (0.012)	0.324 (0.002)		0.642 (0.014)	
9433.6380	0.958	-0.388 (0.009)	0.454 (0.013)	0.328 (0.003)	0.363 (0.003)	0.647 (0.004)	0.292 (0.003)
9436.6308	0.753	-0.386 (0.003)		0.328 (0.018)		0.688 (0.014)	
9439.6236	0.547	-0.388 (0.011)	0.436 (0.014)	0.331 (0.005)	0.368 (0.010)	0.662 (0.006)	0.288 (0.007)
9441.6382	0.082	-0.402 (0.007)	0.411 (0.003)	0.327 (0.010)	0.380 (0.009)	0.656 (0.014)	0.297 (0.003)
9442.6387	0.348	-0.456 (0.005)	0.408 (0.000)	0.279 (0.003)		0.605 (0.005)	0.313 (0.001)
9443.6389	0.614	-0.392 (0.008)	0.428 (0.003)	0.327 (0.009)	0.364 (0.004)	0.661 (0.005)	0.292 (0.005)
9447.6269	0.673	-0.410 (0.006)	0.425 (0.000)	0.324 (0.004)	0.372 (0.010)	0.650 (0.009)	0.299 (0.002)
9448.6195	0.936	-0.389 (0.010)	0.459 (0.006)	0.342 (0.006)	0.359 (0.006)	0.676 (0.011)	0.287 (0.006)
9450.6203	0.467	-0.371 (0.009)	0.407 (0.019)	0.354 (0.009)	0.339 (0.015)	0.686 (0.004)	

^a The internal standard deviation of the data is given in brackets. The empty cells in the table are due to rejection of the data when this number exceeds 0.02 mag (Young et al. 1991).

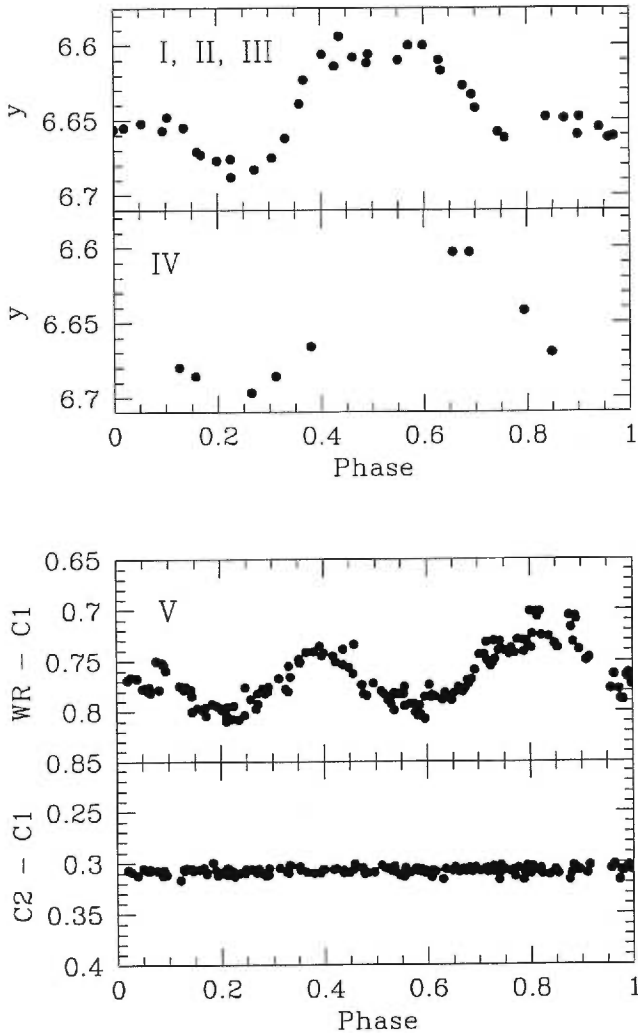


FIGURE 3.1. *Top:* The y -magnitudes of EZ CMa for the periods HJD 2,448,281-2,448,294 (epochs I, II, and III) and HJD 2,448,918-2,448,931 (epoch IV) (Duijsens et al. 1996). *Bottom:* Narrowband light curve of EZ CMa for the period HJD 2,449,038-2,449,089 (epoch V) (Antokhin et al. 1994); *upper*, differential light curve of EZ CMa; *lower*, differential light curve of the comparison stars c1 and c2. The phases, as everywhere in this paper, are calculated according to the ephemeris of Lamontagne, Moffat, & Lamarre (1986). These figures are adapted from Duijsens et al. (1996) and Antokhin et al. (1994), with permission.

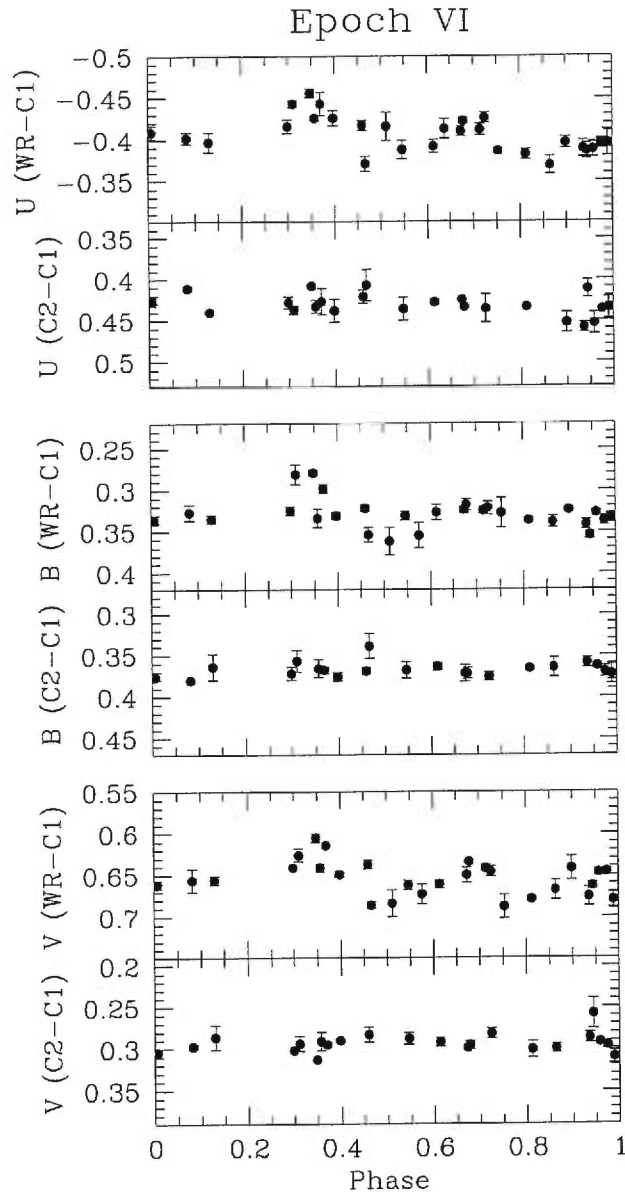


FIGURE 3.2. *UBV* light curves of EZ CMa for the period HJD 2,449,383–2,449,450 (epoch VI). *Upper panels*: differential light curve of EZ CMa. *Lower panels*: differential light curve of the comparison stars C1 and C2. The error bars (2σ) correspond to the internal standard deviations (see Table 3.2).

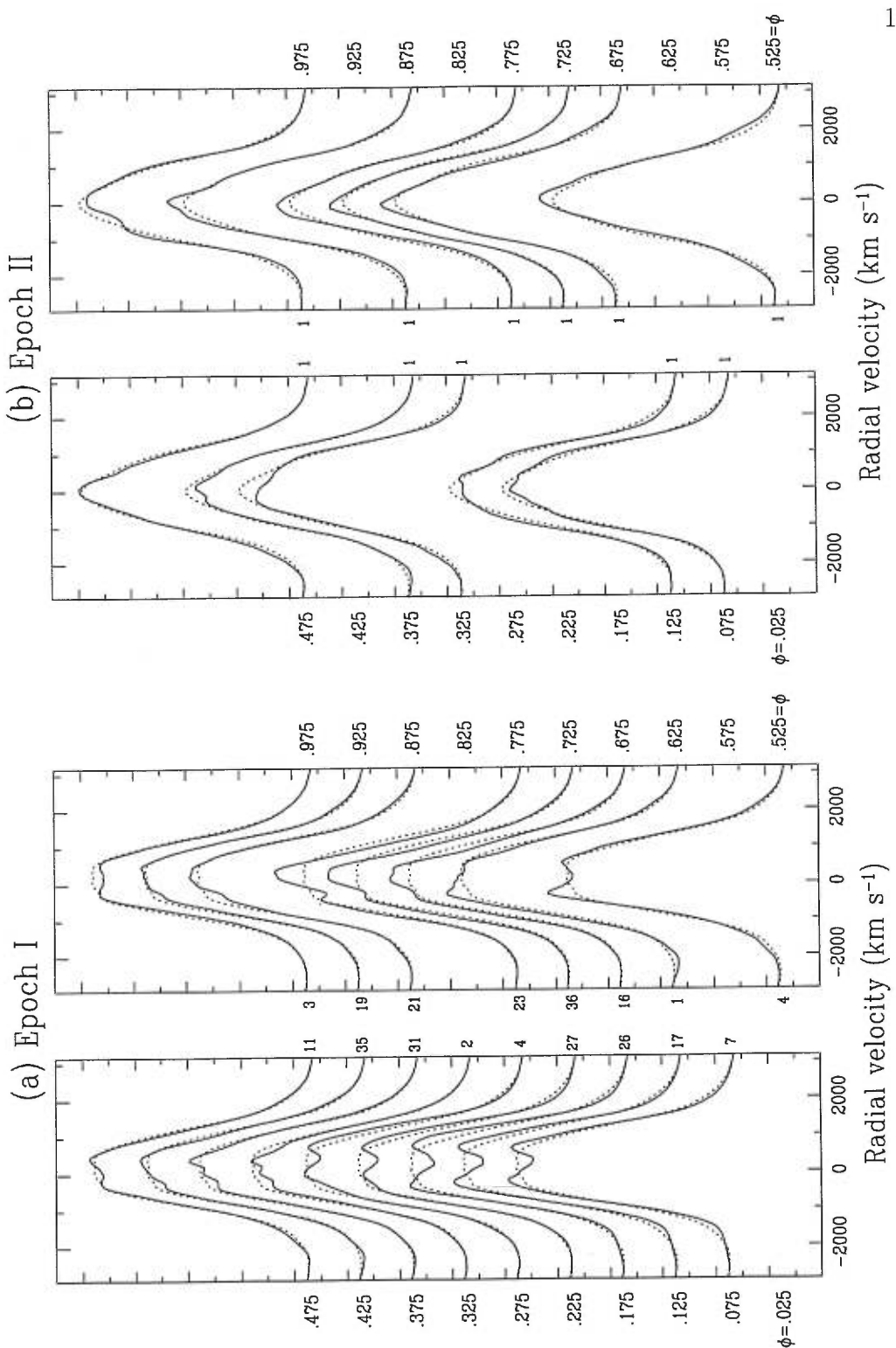


FIGURE 3.3. Time series of He II $\lambda 4686$ for the six different epochs. The rectified spectra were binned to 0.05 phase resolution (the number of spectra averaged to form the corresponding binned spectrum is indicated between the two panels of each figure). The mean phases are also indicated on both sides of these plots. The mean of the binned spectra is overplotted as a dashed line for each epoch. The projected velocities, as everywhere in this paper, are heliocentric and refer to the laboratory rest wavelength.

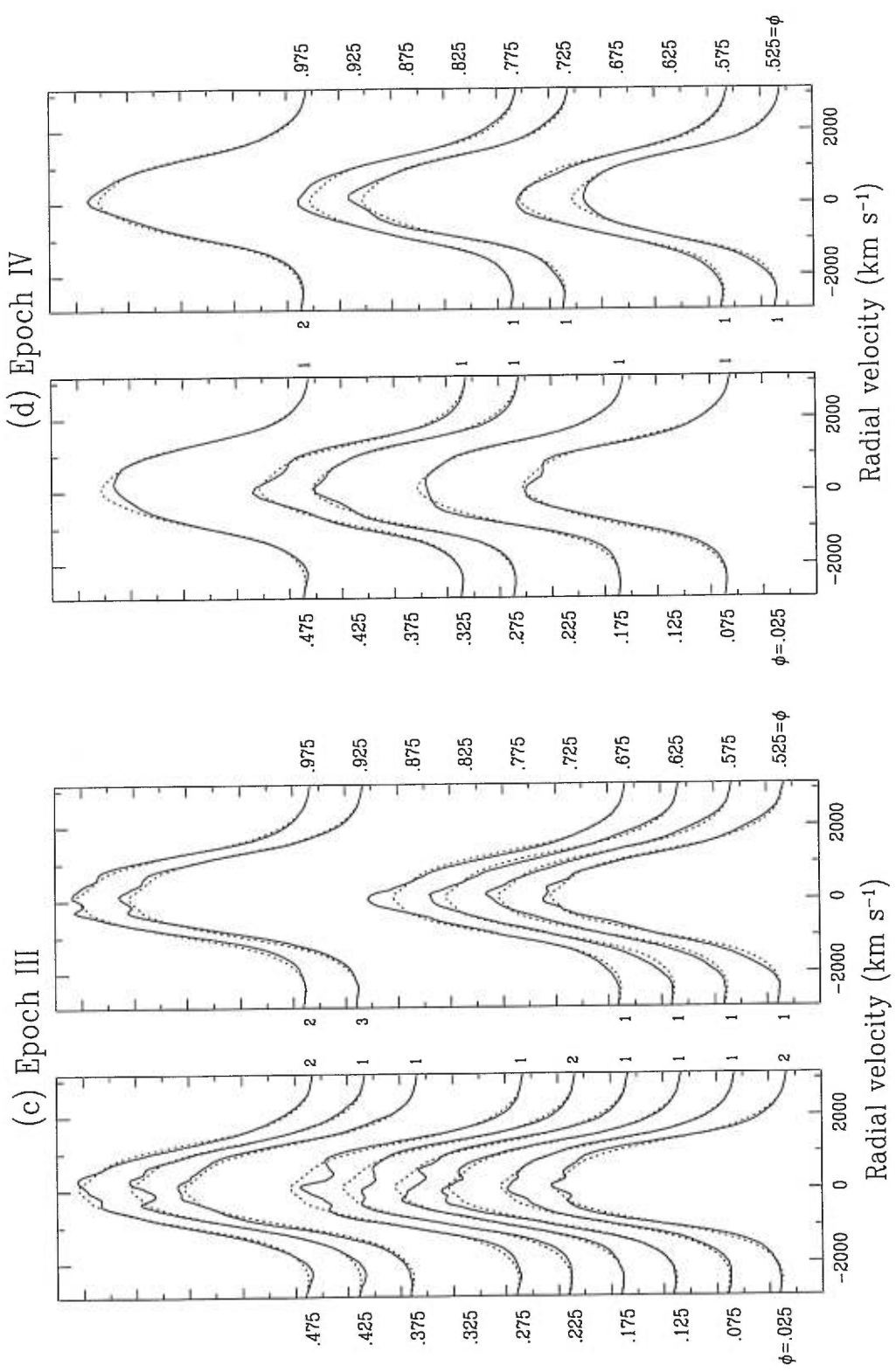


FIGURE 3.3. Continued.

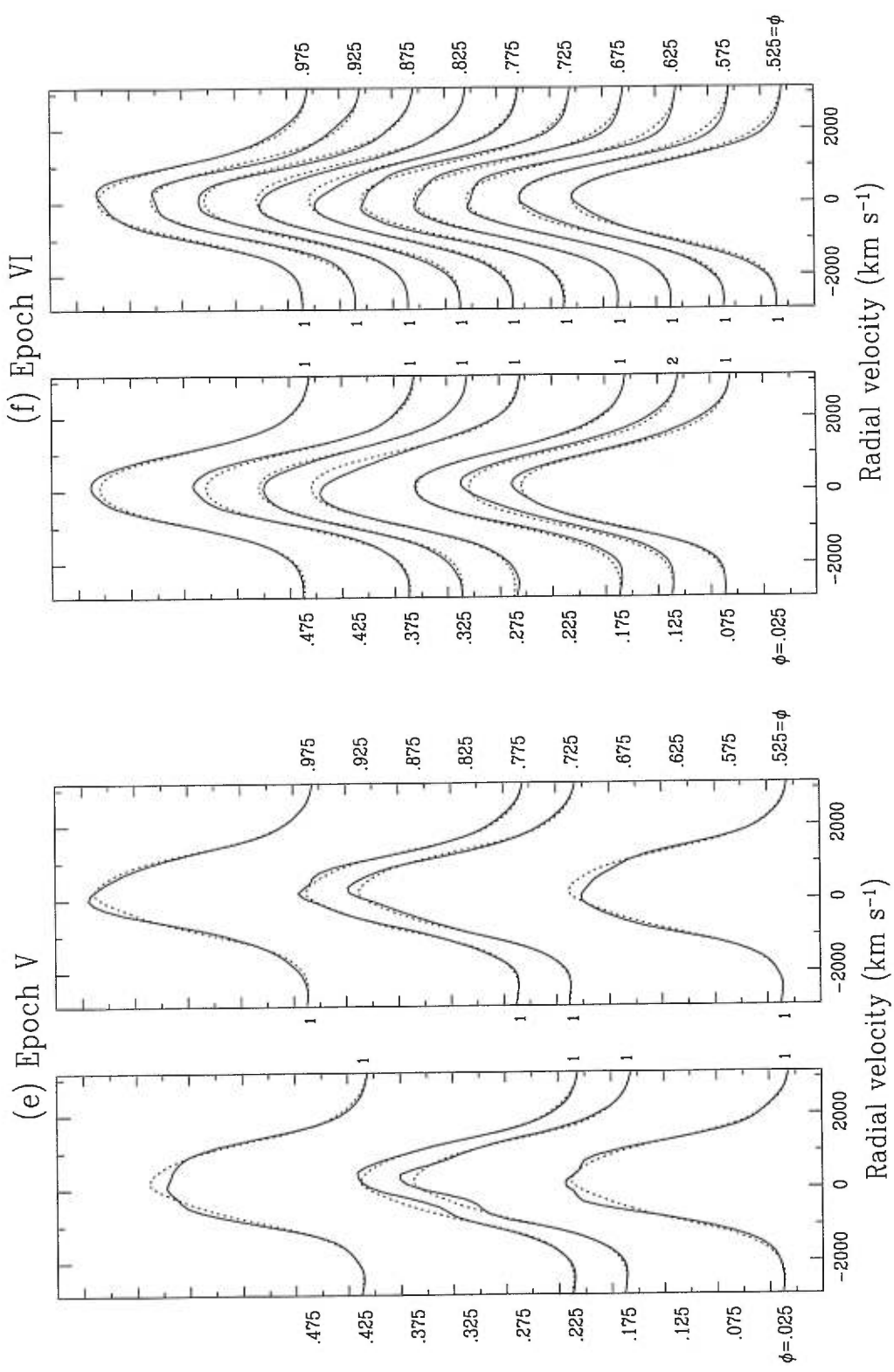


FIGURE 3.3. Continued.

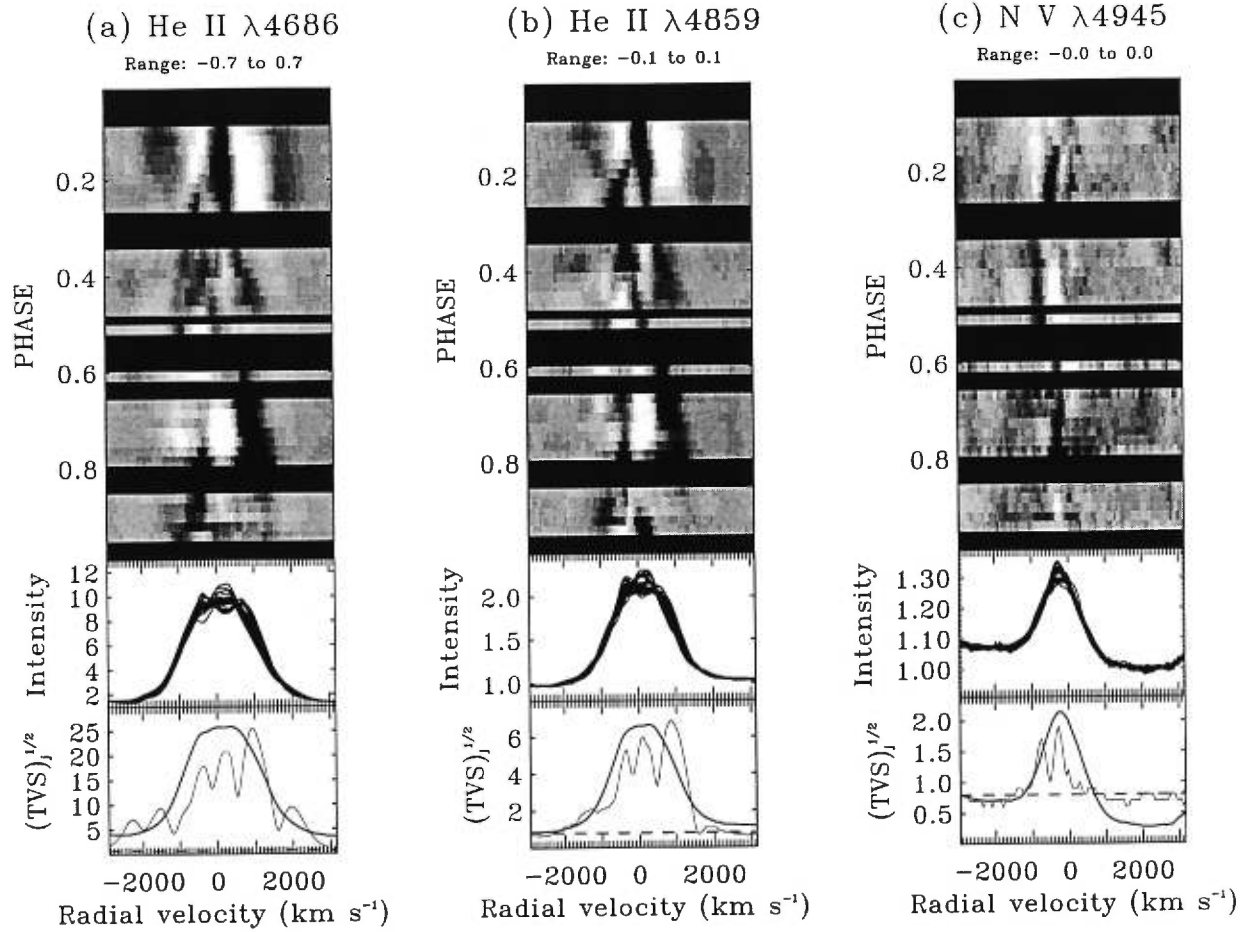


FIGURE 3.4. Gray-scale plots of the time series of the residuals of (a) He II $\lambda 4686$, (b) He II $\lambda 4859$, and (c) N V $\lambda 4945$ for epoch I. These residuals (the mean profile of the epoch subtracted from the individual profiles) were binned to 0.02 phase resolution. Excess emission components appear brighter in these plots. The middle portion of each panel presents the superposition of the different rectified profiles. The values of $(TVS)^{1/2}$ (§3.3.4) and the mean profile (in arbitrary units) are displayed in the lower portion of each panel. The horizontal dashed line indicates the 99.0 % variability detection threshold.

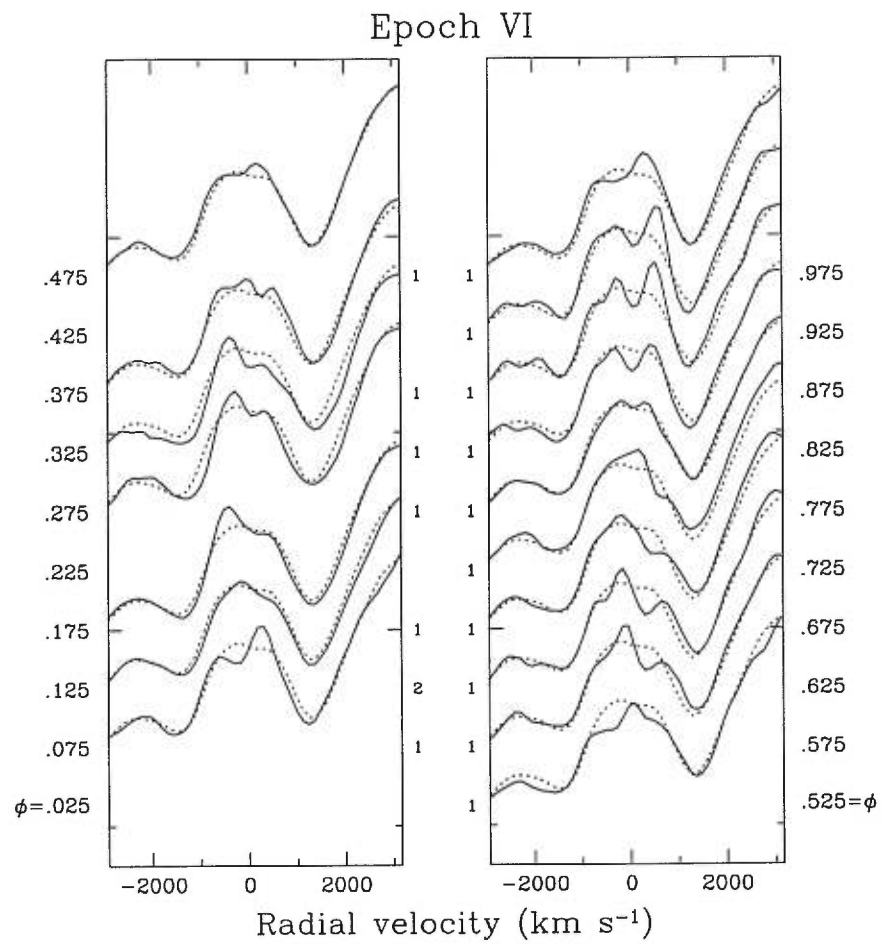


FIGURE 3.5. Time series of N IV λ 4058 for epoch VI.

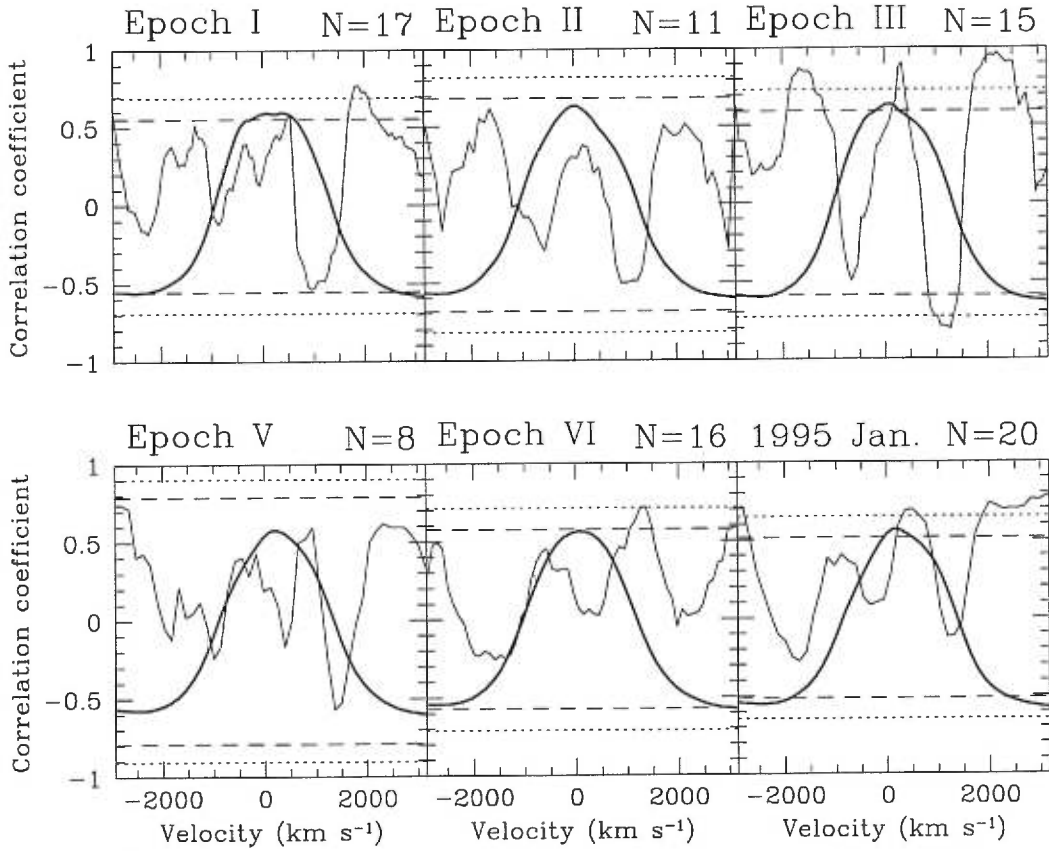


FIGURE 3.6. Correlation functions of He II $\lambda 4686$ for the different epochs. The epoch and the number of spectra used in this procedure are indicated on the top of each panel. The epoch “1995 Jan” refers to the observations of MSM. The dashed and dotted lines give the 99.0 % and 99.9 % confidence levels for a significant (anti)correlation, respectively. The mean profile of each epoch is overplotted by a thick line.

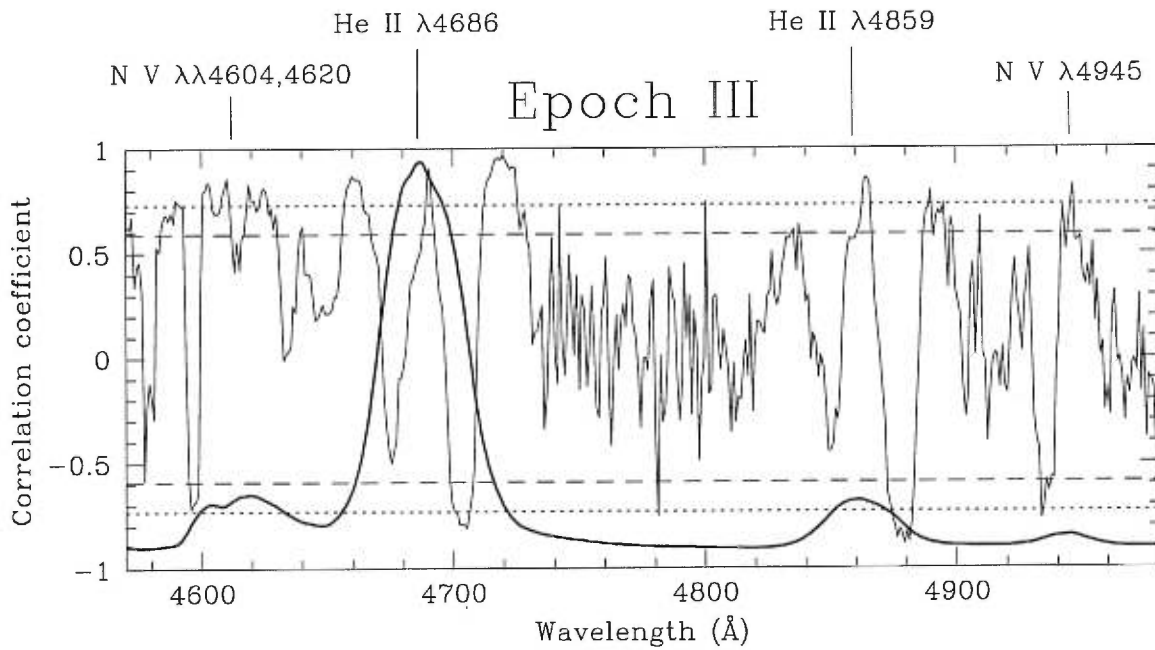


FIGURE 3.7. Correlation function during epoch III for the spectral domain 4570–4980 Å. The dashed and dotted lines give the 99.0 % and 99.9 % confidence levels for a significant (anti)correlation, respectively. The mean profile is overplotted by a thick line.

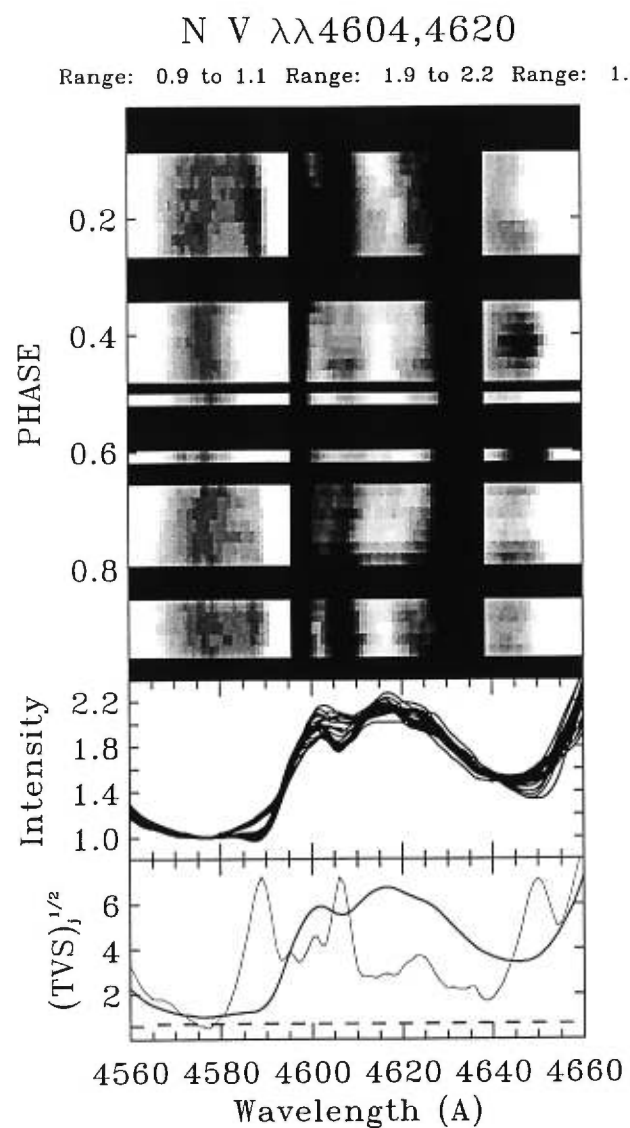


FIGURE 3.8. Gray-scale plot of the time series of the P Cygni components of N V $\lambda\lambda 4604, 4620$ for epoch I. The selected wavelength domain is displayed for three different intensity intervals. The blue wing variability of He II $\lambda 4686$ is seen at the rightmost panel of this figure.

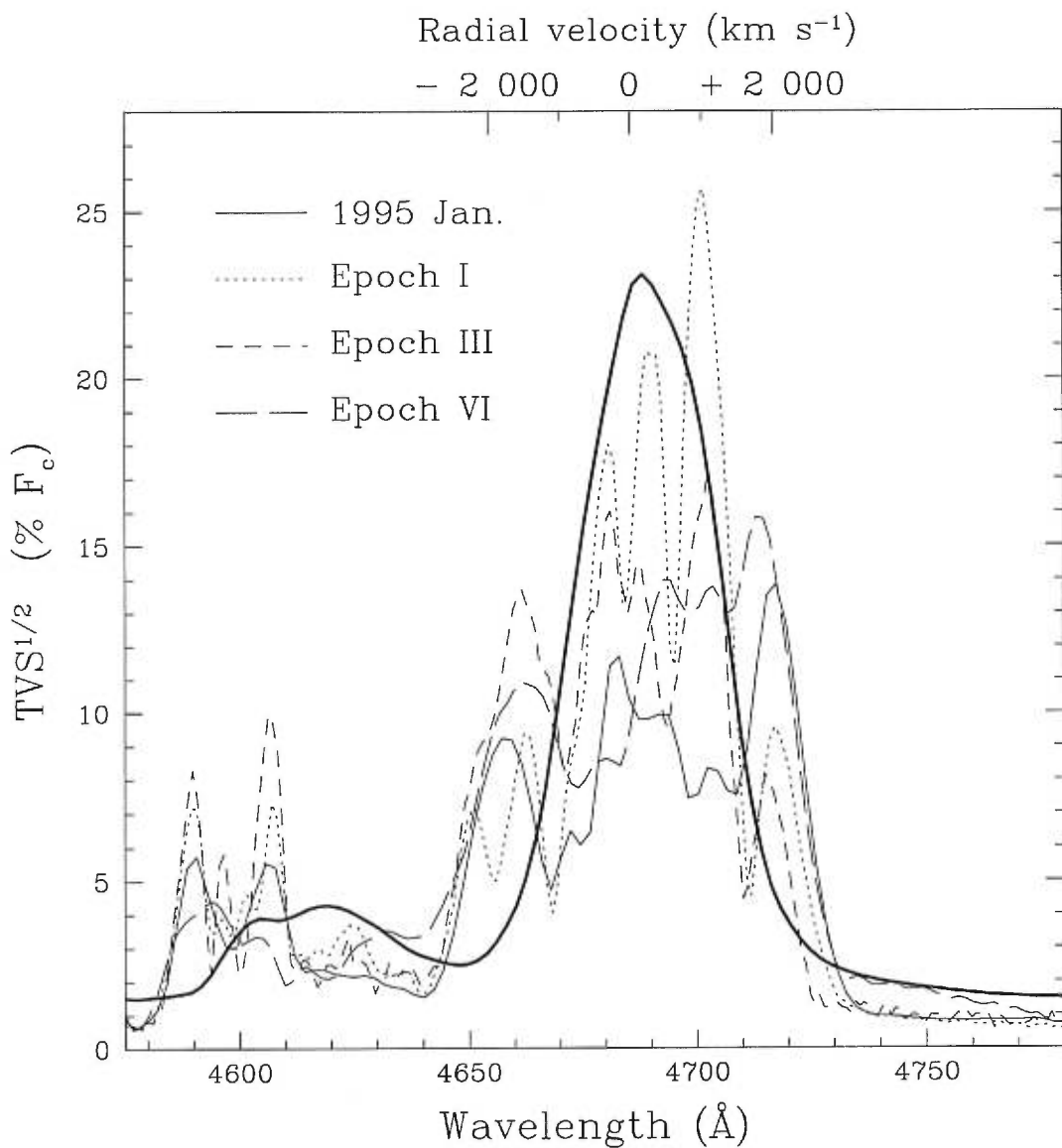


FIGURE 3.9. Superposition of the TVS of epochs I, III, VI, and of 1995 January (MSM) for the spectral domain 4575-4780 Å. A representative mean spectrum is overplotted by a thick line.

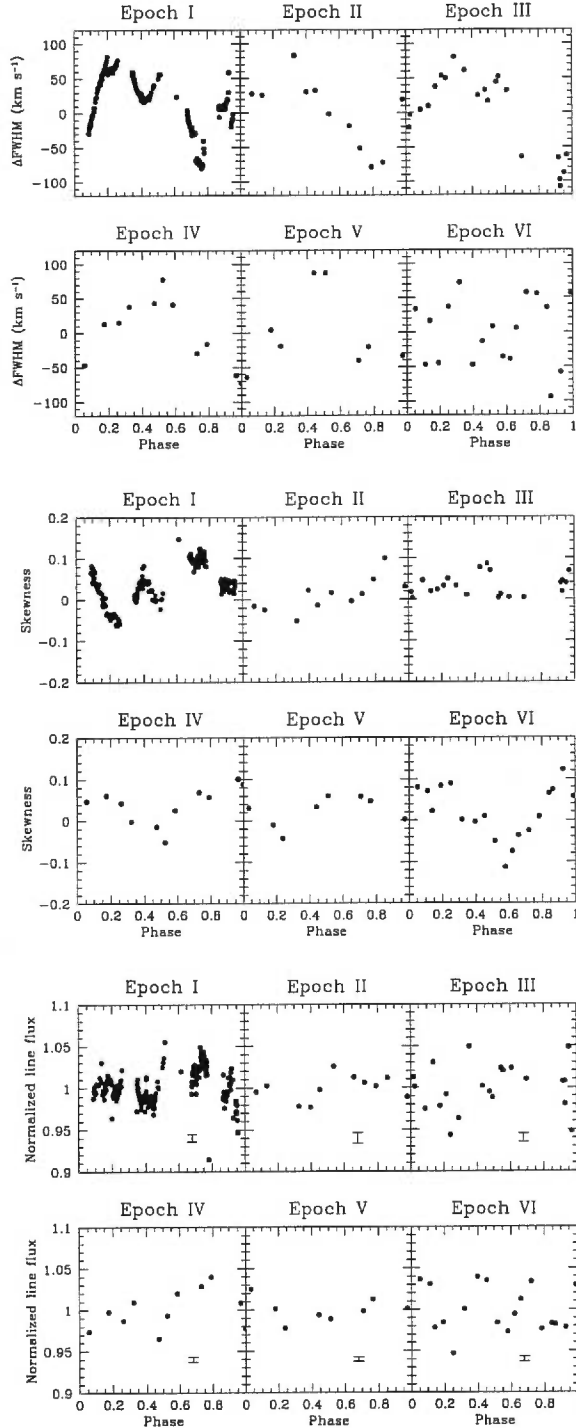


FIGURE 3.10. (a) Deviations of the FWHM for He II $\lambda 4686$ around the mean value (expressed in km s^{-1}), as a function of phase, for the six epochs. (b) Skewness of He II $\lambda 4686$, as a function of phase, for the six epochs. (c) Line flux of He II $\lambda 4686$ (normalized by division to the mean value in each epoch) as a function of phase. The 2σ error bars were calculated according to Chalabaev & Maillard (1983). Note that they only account for the presence of random noise; they do not allow for possible systematic effects, e.g., imperfect rectification of the spectra.

CHAPITRE 4

A 2.3-DAY PERIODIC VARIABILITY IN THE APPARENTLY SINGLE WOLF-RAYET STAR WR 134: COLLAPSED COMPANION OR ROTATIONAL MODULATION?

The Astrophysical Journal, sous presse

**A 2.3-DAY PERIODIC VARIABILITY IN THE
APPARENTLY SINGLE WOLF-RAYET STAR WR
134: COLLAPSED COMPANION OR ROTATIONAL
MODULATION?**

Thierry Morel,¹ Sergey V. Marchenko,¹ Philippe R. J. Eenens,² Anthony F. J. Moffat,¹ Gloria Koenigsberger,³ Igor I. Antokhin,⁴ Thomas Eversberg,¹ Gaghik H. Tovmassian,⁵ Grant M. Hill,⁶ Octavio Cardona,⁷ and Nicole St-Louis¹

Received 1998 April 29;

accepted 1999 January 13

Article submitted to the Astrophysical Journal main section.

¹ Département de Physique, Université de Montréal, C.P. 6128, Succ. Centre-Ville, Montréal, Québec, Canada, H3C 3J7; and Observatoire du Mont Mégantic.

² Departamento de Astronomía, Universidad de Guanajuato, Apdo. Postal 144, 36000 Guanajuato Gto, México.

³ Instituto de Astronomía, UNAM, Apdo. Postal 70-264, México D.F. 04510, México.

⁴ Sternberg Astronomical Institute, Universiteskij Prospect 13, 119899, Moscow, Russia.

⁵ Instituto de Astronomía, Apdo. Postal 877, C. P. 22860, Ensenada, B.C., México.

⁶ McDonald Observatory, HET, P. O. Box 1337, Fort Davis, TX.

⁷ Instituto Nacional de Astrofísica, Optica y Electrónica, Apdo. Postal 51, Puebla, Pue. 72000, México.

ABSTRACT

The apparently single WN 6 type star WR 134 (HD 191765) is distinguished among the Wolf-Rayet star population by its strong, presumably cyclical ($\mathcal{P} \approx 2.3$ day), spectral variations. A true periodicity — which is still very much debated — would render WR 134 a prime candidate for harboring either a collapsed companion or a rotating, large-scale, inhomogeneous outflow.

We have carried out an intensive campaign of spectroscopic and photometric monitoring of WR 134 from 1989 to 1997 in an attempt to reveal the true nature of this object. This unprecedentedly large data set allows us to confirm unambiguously the existence of a coherent 2.25 ± 0.05 day periodicity in the line-profile changes of He II $\lambda 4686$, although the global pattern of variability is different from one epoch to another. This period is only marginally detected in the photometric data set.

Assuming the 2.25 day periodic variability to be induced by orbital motion of a collapsed companion, we develop a simple model aiming to investigate (i) the effect of this strongly ionizing, accreting companion on the Wolf-Rayet wind structure, and (ii) the expected emergent X-ray luminosity. We argue that the predicted and observed X-ray fluxes can only be matched if the accretion on the collapsed star is significantly inhibited. Additionally, we performed simulations of line-profile variations caused by the orbital revolution of a localized, strongly ionized wind cavity surrounding the X-ray source. A reasonable fit is achieved between the observed and modeled phase-dependent line profiles of He II $\lambda 4686$. However, the derived size of the photoionized zone substantially exceeds our expectations, given the observed low-level X-ray flux.

Alternatively, we explore rotational modulation of a persistent, largely anisotropic outflow as the origin of the observed cyclical variability. Although qualitative, this hypothesis leads to greater consistency with the observations.

Subject headings: stars: individual (WR 134) — stars: mass loss — stars: Wolf-Rayet

4.1 Introduction

The recognition in the 1980s that some apparently single Wolf-Rayet (WR) stars exhibit seemingly periodic line profile and/or photometric variations argued for the existence of systems made up of a WR star and a collapsed companion (hereafter WR + c ; where c stands either for a neutron star or a black hole), as predicted by the general theory of massive close-binary evolution (e.g., van den Heuvel & de Loore 1973): $O + O \rightarrow WR + O \rightarrow c + O \rightarrow c + WR \rightarrow c + c$. Due to the recoil of the first supernova explosion leading to $c + O$, the system generally acquires a high systemic velocity. If massive enough, the secondary evolves in turn into a WR star, at which point the system may have reached an unusually high galactic latitude for a population I star. These two peculiarities (runaway velocity and position), along with the existence of a surrounding ring nebula (presumably formed by matter ejected during the secondary mass exchange), were among the criteria initially used to select WR + c candidates (van den Heuvel 1976; Moffat 1982; Cherepashchuk & Aslanov 1984).¹

A major breakthrough in the qualitative scenario described above comes from a recent redetermination of the distribution of the radio pulsar runaway velocities. In sharp contrast with earlier estimations (100-200 km s⁻¹; Gunn & Ostriker 1970; Lyne, Anderson, & Salter 1982), these new values imply a mean pulsar kick velocity at birth of about 450 km s⁻¹ (Lyne & Lorimer 1994; Lorimer, Bailes, & Harrison 1997). Although such a high kick velocity imparted at birth is still much debated (e.g., Hansen & Phinney 1997; Hartman 1997), this result tends to show — as suggested by the apparent paucity of “runaway” OB stars with

¹Since then, only Cygnus X-3 has been shown to probably belong to this class (van Kerkwijk et al. 1996; Schmutz, Geballe, & Schild 1996; but see Mitra 1998). Besides this system, the single-line WN 7 star WR 148 (HD 197406) constitutes one of the most promising candidates (Marchenko et al. 1996a). Two candidates for WR + c in 30 Doradus have also been proposed by Wang (1995).

compact companions (Kumar, Kallman, & Thomas 1983; Gies & Bolton 1986; Philp et al. 1996; Sayer, Nice, & Kaspi 1996) — that the number of systems which would survive the first supernova explosion is probably considerably lower than initially thought (see Brandt & Podsiadlowski 1995 vs Hellings & de Loore 1986). Indeed, the incorporation of up-to-date physics of supernova explosions in the most recent population synthesis models of massive binaries leads to a very small number of observable WR + c systems in the Galaxy ($N \lesssim 5$; De Donder, Vanbeveren, & van Bever 1997). This number contrasts significantly with the number of observationally selected candidates ($N \approx 15$; Vanbeveren 1991), especially considering the necessarily incomplete nature of this sample. At face value, this discrepancy might imply that most of these WR + c candidates are spurious or, more interestingly, that other physical mechanisms are at work to induce the large-scale, periodic variability inherent to *some* objects.

At least in O stars, the progenitors of WR stars, it appears that large-scale periodic variability may be induced by rotating aspherical and structured winds (e.g., Fullerton et al. 1997; Kaper et al. 1997). The incidence of asymmetric outflows among the WR star population is probably lower, although recent spectro-polarimetric (Harries, Hillier, & Howarth 1998), UV (St-Louis et al. 1995), optical (Marchenko et al. 1998a), and radio observations (White & Becker 1996; Williams et al. 1997) have now independently revealed this peculiarity in a substantial number of WR stars. In order to account for the periodic variability inferred for the suspected WR + c candidates, the rotational modulation of a persistent, largely inhomogeneous outflow could thus constitute in some cases an attractive alternative to the binary scenario, and would be consistent with the lack of strong, accretion-type X-ray emission (Wessolowski 1996).

The nature of the variable WN 5 star EZ CMa (HD 50896; WR 6), which is generally considered as a prime candidate for an orbiting collapsed companion (Firmani et al. 1980), has been recently re-investigated by means of extensive

spectropolarimetric (Harries et al. 1999), UV (St-Louis et al. 1995), and optical studies (Morel, St-Louis, & Marchenko 1997; Morel et al. 1998). These studies reveal that the 3.77 day period displayed by this object is more likely induced by the rotational modulation of a structured wind. Hints of long-term (from weeks to months) wind variability triggered by a spatial dependence of the physical conditions prevailing in the vicinity of the hydrostatic stellar “surface” were also found (Morel et al. 1998).

Besides the search for WR + c systems, the mysterious origin of such deep-seated variability (possibly induced by pulsational instabilities or large-scale magnetic structures in the case of EZ CMa) has prompted us to carry out intensive spectroscopic and photometric observations of other WR stars suspected to exhibit such periodic line-profile variations (LPVs). In this context, WR 134 is regarded as a natural target.

4.2 Observational Background

WR 134 is a relatively bright ($v \approx 8.3$) WN 6 star surrounded by a ring-type nebula embedded in the H II region S 109 (Crampton 1971; Esteban & Rosado 1995).

Following the discovery of spectacular line-profile and photometric changes intrinsic to this object (Bappu 1951; Ross 1961), a major effort was directed to establish the periodic nature of these variations. Cherepashchuk (1975) was the first to investigate photometric variability of WR 134 on different timescales. Irregular night-to-night light fluctuations (with rms amplitude $\sigma \approx 0.014$ mag) were observed, without evidence for rapid (\sim hourly) or long-term (\sim monthly) changes. The first claim of periodic variability with $P = 7.44 \pm 0.10$ day was made by Antokhin, Aslanov, & Cherepashchuk (1982) on the basis of a two-month interval of broadband photometric monitoring. The authors also reported

small amplitude radial velocity variations present in simultaneously acquired spectroscopic data ($K_{WR} \approx 20\text{-}40 \text{ km s}^{-1}$), consistent with the above period. This period was subsequently improved to $\mathcal{P} = 7.483 \pm 0.004$ day by Antokhin & Cherepashchuk (1984). Zhilyaev & Khalack (1996) established that the short-term stochastic variability presented by WR 134 is not related to this period, as it would be in the case of an orbiting collapsed companion. Moffat & Shara (1986) were unable to identify this period in their photometric data, although they found evidence for a 1.8 day periodicity, first tentatively reported by Lamontagne (1983) on the basis of radial velocity measurements. Following the recognition that the level of continuum flux from WR 134 is also irregularly variable on a timescale of weeks to months (Antokhin & Volkov 1987), periodic changes of the equivalent widths of He II $\lambda 4859$ with $\mathcal{P} = 1.74 \pm 0.38$ day were reported by Marchenko (1988). Then, Robert (1992) reported the existence of a 2.34 day periodicity in radial velocity variations, which could be a one-day alias of the 1.8 day period claimed in previous studies. A two-day quasi-periodicity in photometric data was also reported by Antokhin et al. (1992). Although not obvious in the spectroscopic data set obtained by Vreux et al. (1992) because of an unfortunate correspondence to a badly sampled frequency domain (see also Gosset, Vreux, & Andrillat 1994; Gosset & Vreux 1996), strong hints toward the reality of this two-day recurrence timescale come from the analysis of an extensive set of optical spectra by McCandliss et al. (1994), who derived a 2.27 ± 0.04 day periodicity in the centroid, second moment and skewness of the line-profile time series. A relatively large-scale, likely cyclical, shift of excess-emission components superposed on the underlying line profiles was also observed.

WR 134 also shows strong variations in broadband polarimetry (Robert et al. 1989) and spectropolarimetry (Schulte-Ladbeck et al. 1992).

Numerous models have been put forward to account for the intricate variability pattern, including: the presence of an orbiting neutron star (Antokhin

& Cherepashchuk 1984), a disk connected to the central star by ever-changing filaments (Underhill et al. 1990), or a bipolar magnetic outflow (Vreux et al. 1992).

No consensus has been reached yet concerning the possible periodic nature of the variations in WR 134. We present in this paper the analysis of a long-term campaign of optical photometric and spectroscopic monitoring, in an attempt to shed new light on this issue. Preliminary results concerning the photometric data subset were presented by Moffat & Marchenko (1993a, b) and Marchenko et al. (1996b).

4.3 Observations and Reduction Procedure

4.3.1 Spectroscopy

WR 134 was observed spectroscopically between 1992 and 1995. A journal of observations is presented in Table 4.1, which lists an epoch number, the dates of the spectroscopic observations, the interval of the observations in Heliocentric Julian Days, the observatory name, the number of CCD spectra obtained, the selected spectral domain, the reciprocal dispersion of the spectra, and the typical signal-to-noise ratio (S/N) in the continuum. The spectra were reduced using the **IRAF**² data reduction packages. Bias subtraction, flat-field division, sky subtraction, extraction of the spectra, and wavelength calibration were carried out in the usual way. Spectra of calibration lamps were taken immediately before, and after the stellar exposure. The rectification of the spectra was carried out by an appropriate choice of line-free regions, subsequently fitted by a low order Legendre polynomial.

²IRAF is distributed by the National Optical Astronomy Observatories, operated by the Association of Universities for Research in Astronomy, Inc., under cooperative agreement with the National Science Foundation.

In order to minimize the spurious velocity shifts induced by an inevitably imperfect wavelength calibration, the spectra were coaligned in velocity space by using the interstellar doublet Na I $\lambda\lambda 5890, 5896$, or the diffuse interstellar band at 4501 Å as fiducial marks.

Each spectrum obtained during epochs I and II generally consists of the sum of three consecutive exposures typically separated by about 10 minutes, with no apparent short-term variability. This is expected in view of the longer timescales required to detect any significant motion of *stochastic, small-scale* emission-excess features travelling on top of the line profiles induced by outwardly moving wind inhomogeneities (Lépine & Moffat 1999).

No attempts have been made to correct for the continuum level variability, owing to its relatively low amplitude and irregularity (§ 4.4.1.2).

4.3.2 Photometry

Previous work led us to expect a fairly complex light curve behavior. Thus, in attempting to reveal regular (i.e., periodic) variations, it was deemed essential to combine multi-epoch observations of high quality. We therefore organized a long-term campaign of *UBV* photometric monitoring of WR 134 in 1990-1997 using the 0.25 m Automatic Photometric Telescope (APT; Young et al. 1991). The APT data collected during the first 3 years of monitoring have been discussed by Moffat & Marchenko (1993a, b). The data generally consist of systematic, \sim day-to-day photometry with 1-2 measurements per night, each of accuracy of $\sigma \approx 0.005\text{-}0.008$ mag. HD 192533 and HD 192934 were used as check and comparison stars, respectively.

In 1992 and 1995, we also organized additional multi-site, very intensive photometric campaigns, in an attempt to support the simultaneous spectroscopy. In 1992, we used the 0.84 m telescope of San Pedro Mártir Observatory (Mexico)

and the 0.6 m telescope of Maidanak Observatory (Uzbekistan, fSU), to observe WR 134 in narrow and broadband filters. In Mexico, the star was observed with a two-channel (WR and guide star) photometer in rapid (5 s resolution) or ultra-rapid (0.01 s; see Marchenko et al. 1994) mode, through filters centered at $\lambda_c = 5185 \text{ \AA}$ (FWHM = 250 \AA , \sim stellar continuum), and $\lambda_c = 4700 \text{ \AA}$ (FWHM = 190 \AA , He II $\lambda 4686$ emission line). By subsequently re-binning the rapid-photometry data into 0.1 day bins, we achieved an accuracy of 0.002-0.003 mag per bin. Additionally, we used the two-channel device as a conventional one-channel photometer to obtain differential *UBV* observations 1-2 times per night (individual accuracy of 0.006-0.007 mag), with HD 192533 and HD 192934 as a check-comparison pair. The single-channel photometer of Maidanak Observatory was equipped with a single $\lambda_c = 6012 \text{ \AA}$ (FWHM = 87 \AA , \sim stellar continuum) filter. HD 191917 was used as a comparison star, resulting in a mean accuracy of 0.003 mag per 0.1 day binned data point.

In 1995, we used the 0.84 m telescope of San Pedro Mártir Observatory and one-channel photometer with a broadband *V* filter in differential photometry mode, providing a typical accuracy of 0.003-0.005 mag per 0.1 day binned point. WR 134 was also monitored by the Crimean Observational Station of GAISH (Crimea, Ukraine) with a one-channel photometer (*V* filter) attached to a 0.6 m telescope, providing a mean accuracy of 0.007 mag per 0.1 day bin.

We also used all the photometric data secured by the *HIPPARCOS* astrometric satellite in 1989-1993 (broadband *Hp* system; see Marchenko et al. 1998b). To match the accuracy of the ground-based observations, we rebinned the *HIPPARCOS* data set to 1 day bins, achieving $\sigma \approx 0.006$ mag per combined data point. All relevant information concerning the photometry is provided in Table 4.2.

4.4 Results

4.4.1 Search for Short-term Periodicity

4.4.1.1 Spectroscopy

Inspired by the previous clear indication of a 2.3-day periodicity in the line-profile variations found by McCandliss et al. (1994), we have performed a similar search in the present data set by calculating the power spectra (PS) using the technique of Scargle (1982) on the skewness, centroid, and FWHM time series of He II $\lambda 4686$, the strongest line. The centroid and skewness were calculated as the first moment, and the ratio of the third and the (3/2 power of the) second central moments of the line profile, respectively. In order to minimize the contributions of blends, both measurements were restricted to the portion of the profile above two in units of the continuum. The FWHM was determined by a Gaussian fit to the entire line profile. A subsequent correction of the frequency spectrum by the CLEAN algorithm was performed in order to remove aliases and spurious features induced by the unevenly spaced nature of the data (see Roberts, Lehár, & Dreher 1987). The period search was performed up to the Nyquist frequency for unevenly spaced data: $\nu_N = (2\Delta t_{min})^{-1}$. However, since no evidence for periodic signals was found at high frequencies, we will only display in the following the PS for frequencies up to $\nu_N = (2\Delta t_{mean})^{-1}$. The data acquired during epoch III suffer from large time gaps and are inadequate in the search for periods of the order of days. Also, because of the larger time span of epoch I compared to epoch II (and of the related higher frequency resolution), the period determination was mainly based on the former data set. The “raw” and CLEANed PS of the skewness, centroid, and FWHM time series of He II $\lambda 4686$ are presented in Figure 4.1. Note that the centroid variations are mainly due to changes in the line profile morphology and thus do *not* reflect a global shift of the profile. The significance of the peaks in the PS can be estimated by means of the 99.0 % and 99.9 %

thresholds (Fig.4.1), giving the probability that a given peak is related to the presence of a deterministic signal in the time series (Scargle 1982). Note that these levels are only indicative in the case of unevenly spaced data (see, e.g., Antokhin et al. 1995).

The “raw” PS display numerous peaks, most of them being induced by the fairly complex temporal window and/or the presence of noise. Very few significant peaks remain in the CLEANed PS. In particular, the highest peaks in the skewness and centroid PS are found at $\nu_0 \approx 0.442$ and 0.447 d^{-1} (with a typical uncertainty of about 0.010 d^{-1} , as determined by the FWHM of the peaks), which translates into periods of 2.26 ± 0.05 and 2.24 ± 0.05 day, respectively. These values are equal, within the uncertainties, to the period proposed by McCandliss et al. (1994): 2.27 ± 0.04 day. The PS for the FWHM time series presents a prominent peak at $\nu_1 \approx 0.884 \text{ d}^{-1}$, which can very likely be identified with the first harmonic of the “fundamental” frequency ν_0 suggested above (we adopt $\nu_0 = 0.444 \text{ d}^{-1}$ in the following). A highly significant signal is also found at $\nu_2 \approx 0.326 \text{ d}^{-1}$ ($\mathcal{P} = 3.07 \pm 0.10$ day); we will return to this point below. Note the absence of any trace of the 7.483 day period ($\nu \approx 0.134 \text{ d}^{-1}$) proposed by Antokhin & Cherepashchuk (1984). The periodic nature of the skewness, centroid, and FWHM variations with a frequency of ν_0 is confirmed — at least for epochs I and II — when the data are plotted as a function of phase (Fig.4.2).³ We have also calculated the equivalent widths (EWs) of He II $\lambda 4686$ by integrating the line flux in the interval 4646–4765 Å. Although significant, the EW variations show no clear evidence for phase-locked variability (Fig.4.2).

After demonstrating that the integrated properties of the line profile are periodic in nature, it is natural to ask whether the same recurrence timescale is present in the detailed LPVs. To this end, we performed pixel-to-pixel CLEANing

³Because our period of 2.25 ± 0.05 day is indistinguishable from the one derived by McCandliss et al. (1994), we adopt their ephemeris in the following: $HJD\ 2,447,015.753 + 2.27\ E$.

of the epoch I and II data sets. All spectra were rebinned in a similar manner and were used as independent time sequences, thus creating 1024 CLEANed PS along the wavelength direction. This procedure confirms the presence of ν_0 , along with its first harmonic at $\nu_1 \approx 0.88 \text{ d}^{-1}$ over the entire line profile of He II $\lambda 4686$ during epoch I, along with weak traces of this period in He II $\lambda 4542$, N V $\lambda\lambda 4604, 4620$ and N III $\lambda 4640$ (Fig.4.3). As in the PS of the FWHM time series of epoch I (Fig.4.1), a periodic signal at $\nu_2 \approx 0.326 \text{ d}^{-1}$ is also present in the pixel-to-pixel CLEANed PS. The occurrence of the same signal at ν_2 in the FWHM and pixel-to-pixel CLEANed PS raises the possibility that this feature is real. However, ν_0 (or its harmonics) is generally (within the uncertainties) recovered in the epoch II PS, contrary to ν_2 . More importantly, the gray-scale plot of He II $\lambda 4686$ does not show a coherent pattern of variability when folded with ν_2 , whereas it does when folded with ν_0 (see below). Also, the phase diagram of the FWHM data of epoch I is considerably noisier when folded with this frequency. Further observations are essential to indicate whether this period is genuinely spurious. Although the LPVs of He II $\lambda 4686$ for epoch II are undoubtedly periodic with a frequency of ν_0 (see below), only a weak signal appears in the pixel-to-pixel PS at this frequency on the top of He II $\lambda 4542$ and He II $\lambda 4686$. This may be related to the more complex pattern of variability compared to epoch I.

The next analysis we have performed consisted in grouping the spectra for each epoch into 0.02 phase bins. The individual, binned He II $\lambda 4686$ line profiles minus their corresponding unweighted means for each epoch are arranged as a function of phase in the upper panels of Figures 4.4a-4.4c. This line transition was chosen because its LPVs are quite representative of (but stronger and clearer than) that of the other He II spectral features (§ 4.4.3). In view of the long time span of the observations (13, 4, and 63 cycles for epochs I, II, and III, respectively), He II $\lambda 4686$ presents a remarkably coherent phase-related pattern of variability. However, it is noteworthy that significant cycle-to-cycle differences in the line-profile morphology are often found, a fact which is reflected in the gray-

scale plots by discontinuities in the pattern of variability between consecutive bins (especially for epoch III; Fig.4.4c). Four main factors can induce this: (i) lack of long-term coherency in the pattern of variability; (ii) artificial loss of coherency induced by the uncertainty in the period; (iii) presence of additional small-scale profile variations created by shocked (and possibly turbulent) material carried out by the global stellar outflow, as observed in other WR stars (Lépine & Moffat 1999); and (iv) continuum flux variations for which no allowance has been made; we deem this last factor as a less important effect because of the small amplitude of the changes (see below). Concerning the first two points, note that the smaller the time span of the observations (Table 4.1), the higher the coherency.

4.4.1.2 Photometry

For the analysis of the broadband photometry, we only use the V -filter data as being less contaminated by emission lines (about 7 % of the total V flux), along with all available mediumband visual-filter photometry, in total 734 observations binned to 0.1 day (1 day for the *HIPPARCOS* data). Note that for WR 134, the small-scale variations observed in U , B , and V are fairly well-correlated in general (Moffat & Marchenko 1993b).

Combining all 1989-1997 data and reducing them to the APT photometric system, we concentrate on a search for relatively short periods; a detailed investigation of the temporal behavior of the “secular” components (i.e., $\mathcal{P} \approx 625$ day and $\mathcal{P} \approx 40$ day variations) being presented in Marchenko et al. (1996b) and Marchenko & Moffat (1998a).

We constructed a CLEANed PS of the whole photometric data set, but failed to find any significant peaks in the range of interest, i.e., around the expected 2.3-day component. This is possibly due to the lack of coherency of the period on long timescales. The long-term component with $\mathcal{P} \approx 625$ day completely dominates

the PS, followed by a less evident power peak at $\mathcal{P} \approx 40$ day. Pre-whitening from both long-period variations does not improve the situation in the high-frequency domain.

In the analysis of the data subsets, we have encountered some limited success. The “subsets” are naturally-imposed segments (e.g., summer monsoon and winter gaps at the APT, short-term campaigns of intense monitoring), with gaps between the segments exceeding, or comparable to, the length of the segment filled by observations. We obtain 14 such segments, covering the period HJD 2,447,859-2,450,636, with the number of observations per segment varying from 9 to 161. The most frequently appearing detail in the CLEANed PS is clustered around $\nu = 1.3\text{-}1.4 \text{ d}^{-1}$ (in 5 out of 14 PS). Twice, we detect a fairly strong signal at $\nu \approx 0.9 \text{ d}^{-1}$: HJD 2,448,896-2,448,976 (43 observations), and HJD 2,450,522-2,450,636 (82 observations). Concerning the most abundant data set secured during the 1992 campaign (161 data points distributed over 135 days; practically all of them are shown on Fig.4.5), the expected signal at $\nu_0 = 0.440 \pm 0.018 \text{ d}^{-1}$ is enhanced only during a few cycles, between HJD 2,448,818-2,448,824 (Fig.4.5). We have used the data shown in the middle section of Figure 4.5 to construct a folded light curve with $\mathcal{P} = 2.27$ day (ephemeris from McCandliss et al. 1994). Despite the fact that the periodic signal found during the interval HJD 2,448,818-2,448,824 is identical to the one found in the independently and practically simultaneously acquired spectroscopic data set — thus demonstrating that this detection is unlikely to be fortuitous —, the very noisy appearance of the folded light curve (Fig.4.6) shows that the detection of the $\mathcal{P} = 2.27$ day periodicity is only marginal in the photometric data set. Adopting $\nu_0 \approx 0.44 \text{ d}^{-1}$ as the principal frequency, we may interpret the $\nu \approx 0.9$ and $1.3\text{-}1.4 \text{ d}^{-1}$ components found in the other subsets as the first and second harmonics, respectively.

Another intensive multi-site monitoring campaign in 1995 reveals the presence of the long-term $\mathcal{P} \approx 40$ day cyclic component (Marchenko et al. 1996b,

and our Fig.4.7), masking the relatively weaker $\nu_1 \approx 0.88 \text{ d}^{-1}$ frequency, along with the possible initiation of $\mathcal{P} \approx 7\text{-}8$ day variations (perhaps as in Antokhin & Cherepashchuk 1984) at HJD 2,449,920–2,449,948. The latter phenomenon points to the transient character of the $\mathcal{P} \approx 7\text{-}8$ day variations.

4.4.2 Similarities of the Variations Across a Given Line Profile

In an attempt to objectively and quantitatively examine a potential relationship in the pattern of variability displayed by different portions of a given line profile, we have calculated the Spearman rank-order correlation matrices (see, e.g., Johns & Basri 1995; Lago & Gameiro 1998) whose elements $r(i, j)$ give the degree of correlation between the line intensity variations at any pixels i and j across the line profile (these matrices are symmetric and a perfect positive correlation is found along the main diagonal where $i = j$). These matrices for He II $\lambda 4686$ are shown for all epochs in Figure 4.8, in the form of contour plots, where the lowest contour indicates a significant positive or negative correlation at the 99.9 % confidence level.

An inspection of these matrices allows one to draw the following general conclusions: (i) There are various regions in the auto-correlation matrices presenting a significant positive or negative correlation; (ii) If the variations were principally induced by the changes in the continuum flux level (§ 4.4.1.2), one would observe a tendency for a positive correlation over a substantial fraction of velocity space; this is clearly not observed; (iii) The main diagonal is not a straight line with a width corresponding to the velocity resolution (at most 100 km s^{-1} in our case), as expected if two contiguous velocity elements would vary in a completely uncorrelated fashion, but is considerably wider. This suggests that the same pattern of variability affects simultaneously a fairly large velocity range of the profile, as independently found by Lépine, Moffat, & Henriksen (1996), who derived a relatively large mean line-of-sight velocity dispersion for the emission

subpeaks travelling across the line profile of WR 134 ($\overline{\sigma_\xi} \approx 440 \text{ km s}^{-1}$) compared to other WR stars in their sample ($\overline{\sigma_\xi} \approx 100 \text{ km s}^{-1}$).

If we turn to a detailed epoch-to-epoch comparison of the matrices in Figure 4.8, we find significant differences (note that the phase coverage is sufficiently similar for all epochs for a direct comparison to be made). For example, a positive correlation is observed for epoch I at $(-500, +2400)$ and $(+200, +1800) \text{ km s}^{-1}$, whereas the variations in these velocity ranges are rather negatively correlated for epoch II. The paucity of contours for epoch III indicates that no significant relationship existed for this epoch between the changes presented by different portions of the He II $\lambda 4686$ line profile. This leads to the conclusion that the global pattern of variability is likely to differ notably in nature on a yearly timescale, although the LPVs are coherent over shorter timescales when phased with the 2.27 day period (Figs.4.4a-4.4c).

4.4.3 Similarities Between the Variations of Different Lines

The similar qualitative behavior of different lines has already been emphasized in the past (McCandliss 1988; Marchenko 1988; Vreux et al. 1992; McCandliss et al. 1994). Here, we re-address this point by calculating the degree of correlation between the LPVs at different projected velocities (referred to the line laboratory rest wavelength) in two given line profiles. The spectra obtained during epoch III are well suited for this purpose because of their wide spectral coverage. The correlation matrices of He II $\lambda 5412$ with He II $\lambda 4542$, He II $\lambda 4686$, He II $\lambda 4859$, and the doublet C IV $\lambda 5806$ are presented for this epoch in Figure 4.9. As revealed by the prevalence of contours along the main diagonal, the LPVs presented by the He II lines are generally well correlated (this is especially true for the relatively unblended lines He II $\lambda 5412$ and He II $\lambda 4686$), emphasizing that they vary in a fairly similar fashion. This is remarkable as the presence of blends and/or noise tends to mask any potential correlation. Only the blue wings of He II $\lambda 5412$ and

C IV $\lambda 5806$ are positively correlated for epoch III. The changes affecting He II $\lambda 4686$ and He II $\lambda 4542$ are also well correlated for epochs I and II.

4.5 Discussion

4.5.1 The Duplicity of WR 134 Questioned

In view of the long-suspected association of WR 134 with an orbiting collapsed companion (Antokhin et al. 1982; Antokhin & Cherepashchuk 1984), we discuss below the implications of these observations with respect to this scenario.

4.5.1.1 The Expected Emergent X-ray Luminosity

An interesting issue is whether the predicted X-ray luminosity produced by the accretion process (after allowance for wind absorption) can be reconciled with the X-ray observations of WR 134.

First, if we associate the 2.27 day periodicity with orbital motion, we can obtain an estimate of the location of the compact object in the WR wind. Assuming for simplicity a circular orbit (i.e., that the circularization timescale is shorter than the evolutionary timescale; Tassoul 1990), a canonical mass for the secondary as a neutron star, $M_X = 1.4 M_\odot$, and a mass for WR 134, $M_* = 11 M_\odot$ (Hamann, Koesterke, & Wessolowski 1995), we obtain an orbital separation of $a \approx 17 R_\odot$, or $a \approx 6$ WR core radii (Hamann et al. 1995).⁴

Second, the *total* X-ray luminosity (in ergs s⁻¹) produced by Bondi-Hoyle

⁴Since the observationally determined masses of WN 6 stars in binary systems show a large scatter ($M_* \approx 14 M_\odot$ in WR 153; St-Louis et al. 1988 — $M_* \approx 48 M_\odot$ in WR 47; Moffat et al. 1990), we use here a value given by atmospheric models of WR stars (adopting $M_* \approx 14 M_\odot$ or $48 M_\odot$ does not qualitatively change the conclusions presented in the following).

accretion of a stellar wind onto a degenerate object can be expressed by the following relation (Stevens & Willis 1988):

$$L_X \approx 2.03 \times 10^{57} \eta \dot{M} M_X^2 a^{-2} v(a)^{-4} \left(1 - \frac{L_X}{L_E}\right)^2, \quad (4.1)$$

where η is the efficiency of the conversion of gravitational energy into X-ray emission; \dot{M} the mass-loss rate of the primary (in $M_\odot \text{ yr}^{-1}$); $v(a)$ the WR wind velocity at the secondary's location (in km s^{-1}), and L_E the Eddington luminosity (in ergs s^{-1}) given by $L_E \approx 5.02 \times 10^{37} M_X / \sigma_e$ (the electron scattering coefficient $\sigma_e = 0.35$). In this expression, we neglect the orbital velocity of the secondary relative to the (much larger) WR wind velocity. For the latter, we start by arbitrarily adopting the well-established mean velocity law for O stars of the form (Pauldrach, Puls, & Kudritzki 1986)⁵:

$$v(r) = v_\infty (1 - R_*/r)^{0.8}. \quad (4.2)$$

Note that at the assumed location of the secondary ($r \approx 6 R_*$; see above) the wind has almost reached its terminal velocity, $v_\infty = 1900 \text{ km s}^{-1}$ (Rochowicz & Niedzielski 1995). We further assume: $\dot{M} = 8 \times 10^{-5} M_\odot \text{ yr}^{-1}$ (Hogg 1989), and $\eta = 0.1$ (McCrory 1977). This yields: $L_X \approx 1.4 \times 10^{37} \text{ ergs s}^{-1}$.

We have modeled the emergent X-ray flux by a power law with energy index α , substituted above a characteristic high-energy cutoff E_c by the function $\exp[(E_c - E)/E_f]$, as commonly observed in accretion powered pulsars (White, Swank, & Holt 1983; Kretschmar et al. 1997). The values of α , E_c , and E_f are chosen to be roughly representative of accreting pulsars: $\alpha \approx -0.2$; $E_c \approx 15 \text{ keV}$; $E_f \approx 15 \text{ keV}$ (White et al. 1983). The X-ray spectrum was normalized to the total X-ray luminosity determined above, i.e., $L_X = 1.4 \times 10^{37} \text{ ergs s}^{-1}$.

The next step is to evaluate the attenuation of the beam of photons as they propagate through the stellar wind. Since the absorption properties of ionized

⁵We explore below the impact on L_X of more recently proposed (but not yet well established) revisions for the velocity law and mass-loss rate of WR stars.

plasmas are dramatically dependent on their ionization state (e.g., Woo et al. 1995), one has first to determine to what degree the accreting compact object ionizes the surrounding stellar wind. The presence of an immersed, strongly ionizing companion is expected to create an extended X-ray photoionized zone in its vicinity (Hatchett & McCray 1977). An investigation of the effect of the ionizing X-ray flux coming from the secondary on the surrounding wind material requires a detailed calculation of the radiative transfer (Kallman & McCray 1982). However, good insight into the ionization state of an *optically thin* gas illuminated by a X-ray point source can be obtained by considering the quantity (Hatchett & McCray 1977):

$$\xi(r, r_X) = \frac{L_X}{n(r)r_X^2} = \frac{4\pi L_X \bar{m}}{\dot{M}} v(r) \left(\frac{r}{r_X} \right)^2, \quad (4.3)$$

with: $n(r)$ the local number density of the gas; r_X the distance from the X-ray source. This expression is derived using the mass continuity equation: $\dot{M} = 4\pi r^2 \bar{m} n(r) v(r)$. Here, \bar{m} is the average mass per ion (we assume a pure helium atmosphere). The velocity of the material as a function of r is given by equation (4.2). The variations of $\log \xi(r, r_X)$ are illustrated as viewed from above the orbital plane in Figure 4.10. In the limit $\xi \rightarrow 0$ ergs cm s⁻¹, the ionization balance of the material is unaffected by the presence of the X-ray emitter, i.e., is principally governed by the radiation field of the WR star. We stress that this model assumes an optically thin plasma. In reality, the mean path length of the X-ray photons is considerably shorter, and it is thus likely that the X-ray photoionized zone would be dramatically less extended — especially in the direction toward the primary — than sketched here.

The predicted (after wind absorption) X-ray luminosities for the wavebands corresponding to the *PSPC* and *IPC* detectors onboard the *ROSAT* and *Einstein* observatories (0.2-2.4 and 0.2-4.0 keV, respectively) have been computed for three illustrative cases spanning a wide range in the wind ionization state, namely $\log \xi = 2.1$, 1.8, and 0 ergs cm s⁻¹. The photoelectric atomic cross sections for

ionized plasmas are taken from Woo et al. (1995). Thompson scattering by the free electrons was also taken into account. The two former values, $\log \xi = 2.1$ and $1.8 \text{ ergs cm s}^{-1}$, are roughly what would be expected in the framework of our model (Fig.4.10), whereas in the latter case, $\log \xi = 0 \text{ ergs cm s}^{-1}$, we explore the (somewhat unrealistic) case in which the presence of the neutron star has no effect on the surrounding stellar wind. In this case, photoelectric cross sections for cold interstellar gas were used (Morrison & McCammon 1983). Because the WR wind material is, by nature, far from neutral, the derived X-ray luminosities are here *strictly lower* limits.

Pollock (1987) reported on two pointed *IPC* observations of WR 134 obtained with the *Einstein* satellite, with no evidence for variability (see his Table 5). The derived (corrected for interstellar extinction) X-ray luminosity in the 0.2-4.0 keV band, $4.6 \pm 1.6 \times 10^{32} \text{ ergs s}^{-1}$, being consistent with the upper limit derived by Sanders et al. (1985): $4.5 \times 10^{32} \text{ ergs s}^{-1}$ (when scaled to the same adopted distance of 2.1 kpc; van der Hucht et al. 1988). On the other hand, a single measurement (due to the *ROSAT* satellite) is available in the 0.2-2.4 keV range (Pollock, Haberl, & Corcoran 1995). With no clear indication of X-ray variability, we will assume in the following that the *typical* observed (and corrected for interstellar extinction) X-ray luminosities from WR 134 are: 0.46 ± 0.22 and $4.6 \pm 1.6 \times 10^{32} \text{ ergs s}^{-1}$ in the 0.2-2.4 and 0.2-4.0 keV bands, respectively.⁶

These values can be directly compared with the predicted X-ray luminosities after wind absorption shown as a function of orbital phase in Figure 4.11. For $\log \xi = 2.1$ and $1.8 \text{ ergs cm s}^{-1}$, the observed luminosities are systematically much lower than expected in the framework of our model, with a deficiency reaching 2-3 orders of magnitude. For $\log \xi = 0 \text{ ergs cm s}^{-1}$, the *ROSAT* data are consistent with the expectations. However, and unless the *Einstein* satellite observed WR

⁶Unfortunately, the relatively large uncertainty in the period (§4.4.1.1) does not allow to fold in phase the *ROSAT* and *Einstein* data, thus preventing the construction of an observed X-ray light curve of WR 134.

134 near X-ray eclipse, the same conclusion does not hold for the data in the 0.2-4.0 keV band, with an order of magnitude deficiency. Although mildly significant, this deficiency shows that, even in the extreme case in which the presence of the accreting neutron star has a negligible effect on the WR wind, the observed and predicted X-ray luminosities can hardly be reconciled. Overall, and although we stress that more detailed and rigorous calculations are necessary, the deficiency of the observed X-ray flux must thus be regarded as serious. This conclusion is bolstered if one considers that wind radiative instabilities may largely account for the observed fluxes (typically 10^{32-33} ergs s $^{-1}$ in the 0.2-2.4 keV range; Wessolowski 1996).

Assuming a lower mass-loss rate due to clumping (Moffat & Robert 1994; Nugis, Crowther, & Willis 1998) may, at best, reduce the discrepancy by one order of magnitude (see equation [4.1]). In contrast, however, assuming a “softer” $v(r)$ law (i.e., $\beta > 0.8$; see equation [4.2]) for WR stars (Schmutz 1997; Lépine & Moffat 1999; Antokhin, Cherepashchuk, & Yagola 1998), or taking into account the existence of a velocity plateau inside the photoionized zone (Blondin 1994), exacerbates the discrepancy.

Considering that the soft X-ray flux of WR 134 is very similar to that of other *bona fide single* WN stars (Pollock 1987), and was even among the lowest found for single WN 6 stars during the *ROSAT* all-sky survey (Pollock et al. 1995), this deficiency of predicted X-ray flux suggests centrifugal (or magnetic) inhibition to prevent the gravitational capture by the compact object of the primary’s wind material (the so-called “propeller effect”; Lipunov 1982; Campana 1997; Cui 1997; Zhang, Yu, & Zhang 1998). Note that orders of magnitude deficiency in the X-ray flux is observed in some high-mass X-ray binaries (HMXRBs; e.g., Taylor et al. 1996).

4.5.1.2 Modeling the Line-profile Variations Caused by an Ionizing X-ray Source

Keeping in mind that the accretion process would be, as suggested above, much less efficient than expected in the Bondi-Hoyle approximation — and therefore that the influence of the X-ray source on the surrounding wind material would be far less severe than sketched in Figure 4.10 — we performed simulations of the LPVs caused by the orbital revolution of a localized, strongly ionized wind cavity.

We proceed with numerical simulations of the observed LPVs of the representative He II $\lambda 4686$ line, binning the epoch I spectra to 0.1 phase resolution. We modify the SEI code (Sobolev method with exact integration: Lamers, Cerruti-Sola, & Perinotto 1987; hereafter LCP) to allow for the variation of the source function in a 3-D space, thus breaking the initially assumed spherical symmetry of the WR wind. The variation of the unperturbed source function as a function of the radial distance from the star is described by equation (4) of LCP. The wind dynamics is assumed to be identical inside, and outside the photoionized cavity. Specifically, we adopt a β -velocity law with an exponent $\beta = 3$ and a ratio of the wind velocity at the inner boundary of the optically thin part of the WR wind to the terminal velocity, w_0 , of 0.25 (see equation [35] of LCP).

We start from the assumption that the underlying, unperturbed line profile is not affected by any phase-dependent variations. We fit this reference profile with the standard SEI code, preserving complete spherical symmetry. Throughout these simulations, we adopt $\tau_T = 0.60$, $\alpha_1 = 6.0$, $\alpha_2 = 0.5$, $\epsilon'_0 = 12.0$, $B_0 = 1.2$, $a_T = 0.2$, and $w_D = 0.25$ (these values are uncertain to about 30 %). We refer the reader to LCP for a complete description of these parameters. Note that these values slightly differ from those adopted by Marchenko & Moffat (1998b) due to a different approach in modelling (adopting their values, however, would not

qualitatively modify the conclusions drawn in the following). Note that while the issue of the flattened, asymmetric wind in WR 134 is appealing (Schulte-Ladbeck et al. 1992; Moffat & Marchenko 1993b), this inevitably introduces a great and probably unnecessary complexity into the simulations.

There are two obvious choices for the reference profile of the unperturbed wind: a minimum-emission or maximum-emission profile, derived from a smoothed minimum/maximum emissivity at a given wavelength for a given phase (Fig.4.12). By introducing 3-D variations into the source function of the unperturbed wind corresponding to the minimum-emission reference profile, we immediately find that we are not able to reproduce the observed LPVs with any reasonable choice of the parameters. Thus we adopt the maximum-emission representation of the unperturbed profile as a starting approximation.

To simulate the X-ray induced cavity in the otherwise spherically symmetric wind, we require the following free parameters: Θ — the azimuthal extension of the cavity; $\Delta z = \Delta p$ — line-of-sight and impact-parameter extension of the cavity; Δz_0 — line-of-sight distance of the cavity's inner boundary from the stellar core; i — orbital inclination; k — coefficient describing the deviation of the source function within the cavity, namely $S(\text{cavity}) = k \times S(\text{wind})$; ϕ_0 — cross-over phase (frontal passage of the cavity). We assume a circular orbit. A sketch of the adopted geometry is shown in Figure 4.13.

With these parameters, we attempt to fit all the phase-binned profiles, minimizing the observed minus model deviations in the χ^2 sense, while reproducing the observed TVS of He II $\lambda 4686$ (Fig.4.12). We also attempt to make the (O – C) profile deviations distributed as evenly as possible over the entire phase interval. We concentrate on the goodness of the fit for the velocities not exceeding $\pm 0.8 v_\infty$, since it is impossible to match the red wing of the He II $\lambda 4686$ profile (electron scattering effect; see Hillier 1991) as well as the bluest portion (partial blending with N III transitions).

After an extensive search for optimal parameters, we find that the following set reproduces the observed LPVs reasonably well (Fig.4.14): $\Theta = 140 \pm 10^\circ$, $\Delta z = \Delta p = 8 \pm 0.5 R_*$, $\Delta z_0 = 2.7 \pm 0.2 R_*$, $i = 65 \pm 5^\circ$, $k = 0.07 \pm 0.01$ (i.e., practically zero emissivity from the X-ray eroded wind), and $\phi_0 = 0.55 \pm 0.03$. This value of ϕ_0 means that the X-ray source passes in front when the continuum flux undergoes a shallow minimum (Fig.4.6). The largest (O – C) deviations are concentrated around phases 0.0 and 0.5. By no means are we able to reproduce the extended emissivity excesses at $v \approx -0.5 v_\infty$ ($\phi = 0.35$) and $v = + (0.5-0.7) v_\infty$ ($\phi = 0.65$ and 0.75). These deviations *might* be generated by a low-amplitude velocity shift of the underlying profile as a whole, due to binary motion (partially inducing the centroid variations seen in Fig.4.2). We will not consider this possibility further, as it will add more free parameters into the model. We are able to reproduce only the general appearance of the TVS as a structured, non-monotonic function with 3 distinct maxima, without precise match of their amplitudes and positions (Fig.4.12).

According to Model 5 of Kallman & McCray (1982), helium is fully ionized for $\log \xi \gtrsim 1.5$ ergs cm s⁻¹. The derived azimuthal and radial extensions of the cavity indeed match fairly well the size of the highly ionized zone with $\log \xi \approx 1.5$ ergs cm s⁻¹ (Fig.4.10), especially if we take into account its large azimuthal extension. However, since the accretion is likely to be partially inhibited and the WR wind is not optically thin, the real photoionized cavity will be much less extended than sketched in Figure 4.10. For example, reduction of the efficiency of the X-ray generation by 1-2 orders of magnitude would dramatically reduce the dimension of the $\log \xi \approx 1.5$ cavity (to the size of the $\log \xi \gtrsim 2.5$ cavities sketched in Figure 4.10; see equation [4.3]). The local nature of this putative zone is also suggested by an inspection of the P Cygni absorption profile variations of He I $\lambda 4471$ and N V $\lambda 4604$. The epoch I spectra have been grouped into broad phase bins of width 0.2 (the P Cygni absorptions are very weak, thus requiring an extremely high S/N), and are overplotted in Figure 4.15. It is apparent that

potential phase-related variations do not significantly exceed the observationally-inflicted accuracy. Thus, neither the base of the wind ($\text{N V } \lambda 4604$), nor the relatively distant regions ($\text{He I } \lambda 4471$) are *seriously* affected by the presence of the photoionized cavity. An inspection of 16 archive *IUE* SWP spectra of WR 134 obtained during the period 1989 November 30 - December 6 (see Table 4.3) also shows that no UV lines with well-developed P Cygni absorption components show any significant variability in their absorption troughs. Hints of relatively weak, *possibly* phase-locked variations are only evident in the emission parts.

We conclude that despite the encouraging similarity between the observed and modeled line-profiles, the relatively large derived size of the cavity ($R \approx 8 R_*$) along with its large azimuthal extension seem to enter in conflict with the low level of X-ray flux observed from WR 134.

4.5.1.3 On the Origin of the Long-term Modulations

Another question we may ask is whether this model is able to account for the $\mathcal{P} \approx 40$ and $\mathcal{P} \approx 625$ day recurrence timescales present in the photometric data (Marchenko et al. 1996b; Marchenko & Moffat 1998a), as well as the epoch-dependent nature of the LPVs (Figs.4.2 and 4.4).

As the wind approaches the compact object, it is gravitationally focused, forming a standing bow shock. This leads to the formation of an extended wake downstream (Blondin et al. 1990). This process is suspected to be non-stationary in HMXRBs, with the possible formation of a quasi-cyclical “flip-flop” instability (Benenohn, Lamb, & Taam 1997; but see Ruffert 1997), with characteristic timescales comparable to the flow time across the accretion zone (\approx minutes); too short a timescale to account for *any* observed long-term variations in WR 134.

Alternatively, it is tempting to associate the 40 day recurrence timescale to

the precession of a tilted accretion disk as suggested in some HMXRBs (Heermanskerk & van Paradijs 1989; Wijnands, Kuulkers, & Smale 1996). The condition for the creation of a persistent accretion disk around a wind-fed neutron star orbiting an early-type companion can be written as (Shapiro & Lightman 1976):

$$2.7 \times 10^{-11} \gamma^8 B_{12}^{-4/7} R_{10}^{-10/7} M_X^{20/7} M_*^{-4} P^{-2} R_*^4 L_X^{2/7} \gtrsim 1 \quad (4.4)$$

With B_{12} the surface magnetic field of the neutron star in units of 10^{12} Gauss, R_{10} the radius of the neutron star in units of 10 km, M_X and M_* in units of solar masses, P in units of days, R_* in units of solar radii, and L_X in units of ergs s $^{-1}$. γ is expressed by the relation: $\gamma \approx \zeta^{1/2} [v_{esc}/v(a)]$ where ζ is a dimensionless quantity accounting for the deviation from the Hoyle-Lyttleton treatment, and v_{esc} the escape velocity at the WR “photosphere” (we neglect the orbital velocity of the neutron star relative to the WR wind velocity). Taking $B_{12} = R_{10} = \zeta = 1$, we obtain a value much below unity ($\sim 10^{-4}$), suggesting that accretion mediated by a persistent disk in WR 134 would be very unlikely.

A viable mechanism that might, however, account for the monthly changes in the spectroscopic pattern of variability (Figs.4.2 and 4.4) is to consider long-term changes in the accretion rate (thus varying the size of the ionized cavity surrounding the compact companion).

4.5.2 Wind-related Variability?

Although the encouraging agreement between the observed and modeled LPVs (Fig.4.14) leads to the conclusion that the model involving an accreting compact companion cannot be completely ruled out by the present observations, the very low observed X-ray flux of WR 134 which imposes inhibited accretion, as well as the long-term changes in the accretion rate required to account for the epoch-dependent nature of the LPVs, set serious constraints on this model. This, together with the inconclusive search for rapid *periodic* photometric variations,

possibly induced by a spinning neutron star (Antokhin et al. 1982; Marchenko et al. 1994) can be used to argue that the existence of such a low-mass collapsed companion is questionable.

Alternatively, it is conceivable that we observe rotationally-modulated variability in WR 134. Indeed, the global pattern of spectral variability resembles in some aspects that of the apparently single WR star EZ CMa, for which the existence of a rotation-modulated, structured wind has been proposed (St-Louis et al. 1995; Morel et al. 1997, 1998; Harries et al. 1999). By analogy with EZ CMa, the He II line profiles vary in a fairly similar fashion (Vreux et al. 1992, and our Fig.4.9), changes in line skewness or FWHM generally demonstrate a rather simple and well-defined behavior when phased with the 2.27 day period (Fig.4.2), and a positive/negative correlation between the pattern of variability presented by different parts of the same line profile is occasionally found (Fig.4.8). Other outstanding properties shared by WR 134 and EZ CMa are the epoch-dependent nature of the variations, as well as the substantial depolarization of the emission lines (Harries et al. 1998); this last point being generally attributed to an equatorial density enhancement (see also Ignace et al. 1998).

Another piece of evidence pointing to the similarity between WR 134 and EZ CMa comes from the broadband (\sim continuum) polarimetric observations of Robert et al. (1989). Plots of the Stokes parameters Q and U of WR 134 versus phase are shown in Figure 4.16 (because of a likely loss of coherency over long timescales, the two data subsets separated by a year are plotted separately). The data show strong epoch-dependent variations, with a clear single-wave variation in U (less clear in Q) in 1985, and a fairly clear double-wave modulation in Q (less clear in U) in 1986. This behavior is qualitatively very similar to what is observed in EZ CMa (e.g., Robert et al. 1992), although the polarimetric variations are not as clearly phase-locked in WR 134. Such a drastic change from a single-wave to a double-wave modulation in data taken one year apart is not easily

acommodated by a binary hypothesis. However, neither the amount, nor the time coverage of the polarimetric data allow to regard it as a decisive evidence favoring the single-star interpretation. Although the 7 nights of linear spectropolarimetry of WR 134 by Schulte-Ladbeck et al. (1992) do show variations, both in the continuum and in the lines, the data are sparsely spread out over 6 months, making it impossible to separate variations on the 2.3-day cycle from long-term epoch-dependent variations. Certainly, further more intense spectropolarimetry on different timescales in all 4 Stokes' parameters will prove quite interesting.

Relying on the EZ CMa and WR 134 similarities, one may speculate that the 2.3-day periodicity in WR 134 is induced by a small number of spatially extended, relatively long-living and rotating wind streams whose formation is possibly triggered by photospheric perturbations, such as magnetic structures or pulsations (e.g., Cranmer & Owocki 1996; Kaper et al. 1997). Contrary to EZ CMa, however, WR 134 does not show any detectable phase-related changes in the UV or optical P Cygni absorption troughs, nor a clear correlation between changes occurring near the hydrostatic stellar “surface” and in the wind.

By speculating about the existence of (non)radial pulsations in WR 134 (although a search for related rapid light variations has been hitherto inconclusive; Cherepashchuk 1975; Antokhin et al. 1992), and exploring the idea of interactions between different pulsational modes, one is led to the notion of quasi-periodic ejection of shell-like structures. This idea can be explored via the application of the model introduced above for the anisotropic wind (§ 4.5.1.2). We allow for the formation of a shell with enhanced optical depth in the otherwise spherically symmetric wind. The shell geometry may be variable but, for the sake of simplicity, we mainly explore the spherically symmetric case. The shell can slowly propagate outwards at a given rate, slightly expanding and gradually approaching the physical conditions in the unperturbed surrounding wind. Indeed, at least the variations in the blue wing of He II $\lambda 4686$ (Figs.4.4a and 4.14) somewhat mimic

the expected behavior of such an outwardly-moving structure. However, there is also pronounced asymmetry between the blue and red parts of the He II $\lambda 4686$ profile, especially obvious around $\phi = 0.35\text{--}0.55$ (Fig.4.14). This asymmetry cannot be reproduced by any adjustment of the model free parameters, unless one makes the contrived assumption that the front- and back-side lobes of the shell are formed under different physical conditions. This leads us to discard the model of an expanding shell with central symmetry.

Although the existence of a globally inhomogeneous outflow in WR 134 is attractive, such an interpretation is also not without difficulties. For instance, the origin of the long-term (quasi)periodic changes in continuum flux, and of the epoch-dependency of the spectral changes remains unexplained. Magnetic activity, by inducing long-term changes in the global wind structure, may constitute a convenient, although largely ad hoc, way to accomodate this aspect of the variability.

Acknowledgments: We wish to thank J. W. Woo for kindly providing us with the photoelectric cross sections for ionized plasmas. We acknowledge Alex W. Fullerton and the referee, Mike Corcoran, for their detailed and helpful comments. T. M., S. V. M., A. F. J. M., and N. S.-L. wish to thank the Natural Sciences and Engineering Research Council (NSERC) of Canada and the Fonds pour la Formation de Chercheurs et l'Aide à la Recherche (FCAR) of Québec for financial support. P. R. J. E. is grateful to CONACyT. I. I. A. acknowledges financial support from Russian Foundation for Basic Research through the grants No. 96-02-19017 and 96-15-96489. T. E. is grateful for full financial aid from the Evangelisches Studienwerk/Germany which is supported by the German Government.

RÉFÉRENCES

- Antokhin, I. I., Aslanov, A. A., & Cherepashchuk, A. M. 1982, Sov. Astron. Lett., 8, 156
- Antokhin, I. I., & Cherepashchuk, A. M. 1984, Sov. Astron. Lett., 10, 155
- Antokhin, I. I., & Volkov, I. M. 1987, Inf. Bull. Var. Stars, 2973, 1
- Antokhin, I. I., Irsmambetova, T. R., Moffat, A. F. J., Cherepashchuk, A. M., & Marchenko, S. V. 1992, ApJS, 82, 395
- Antokhin, I. I., Bertrand, J.-F., Lamontagne, R., Moffat, A. F. J., & Matthews, J. M. 1995, AJ, 109, 817
- Antokhin, I. I., Cherepashchuk, A. M., & Yagola, A. G. 1998, Ap&SS, 354, 111
- Bappu, M. K. V. 1951, AJ, 56, 120
- Benensohn, J. S., Lamb, D. Q., & Taam, R. E. 1997, ApJ, 478, 723
- Blondin, J. M., Kallman, T. R., Fryxell, B. A., & Taam, R. E. 1990, ApJ, 356, 591
- Blondin, J. M. 1994, ApJ, 435, 756
- Brandt, N., & Podsiadlowski, P. 1995, MNRAS, 274, 461
- Campana, S. 1997, A&A, 320, 840
- Chalabaev, A., & Maillard, J. P. 1983, A&A, 127, 279
- Cherepashchuk, A. M. 1975, Astrophysics, 10, 218
- Cherepashchuk, A. M., & Aslanov, A. A. 1984, Ap&SS, 102, 97
- Crampton, D. 1971, MNRAS, 153, 303
- Cranmer, S. R., & Owocki, S. P. 1996, ApJ, 462, 469

- Cui, W. 1997, ApJ, 482, L163
- De Donder, E., Vanbeveren, D., & van Bever, J. 1997, A&A, 318, 812
- Esteban, C., & Rosado, M. 1995, A&A, 304, 491
- Firmani, C., Koenigsberger, G., Bisiacchi, G. F., Moffat, A. F. J., & Isserstedt, J. 1980, ApJ, 239, 607
- Fullerton, A. W., Gies, D. R., & Bolton, C. T. 1996, ApJS, 103, 475
- Fullerton, A. W., Massa, D. L., Prinja, R. K., Owocki, S. P., & Cranmer, S. R. 1997, A&A, 327, 699
- Gies, D. R., & Bolton, C. T. 1986, ApJS, 61, 419
- Gosset, E., Vreux, J.-M., & Andrillat, Y. 1994, Ap&SS, 221, 181
- Gosset, E., & Vreux, J.-M. 1996, in Proceedings of the 33rd Liège International Astrophysical Colloquium, ed. J.-M. Vreux et al., 231
- Gunn, J. E., & Ostriker, J. P. 1970, ApJ, 160, 979
- Hamann, W.-R., Koesterke, L., & Wesselowski, U. 1995, A&A, 299, 151
- Hansen, B. M. S., & Phinney, E. S. 1997, MNRAS, 291, 569
- Harries, T. J., Hillier, D. J., & Howarth, I. D. 1998, MNRAS, 296, 1072
- Harries, T. J., Howarth, I. D., Schulte-Ladbeck, R. E., & Hillier, D. J. 1999, MNRAS, in press
- Hartman, J. W. 1997, A&A, 322, 127
- Hatchett, S., & McCray, R. 1977, ApJ, 211, 552
- Heemskerk, M. H. M., & van Paradijs, J. 1989, A&A, 223, 154
- Hellings, P., & de Loore, C. 1986, A&A, 161, 75
- Hillier, D. J. 1991, A&A, 247, 455
- Hogg, D. E. 1989, AJ, 98, 282
- Ignace, R., Cassinelli, J. P., Morris, P., & Brown, J. C. 1998, in ESO Proceedings, Cyclical Variability in Stellar Winds, ed. L. Kaper & A. W. Fullerton, 29

- Johns, C. M., & Basri, G. 1995, AJ, 109, 2800
- Kallman, T. R., & McCray, R. 1982, ApJS, 50, 263
- Kaper, L., et al. 1997, A&A, 327, 281
- Kretschmar, P., et al. 1997, A&A, 325, 623
- Kumar, C. K., Kallman, T. R., & Thomas, R. J. 1983, ApJ, 272, 219
- Lago, M. T. V. T., & Gameiro, J. F. 1998, MNRAS, 294, 272
- Lamers, H. J. G. L. M., Cerruti-Sola, M., & Perinotto, M. 1987, ApJ, 314, 726
(LCP)
- Lamontagne, R. 1983, Ph.D. Thesis, Univ. Montréal
- Lépine, S., Moffat, A. F. J., & Henriksen, R. N. 1996, ApJ, 466, 392
- Lépine, S., & Moffat, A. F. J. 1999, ApJ, in press
- Lipunov, V. M. 1982, Sov. Astron. Lett., 8, 194
- Lorimer, D. R., Bailes, M., & Harrison, P. A. 1997, MNRAS, 289, 592
- Lyne, A. G., Anderson, B., & Salter, M. J. 1982, MNRAS, 201, 503
- Lyne, A. G., & Lorimer, D. R. 1994, Nature, 369, 127
- McCandliss, S. R. 1988, Ph.D. Thesis, Univ. Colorado
- McCandliss, S. R., Bohannan, B., Robert, C., & Moffat, A. F. J. 1994, Ap&SS, 221, 155
- McCray, R. 1977, Highlights Astr., 4, 155
- Marchenko, S. V. 1988, Kinemat. Phys. Celest. Bodies, Vol.4, 5, 25
- Marchenko, S. V., Antokhin, I. I., Bertrand, J.-F., Lamontagne, R., Moffat, A. F. J., Piceno, A., & Matthews, J. M. 1994, AJ, 108, 678
- Marchenko, S. V., Moffat, A. F. J., Lamontagne, R., Tovmassian, G. H. 1996a, ApJ, 461, 386

- Marchenko, S. V., Moffat, A. F. J., Antokhin, I. I., Eversberg, T., & Tovmassian, G. H. 1996b, in Proceedings of the 33rd Liège International Astrophysical Colloquium, ed. J.-M. Vreux et al., 261
- Marchenko, S. V., & Moffat, A. F. J. 1998a, ApJ, 499, L195
- Marchenko, S. V., Moffat, A. F. J., Eversberg, T., Hill, G. M., Tovmassian, G. H., Morel, T., & Seggewiss, W. 1998a, MNRAS, 294, 642
- Marchenko, S. V., & Moffat, A. F. J. 1998b, A&A, in press
- Marchenko, S. V., et al. 1998b, A&A, 331, 1022
- Mitra, A. 1998, ApJ, 499, 385
- Moffat, A. F. J. 1982, in IAU Symp. 99, Wolf-Rayet Stars: Observations, Physics, Evolution, ed. C. W. H. de Loore & A. J. Willis (Dordrecht: Kluwer), 263
- Moffat, A. F. J., & Shara, M. M. 1986, AJ, 92, 952
- Moffat, A. F. J., et al. 1990, ApJ, 350, 767
- Moffat, A. F. J., & Marchenko, S. V. 1993a, in ASP Conf. Ser. 35, Massive Stars: Their Lives in the Interstellar Medium, ed. J. P. Cassinelli, & E. B. Churchwell (San Francisco: ASP), 250
- Moffat, A. F. J., & Marchenko, S. V. 1993b, AJ, 105, 339
- Moffat, A. F. J., & Robert, C. 1994, ApJ, 421, 310
- Morel, T., St-Louis, N., & Marchenko, S. V. 1997, ApJ, 482, 470
- Morel, T., St-Louis, N., Moffat, A. F. J., Cardona, O., Koenigsberger, G., & Hill, G. M. 1998, ApJ, 498, 413
- Morrison, R., & McCammon, D. 1983, ApJ, 270, 119
- Nugis, T., Crowther, P. A., & Willis, A. J. 1998, A&A, 333, 956
- Pauldrach, A., Puls, J., Kudritzki, R. P. 1986, A&A, 164, 86
- Philp, C. J., Evans, C. R., Leonard, P. J. T., & Frail, D. A. 1996, AJ, 111, 1220
- Pollock, A. M. T. 1987, ApJ, 320, 283

- Pollock, A. M. T., Haberl, F., & Corcoran, M. F. 1995, in IAU Symp. 163, Wolf-Rayet Stars: Binaries, Colliding Winds, Evolution, ed. K. A. van der Hucht & P. M. Williams (Dordrecht: Kluwer), 512
- Robert, C., Moffat, A. F. J., Bastien, P., Drissen, L., & St-Louis, N. 1989, ApJ, 347, 1034
- Robert, C. 1992, Ph.D. Thesis, Univ. Montréal
- Robert, C., et al. 1992, ApJ, 397, 277
- Roberts, D. H., Lehár, J., & Dreher, J. W. 1987, AJ, 93, 968
- Rochowicz, K., & Niedzielski, A. 1995, Acta Astron., 45, 307
- Ross, L. W. 1961, PASP, 73, 354
- Ruffert, M. 1997, A&A, 317, 793
- Sanders, W. T., Cassinelli, J. P., Myers, R. V., & van der Hucht, K. A. 1985, ApJ, 288, 756
- Sayer, R. W., Nice, D. J., & Kaspi, V. M. 1996, ApJ, 461, 357
- Scargle, J. D. 1982, ApJ, 263, 835
- Schmutz, W., Geballe, T. R., & Schild, H. 1996, A&A, 311, L25
- Schmutz, W. 1997, A&A, 321, 268
- Schulte-Ladbeck, R. E., Nordsieck, K. H., Taylor, M., Bjorkman, K. S., Magalhães, A. M., & Wolff, M. J. 1992, ApJ, 387, 347
- Shapiro, S. L., & Lightman, A. P. 1976, ApJ, 204, 555
- Stevens, I. R., & Willis, A. J. 1988, MNRAS, 234, 783
- St-Louis, N., Moffat, A. F. J., Drissen, L., Bastien, P., Robert, C. 1988, ApJ, 330, 286
- St-Louis, N., Dalton, M. J., Marchenko, S. V., Moffat, A. F. J., & Willis, A. J. 1995, ApJ, 452, L57
- Tassoul, J.-L. 1990, ApJ, 358, 196

- Taylor, A. R., Young, G., Peracaula, M., Kenny, H. T., Gregory, P. C. 1996, A&A, 305, 817
- Underhill, A. B., Gilroy, K. K., Hill, G. M., & Dinshaw, N. 1990, ApJ, 351, 666
- Vanbeveren, D. 1991, Space Sci. Rev., 56, 249
- van den Heuvel, E. P. J., & De Loore, C. 1973, A&A, 25, 387
- van den Heuvel, E. P. J. 1976, in IAU Symp. 73, Structure and Evolution of Close Binary Systems, ed. P. Eggleton, S. Mitton, & J. Whelan (Dordrecht: Reidel), 35
- van der Hucht, K. A., Hidayat, B., Admiranto, A. G., Supelli, K. R., & Doom, C. 1988, A&A, 199, 217
- van Kerkwijk, M. H., Geballe, T. R., King, D. L., van der Klis, M., & van Paradijs, J. 1996, A&A, 314, 521
- van Leeuwen, F., Evans, D. W., Grenon, M., Großmann, V., Mignard, F., & Perryman, M. A. C. 1997, A&A, 323, L61
- Vreux, J.-M., Gosset, E., Bohannan, B., & Conti, P. S. 1992, A&A, 256, 148
- Wang, Q. D. 1995, ApJ, 453, 783
- Wessolowski, U. 1996, in Proceedings of the 33rd Liège International Astrophysical Colloquium, ed. J.-M. Vreux et al., 345
- White, N. E., Swank, J. H., & Holt, S. S. 1983, ApJ, 270, 711
- White, R. L., & Becker, R. H. 1996, ApJ, 451, 352
- Wijnands, R. A. D., Kuulkers, E., & Smale, A. P. 1996, ApJ, 473, L45
- Williams, P. M., Dougherty, J. M., Davis, R. J., van der Hucht, K. A., Bode, M. F., & Gunawan, D. Y. A. 1997, MNRAS, 289, 10
- Woo, J. W., Clark, G. W., Blondin, J. M., Kallman, T. R., & Nagase, F. 1995, ApJ, 445, 896
- Young, A. T., et al. 1991, PASP, 103, 221

Zhang, S. N., Yu, W., & Zhang, W. 1998, ApJ, 494, L71

Zhilyaev, B. E., & Khalack, V. R. 1996, Kinemat. Phys. Celest. Bodies, Vol.12, 2, 14

TABLEAU 4.1. Journal of spectroscopic observations

Epoch	Date	HJD - 2,440,000	Observatory ^a	Number of Spectra	Reciprocal		
					Spectral Coverage (Å)	Dispersion (Å pix ⁻¹)	S/N
I	92 Jul - Aug	8813-8843	SPM	65	4380-4790	0.41	~ 160
II	93 Oct	9258-9269	SPM	38	3990-4840	0.83	~ 115
III	95 May - Oct	9860-10005	OMM, DAO	32	4360-5080	1.62	~ 210
				30	5050-5945	1.62	~ 290

^a SPM: San Pedro Mártir Observatory 2.1 m (Mexico); OMM: Observatoire du Mont Mégantic 1.6 m (Canada); DAO: Dominion Astrophysical Observatory 1.2 m (Canada).

TABLEAU 4.2. Journal of photometric observations

Date	HJD - 2,440,000	Observatory ^a	Number		Mode of Observation	Filter Set ^b
			of Binned Observations	—		
89 Nov - 93 Feb	7859-9045	HIPPARCOS	44	—	H_p ($\sim B + V$) ^c	
90 May - 97 Jul	8025-10636	APT	483	Diff. phot.	V	
92 Jun - Jul	8800-8828	SPM	28	2-ch. phot.	5185 (250)	
92 Jun - Jul	8800-8832	SPM	23	Diff. phot.	V	
92 Jul	8819-8833	MO	55	Diff. phot.	6012 (87)	
95 Jun - Jul	9885-9903	CR	13	Diff. phot.	V	
95 Jun - Aug	9891-9949	SPM	88	Diff. phot.	V	

^a APT: Automatic Photometric Telescope 0.25 m (USA); SPM: San Pedro Mártir Observatory 0.84 m (Mexico); MO: Maidanak Observatory 0.6 m (Uzbekistan); CR: Observational Station in Crimea 0.6 m (Ukraine).

^b For the midband filters, we provide the central wavelength and FWHM (in Å).

^c See van Leeuwen et al. (1997).

TABLEAU 4.3. *IUE* SWP high resolution spectra of WR 134

SWP Image Number	JD - 2,440,000 ^a	Phase ^b
37705	7861.092	0.396
37707	7861.213	0.449
37718	7863.008	0.240
37725	7863.981	0.669
37727	7864.097	0.720
37734	7865.136	0.178
37735	7865.184	0.199
37737	7865.315	0.256
37739	7865.427	0.306
37741	7865.543	0.357
37743	7865.655	0.406
37745	7865.765	0.455
37748	7865.972	0.546
37750	7866.095	0.600
37755	7866.976	0.988
37757	7867.103	0.044

^a Julian Date at the midpoint of the exposure (2400 s for all spectra).

^b According to the ephemeris of McCandliss et al. (1994): $JD\ 2,447,015.753 + 2.27\ E$.

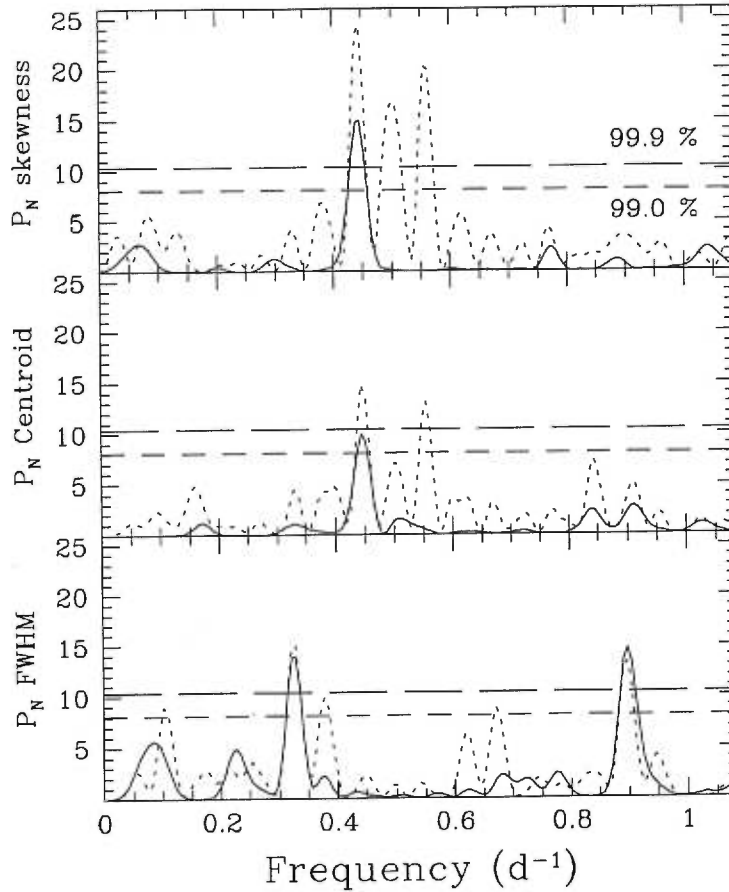


FIGURE 4.1. Power spectra (normalized to the total variance of the data) of the skewness, centroid, and FWHM time series of He II $\lambda 4686$ for epoch I. *Dotted line:* raw PS; *solid line:* CLEANed PS. The short- and long-dashed horizontal lines indicate the 99.0 % and 99.9 % confidence levels for the presence of a deterministic signal in the time series, respectively. The number of iterations of the CLEAN algorithm, N , has been set to 3400 (skewness), 380 (centroid), and 4500 (FWHM); a gain $g = 0.2$ has been used throughout. The algorithm is generally insensitive to the combination of these two parameters in the range $N \gtrsim 100$ and $g \leq 0.5\text{--}0.8$.

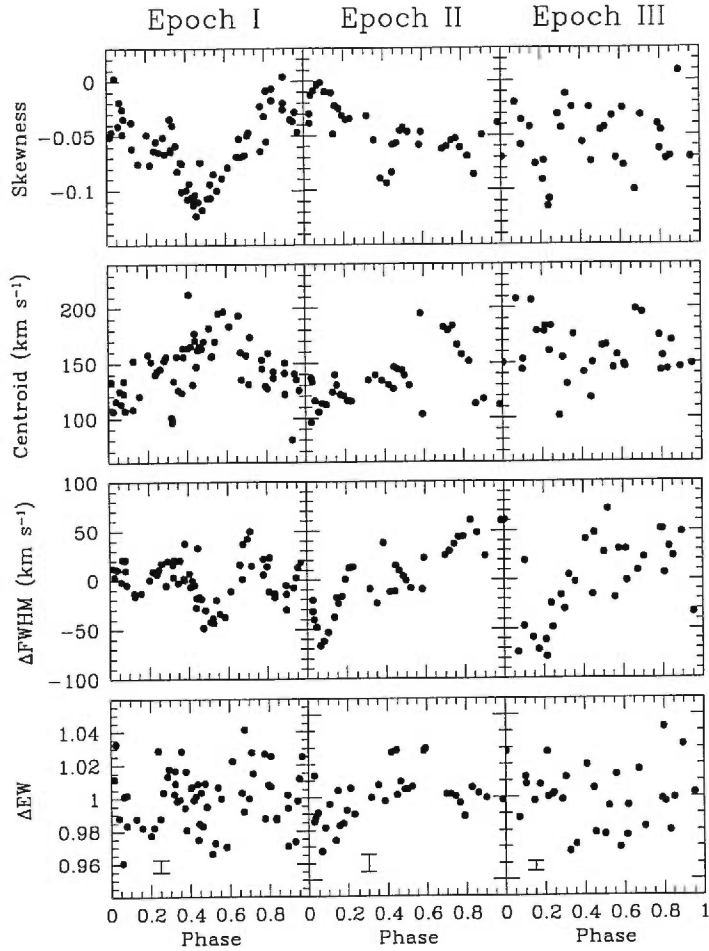


FIGURE 4.2. Skewness and centroid variations, deviations of the FWHM around the mean value (in km s^{-1}), and EW variations (normalized by division to the mean value) of He II $\lambda 4686$ for each epoch, as a function of phase. The 2σ error bars for the EW values were calculated according to Chalabaev & Maillard (1983). As everywhere in this paper, the ephemeris of McCandliss et al. (1994) has been adopted: $HJD 2,447,015.753 + 2.27 E$.

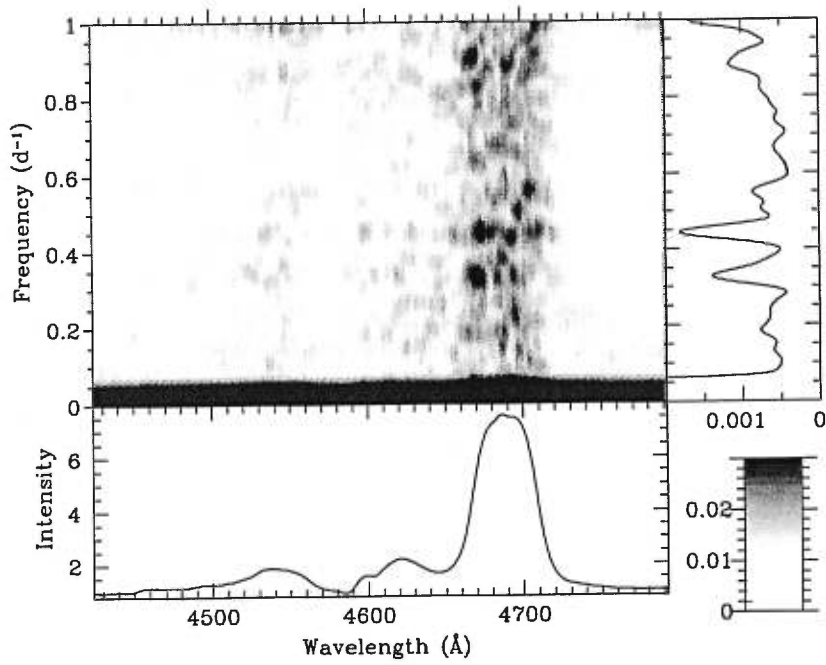


FIGURE 4.3. The pixel-to-pixel CLEANed PS of the rectified spectra of epoch I. The lower and right-hand panels show the mean spectrum and the normalized, integrated power over all pixels, respectively. The highest peak corresponds to a frequency: $\nu_0 \approx 0.444 \text{ d}^{-1}$. The gain and the number of iterations have been set to 0.3 and 250, respectively.

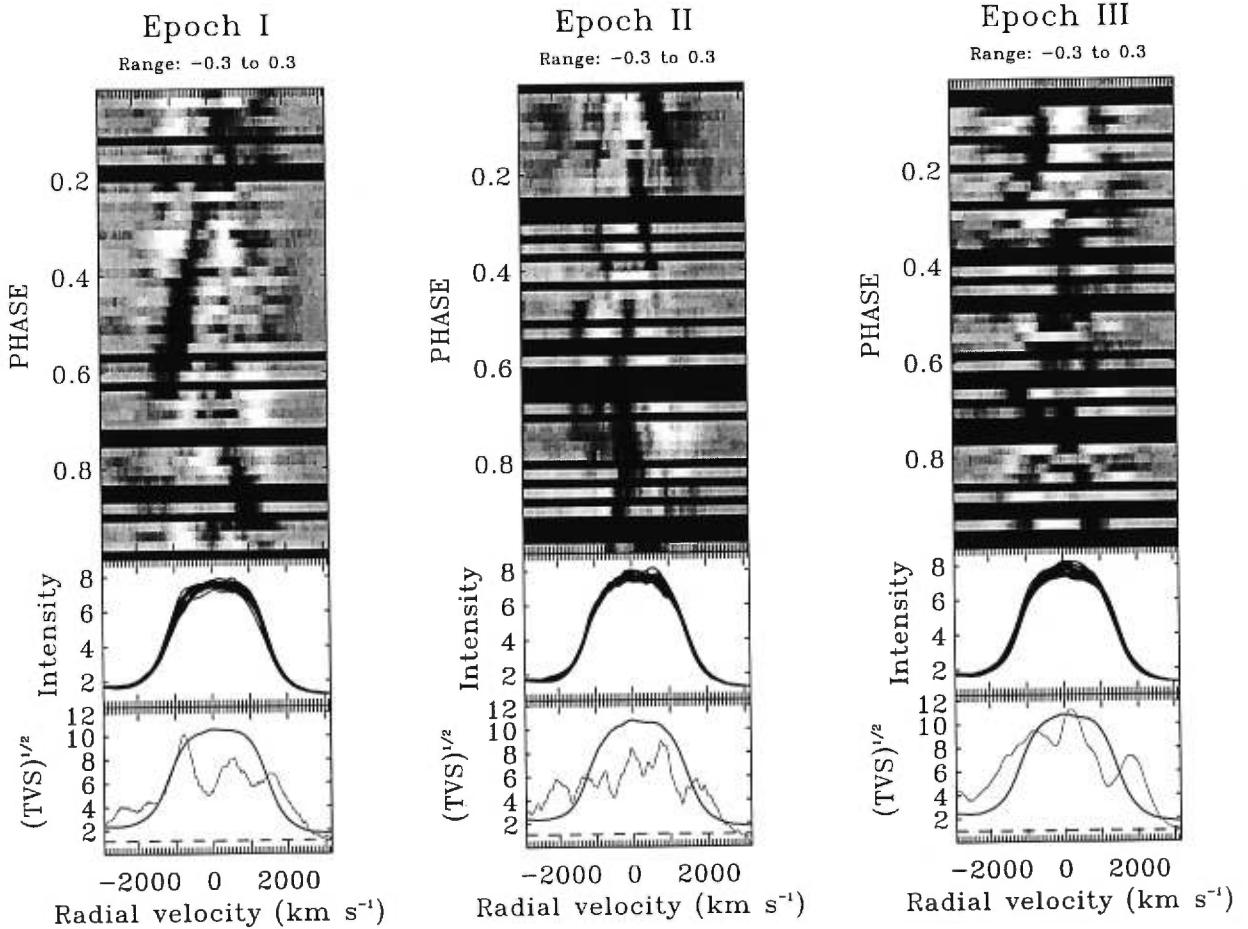


FIGURE 4.4. Gray-scale plots of the time series of the residuals of He II $\lambda 4686$ for each epoch, as a function of phase. The residuals are the binned (to 0.02 phase resolution) He II $\lambda 4686$ line profiles minus their corresponding unweighted means for each epoch. Excess emission components appear brighter in these plots. The middle portion of each panel shows a superposition of the rectified profiles. The values of the temporal variance spectrum (TVS; Fullerton, Gies, & Bolton 1996), along with the horizontal dashed line indicating the 99.0 % confidence level for significant variability, are displayed in the lower portion of each panel. The mean profile (in arbitrary units) of the epoch is overplotted. The gray-scales plots are displayed in the radial velocity frame (the radial velocities are referred to the line laboratory rest wavelength).

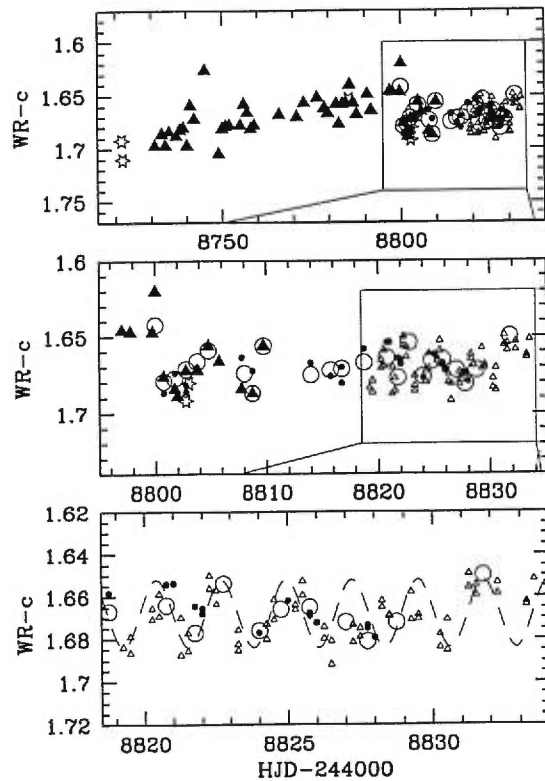


FIGURE 4.5. Photometry of WR 134 in 1992. *Filled triangles*: APT; *open circles*: SPM (Mexico) 1-channel photometry; *filled circles*: SPM 2-channel photometry; *open triangles*: Maidanak Observatory; *open stars*: HIPPARCOS. The bottom panel is an enlargement of the insert in the central panel. The sizes of the symbols correspond to 2σ error bars. In order to guide the eye in the bottom frame, a sinusoid with a period of 2.27 days (ephemeris of McCandliss et al. 1994) has been overplotted.

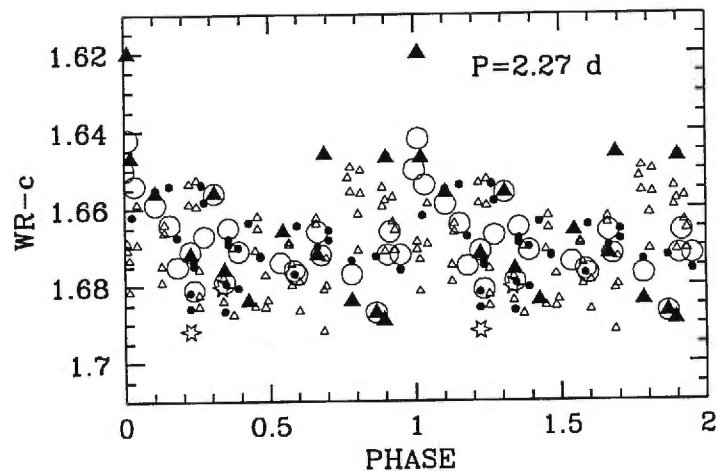


FIGURE 4.6. Photometry of WR 134 in 1992, folded with the $P = 2.27$ day period. Only the data plotted in the middle panel of Figure 4.5 have been used. The symbols are coded as in Figure 4.5.

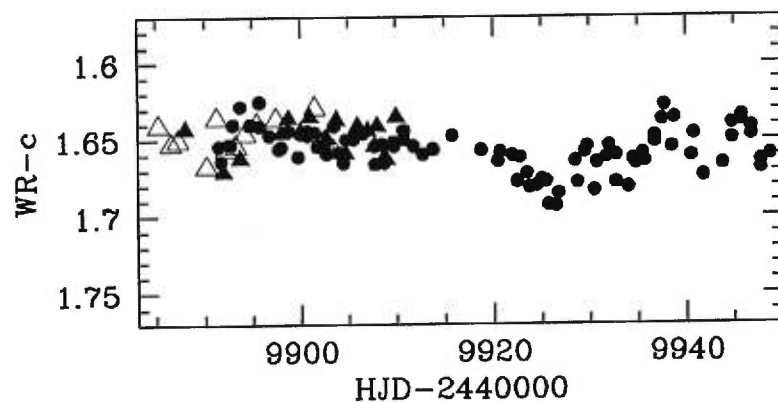


FIGURE 4.7. Photometry of WR 134 in 1995. *Filled triangles*: APT; *filled circles*: SPM (Mexico); *open triangles*: Crimean Observational Station. The sizes of the symbols correspond to 2σ error bars.

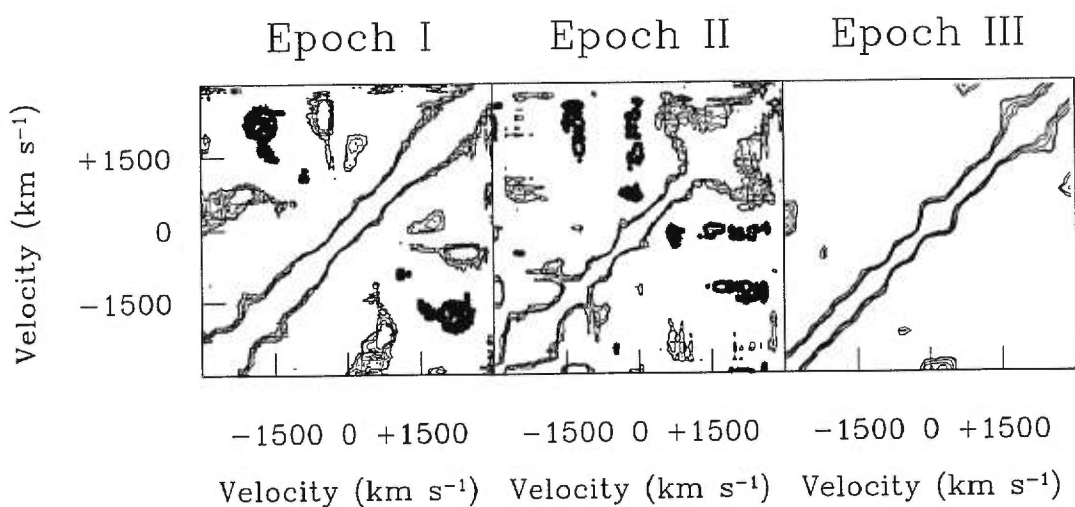


FIGURE 4.8. Auto-correlation matrices of He II $\lambda 4686$ for each epoch. Thick and thin contours indicate a negative or positive correlation in the pattern of variability presented by the same line profile at different radial velocities, respectively. The lowest contour is drawn for a significant correlation at the 99.9 % confidence level.

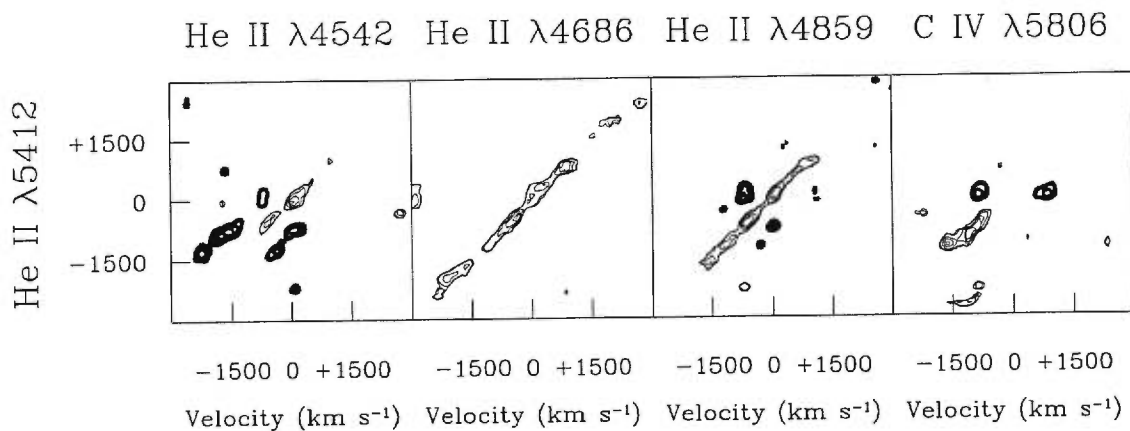


FIGURE 4.9. Correlation matrices of He II λ 5412 with He II λ 4542, He II λ 4686, He II λ 4859, and C IV λ 5806 for epoch III. Thick and thin contours indicate a negative or positive correlation in the pattern of variability presented by two line profiles at different radial velocities (referred to the line laboratory rest wavelength), respectively. The lowest contour is drawn for a significant correlation at the 99.9 % confidence level.

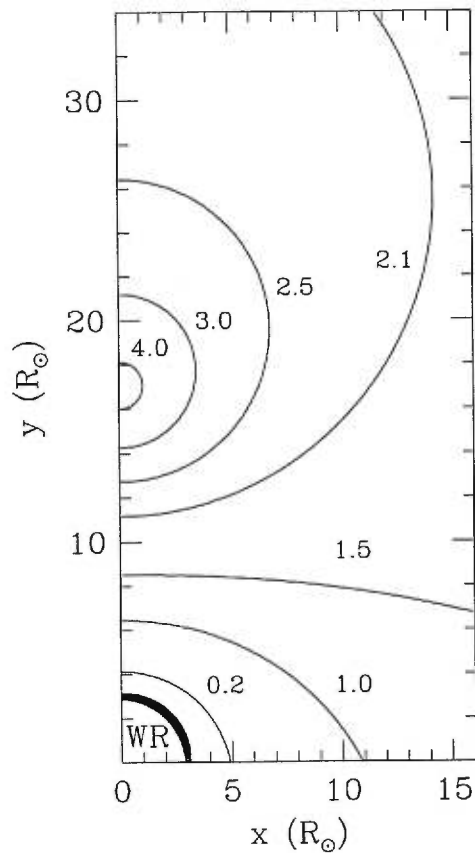


FIGURE 4.10. Contours of constant ionization parameter $\log \xi$ (in ergs cm s^{-1}). The accreting, strongly ionizing compact companion is located at $(0, 17)$. The WR star is placed at the origin of this plot.

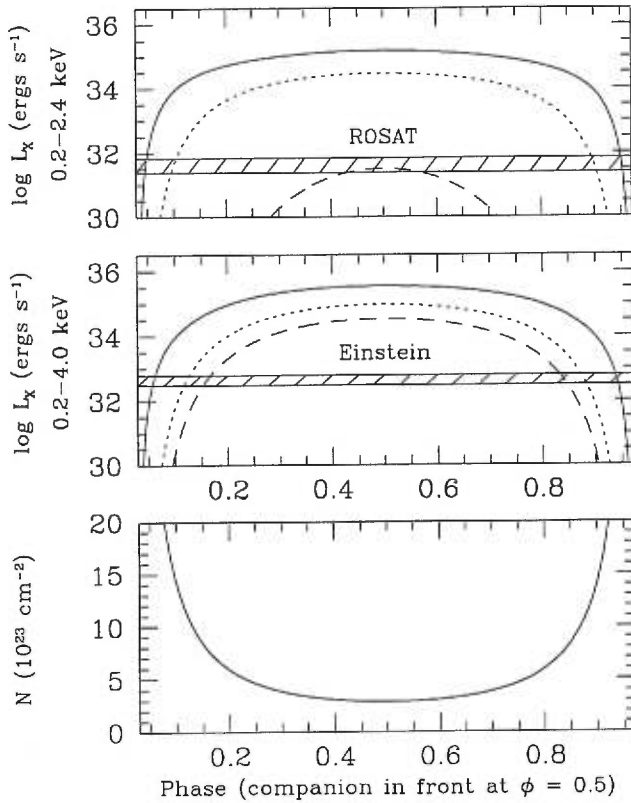


FIGURE 4.11. *Upper and middle panels:* predicted X-ray luminosities after allowance for wind absorption in the 0.2-2.4 and 0.2-4.0 keV bands as a function of the orbital phase ϕ , and for different values of the ionization parameter ξ : $\log \xi = 2.1$ ergs cm s $^{-1}$ (*solid line*), $\log \xi = 1.8$ ergs cm s $^{-1}$ (*short-dashed line*), and $\log \xi = 0$ ergs cm s $^{-1}$ (*long-dashed line*). The shaded areas show the range of the *ROSAT* and *Einstein* count rates for WR 134, namely 0.46 ± 0.22 and $4.6 \pm 1.6 \times 10^{32}$ ergs s $^{-1}$ in the 0.2-2.4 and 0.2-4.0 keV bands, respectively (Pollock, Haberl, & Corcoran 1995; Pollock 1987). The luminosities have been scaled to a distance of 2.1 kpc (van der Hucht et al. 1988). Note that the calculations do not consider the X-ray emission intrinsic to the WR wind (generally ascribed to radiative instabilities), nor the scattering of the neutron star emission in the WR wind which may cause extra emission at X-ray eclipse. *Lower panel:* column density of the absorbing wind material in units of 10^{23} cm $^{-2}$, as a function of ϕ .

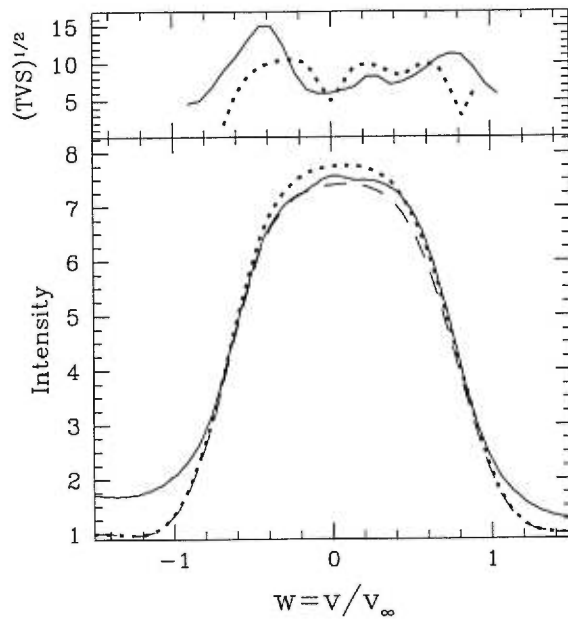


FIGURE 4.12. *Upper panel:* solid line — the observed TVS; dotted line — the modeled TVS within the maximum-emission approach. *Lower panel:* solid line — mean epoch I profile of He II $\lambda 4686$; dotted line — the SEI model fit within the maximum-emission approach; dashed line — the SEI model fit applying the minimum-emission approach. Note that the model is unable to fit the bluest and reddest parts of the line profile because of partial blending and electron scattering effect, respectively. The projected velocity, w , is normalized to $v_\infty = 1900 \text{ km s}^{-1}$.

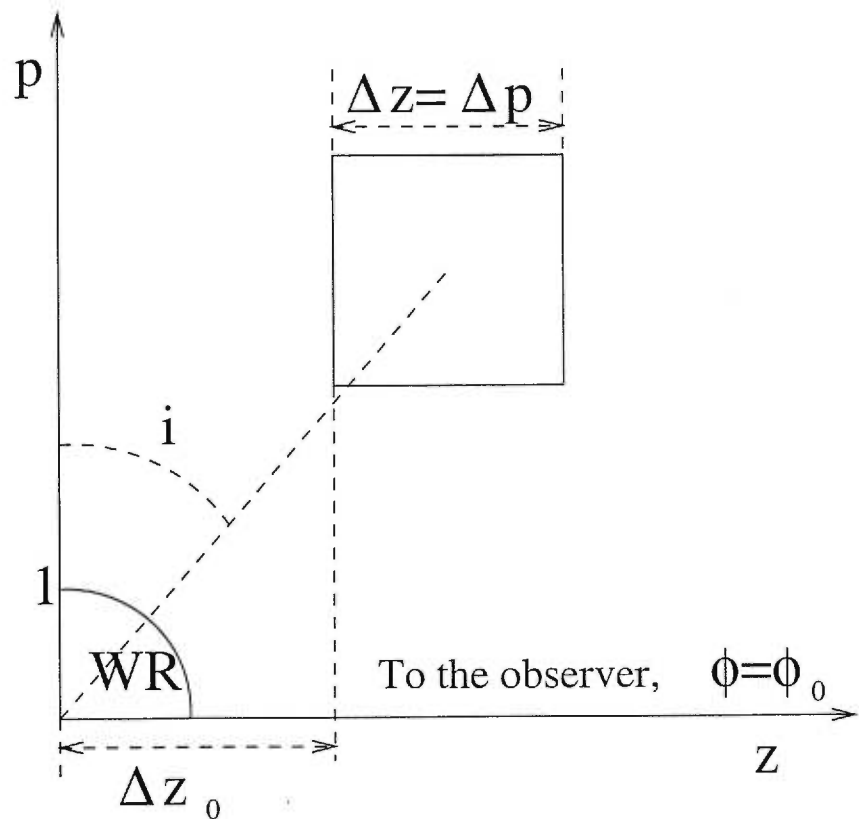


FIGURE 4.13. Sketch of the geometry adopted for the photoionization cavity. The azimuthal extension of the cavity, Θ , is in the direction perpendicular to the plane of the figure.

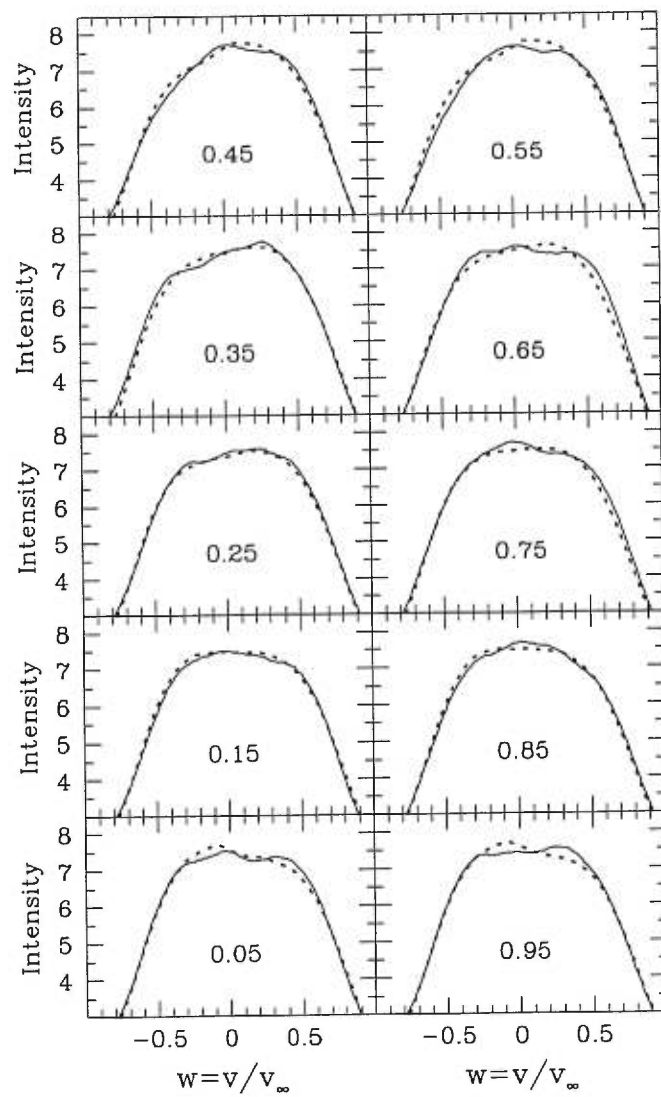


FIGURE 4.14. The observed (*solid line*) and modeled (*dotted line*) phase-dependent variations of He II $\lambda 4686$. All epoch I spectra are binned to 0.1 phase resolution; the bin mid-phase is shown in each panel.

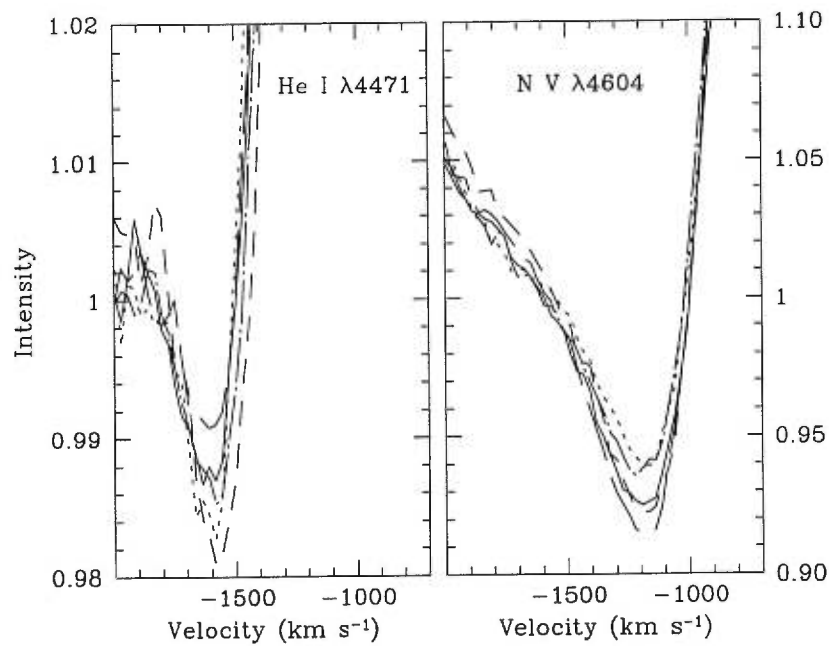


FIGURE 4.15. Variations of the P Cygni absorption troughs of He I $\lambda 4471$ and N V $\lambda 4604$ with phase. All epoch I observations are binned to 0.2 phase resolution: *dashed-dotted line*: $\phi = 0.15-0.35$; *long-dashed line*: $\phi = 0.35-0.55$; *short-dashed line*: $\phi = 0.55-0.75$; *dotted line*: $\phi = 0.75-0.95$; *solid line*: $\phi = 0.95-1.15$. Note that the intensity scale is different for the two panels.

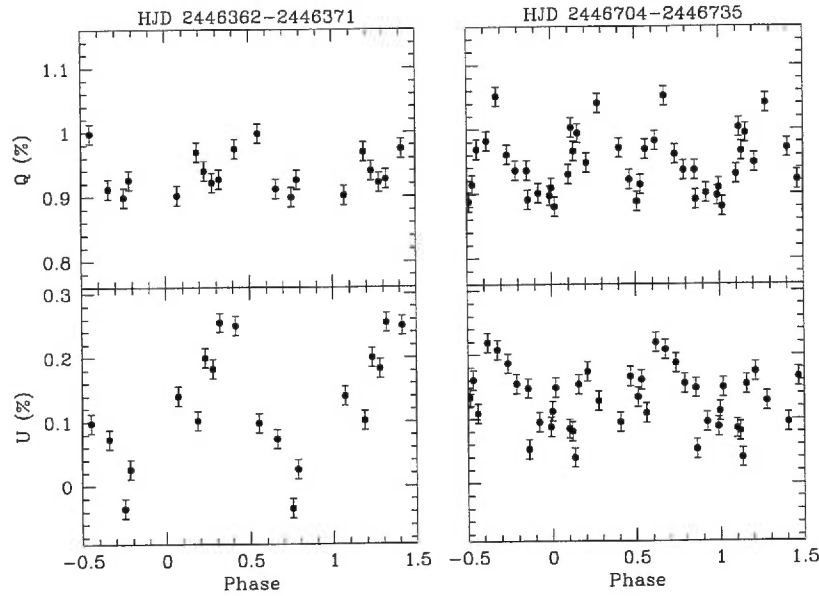


FIGURE 4.16. The Stokes parameters Q and U of WR 134 in 1985-1986 (Robert et al. 1989) plotted in phase according to the ephemeris of McCandliss et al. (1994). *Left and right panels:* data (with 2σ error bars) for the intervals HJD 2,446,362-2,446,371 (1985) and HJD 2,446,704-2,446,735 (1986), respectively.

CHAPITRE 5

AN INVESTIGATION OF THE LARGE-SCALE VARIABILITY OF THE APPARENTLY SINGLE WOLF-RAYET STAR WR 1

Soumis à *Astronomy & Astrophysics*

AN INVESTIGATION OF THE LARGE-SCALE VARIABILITY OF THE APPARENTLY SINGLE WOLF-RAYET STAR WR 1

Thierry Morel,¹ Leonid N. Georgiev,² Yves Grosdidier,^{1,3} Nicole St-Louis,¹
Thomas Eversberg,¹ and Grant M. Hill⁴

Received ; accepted

Article submitted to Astronomy & Astrophysics.

¹ Département de Physique, Université de Montréal, C.P. 6128, Succ. Centre-Ville, Montréal, Québec, Canada, H3C 3J7; and Observatoire du Mont Mégantic.

² Instituto de Astronomía, UNAM, Apdo. Postal 70-264, México D.F. 04510, México.

³ Observatoire Astronomique de Strasbourg, Université Louis Pasteur, 11 rue de l'Université, 67000, Strasbourg, France.

⁴ McDonald Observatory, HET, P. O. Box 1337, Fort Davis, TX.

ABSTRACT

Despite its apparently single nature, the Wolf-Rayet star WR 1 has been recently shown to present a *possibly* periodic, unusually large-scale pattern of spectral variability. This peculiar behavior suggests the existence of an unseen (collapsed?) companion or a strongly time-dependent wind structure.

Photometric and spectroscopic campaigns of observations of WR 1 have been carried out in 1995 and 1996 in an effort to reveal the true driver of the variability. Our narrowband photometric observations reveal an unusual behavior with a gradual increase in the stellar continuum flux amounting to $\Delta v \approx 0.09$ mag followed by a decline on a total timescale of about 7 days. Only marginal variability is found during the 11 following nights.

Strong, daily line-profile variations are also observed but they cannot be easily linked to the photometric variations. Similarly to the continuum flux variations, *coherent* time-dependent changes are observed in 1996 in the centroid, equivalent width and skewness of He II $\lambda 4686$.

Despite the apparently well-defined pattern of variability observed, these data question the existence of a *strictly* periodic pattern of variability in WR 1. If any, relatively long periods ($P \gtrsim 5$ days) are more consistent with our observations. The origin of the variations is discussed in the context of scenarios involving a single or binary star.

Subject headings: stars: individual (WR 1; HD 4004) — stars: mass loss — stars: Wolf-Rayet

5.1 Introduction

It is now relatively well established that *apparently single* Wolf-Rayet (WR) stars may display two distinct (but probably non exclusive) spectroscopic patterns of variability: (a) small-scale emission features systematically moving from the line center to the line wings on an hourly timescale (e.g., Lépine 1998); (b) dramatically larger line-profile deformations operating on a much longer basis (\sim days, e.g., Smith & Willis 1994). Although the first phenomenon, observed in most (if not all) WR stars, is believed to be the consequence of the fragmented, possibly turbulent nature of the outflow, the origin of the latter type of variability is still very much elusive.

Remarkable in this respect, is the existence of a well-established, although strongly epoch-dependent, large-scale *cyclical* pattern of variability in the two apparently single WR stars WR 6 ($P \approx 3.77$ d; Firmani et al. 1980) and WR 134 ($P \approx 2.3$ d; McCandliss et al. 1994; Morel et al. 1999). A major observational effort has been directed on establishing the true nature of these peculiar objects, i.e., whether this cyclical variability is induced by an orbiting unseen (collapsed?) companion or by the rotational modulation of large-scale wind structures (e.g., Vreux et al. 1992; Harries et al. 1999, and references therein). Although the very nature of these stars has yet to be unambiguously settled, these studies reveal that rotational modulation constitutes an attractive alternative to the binary hypothesis, especially considering the recent recognition that some O stars (the progenitors of WR stars) might possess such azimuthally structured outflows (Fullerton et al. 1997; Kaper et al. 1997).

A prime target for further investigations is the seldom-studied, apparently single WN 5 star WR 1 (HD 4004) that has recently been shown to present a spectral pattern of variability very similar to that of WR 6 (Niedzielski 1995, 1996a, b; Wessolowski & Niedzielski 1996; Niedzielski 1999). Large-scale line-

profile variability was observed, as well as apparently cyclical (according to $\mathcal{P} \approx 2.667$ days) variations in the EWs of He II $\lambda 4686$ and He II $\lambda 5412$ (Niedzielski 1996a). The first claim of periodic variability in WR 1 with $\mathcal{P} \approx 7.7$ days was made by Lamontagne (1983) from an analysis of the radial velocity variations of He II $\lambda 4686$. The first photometric monitoring of this object has shown WR 1 to be variable, with an indication of a 6.1 day period (Moffat & Shara 1986). Recently, Marchenko et al. (1998a) discussed *HIPPARCOS* broadband photometric data which revealed that WR 1 also displays relatively long-term photometric variations, with a marginal evidence for a $\mathcal{P} = 11.68 \pm 0.14$ day periodicity.

As can be seen, controversy persists in the literature concerning the possible cyclical nature of the variations in WR 1. We present in this paper the results of spectroscopic and photometric monitoring of WR 1 carried out in 1995 and 1996 aiming at shedding some light on this issue.

5.2 Observations and Reduction Procedure

5.2.1 Photometry

The photometric variability of WR 1 has been investigated during the interval 1996 September 18–October 5 by use of the single channel photometer *CUENTA-PULSOS* on the 0.84 m telescope of the Observatorio Astronómico Nacional at San Pedro Mártir (Mexico). Two additional objects were monitored during this observing run, WR 3, and WR 153. The nights were clear, albeit generally nonphotometric. WR 1 was observed through a narrowband v filter centered on 5140 Å (FWHM = 90 Å). This filter samples a continuum-dominated region of the WR spectrum. We applied the following sequence of 60 s integration through a 25" diaphragm: sky, C2, C1, WR, C1, WR, C1, C2, sky. The same nearby comparison stars as used by Moffat & Shara (1986) have been chosen. These comparison stars are similar in terms of their magnitude and colour to WR 1: C1

($\Delta B = + 0.17$; $\Delta[B - V] = + 0.17$); C2 ($\Delta B = + 0.26$; $\Delta[B - V] = + 0.19$). An extinction coefficient $k_v = 0.20$ was used for the data reduction. The scatter in the (C2 – C1) data for the whole dataset amounts to $\sigma \approx 4.7$ mmag. The differential magnitudes quoted in Table 5.1 are averaged over two consecutive cycles typically separated by about 20 minutes.

5.2.2 Spectroscopy

5.2.2.1 Long-slit and Reticon Spectra

Long-slit spectra of WR 1 have been obtained during various campaigns at the Observatoire du Mont Mégantic and Dominion Astrophysical Observatory (Canada) in 1995 October and 1996 September. Reticon spectra were also obtained at DAO in 1996 November. The 1996 campaign at the Observatoire du Mont Mégantic was coordinated to support the photometric campaign described above. Table 5.2 lists the mode of observation, the dates of the spectroscopic observations, the interval of the observations in Heliocentric Julian Days, the observatory name, the number of CCD spectra obtained, the selected spectral domain, the reciprocal dispersion of the spectra, and the typical signal-to-noise ratio (S/N) in the continuum.

The spectra were reduced using the **IRAF**¹ data reduction packages. The bias and sky subtraction, flat-field division, removal of cosmic ray events, extraction of the spectra, and wavelength calibration were carried out in the usual way. Spectra of calibration lamps were taken immediately before, and after the stellar exposure. The stellar spectra were subsequently continuum normalized by fitting a low-order Legendre polynomial to carefully selected line-free regions. In order to minimize

¹IRAF is distributed by the National Optical Astronomy Observatories, operated by the Association of Universities for Research in Astronomy, Inc., under cooperative agreement with the National Science Foundation.

the spurious velocity shifts induced by an inevitably imperfect wavelength calibration, the spectra were coaligned in the radial velocity space by using the interstellar doublet Na I $\lambda\lambda 5890, 5896$ as fiducial marks. When not available, the doublet Ca II $\lambda\lambda 3934, 3968$, or the diffuse interstellar band at 4501 Å were used. A trend for a systematic shift of the zero point of the wavelength scale has been corrected by redshifting most of the spectra by an average value of 35 km s^{-1} .

5.2.2.2 Echelle Spectra

Echelle spectra have been obtained during the period 1996 September 16–19 with the Echelle spectrograph *ESPRESSO* (Levine & Chakrabarty 1995) on the 2.1 m telescope of the San Pedro Mártir Observatory. The UCL camera and a 1024×1024 coated CCD-Tek chip have been used. The selected grating (300 lines mm^{-1}) yields a reciprocal dispersion of 0.16 and $0.23 \text{ \AA pixel}^{-1}$ at H γ and H α , respectively. The spectra cover 27 orders and span the spectral range 3720–6900 Å.

The reduction procedure (bias subtraction, division by a normalized flat field, removing of scattered light, extraction of the orders) was carried out using the reduction tasks in the IRAF package `echelle`. Comparison spectra of Th-Ar lamps have been used for the wavelength calibration. The typical accuracy of the wavelength calibration can be judged by the dispersion in the measured heliocentric radial velocities of the interstellar line Na I $\lambda 5890$: $\sigma \approx 2 \text{ km s}^{-1}$. The instrumental response has been removed by fitting a low-order Legendre polynomial to the continuum sections of each order of an O-star spectrum, and then dividing the corresponding order of the WR 1 spectra by this polynomial. The resultant, almost flat, orders were then combined using the IRAF task `scomb`. This procedure proved to be satisfactory, except when the overlapping regions fall in a spectral domain with very steep intensity gradients, as in the blue wing of He II $\lambda 4686$ (see Fig.5.2). The combined spectra were then subdivided into

spectral regions roughly corresponding to those of the long-slit spectra discussed above (§5.2.2.1). For consistency purposes, these spectra have been continuum normalized by fitting a low-order Legendre polynomial to the *same* continuum sections as selected for the long-slit spectra.

5.3 Results

5.3.1 Continuum Flux Variations

The light curve of WR 1 is plotted, as a function of the Heliocentric Julian Date of observation, in Figure 5.1. The main and obvious event during our photometric monitoring of WR 1 is the gradual increase of the stellar continuum flux by $\Delta v \approx 0.09$ mag beginning at HJD 2,450,346 followed by its decline on about the same timescale after HJD 2,450,350. During the last 11 nights (after HJD 2,450,353), only marginal evidence for variability is found, with $\sigma(\text{WR} - \text{C})/\sigma(\text{C}_2 - \text{C}_1) \approx 1.3$. This can be compared with a value of 1.9 obtained by Moffat & Shara (1986) on the basis of 14 nights of broadband *B* observations in 1984. Noticeable is also the striking lack of recurrence in the continuum flux data. A periodicity search in the $(\text{WR} - \text{C}_1)$ and $(\text{WR} - \text{C}_2)$ data acquired after HJD 2,450,353 yields no evidence for any periodic signals in the range 6–8 days that would possibly account for the variations observed before this date. The highest peaks in the power spectra of these two datasets (after correction by the CLEAN algorithm; see Roberts et al. 1987) appear (with considerable uncertainty) for periods of about 4 days. However, the significance of these periodic signals is very low and they must thus be regarded as spurious. The periods proposed by Niedzielski (1996a; 2.667 days) and Marchenko et al. (1998a; 11.68 days) are inconsistent with the global light curve morphology. On the other hand, the periods claimed by Lamontagne (1983; 7.7 days) and Moffat & Shara (1986; 6.1 days) are only consistent with part of the data (before HJD 2,450,353). We will

come back to this point later (§5.4).

5.3.2 An Overview of the Line-profile Variations

In the following, we will generally illustrate the line-profile variations of WR 1 by means of the strong He II $\lambda 4686$ line as its variations are qualitatively similar to those affecting the other He II features (see §5.3.5; Niedzielski 1996a). One of the most outstanding features of the line-profile variability is the relatively low level of variability observed within one night.² Such a gradual pattern of variability has been observed whenever several spectra have been obtained during a single night of observation. This phenomenon is illustrated in Figure 5.2 where we show a superposition of the 21 He II $\lambda 4686$ line profiles obtained on the night of 1996 September 18 (around HJD 2,450,344.873). In sharp contrast, however, noticeable night-to-night variations are observed. This is illustrated in Figure 5.3 which shows a montage of the nightly mean spectra obtained in 1995 October (*left panel*) and 1996 September (*right panel*) for the spectral region encompassing He II $\lambda 4686$ (it has to be kept in mind that because of the paucity of the photometric data, the strength of the spectral lines in these continuum-normalized spectra has not been corrected for the varying continuum flux level).

5.3.3 Temporal Variance Spectrum Analysis

The Temporal Variance Spectrum analysis (TVS; Fullerton et al. 1996) has been used to assess the level of spectral variability as a function of wavelength. The (square root of the) TVS, giving the typical “size” of the deviations from a template-weighted mean spectrum (expressed in percentage of the continuum

²Note that although probably present in WR 1, the small-scale emission-excess features travelling on an hourly timescale on the top of the line profiles — probably induced in WR stars by outwardly moving shocked and/or turbulent material (Lépine & Moffat 1999) — cannot be studied here, owing to the insufficient S/N achieved for the Echelle spectra.

flux) is shown, along with the 99.0 % confidence level for variability, in Figure 5.4. As can be seen, highly significant variability affects the emission lines with the notable exception of N V λ 4945 for which only marginal evidence for variability is found. Many peaks (i.e., locations of “preferential” variability) can be distinguished in the TVS. The locations of these peaks (in terms of the projected velocity referred to the rest laboratory wavelength of the spectral feature in question) are quoted in Table 5.3. The results of this investigation show that: (a) the variability often extends to velocities comparable to the wind terminal velocity ($v_\infty \approx 2135 \text{ km s}^{-1}$; Rochowicz & Niedzielski 1995), e.g., $v \approx -1790 \text{ km s}^{-1}$ for the relatively unblended line He II λ 4859; (b) the TVS structure — constituted of several subpeaks — presents some similarities for the various He II features. However, the velocities quoted in Table 5.3 are certainly entached of considerable uncertainties (due, e.g., to blend of TVS subpeaks) making difficult a clear statement as to as the variability takes place at the same characteristic velocities in different lines.

5.3.4 The P Cygni Profile Variability

The TVS analysis also reveals substantial variability at the location of the P Cygni absorption component of N V λ 4604 (Fig.5.4). This mainly results from the transition of the N V λ 4604 feature from a pure emission line-profile in 1995 October to a P Cygni line-profile in 1996 September (Fig.5.5). No clear variations in the strength of this absorption trough on a daily timescale are observed.

An enhanced peak in the TVS can also be found at the location where the carbon triplet C IV λ 5806 and He I λ 5876 merge (Fig.5.4). The large daily changes affecting C IV λ 5806 and/or He I λ 5876 in October 1995 and September 1996 are illustrated in Figure 5.6 (this phenomenon is not observed in 1996 November). The high level of variability observed at this particular location is likely due to the superposition of two distinct type of variability: (a) red-wing variability of

C IV $\lambda 5806$ as observed in other spectral features (e.g., He II $\lambda 4686$; Fig.5.4); (b) variations in the P Cygni absorption component strength of He I $\lambda 5876$.³ The latter interpretation is supported by the fact that the projected velocity of the peak in the TVS ($v \approx -1980 \text{ km s}^{-1}$, referred to the He I rest laboratory wavelength) matches fairly well the wind terminal velocity ($v_\infty \approx 2135 \text{ km s}^{-1}$). Considering the relatively modest variability affecting the red-wing parts of the line profiles in WR 1 (Fig.5.4) it is conceivable that changes in the strength of the P Cygni absorption component of the He I feature *mostly* contribute to the observed changes.

5.3.5 Correlated Line-profile Variations in Different Lines?

A possible correlated pattern of variability in two different spectral features has been investigated by calculating the Spearman rank-order correlation matrices (see, e.g., Johns & Basri 1995) whose elements $r(i, j)$ give the degree of correlation between the line intensity variations at pixels i and j in each line profile, respectively. In the case of perfectly, positively correlated variations, a matrix unity is obtained. The correlation matrices of He II $\lambda 5412$ with He II $\lambda 4686$, He II $\lambda 4859$, and N V $\lambda 4945$ are shown in Figure 5.7 in the form of contour plots, where the lowest contour indicates a significant positive (or negative) correlation at the 99.5 % confidence level (the other spectral lines were not covered enough to be included in the analysis). These matrices are displayed in the projected velocity frame (referred to the line laboratory rest wavelength). A significant positive correlation is found between the pattern of variability presented by He II $\lambda 5412$ and He II $\lambda 4686$. The same conclusion, however restricted to the velocity range ($-1000, +1000$) km s^{-1} , holds for the variations affecting He II $\lambda 5412$ and He II $\lambda 4859$. In contrast, the (weak) variations of N V $\lambda 4945$ are apparently not

³Such P Cygni absorption troughs of He I $\lambda 5876$ are commonly (and more clearly) observed in other WN stars (e.g., Robert 1992).

linked to those of He II $\lambda 5412$ (the same is true for C IV $\lambda 5806$ and He I $\lambda 5876$). Various factors are susceptible to mask any potential correlated pattern (e.g., noise, blends). Also, due to the stratified nature of WR winds, it is conceivable that two given features may present similar, yet delayed, patterns of variability. This would also result in an apparent lack of correlation. Overall, the results of this analysis tend to show that the He II features vary in a fairly similar fashion. The small number of spectral features included in the analysis prevents, however, to draw at this stage more general conclusions.

5.3.6 Centroid, FWHM, EW, and Skewness Variations

We have investigated the time-dependent changes in the global line-profile properties by calculating the centroid, FWHM, EW, and skewness of He II $\lambda 4686$, the strongest line. The centroid and skewness were calculated as the first moment, and the ratio of the third and the (3/2 power of the) second central moments of the portion of the profile above two in units of the continuum (in order to avoid the contribution of blends). The FWHM was determined by a Gaussian fit to the entire line profile. The EWs were calculated by integrating the line flux in the interval 4643–4780 Å. As can be seen in Figure 5.8 (*right panel*), the data of 1996 September show generally *coherent* time-dependent variations. This is especially clear for the skewness time series, with the timescale of the variations being of the same order of magnitude as the variations of the continuum flux shown in the uppermost part of Figure 5.8, that is to say about 5–7 days. On the other hand, however, and although this may be induced by the paucity of the data, no clear time-dependent behavior is noticeable for the 1995 October dataset (*left panel*).

5.4 Comparison with Previous Studies

Niedzielski (1996a) reported on a spectroscopic pattern of variability of WR 1 very much reminiscent of the one presented by the apparently single WN 5 star WR 6 that displays tightly phase-locked (although strongly epoch-dependent) spectral variations according to $\mathcal{P} \approx 3.77$ days (Morel et al. 1998, and references therein). The results of our investigation of the spectral variability of WR 1 are broadly consistent with this suggestion. In particular, as general features of the spectroscopic pattern of variability, one can note in both objects the substantial variations in the strength of the absorption component of the optical P Cygni profiles (readily observable in N V $\lambda\lambda 4604, 4620$ where the absorption component occasionally disappears; Fig.5.5) or the coherent time-dependent changes in the global line-profile properties (e.g., skewness; Fig.5.8). Similarities can also be found with WR 134, another very rare example of single-line WR star displaying cyclical variations (Morel et al. 1999).

Evidence was also presented by Niedzielski (1996a) for cyclical (according to $\mathcal{P} \approx 2.667$ days), correlated changes in the EWs of He II $\lambda 4686$ and He II $\lambda 5412$. The data presented in the present paper do not, however, support a claim of such periodicity. In particular, a period search in our EW data (but also in our centroid, FWHM and skewness data; Fig.5.8) yields no significant signal at the expected frequency. Also, this 2.667 day period could hardly account for our global light curve morphology (Fig.5.1). This apparent disagreement between our results and those presented by Niedzielski (1996a) *may* point to a possible multiperiodic nature of the variability in WR 1, with the 2.667 day period being present in 1994-1995 but being dominated by other longer (non)cyclical processes during our observations. It has to be noted that based on a more comprehensive analysis of the data, Niedzielski (private communication) recently questioned the strictly periodic nature of the spectral variations.

As already noted by Niedzielski (1995, 1996b) and Wessolowski & Niedzielski (1996), our data provide evidence for a more gradual spectral pattern of variability compared to WR 6; a fact which may imply that the period (if any) is longer than 3.77 days. In support of this view, the centroid, EW, and skewness data of He II $\lambda 4686$ show coherent time-dependent patterns of variability (Fig.5.8), with timescales in the range 5–6 days after a formal periodicity search. However, we caution the reader that this period should not be taken too literally because of the limited time sampling of these data. In particular, a cyclical pattern in this range, as proposed by Lamontagne (1983) and Moffat & Shara (1986), is clearly inconsistent with the lack of continuum flux variations observed after HJD 2,450,353 (Fig.5.1) unless one invokes a sudden period of “quiescence” after this date, with the small amplitude of the variations masking any periodic pattern.

5.5 On the Presence of a Companion

Although a possible cyclical pattern of variability has yet to be unambiguously established in WR 1, general considerations are made below regarding the model assuming an orbiting (unseen) companion as the origin of the variability.

5.5.1 A Non-degenerate Companion?

Some constraints can be set on the mass, M_* , of this putative companion on the basis of the centroid measurements of He II $\lambda 4686$ presented in Figure 5.8. Assuming that these variations are *entirely* attributable to orbital motion (i.e., $K_{WR} \approx 70 \text{ km s}^{-1}$), one can explore the values of (P, M_*) allowed by this adopted value of K_{WR} . The solid lines in Figure 5.9 show the result of this investigation for three illustrative values of the orbital inclination ($i = 30^\circ, 60^\circ, \text{ and } 90^\circ$). In these calculations, we assume a circular orbit and a mass for WR 1 of $9.1 M_\odot$ (Hamann, Koesterke, & Wessolowski 1995). For a wide range in orbital inclination ($i \gtrsim 30^\circ$)

and in orbital period ($\mathcal{P} \lesssim 20$ days), an upper limit for the companion's mass of $15 M_{\odot}$ is obtained. Assuming the companion to be a main sequence star, this constrains the spectral type to be later than B1. In this case, the companion's wind is too weak (Grigsby & Morrison 1995) to induce wind-wind collision effects that might induce the large spectral changes observed here. For a system observed nearly face-on ($i \lesssim 30^\circ$), larger masses are evidently consistent with the value of K_{WR} adopted above. However, no direct evidences (e.g., photospheric lines in the integrated spectrum, dilution of the WR continuum) support the presence of a luminous, early-type companion. In presence of a non-degenerate companion, one would also expect a flat or eclipsing-type light curve. Yet, the *opposite* behavior is observed in Figure 5.1. These arguments strongly argue against the presence of a non-degenerate star orbiting WR 1.

5.5.2 A Collapsed Companion?

For a canonical mass of the companion as a neutron star, $M_{\star} \approx 1.4 M_{\odot}$, improbably small periods below one day are consistent with the adopted K_{WR} value (Fig.5.9). However, it has to be kept in mind that the centroid measurements of He II $\lambda 4686$ included the highly variable uppermost part of the profile which is unlikely to purely reflect orbital motion. Therefore, this K_{WR} value is probably grossly overestimated. If one considers lower K_{WR} values (as Lamontagne 1983: $K_{WR} = 22 \pm 5 \text{ km s}^{-1}$; the allowed values of $[\mathcal{P}, M_{\star}]$ are shown for this case by short-dashed lines in Fig.5.9), much larger \mathcal{P} values (as in fact suggested by our study) are allowed. Thus, these considerations are not sufficient by themselves to rule out the presence of a neutron star companion (a black hole companion, on the other hand, would require long periods and/or small orbital inclinations). ⁴

In the presence of a collapsed companion, one may expect fairly strong, accretion-type X-ray emission. Earliest observations by the *HEAO A-1* experiment

⁴Considering a lower value of K_{WR} in §5.5.1 does not qualitatively modify our conclusions.

gave an upper limit $L_X \approx 4.4 \times 10^{33}$ erg s $^{-1}$ on the emission in the 0.5–20 keV range (Helfand 1980). A value $L_X = 7.07 \pm 2.85 \times 10^{32}$ erg s $^{-1}$ in the 0.2–2.4 keV range has been reported for WR 1 during the *ROSAT* all-sky survey (Pollock, Haberl, & Corcoran 1995). WR 1 is a fairly strong X-ray emitter compared to other (apparently) single WN stars. However, its emission is by no means unusual when only considering the WNE-s subclass (Wessolowski 1996). Two subsequent pointed *ROSAT* PSPC observations showed that a satisfactory fit to the X-ray spectrum can be achieved, either with a *Raymond-Smith* thermal plasma of about 1 keV, or by the model developed by Baum et al. (1992), assuming a mixture of “cool” (in radiative equilibrium) and “hot” (shocked) material (Wessolowski et al. 1995; Wessolowski 1996). This picture agrees with our current understanding of the X-ray production in bona fide single WR stars, as being due to radiatively-induced instabilities taking place in the outer parts of their winds (e.g., Willis & Stevens 1996). This “normal” level of X-ray emission from WR 1 does not constitute, however, a decisive argument arguing against the presence of a collapsed companion, as the accretion of the wind material onto the neutron star might be inhibited (e.g., Zhang et al. 1998).

Because of the spiral-in process that massive close binaries are believed to experience in the course of their evolution, one is led to expect periods of some hours for systems made up of a WR star and a compact companion, not days (e.g., De Donder et al. 1997). A period of 4.8 hr is observed in Cygnus X-3, the prime candidate for a WR + compact companion system (van Kerkwijk et al. 1996).

5.6 Concluding Remarks

The single-star hypothesis appears appealing when considering the similarities between the optical spectral pattern of variability of WR 1 with the ones of the two peculiar stars WR 6 and WR 134. In this respect, spectropolarimetric monitoring

aiming at revealing – as in the two aformentionned WR stars (Schulte-Ladbeck et al. 1991, 1992) – a substantial depolarization of the emission lines may shed some light on the true nature of WR 1.

Although the light curve morphology of WR 1 (a “bump” followed by a plateau) has, to our knowledge, no example among the WR population (Moffat & Shara 1986; Lamontagne & Moffat 1987; Antokhin et al. 1995; Marchenko et al. 1998b), such a well-defined light-curve pattern is reminiscent of what is observed in WR 6 (Robert et al. 1992).⁵ A repeatable pattern — as observed in WR 6 — would, however, imply an unlikely large value for the period in the context of this single-star hypothesis ($\mathcal{P} \gtrsim 18$ days).

If this single star interpretation is revealed to be correct, WR 1 might constitute in the future a cornerstone for our understanding of the mechanisms leading to the formation of largely anisotropic outflows in WR stars.

Acknowledgments: We acknowledge an anonymous referee and Alex W. Fullerton whose comments have stimulated a substantial improvement of this manuscript. T. M., Y. G., and N. S.-L. wish to thank the Natural Sciences and Engineering Research Council (NSERC) of Canada and the Fonds pour la Formation de Chercheurs et l’Aide à la Recherche (FCAR) of Québec for financial support. T. E. is grateful for full financial aid from the Evangelisches Studienwerk/Germany which is supported by the German Government.

⁵Curiously, a very similar light curve morphology (both in terms of the timescales involved and of the amplitude of the variations) has been noticed in the Be star FV CMa (Balona et al. 1992).

RÉFÉRENCES

- Antokhin, I., Bertrand, J.-F., Lamontagne, R., Moffat, A. F. J., Matthews, J. 1995, AJ, 109, 817
- Balona, L. A., Cuypers, J., & Marang, F. 1992, A&AS, 92, 533
- Baum, E., Hamann, W. -R., Koesterke, L., & Wesselowski, U. 1992, A&A, 266, 402
- De Donder, E., Vanbeveren, D., & van Bever, J. 1997, A&A, 318, 812
- Firmani, C., Koenigsberger, G., Bisiacchi, G. F., Moffat, A. F. J., & Isserstedt, J. 1980, ApJ, 239, 607
- Fullerton, A. W., Gies, D. R., & Bolton, C. T. 1996, ApJS, 103, 475
- Fullerton, A. W., Massa, D. L., Prinja, R. K., Owocki, S. P., & Cranmer, S. R. 1997, A&A, 327, 699
- Grigsby, J. A., & Morrison, N. D. 1995, ApJ, 442, 794
- Hamann, W.-R., Koesterke, L., & Wesselowski, U. 1995, A&A, 295, 151
- Harries, T. J., Howarth, I. D., Schulte-Ladbeck, R. E., & Hillier, D. J. 1999, MNRAS, in press
- Helfand, D. J. 1980, PASP, 92, 691
- Johns, C. M., & Basri, G. 1995, AJ, 109, 2800
- Kaper, L., et al. 1997, A&A, 327, 281
- Lamontagne, R. 1983, Ph.D. Thesis, Univ. Montréal

- Lamontagne, R., & Moffat, A. F. J. 1987, AJ, 94, 1008
- Lépine, S. 1998, Ph.D. Thesis, Univ. Montréal
- Lépine, S., & Moffat, A. F. J. 1999, ApJ, in press
- Levine, S., & Chakrabarty, D. 1995, IA-UNAM Technical Report #MU-94-04
- McCandliss, S. R., Bohannan, B., Robert, C., & Moffat, A. F. J. 1994, Ap&SS, 221, 155
- Marchenko, S. V., et al. 1998a, A&A, 331, 1022
- Marchenko, S. V., Moffat, A. F. J., Eversberg, T., Hill, G. M., Tovmassian, G. H., Morel, T., & Seggewiss, W. 1998b, MNRAS, 294, 642
- Moffat, A. F. J., & Shara, M. M. 1986, AJ, 92, 952
- Morel, T., St-Louis, N., Moffat, A. F. J., Cardona, O., Koenigsberger, G., & Hill, G. M. 1998, ApJ, 498, 413
- Morel, T., et al. 1999, ApJ, in press
- Niedzielski, A. 1995, in Proc. IAU Symp. 163, Wolf-Rayet Stars: Binaries, Colliding Winds, Evolution, ed. K. A. van der Hucht & P.M. Williams (Dordrecht: Kluwer), 52
- Niedzielski, A. 1996a, in Proceedings of the 33rd Liège International Astrophysical Colloquium, ed. J. M. Vreux et al., 277
- Niedzielski, A. 1996b, in Proceedings of the 27th Meeting of the Pol. Astron. Soc., 98
- Niedzielski, A. 1999, Acta Astron., in press
- Pollock, A. M. T., Haberl, F., & Corcoran, M. F. 1995, in Proc. IAU Symp. 163, Wolf-Rayet Stars: Binaries, Colliding Winds, Evolution, ed. K. A. van der Hucht & P.M. Williams (Dordrecht: Kluwer), 512

- Robert, C. 1992, Ph.D. Thesis, Univ. Montréal
- Robert, C., et al. 1992, ApJ, 397, 277
- Roberts, D. H., Lehár, J., & Dreher, J. W. 1987, AJ, 93, 968
- Rochowicz, K., & Niedzielski, A. 1995, Acta Astron., 45, 307
- Schulte-Ladbeck, R. E., Nordsieck, K. H., Taylor, M., Nook, M. A., Bjorkman, K. S., Magalhães, A. M., & Anderson, C. M. 1991, ApJ, 382, 301
- Schulte-Ladbeck, R. E., Nordsieck, K. H., Taylor, M., Bjorkman, K. S., Magalhães, A. M., & Wolff, M. J. 1992, ApJ, 387, 347
- Smith, L. J., & Willis, A. J. 1994, Ap&SS, 221, 189
- van Kerkwijk, M. H., Geballe, T. R., King, D. L., van der Klis, M., & van Paradijs, J. 1996, A&A, 314, 521
- Vreux, J.-M., Gosset, E., Bohannan, B., & Conti, P. S. 1992, A&A, 256, 148
- Wessolowski, U., Hamann, W. -R., Koesterke, L., Hillier, D. J., & Puls, J. 1995, in Proc. IAU Symp. 163, Wolf-Rayet Stars: Binaries, Colliding Winds, Evolution, ed. K. A. van der Hucht & P.M. Williams (Dordrecht: Kluwer), 174
- Wessolowski, U. 1996, in Proceedings of the 33rd Liège International Astrophysical Colloquium, ed. J. M. Vreux et al., 345
- Wessolowski, U., & Niedzielski, A. 1996, in Proc. Röntgenstrahlung from the Universe, ed. Zimmermann, H. U., Trümper, J., & Yorke, H., MPE Report, 263, 73
- Willis, A. J., & Stevens, I. R. 1996, A&A, 310, 577
- Zhang, S. N., Yu, W., & Zhang, W. 1998, ApJ, 494, L71

TABLEAU 5.1. Journal of photometric observations

HJD - 2,449,000	WR - C1	WR - C2	C2 - C1	HJD - 2,449,000	WR - C1	WR - C2	C2 - C1
1345.721	0.043	0.114	- 0.071	1356.693	0.054	0.121	- 0.067
1347.702	0.074	0.134	- 0.061	1356.773	0.057	0.128	- 0.071
1347.731	0.063	0.121	- 0.058	1356.847	0.065	0.130	- 0.065
1347.760	0.064	0.137	- 0.073	1356.902	0.054	0.127	- 0.073
1347.846	0.065	0.134	- 0.069	1356.984	0.054	0.130	- 0.076
1347.882	0.066	0.141	- 0.075	1357.656	0.064	0.139	- 0.075
1348.807	0.095	0.163	- 0.068	1357.723	0.064	0.129	- 0.065
1348.831	0.105	0.173	- 0.067	1357.781	0.055	0.121	- 0.066
1348.857	0.094	0.170	- 0.076	1357.847	0.058	0.127	- 0.070
1348.886	0.103	0.161	- 0.058	1357.914	0.057	0.129	- 0.072
1349.678	0.126	0.197	- 0.071	1358.735	0.055	0.126	- 0.071
1349.761	0.119	0.185	- 0.066	1358.773	0.059	0.125	- 0.066
1349.854	0.129	0.195	- 0.065	1358.829	0.048	0.109	- 0.061
1349.933	0.127	0.193	- 0.065	1358.881	0.061	0.123	- 0.062
1349.991	0.130	0.194	- 0.064	1358.943	0.051	0.117	- 0.066
1350.873	0.101	0.164	- 0.063	1358.992	0.058	0.120	- 0.062
1350.947	0.104	0.167	- 0.063	1359.642	0.051	0.118	- 0.067
1351.006	0.100	0.164	- 0.064	1359.702	0.040	0.112	- 0.072
1352.851	0.059	0.123	- 0.064	1359.767	0.043	0.115	- 0.071
1352.913	0.053	0.126	- 0.073	1359.832	0.049	0.116	- 0.067
1352.953	0.054	0.119	- 0.065	1359.909	0.051	0.117	- 0.066
1352.964	0.052	0.118	- 0.066	1359.958	0.050	0.122	- 0.072
1353.000	0.058	0.125	- 0.067	1360.004	0.059	0.122	- 0.063
1353.649	0.062	0.125	- 0.063	1360.632	0.063	0.133	- 0.070
1353.747	0.058	0.126	- 0.067	1360.697	0.046	0.114	- 0.067
1353.836	0.048	0.115	- 0.067	1360.761	0.059	0.126	- 0.067
1353.936	0.049	0.115	- 0.066	1360.842	0.057	0.116	- 0.060
1354.013	0.060	0.126	- 0.066	1360.912	0.061	0.123	- 0.062
1354.671	0.051	0.124	- 0.073	1361.637	0.060	0.122	- 0.061
1354.754	0.057	0.133	- 0.076	1361.694	0.060	0.132	- 0.073
1354.810	0.048	0.124	- 0.076	1361.768	0.061	0.121	- 0.060
1354.875	0.047	0.113	- 0.066	1361.851	0.065	0.124	- 0.060
1354.948	0.062	0.129	- 0.067	1361.952	0.065	0.131	- 0.066
1355.002	0.054	0.121	- 0.068	1361.997	0.058	0.126	- 0.069
1355.668	0.044	0.113	- 0.070	1362.625	0.053	0.118	- 0.066
1355.735	0.056	0.124	- 0.068	1362.720	0.060	0.124	- 0.064
1355.792	0.058	0.121	- 0.063	1362.846	0.052	0.121	- 0.069
1355.860	0.060	0.123	- 0.063	1362.910	0.055	0.123	- 0.068
1355.912	0.050	0.121	- 0.071	1362.983	0.053	0.123	- 0.070
1355.993	0.064	0.116	- 0.052				

TABLEAU 5.2. Journal of spectroscopic observations

Mode of Observation	Date	HJD — 2,449,000	Observatory ^a	Number of Spectra	Spectral Coverage (Å)	Reciprocal Dispersion (Å pix ⁻¹)	S/N
Long-slit	95 Oct	992-1005	OMM, DAO	7	3830-4300	1.6	≈ 160
				15	4360-5080	1.6	≈ 170
				11	5050-5945	1.6	≈ 290
Echelle	96 Sep	1342-1345	SPM	72	3720-6900	0.16 (H _γ) — 0.23 (H _α)	≈ 25 (H _γ) — 50 (H _α)
Long-slit	96 Sep	1346-1352	OMM	13	4400-5080	1.3	≈ 120
				14	5050-6500	1.3	≈ 190
Reticon	96 Nov	1386-1389	DAO	12	5100-6110	0.5	≈ 75

^a OMM: Observatoire du Mont Mégantic 1.6 m; DAO: Dominion Astrophysical Observatory 1.8 m; SPM: San Pedro Mártir Observatory 2.1 m.

TABLEAU 5.3. Projected velocities of the TVS subpeaks observed in He II λ 4686,
He II λ 4859 and He II λ 5412.^a

He II λ 4686	He II λ 4859	He II λ 5412
– 2260	– 1790	– 1880
– 1060	– 1060	– 1040
	– 550	
+ 430	+ 290	+ 690
+ 1560	+ 1390	+ 1430
+ 2460		

^a In km s^{–1} and referred to the laboratory rest wavelength.

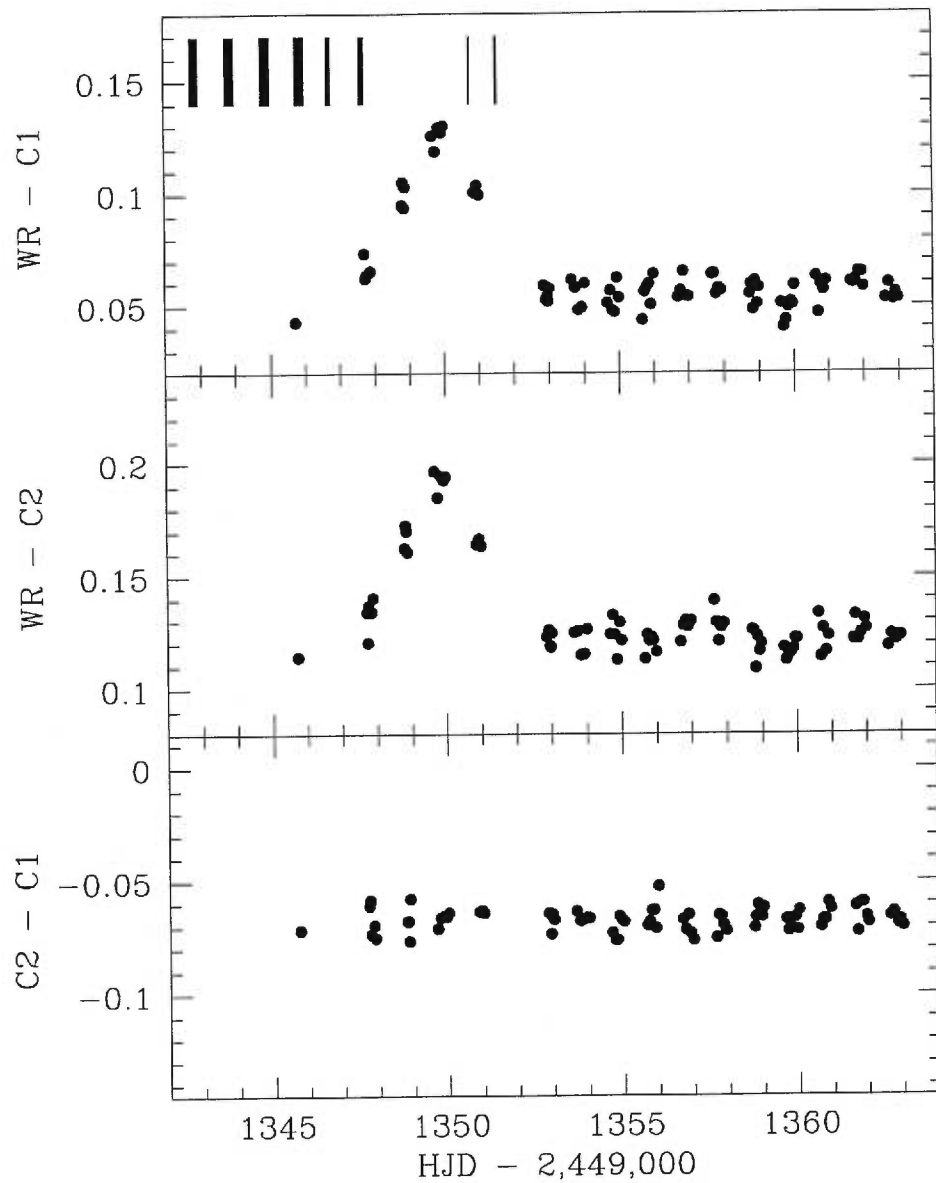


FIGURE 5.1. *Two upper panels:* differential v magnitudes of WR 1 in 1996 September relative to the two comparison stars C1 and C2. *Lower panel:* differential ($C2 - C1$) magnitudes. Dates when simultaneous spectroscopic observations were performed are indicated by vertical tick lines in the uppermost panel.

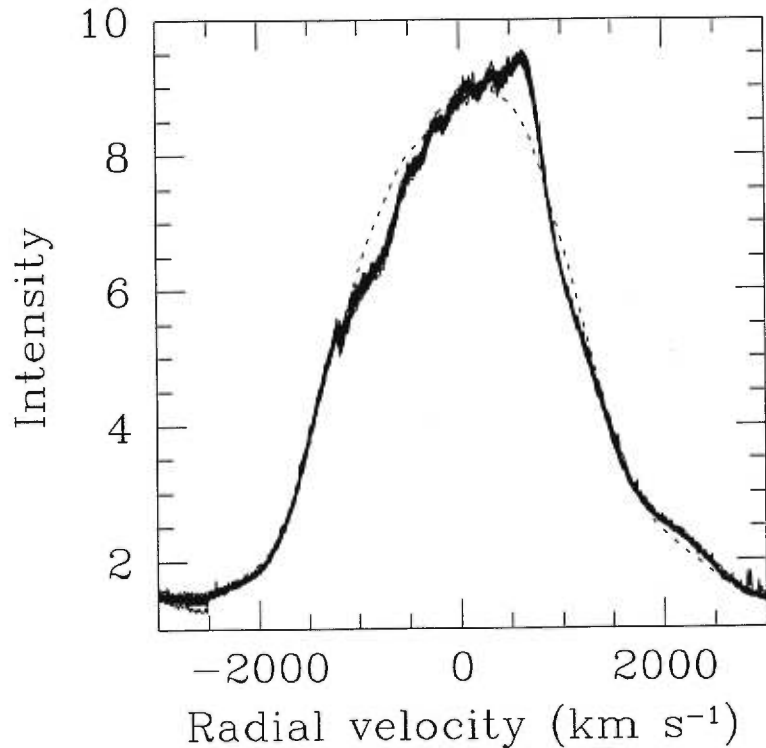


FIGURE 5.2. Superposition of the 21 Echelle spectra acquired on 1996 September 18 (around HJD 2,450,344.873) for the spectral range encompassing He II $\lambda 4686$. These spectra have been acquired on a total time interval of about 5.5 hours. For comparison purposes, the dashed line shows the mean spectrum of the 1996 September dataset. The discontinuities observed at about -2500 km s^{-1} and -1200 km s^{-1} are artefacts of an imperfect connection of the orders. The projected velocities, as everywhere in this paper, are heliocentric and refer to the laboratory rest wavelength.

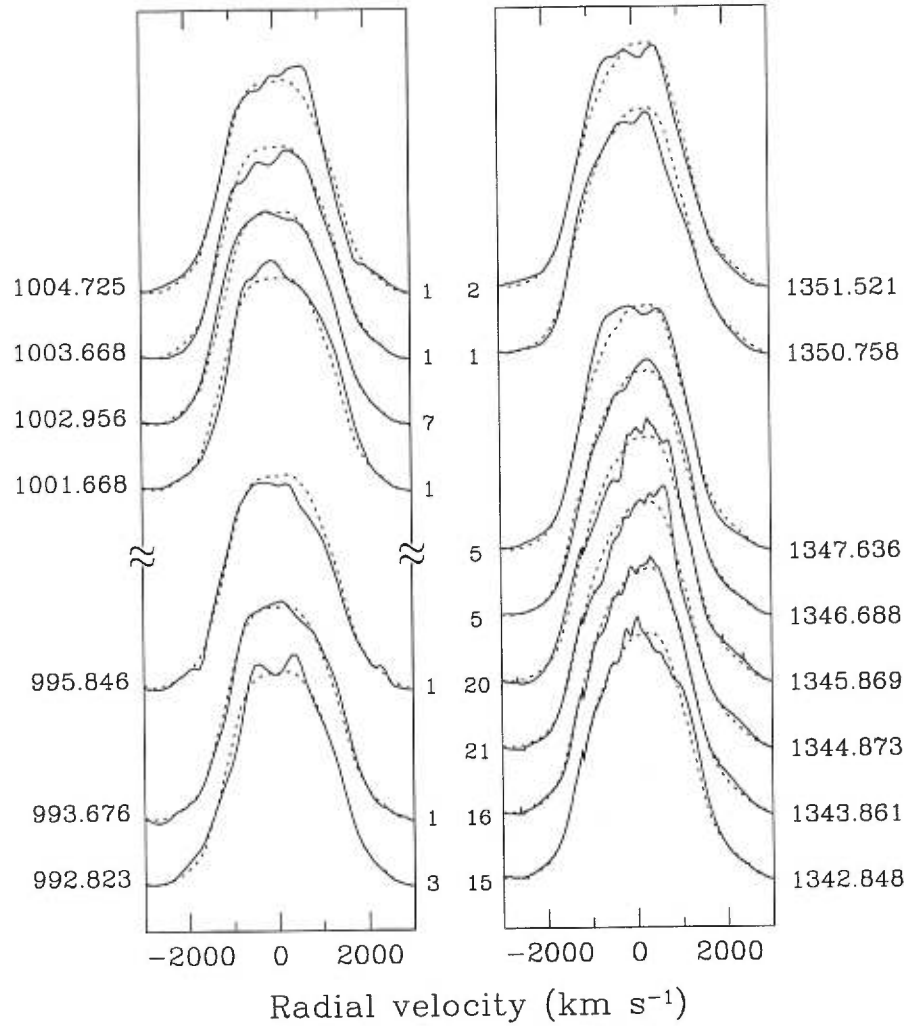


FIGURE 5.3. Montage of the continuum-normalized, nightly mean spectra obtained in 1995 October (*left panel*) and 1996 September (*right panel*) for the spectral range encompassing He II λ 4686 (the number of individual spectra averaged to form the corresponding nightly mean is indicated between the two panels). The mean Heliocentric Julian Date of the observations ($-2,449,000$) is indicated on both sides of the panels. For comparison purposes, the unweighted means for 1995 October (7 spectra) and 1996 September (8 spectra) are overplotted as a dashed line. The spectra of consecutive nights are offset by 2.5 units of continuum in the intensity scale.

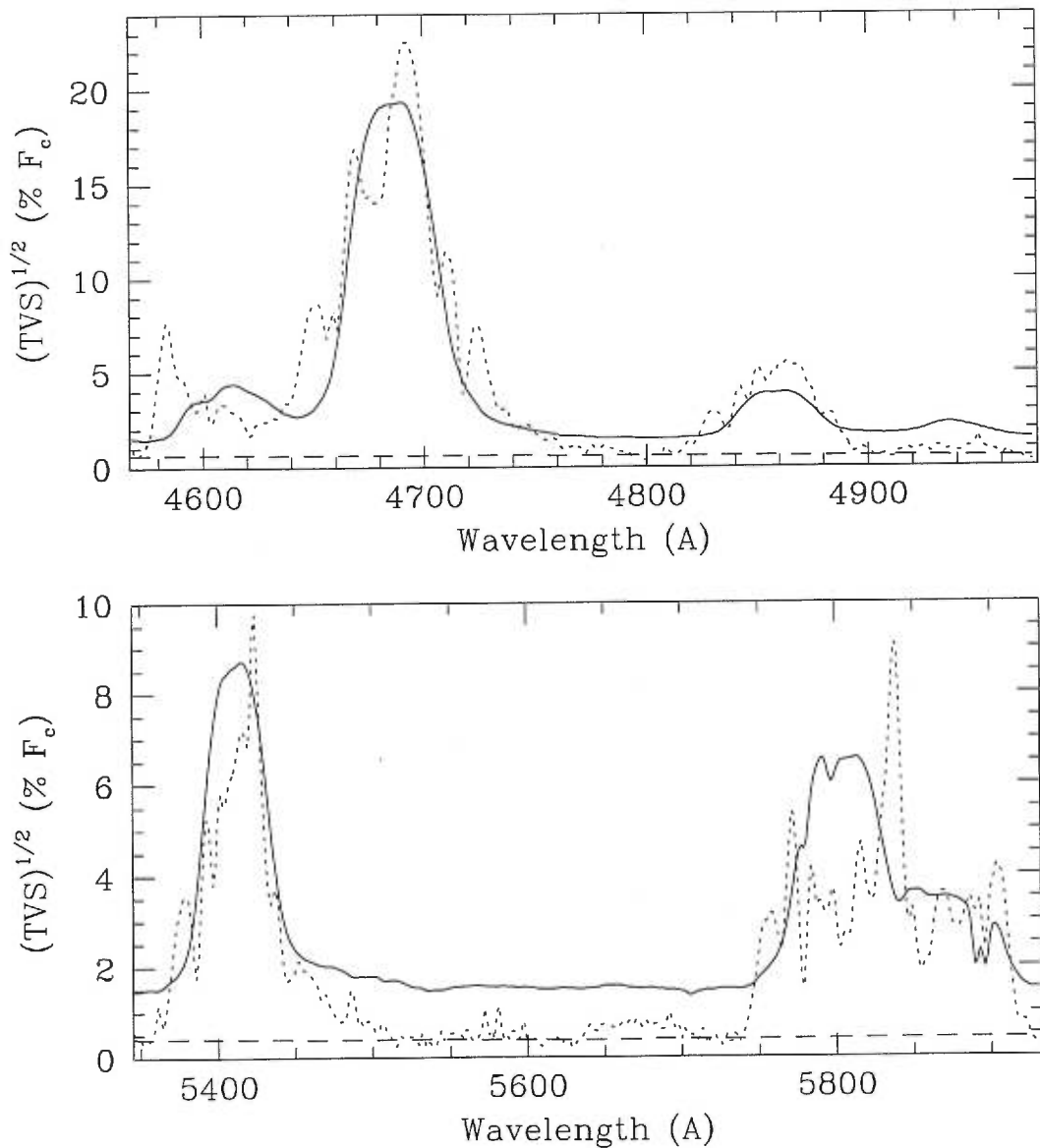


FIGURE 5.4. Square root of the Temporal Variance Spectrum (*short-dashed line*), along with the threshold indicating the 99.0 % confidence level for significant variability (*long-dashed line*). The mean of the spectra used in the calculations is overplotted in arbitrary units (*solid line*).

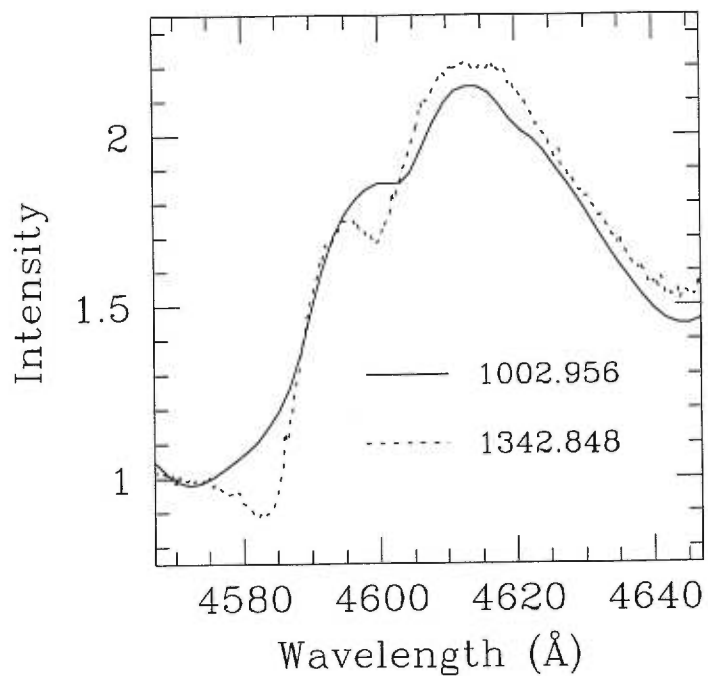


FIGURE 5.5. Superposition for the spectral range encompassing N V $\lambda\lambda 4604, 4620$ of the nightly means of 1995 October 12 (*solid line*) and 1996 September 16 (*short-dashed line*). The mean Heliocentric Julian Dates of the observations ($-2,449,000$) are indicated.

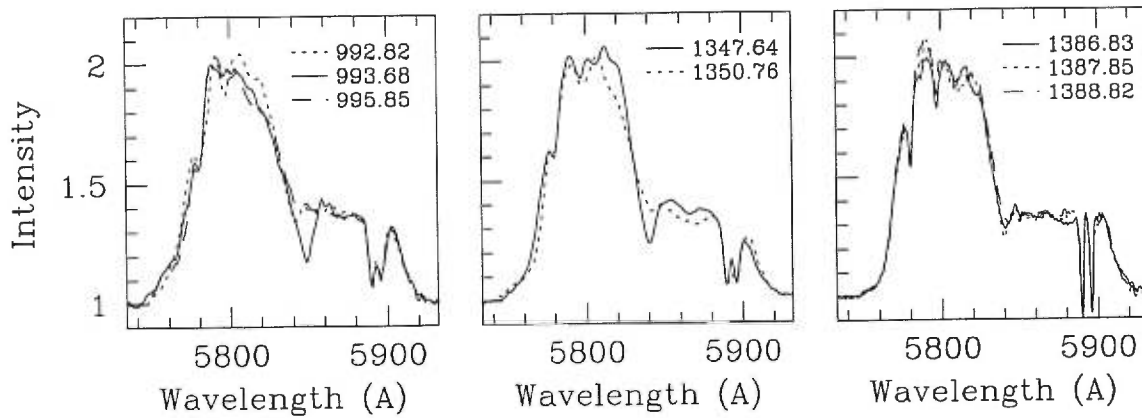


FIGURE 5.6. Superposition for the spectral range encompassing C IV λ 5806 and He I λ 5876 of nightly means observed in 1995 October (*left panel*), 1996 September (*middle panel*) and 1996 November (*right panel*). The mean Heliocentric Julian Dates of the observations ($-2,449,000$) are indicated in each panel.

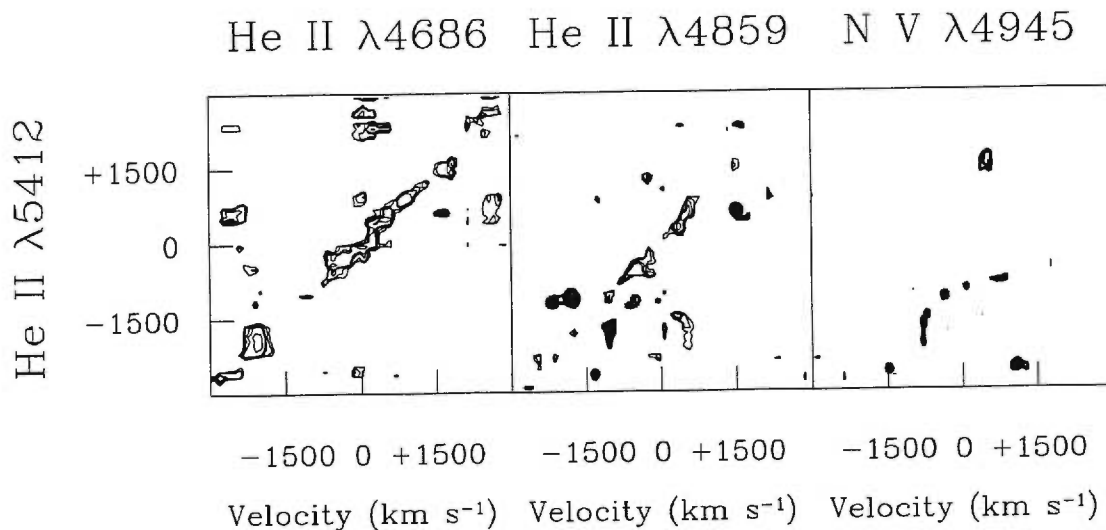


FIGURE 5.7. Correlation matrices of He II λ 5412 with He II λ 4686, He II λ 4859, and N V λ 4945. Thick and thin contours indicate a negative or positive correlation in the pattern of variability presented by two line profiles at different projected velocities (referred to the line laboratory rest wavelength), respectively. The lowest contour is drawn for a significant correlation at the 99.5 % confidence level.

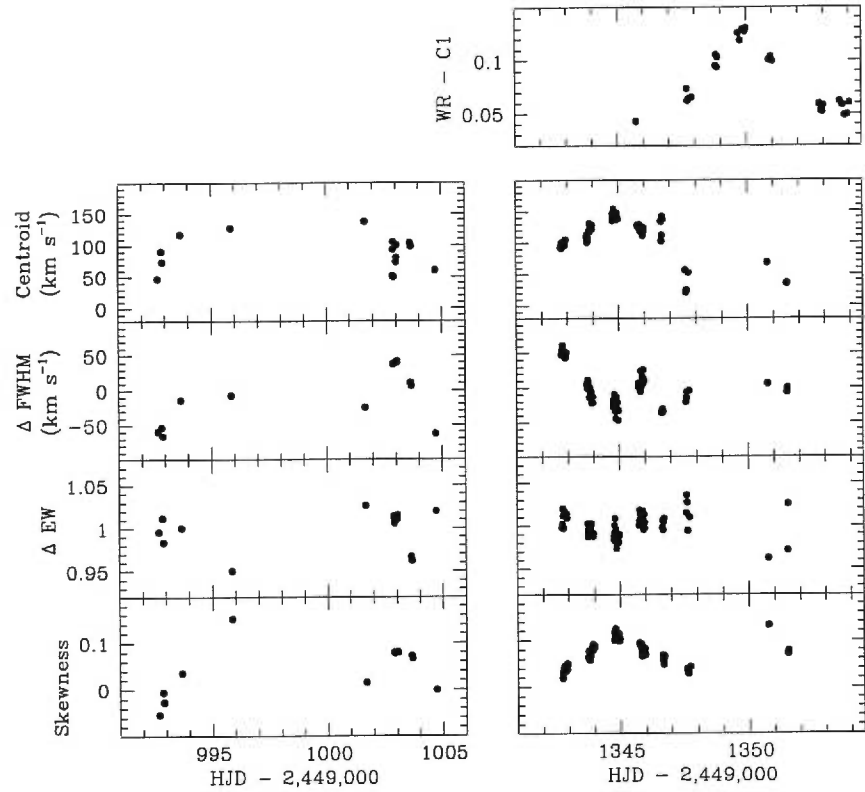


FIGURE 5.8. From top to bottom: continuum flux level variations, centroid variations (in km s^{-1}), deviations of the FWHM around the mean value (in km s^{-1}), EW variations (normalized by division to the mean value), and skewness variations of He II $\lambda 4686$, as a function of the Heliocentric Julian Date of observation. *Left panel:* 1995 October; *right panel:* 1996 September.

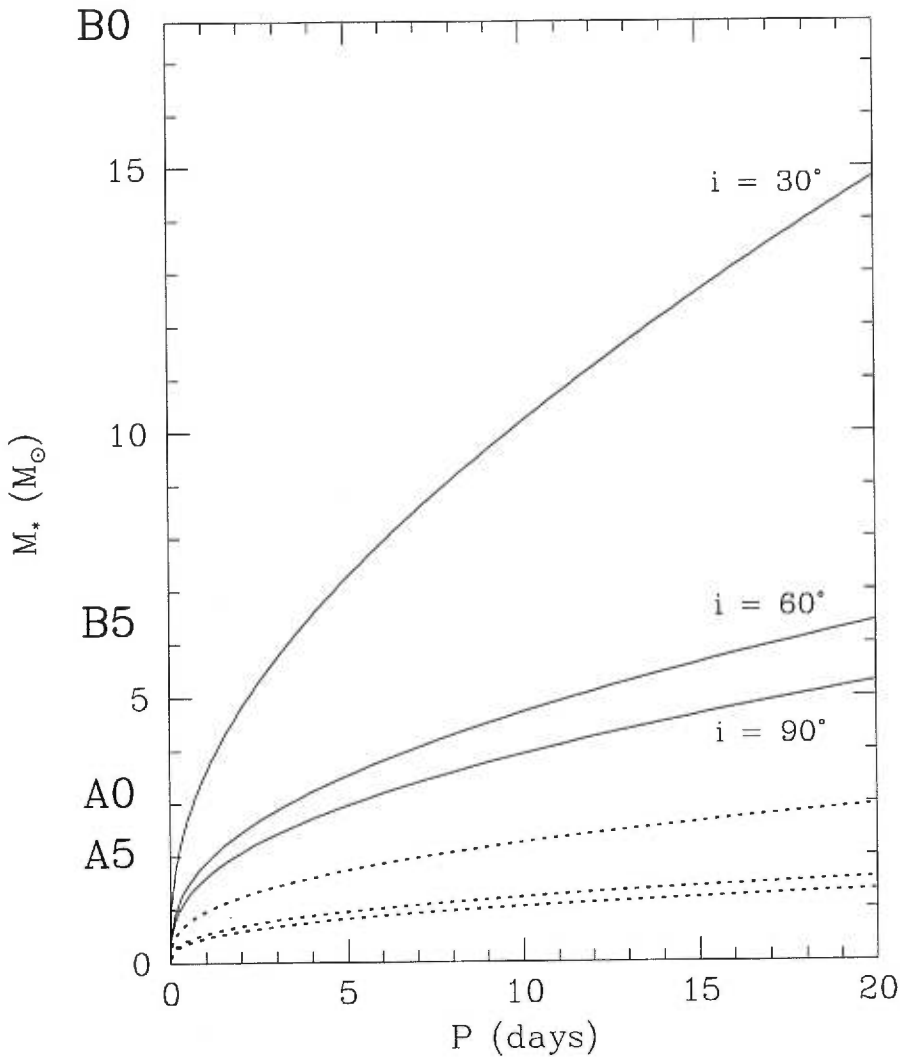


FIGURE 5.9. Allowed values of (P, M_*) when adopting $K_{WR} \approx 70 \text{ km s}^{-1}$ (solid lines) and $K_{WR} \approx 22 \text{ km s}^{-1}$ (short-dashed lines). These values are shown for different orbital inclinations i : 90° , 60° , and 30° . The spectral type of the companion (assuming a main-sequence type star) is indicated at the leftmost part of this figure.

CHAPITRE 6

CONCLUSION

A l'origine, ce projet visait essentiellement à reconsidérer la proposition selon laquelle la variabilité périodique présentée par les étoiles WR 6 et WR 134 était induite par la révolution orbitale d'un compagnon dégénéré. Cette tâche est rendue difficile par le fait que les déformations qui affectent les profils de raie masquent la signature non équivoque de la présence d'un compagnon que serait la détection de (faibles) variations de vitesse radiale. De ce fait, les arguments pour, ou contre, l'éventuelle association de ces étoiles WR avec un compagnon ne reposent que sur des critères secondaires (e.g., chapitres 2 et 4).¹

Notre étude a notamment permis de démontrer le relativement faible flux de rayons-X émanant de ces objets dans l'hypothèse d'un compagnon compact accrétant le vent de l'étoile WR (voir les calculs détaillés du chapitre 4), la nature causale des variations affectant les parties internes et externes du vent (chapitre 3), le caractère périodique des variations présentées par les raies spectrales formées à proximité du cœur stellaire (e.g., N V λ 4945; chapitre 3), ainsi que le caractère globalement variable des variations selon l'époque d'observation (chapitres 3 et 4). Bien que nous voudrions souligner qu'aucun de ces critères ne constitue en lui-même un argument péremptoire permettant d'exclure définitivement le modèle impliquant la présence d'un compagnon dégénéré (par exemple, la déficience de

¹En tout état de cause, et quelle que soit l'origine des importantes variations spectrales observées, le choix de WR 6 et WR 134 comme prototypes des classes WN 5 et WN 6 pour les modèles atmosphériques des étoiles WR (Hillier 1988; Hamann, Schmutz, & Wessolowski 1988; Crowther & Smith 1996) se doit d'être abandonné.

rayons-X observée peut être expliquée par des processus menant à l'inhibition de l'accrétion sur le compagnon), la conjonction de ces arguments nous amène à penser que l'hypothèse selon laquelle WR 6 et, dans une moindre mesure, WR 134, sont associées à un compagnon dégénéré est sérieusement mise en doute (l'association avec une étoile de classe de luminosité V-III semble également improbable). Après achèvement de ce projet, cette conclusion a été d'autre part supportée en ce qui concerne WR 6 par la non-détection de rayons-X de hautes énergies ($E \gtrsim 5$ keV) prédis dans le contexte d'un vent stellaire accrétré par une étoile à neutron (Skinner, Itoh, & Nagase 1998). Cette probable non-association de WR 6 et WR 134 avec un compagnon dégénéré semble conforter les modèles d'explosion de supernova les plus récents, où le taux de survie de systèmes binaires massifs à cet événement est peu élevé (e.g., Brandt & Podsiadłowski 1995).²

Inversement, et ceci est peut-être potentiellement plus riche en enseignements, les variations observées seraient plus vraisemblablement induites par la modulation par rotation de structures étendues dans le vent (quelque peu similaires à celles idéalisées sur la Fig.1.7). Des observations spectropolarimétriques de l'étoile WR 6 ont récemment permis de favoriser ce modèle (Harries et al. 1999). Le caractère globalement variable des variations selon l'époque d'observation pour WR 6 et WR 134 semble indiquer que, pour une raison qui reste à déterminer, la morphologie à grande échelle du vent stellaire change fondamentalement sur une base de temps variant de quelques semaines à quelques mois. De plus, des présomptions laissent penser que ces structures dans le vent de WR 6 prennent naissance à la base du vent, voire même à toute proximité de la photosphère stellaire (chapitre 3).

Durant l'élaboration de ce projet, nombre d'études observationnelles (notam-

²Il n'est nullement exclu que ces étoiles n'aient été, au début de leur évolution, associées à un compagnon; le système ayant pu être par la suite dissocié lorsque l'étoile primaire a explosé en supernova (§1.2.2.1). Ceci expliquerait leurs distances perpendiculairement au plan galactique, ainsi que leurs vitesses tangentielles particulières relativement élevées (Tableau 1.2).

ment avec le satellite *IUE*) ont permis de mieux cerner les mécanismes à l'origine de la variabilité spectrale affectant les progénitrices des étoiles WR que sont les étoiles O (e.g., Kaper et al. 1997, et références citées). Ces études ont démontré que des vents nettement anisotropiques, probablement constitués de structures azimutales à grande échelle émanant de la photosphère stellaire, étaient sans doute l'apanage d'un nombre non négligeable d'étoiles de type précoce. Il est intéressant de constater que ces conclusions, quant à l'origine de la variabilité, concordent dans leurs grandes lignes avec celles de notre étude.

Nos observations suggèrent que le vent de ces étoiles WR se compose, d'une part, de structures à grande échelle (de l'ordre du rayon stellaire) dont la formation est possiblement induite par des perturbations photosphériques et, d'autre part, par des structures à petite échelle dues à des instabilités radiatives et/ou des phénomènes de turbulence (Lépine & Moffat 1999). La question qui vient immédiatement à l'esprit est de savoir si ces deux types distincts de structures peuvent cohabiter et, si oui, de quelle façon elles s'influencent mutuellement. La réponse à la première interrogation semble devoir être affirmative. De récentes simulations hydrodynamiques s'attachant à modéliser le vent d'une étoile de type précoce soumis à ces deux types de perturbations suggèrent que, si l'amplitude des chocs induits par des instabilités radiatives n'est pas trop élevée, la formation de structures à grande échelle n'est pas inhibée par l'existence de chocs, et *vice versa* (Owocki 1999). Cette proposition est supportée observationnellement par la présence simultanée de structures à petite et grande échelle se déplaçant sur les profils de raie de l'étoile WR 11 (γ^2 Vel; Lépine, Eversberg, & Moffat 1999). Nous pouvons également noter dans la Figure 2.15 que le profil de la raie N IV λ 1718 — de par son caractère différent de ce qui serait attendu dans l'approximation Sobolev — révèle à la fois pour le flot “rapide” *et* pour le flot “lent” l'existence de champs de vitesse non monotones (i.e., chocs) dans les parties externes du vent. L'élaboration d'une nouvelle génération de modèles permettra éventuellement d'évaluer de façon précise si les propriétés des surdensités de matière formées

sous l'action d'instabilités radiatives (e.g., dimension, champ de vitesse) différent à l'intérieur et à l'extérieur des structures étendues.

Comme le suggèrent les modèles hydrodynamiques de Cranmer & Owocki (1996), nous pouvons spéculer que cette anisotropie du vent des étoiles WR 6 et WR 134 est engendrée par une quelconque activité photosphérique (nos données semblent d'ailleurs supporter cette assertion pour WR 6; chapitre 3). Les processus physiques engendrant cette activité restent particulièrement mystérieux. Des structures magnétiques ou des pulsations constituent, dans l'état de nos connaissances actuelles, les mécanismes qui semblent pouvoir être raisonnablement avancés. L'existence de structures magnétiques pour initier la variabilité observée semble néanmoins favorisée, et ce pour diverses raisons:

- Les modèles s'intéressant à la stabilité des étoiles WR suggèrent que des modes "étranges" sont susceptibles de se développer dans ces étoiles, avec des périodes de l'ordre de 5-10 minutes (Glatzel, Kiriakidis, & Fricke 1993). Cependant, ce phénomène de pulsations éprouve, entre autres, des difficultés pour expliquer la modulation du patron de variabilité sur une base de temps de quelques semaines, ainsi que l'amplitude élevée des variations photométriques (occasionnellement ≈ 0.1 mag).
- De par son effet sur l'émergence du vent à grande échelle, le comportement à long terme de structures magnétiques serait éventuellement susceptible de rendre compte de la nature globalement variable des variations selon l'époque d'observation. Bien que largement *ad hoc*, cette interprétation a d'ores-et-déjà été proposée pour d'autres étoiles variables de type précoce (Fullerton et al. 1997; Balona, Sterken, & Manfroid 1991). Les étoiles WR étant dépourvues de couche convective à leur surface, il est fort probable que ces structures magnétiques ne soient pas, le cas échéant, engendrées par le processus "dynamo", comme cela est le cas pour le Soleil, par exemple. Il est vraisemblable que le champ magnétique soit au contraire d'origine

fossile. Un effort majeur est actuellement entrepris afin de détecter de tels champs magnétiques dans les étoiles O et WR (Eversberg 1998; Henrichs et al. 1998). Il est cependant à noter qu'un champ magnétique de relativement faible intensité — voire même en deçà des possibilités de détection instrumentales actuelles ($B \lesssim 100$ G) — peut possiblement avoir un effet notable sur la dynamique d'un vent supporté par la pression de radiation (Owocki 1994). Cette possibilité mériterait sans doute d'être explorée théoriquement dans un proche avenir.

Schématiquement, les étoiles WR apparemment isolées peuvent être subdivisées en trois classes exhibant différents types de variabilité (Tableau 6.1). La variabilité de type I — bien qu'indécelable dans les objets présentant des variabilités de type II et III — est sans nul doute présente puisque les instabilités radiatives semblent se développer naturellement dans les vents mus par la pression de radiation. Il n'est pas exclu que certains objets de la classe II puissent en fait être reclassifiés à l'intérieur de la classe III; ceci est notamment le cas pour les étoiles de type WN 8 dont les raies étroites rendent difficile l'identification d'un comportement périodique.

L'étoile WR 134, malgré un caractère (quasi)périodique de la variabilité maintenant bien établi, a un comportement se rapprochant quelque peu de celui de la classe II dans le sens qu'une perte de cohérence est rapidement observée. Ceci contraste avec le patron de variabilité de WR 6 qui est très cohérent sur plusieurs cycles (e.g., Fig.2.3), bien que dépendant de l'époque d'observation. Ces deux étoiles semblent se distinguer nettement de l'ensemble de la population d'étoiles WR par leur dépolarisation élevée dans leurs profils de raie comparée au continuum; ceci étant généralement attribué à un vent concentré dans le plan équatorial (Schulte-Ladbeck et al. 1991, 1992). Il importe de constater que ces deux phénomènes (variabilité de type III et formation d'une "zone de compression équatoriale" telle que définie par Ignace, Cassinelli, & Bjorkman [1996]) sont

possiblement intimement reliés.

Nos observations de l'étoile WR 1 ont permis de démontrer la grande similitude entre son patron de variabilité spectrale et ceux de WR 6 et WR 134, ainsi que le caractère atypique de ses variations photométriques (chapitre 5). Néanmoins, le caractère apparemment non cyclique du patron de variabilité la rapproche des objets de la classe II.

Une hypothèse hardie serait d'avancer que les processus physiques à l'œuvre dans les objets de la classe II et III sont en fait fondamentalement identiques mais que la durée de vie caractéristique des structures étendues varie d'une étoile à l'autre (les structures étant particulièrement instables pour les étoiles de type WN 8 mais relativement stables pour WR 6). Le comportement temporel de structures magnétiques et/ou des instabilités radiatives pourraient éventuellement contribuer à empêcher l'établissement de ces structures à grande échelle.

Il est à noter que les objets présentant un niveau inhabituel (et a fortiori périodique) de variabilité sont confinés aux sous-types WN 8-WN 5; une notable exception étant WR 11 de type WC 8. Il reste à établir si cela résulte tout simplement d'un biais observationnel ou est révélateur de propriétés intrinsèques aux étoiles venant d'entrer relativement récemment dans la phase WR, e.g., telles un champ magnétique fossile disparaissant en allant vers les sous-types WC et/ou une structure interne durant la phase WNL propice aux phénomènes de pulsations. Elargir l'échantillon d'étoiles WR de la classe III permettrait d'évaluer si ces étoiles se distinguent, de par leurs paramètres fondamentaux (notamment z , $(v_t)_{pec}$, η ; voir Tableau 1.2), de l'ensemble de la population d'étoiles WR. Ceci pourrait nous fournir de précieuses indications quant à la nature exacte des mécanismes physiques sous-jacents.

RÉFÉRENCES

- Balona, L. A., Sterken, C., & Manfroid, J. 1991, MNRAS, 252, 93
- Brandt, N., & Podsiadlowski, P. 1995, MNRAS, 274, 461
- Chalabaev, A., & Maillard, J. P. 1983, A&A, 127, 279
- Cranmer, S. R., & Owocki, S. P. 1996, ApJ, 462, 469
- Crowther, P. A., Smith, L. J. 1996, A&A, 305, 541
- Eversberg, T. 1998, Thèse de doctorat, Univ. Montréal
- Fullerton, A. W., Massa, D. L., Prinja, R. K., Owocki, S. P., & Cranmer, S. R. 1997, A&A, 327, 699
- Glatzel, W., Kiriakidis, M., & Fricke, K. J. 1993, MNRAS, 262, L7
- Hamann, W.-R., Schmutz, W., & Wessolowski, U. 1988, A&A, 194, 190
- Harries, T. J., Howarth, I. D., Schulte-Ladbeck, R. E., & Hillier, D. J. 1999, MNRAS, sous presse
- Henrichs, H., et al. 1998, in ESO Proceedings, Cyclical Variability in Stellar Winds, ed. L. Kaper & A. W. Fullerton, 374
- Hillier, D. J. 1988, ApJ, 327, 822
- Ignace, R., Cassinelli, J. P., & Bjorkman, J. E. 1996, ApJ, 459, 671
- Kaper, L., et al. 1997, A&A, 327, 281
- Lépine, S., & Moffat, A. F. J. 1999, ApJ, sous presse
- Lépine, S., Eversberg, T., & Moffat, A. F. J. 1999, AJ, sous presse
- Owocki, S. P. 1994, Ap&SS, 221, 3

Owocki, S. P. 1999, in IAU Symp. 169, Variable and Non-spherical Stellar Winds in Luminous Hot Stars, ed. B. Wolf, A. W. Fullerton, & O. Stahl (Springer Verlag), sous presse

Schulte-Ladbeck, R. E., Nordsieck, K. H., Taylor, M., Nook, M. A., Bjorkman, K. S., Magalhães, A. M., & Anderson, C. M. 1991, ApJ, 382, 301

Schulte-Ladbeck, R. E., Nordsieck, K. H., Taylor, M., Bjorkman, K. S., Magalhães, A. M., & Wolff, M. J. 1992, ApJ, 387, 347

Skinner, S. L., Itoh, M., & Nagase, F. 1998, New Astronomy, 3, 37

TABLEAU 6.1. Caractéristiques générales de la variabilité d'étoiles WR apparemment isolées.

Type	Caractéristiques observationnelles de la variabilité (photométrie, spectroscopie, polarimétrie)	Objets	Cause physique
I	Faible amplitude, stochastique	Tous?	Instabilités radiatives
II	Grande amplitude Stochastique?, (quasi)périodique?	WN 8, WR 1 (WN 5), WR 11 (WC 8)? Pulsations?	Champs magnétiques? (Compagnon?)
III	Grande amplitude, (quasi)périodique	WR 6 (WN 5), WR 134 (WN 6)	Pulsations? Champs magnétiques?

APPENDICE A

MONTAGE DES SPECTRES DE L'ETOILE WR 136

Cet Appendice présente les spectres de l'étoile WR 136 acquis à l'Observatoire du Mont Mégantic entre mai et octobre 1995. Ceux-ci sont respectivement présentés pour les domaines spectraux 4440-5005 Å et 5345-5930 Å sur les figures A1 et A2. Les valeurs de la TVS (voir §2.3.2.3) sont présentées sur la figure A3. La figure A4 présente, quant à elle, les variations selon le jour Julien d'observation de l'inclinaison, premier moment, largeur à mi-hauteur et largeur équivalente de la raie He II λ 4686.

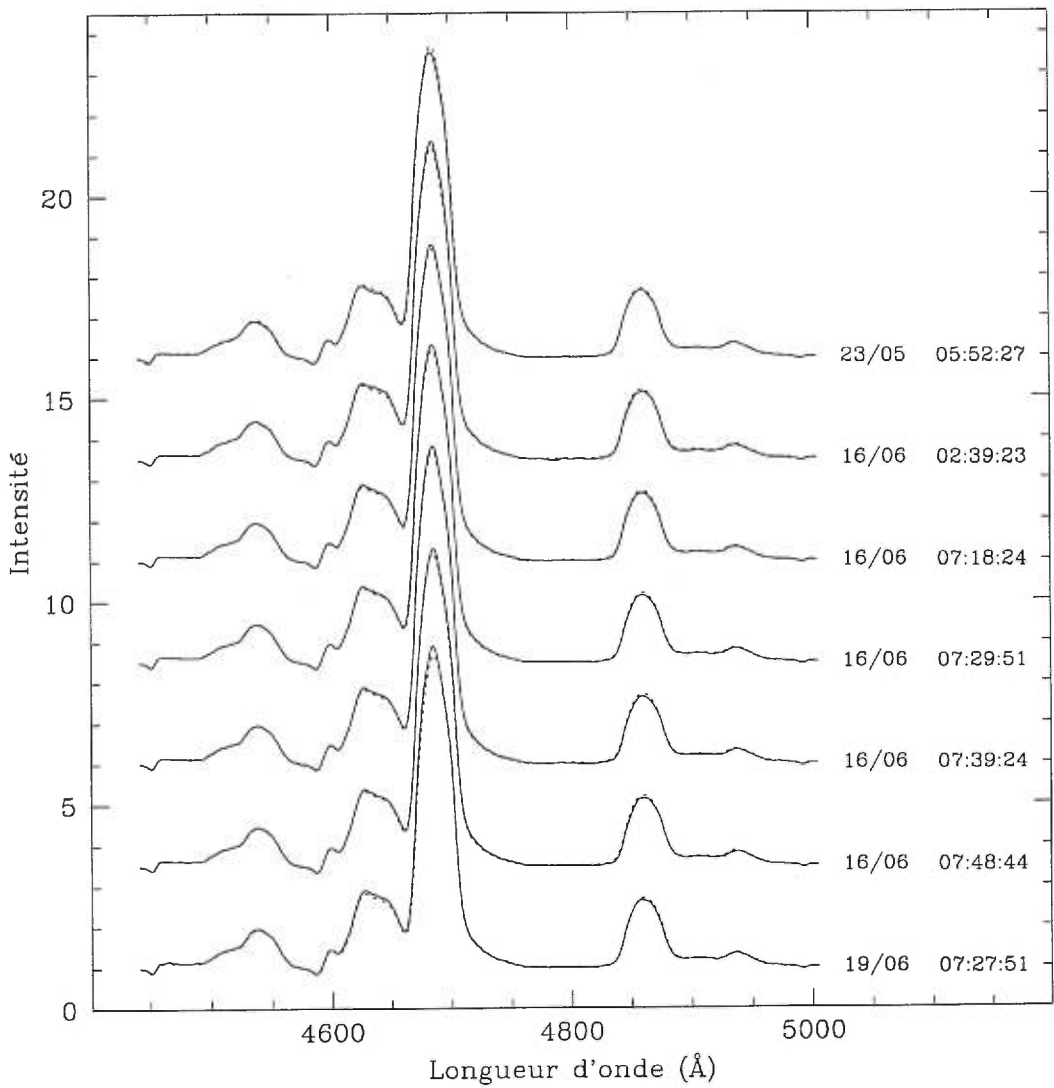


FIGURE A.1. Montage des spectres de l'étoile WR 136 pour le domaine spectral 4440-5005 Å. Le continuum stellaire a été fixé à l'unité. Les spectres ont été coalignés dans l'espace des vitesses radiales grâce aux raies interstellaires du calcium et du sodium ou, par défaut, grâce à la bande diffuse interstellaire à 4501 Å. Par souci de clarté, deux spectres consécutifs sont séparés par 2.5 unités du continuum. Un spectre moyen non pondéré de l'ensemble de ces spectres est superposé à titre indicatif en trait pointillé. La date, ainsi que l'heure de l'acquisition du spectre (en temps universel et référant au début de l'exposition), sont indiquées sur la droite de la figure.

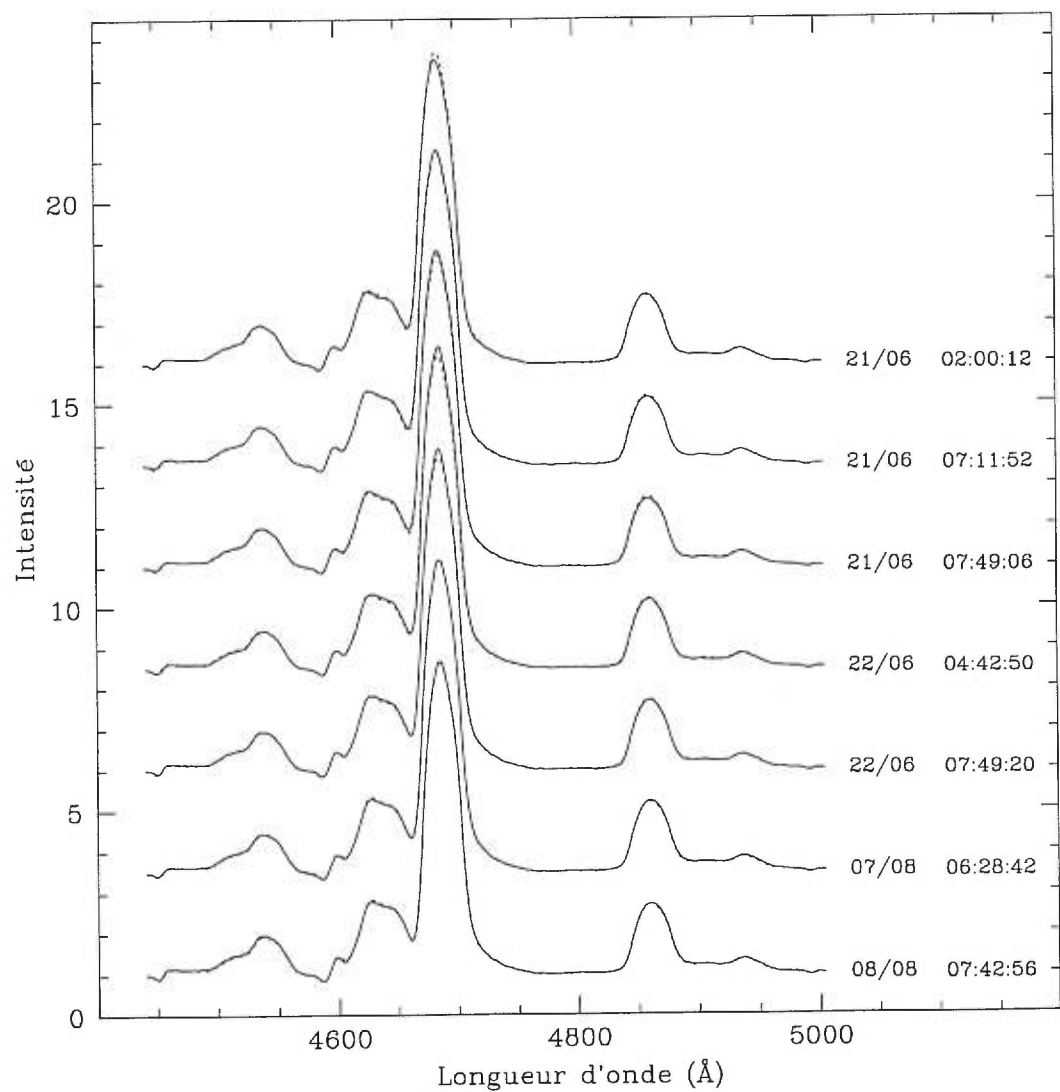


FIGURE A.1. Suite.

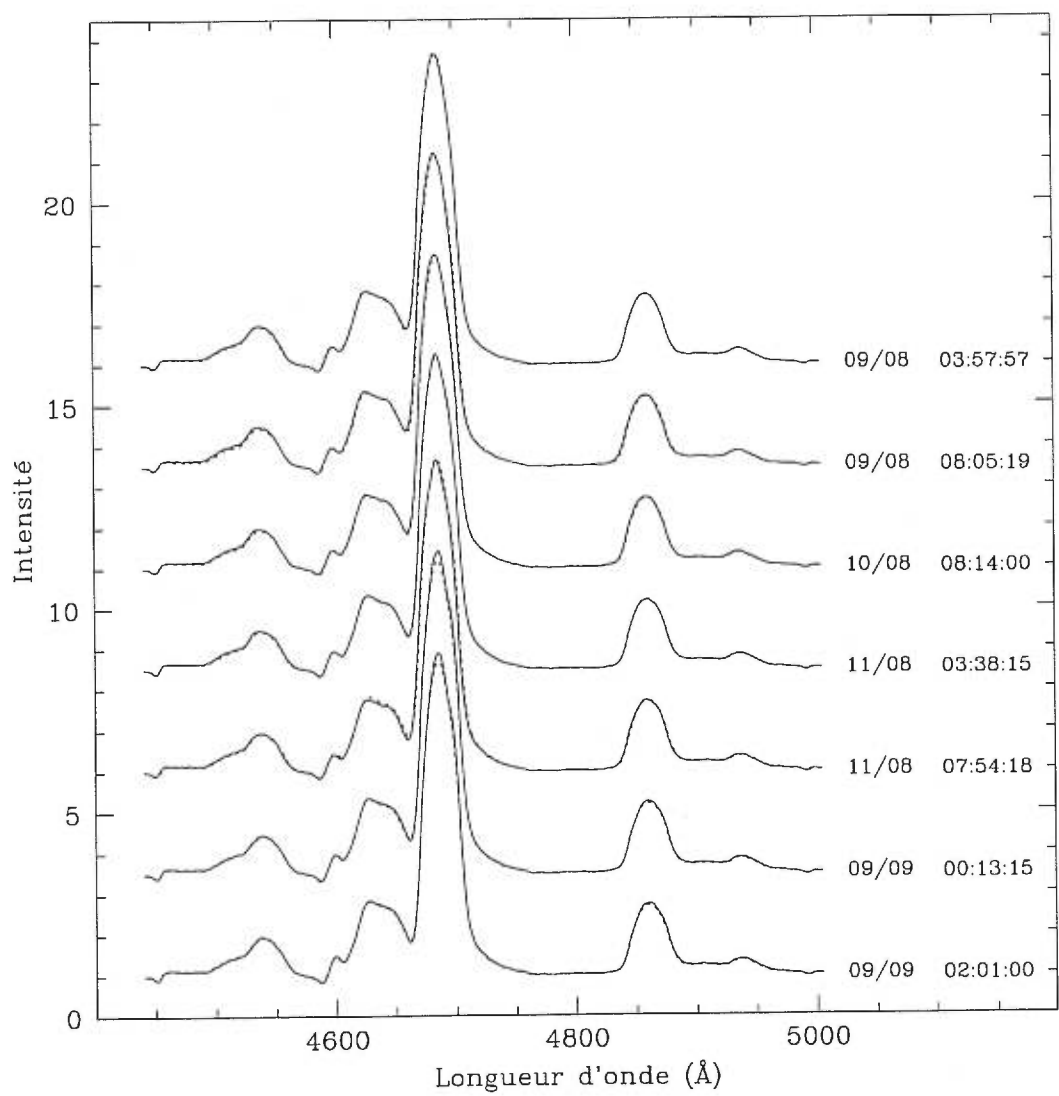


FIGURE A.1. Suite.

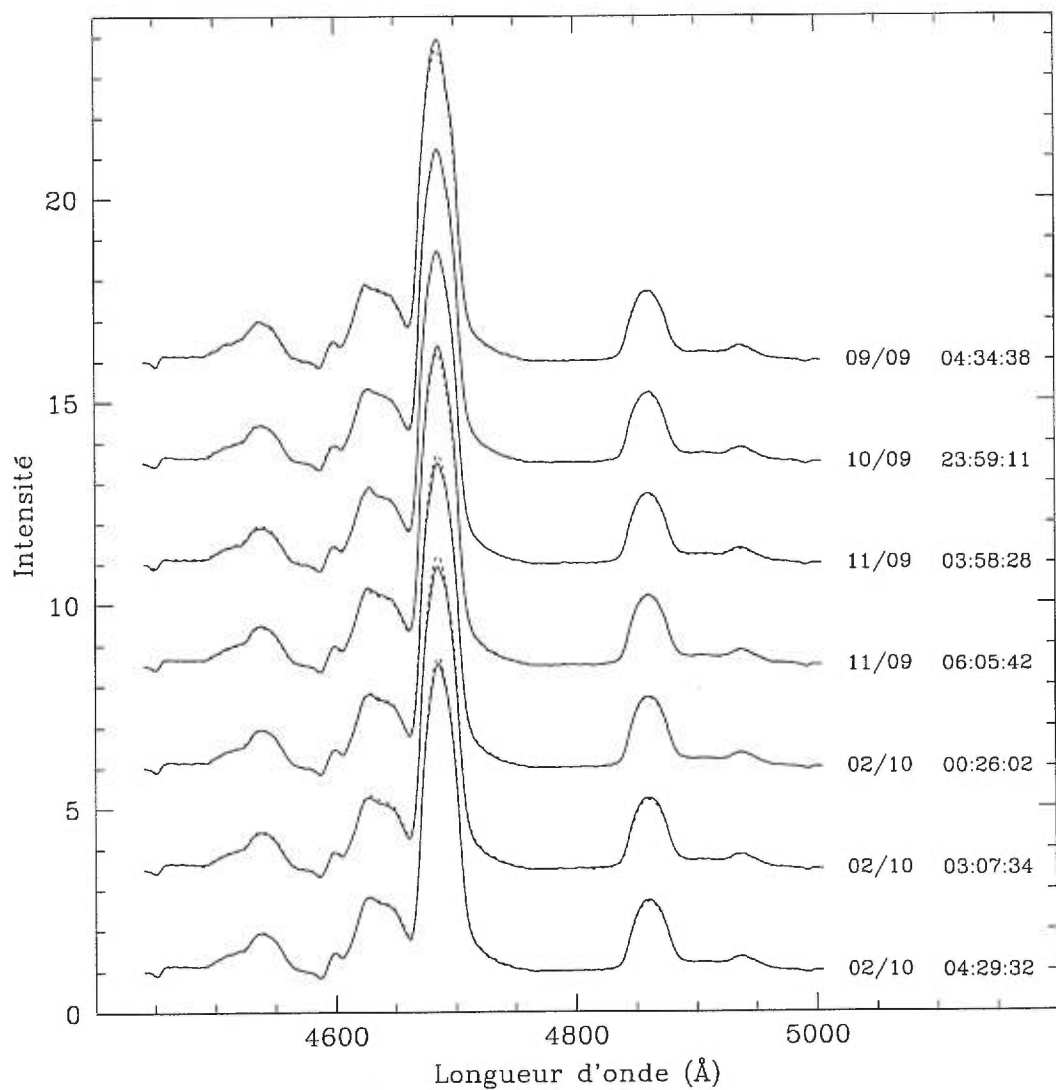


FIGURE A.1. Suite.

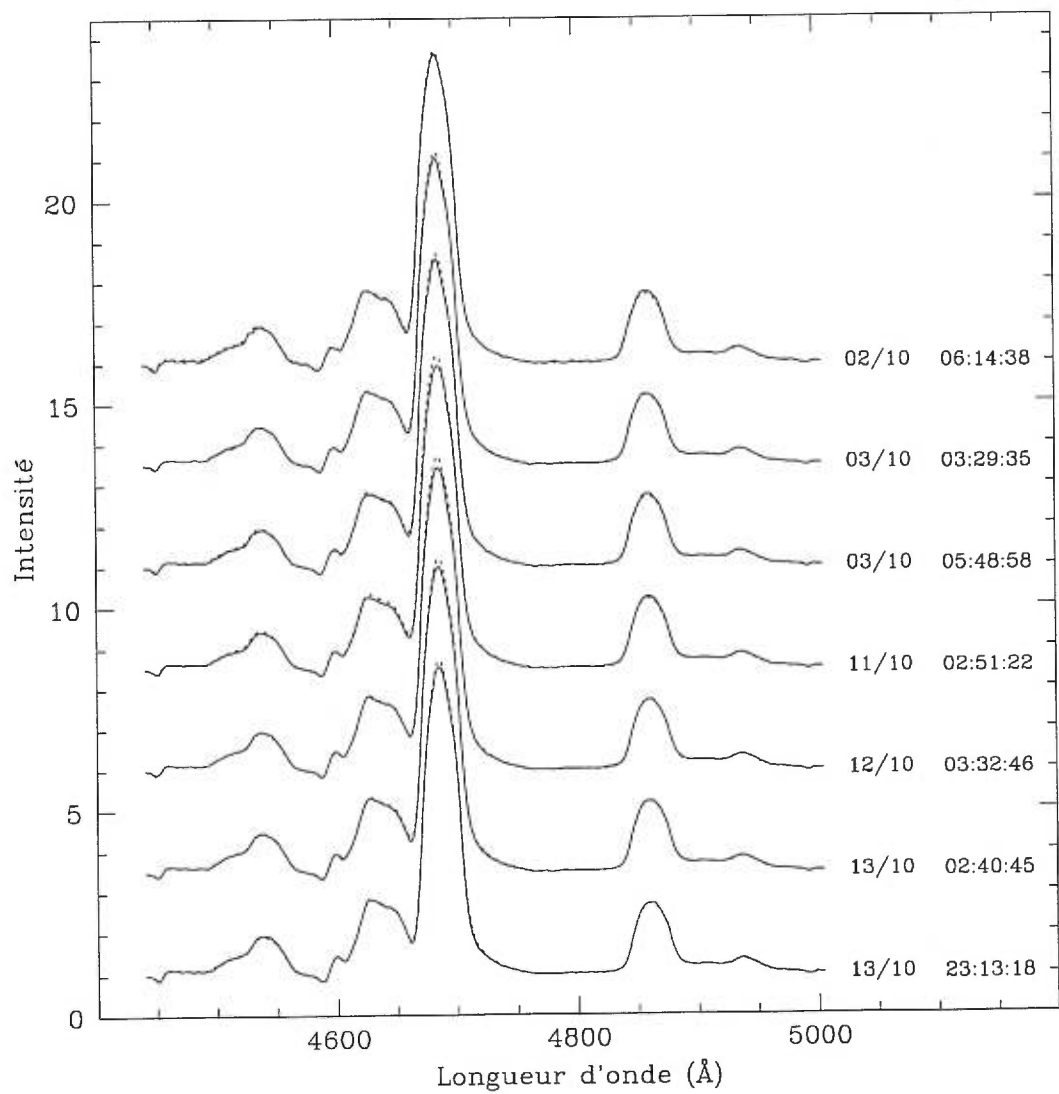


FIGURE A.1. Suite.

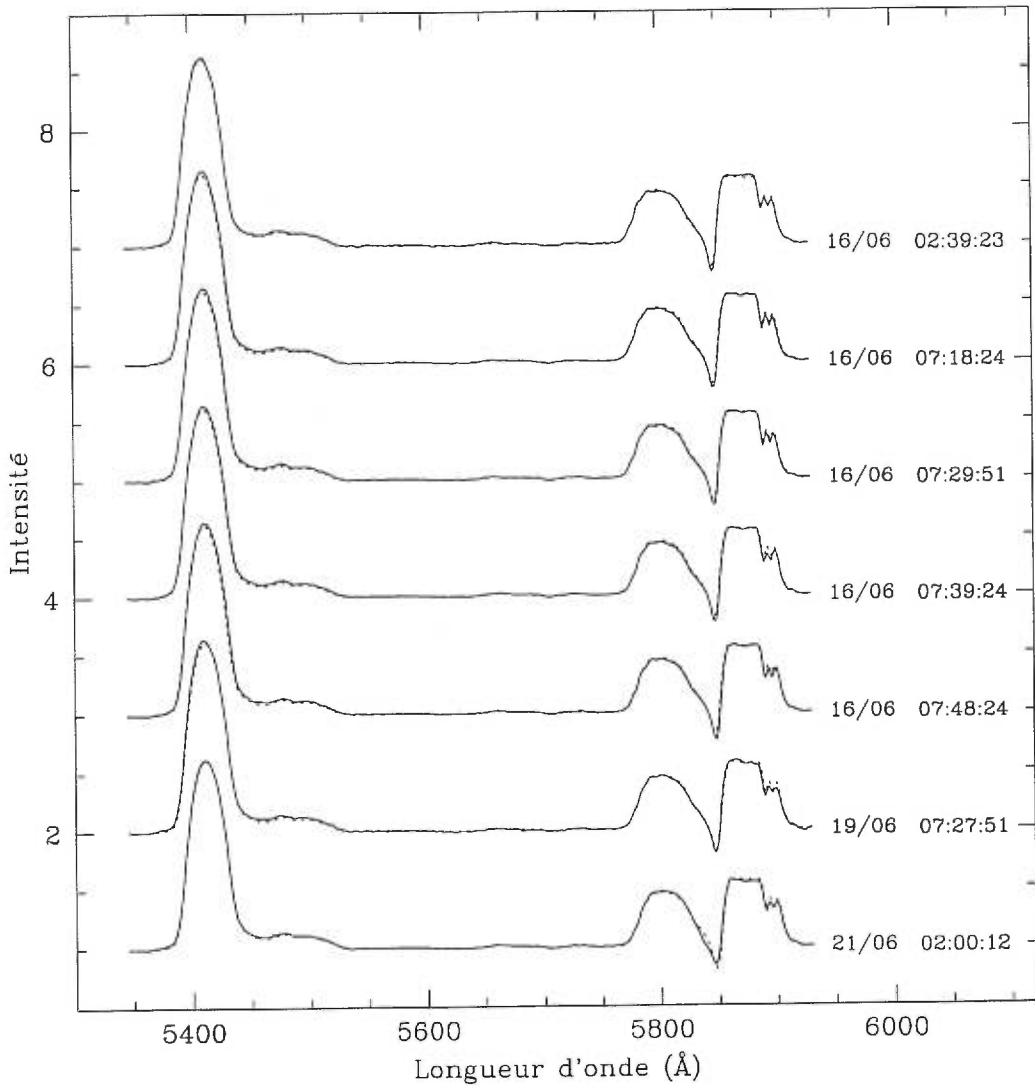


FIGURE A.2. Montage des spectres de l'étoile WR 136 pour le domaine spectral 5345-5930 Å. Le continuum stellaire a été fixé à l'unité. Les spectres ont été coalignés dans l'espace des vitesses radiales grâce aux raies interstellaires Na I $\lambda\lambda 5890, 5896$ Å. Par souci de clarté, deux spectres consécutifs sont séparés par une unité du continuum. Un spectre moyen non pondéré de l'ensemble de ces spectres est superposé à titre indicatif en trait pointillé. La date, ainsi que l'heure de l'acquisition du spectre (en temps universel et référant au début de l'exposition), sont indiquées sur la droite de la figure.

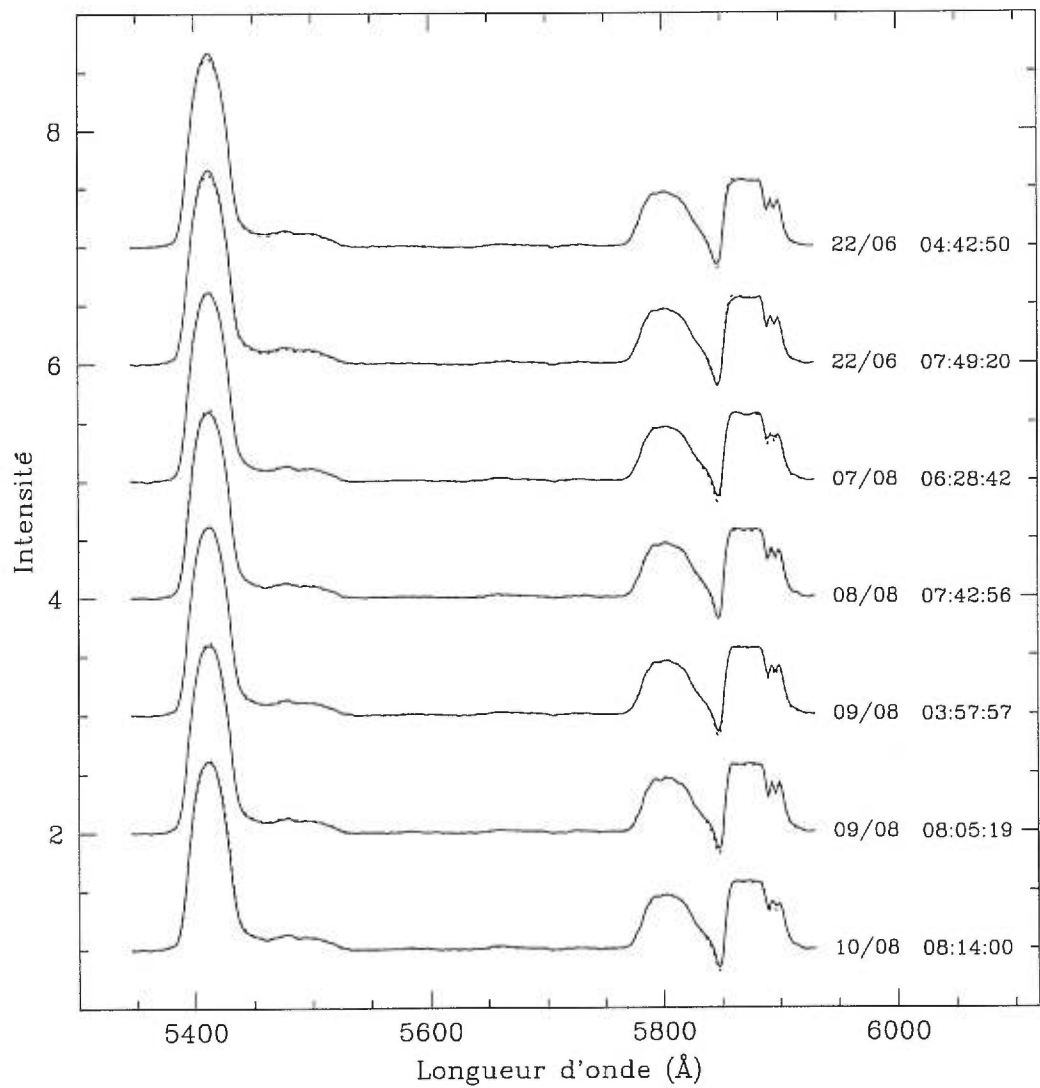


FIGURE A.2. Suite.

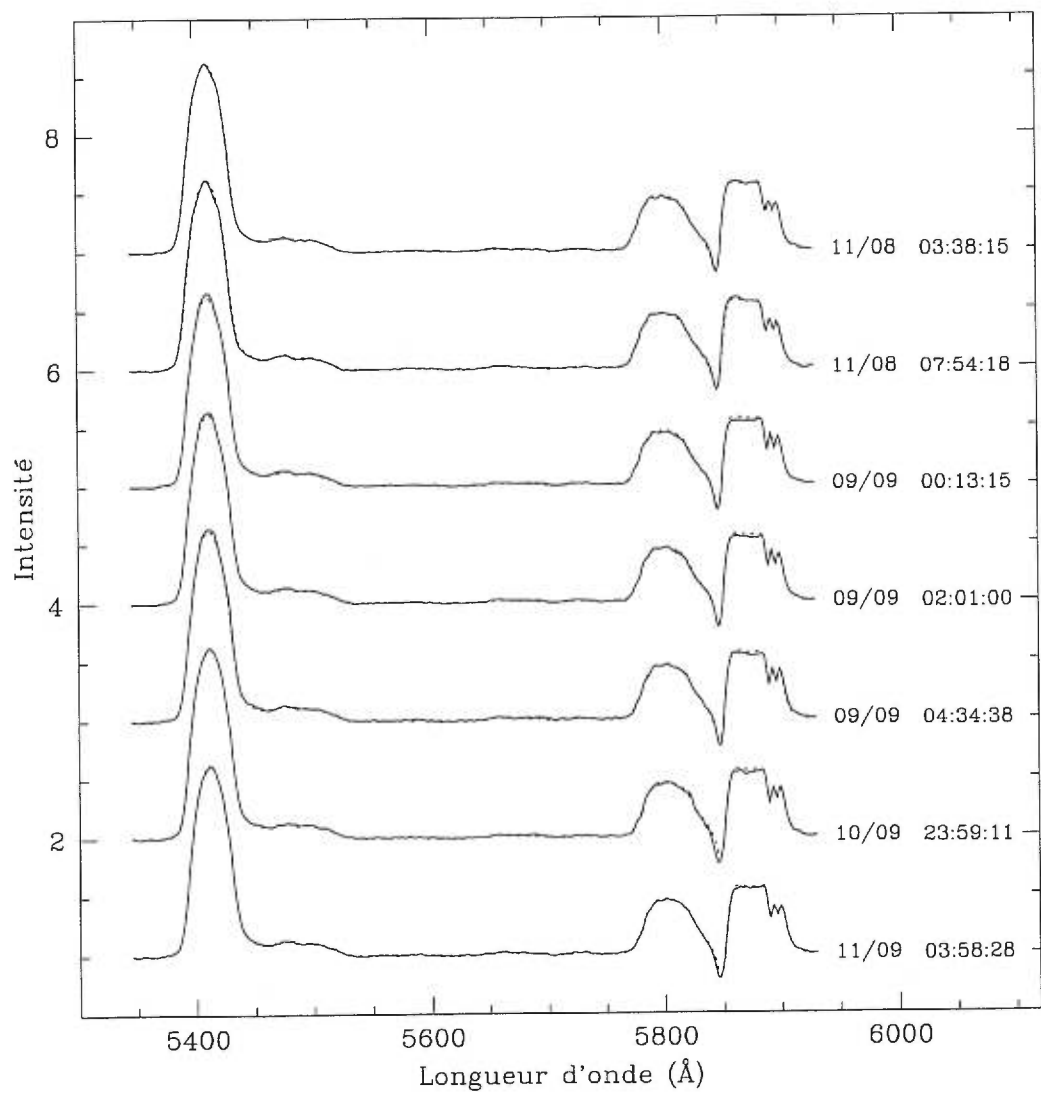


FIGURE A.2. Suite.

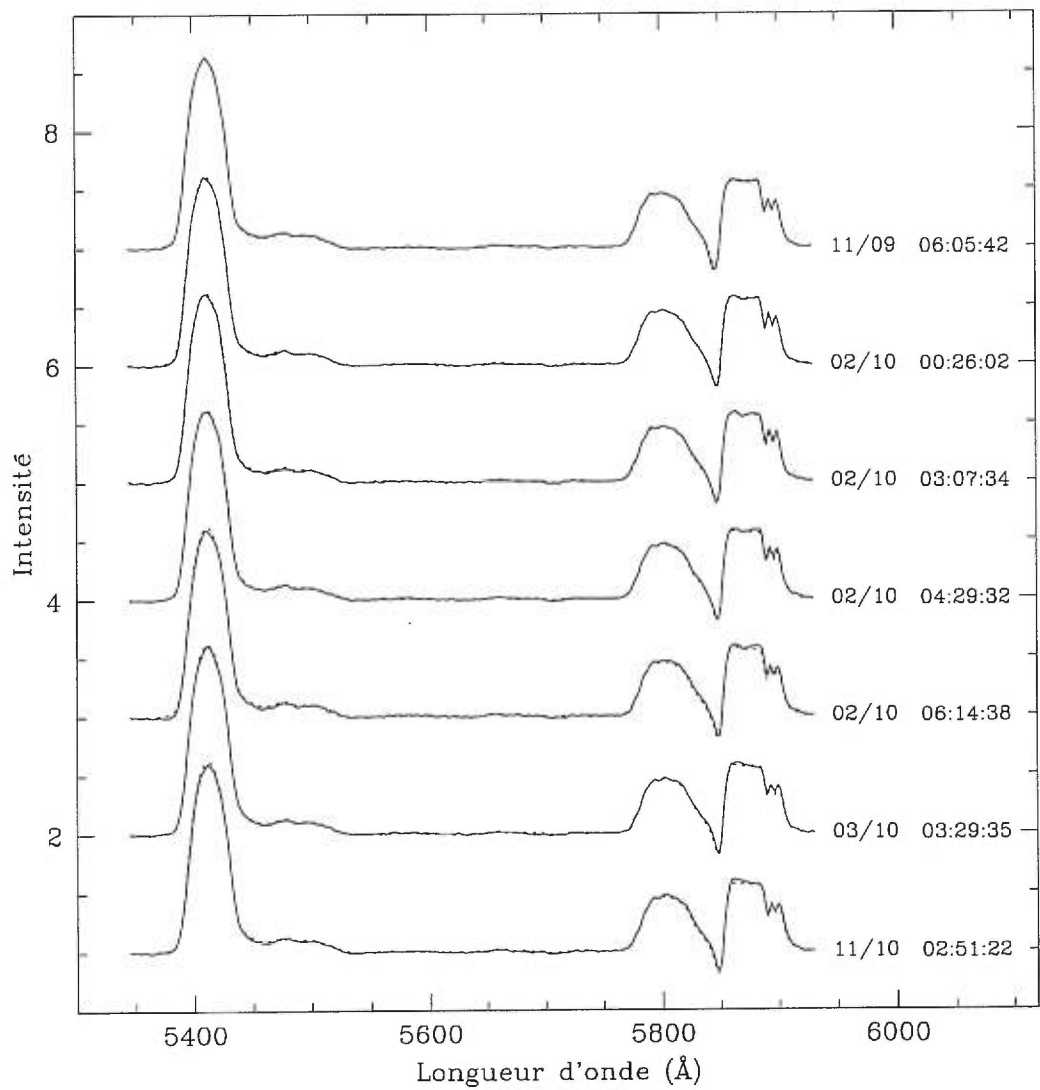


FIGURE A.2. Suite.

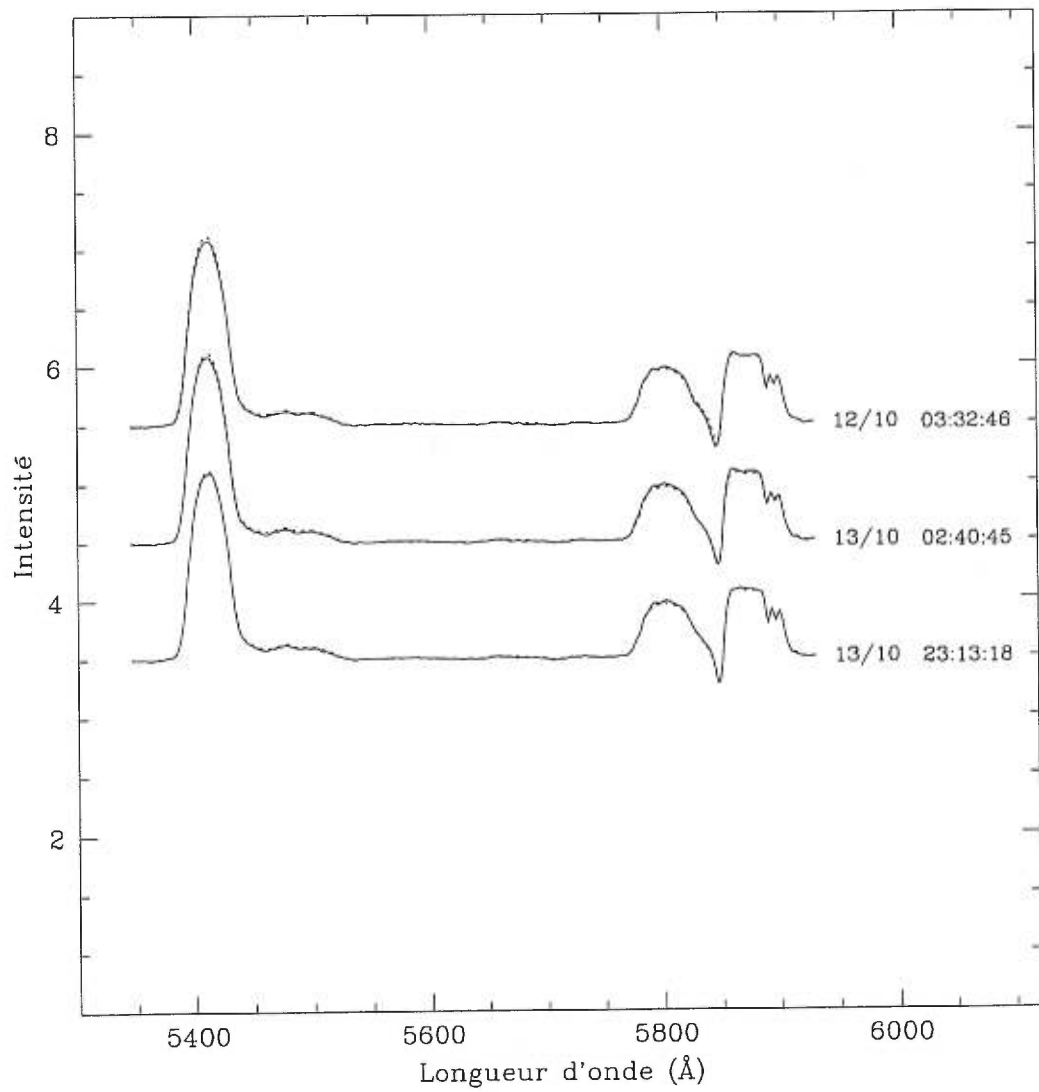


FIGURE A.2. Suite.

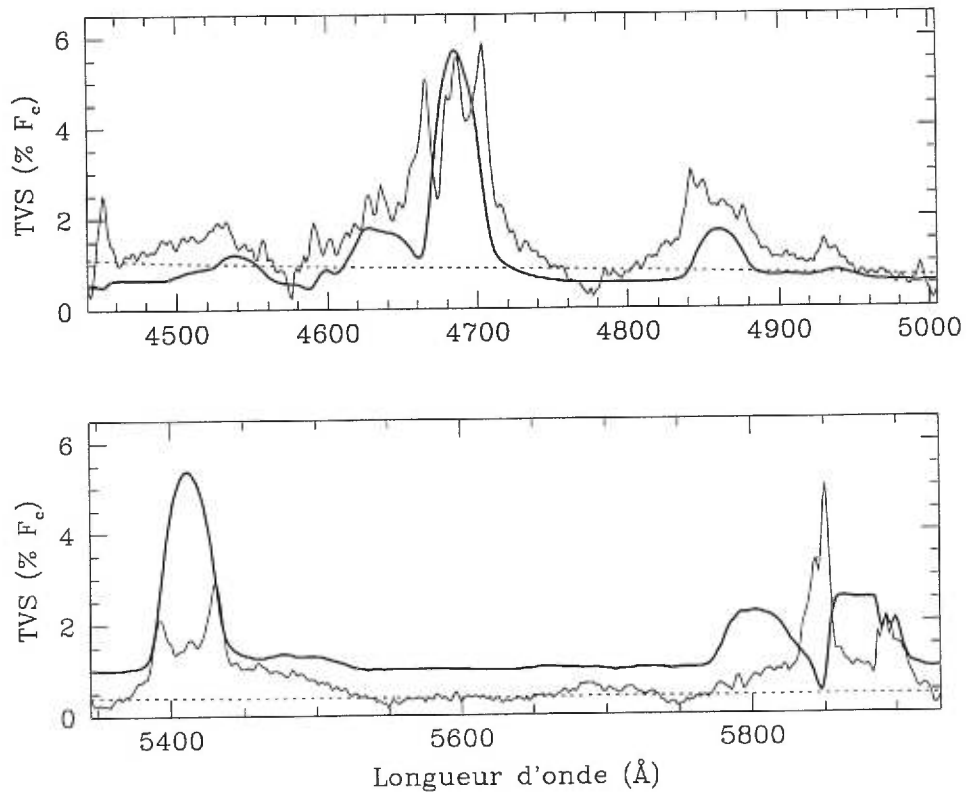


FIGURE A.3. Valeurs de la TVS pour l'étoile WR 136 en 1995 (exprimées en terme de l'amplitude des variations en pourcentage du continuum normalisé). Un spectre moyen est superposé en unités arbitraires. Une correction dans l'espace des vitesses radiales selon $\delta_j = 7.5 \text{ km s}^{-1}$ a été appliquée (§2.3.2.3). La ligne pointillée indique le seuil pour une variabilité significative à un taux de confiance de 99.0 %.

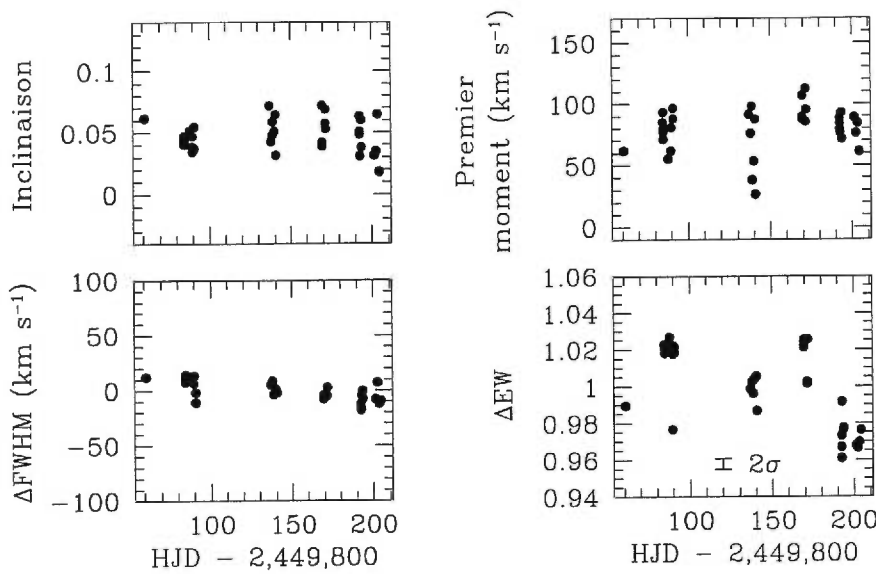


FIGURE A.4. Variations selon le jour Julien d'observation de l'inclinaison (*skewness*), premier moment (*centroid*) (en km s^{-1}), largeur à mi-hauteur (en km s^{-1} et exprimée en terme des déviations autour de la valeur moyenne) et largeur équivalente (normalisée par division par la valeur moyenne) de la raie He II $\lambda 4686$ de l'étoile WR 136. A des fins de comparaison avec l'étoile WR 134, l'échelle est la même que sur la figure 4.2. Les calculs de l'inclinaison et du premier moment ont été restreints à la portion de la raie caractérisée par une intensité relative supérieure à 2.5 unités du continuum. Les largeurs équivalentes ont été calculées en intégrant le flux de la raie dans l'intervalle 4661-4765 Å (la barre d'erreur a été calculée selon la méthode prescrite par Chalabaev & Maillard [1983]).

PUBLICATIONS DE L'AUTEUR

Cette thèse est basée sur les publications suivantes:

- **T. Morel**, N. St-Louis, & S. V. Marchenko, *Optical Spectroscopy of EZ Canis Majoris: Indication for Large-Scale Structures in a Wolf-Rayet Wind*, The Astrophysical Journal, 482, 470 (1997)
- **T. Morel**, N. St-Louis, A. F. J. Moffat, O. Cardona, G. Koenigsberger, & G. M. Hill, *Coupled Line-Profile and Continuum Variations in EZ Canis Majoris: Implications for the Driving Mechanism of Global Wind Structures in Wolf-Rayet Winds*, The Astrophysical Journal, 498, 413 (1998)
- **T. Morel**, S. V. Marchenko, P. R. J. Eeenens, A. F. J. Moffat, G. Koenigsberger, I. I. Antokhin, T. Eversberg, G. H. Tovmassian, G. M. Hill, & O. Cardona, *A 2.3-Day Periodic Variability in the Apparently Single Wolf-Rayet Star WR 134: Collapsed Companion or Rotational Modulation?*, The Astrophysical Journal, sous presse (1999)
- **T. Morel**, L. N. Georgiev, Y. Grosdidier, N. St-Louis, T. Eversberg, & G. M. Hill, *An Investigation of the Large-Scale Variability of the Apparently Single Wolf-Rayet Star WR 1*, Soumis à Astronomy & Astrophysics (1998)

L'auteur a également contribué aux articles suivants:

- **T. Morel**, N. St-Louis, & S. V. Marchenko, *The Photosphere-Wind Connection in Wolf-Rayet Stars: Simultaneous Photometry and Spectroscopy of EZ CMa*, 33rd Liège International Astrophysical Colloquium Proceedings: “WR Stars in the Framework of Stellar Evolution”, 271 (1996)
- S. V. Marchenko, A. F. J. Moffat, T. Eversberg, G. M. Hill, G. H. Tovmassian, **T. Morel**, I. I. Antokhin, & W. Seggewiss, *The All-Variable WN 8 Stars*:

the Stellar Core as Driver, 33rd Liège International Astrophysical Colloquium Proceedings: “WR Stars in the Framework of Stellar Evolution”, 265 (1996)

- S. V. Marchenko, A. F. J. Moffat, T. Eversberg, G. M. Hill, G. H. Tovmassian, **T. Morel**, & W. Seggewiss, *A Comprehensive Variability Study of the Enigmatic WN 8 Stars: Final Results*, Monthly Notices of the Royal Astronomical Society, 294, 642 (1998)
- **T. Morel**, S. V. Marchenko, P. R. J. Eenens, A. F. J. Moffat, G. Koenigsberger, T. Eversberg, G. H. Tovmassian, G. M. Hill, & O. Cardona, *Confirmation of a 2.3-Day Periodicity in the Wolf-Rayet Star WR 134: a Twin of EZ CMa?*, ESO Proceedings: “Cyclical Variability in Stellar Winds”, 109 (1998)
- **T. Morel**, S. V. Marchenko, P. R. J. Eenens, A. F. J. Moffat, G. Koenigsberger, I. I. Antokhin, T. Eversberg, G. H. Tovmassian, G. M. Hill, & O. Cardona, *Cyclical Spectral and Photometric Variations of the Apparently Single Wolf-Rayet Star WR 134*, Astrophysics and Space Science, sous presse (1999)

REMERCIEMENTS

Je suis en premier lieu particulièrement reconnaissant à Nicole St-Louis pour son excellent encadrement, ainsi que pour l'ensemble des moyens qu'elle a mis à ma disposition tout au long de cette collaboration. Sa bonne humeur et son soutien indéfectibles ont été salvateurs en de nombreuses circonstances.

Ce projet de thèse a également largement bénéficié de fructueuses discussions avec Leonid Georgiev, Grant Hill, Gloria Koenigsberger, Sergey Marchenko et Tony Moffat; qu'ils en soient ici vivement remerciés.

Je remercie Alex W. Fullerton, Robert Lamontagne, ainsi que Daniel Nadeau pour m'avoir fait l'honneur de bien vouloir composer mon jury de soutenance.

Je tiens également à exprimer ma gratitude à Agnès Acker grâce à qui j'ai pu poursuivre mes études à l'Université de Montréal.

Mes remerciements vont également à John M. Blondin, Steve R. Cranmer, Achim Feldmeier et Sébastien Lépine pour m'avoir autorisé à inclure dans cet ouvrage des figures issues de leurs travaux.

Une pensée particulière va aux ami(e)s que j'ai eu la chance de rencontrer durant ces quatre années; ils ont pour beaucoup contribué à faire de mon séjour dans la Belle Province une expérience extrêmement enrichissante.

Enfin, je remercie la Faculté des Etudes Supérieures pour son précieux soutien financier.